N^o ORDRE : 40674

École doctorale régionale Sciences Pour l'Ingénieur Lille Nord–de–France

Université Lille 1 Sciences et Technologies & Université Gaston Berger

ANALYSE MATHÉMATIQUE ET NUMÉRIQUE DE MODÈLES DE COAGULATION-FRAGMENTATION

THÈSE EN COTUTELLE

soutenue publiquement le 9 décembre 2011 pour l'obtention

Doctorat de l'université Lille 1

Spécialité : Mathématiques appliquées

Doctorat de l'université Gaston Berger

Spécialité : Mathématiques appliquées

présentée par

Léon Matar S. TINE

Composition du jury

Francis FILBET	Rapporteur	Université Lyon 1
Hamidou TOURE	Rapporteur	Université Ouagadougou
François CASTELA	Rapporteur	Université de Rennes 1
Thierry GOUDON	Directeur	INRIA Lille Nord-Europe
Mamadou SY	Co-encadrant	Université Gaston Berger
Frédéric LAGOUTIERE	Co-encadrant	Université Paris-Sud 11
Claire CHAINAIS	Examinatrice	Université Lille 1

Laboratoires Paul Painlevé & LANI **Equipe SIMPAF (INRIA Lille Nord–Europe)**

Mis en page avec la classe thloria.

Résumé

Ce mémoire de thèse concerne l'analyse mathématique et numérique du comportement asymptotique de certains modèles de type coagulation-fragmentation intervenant en physique ou en biologie. Dans la première partie on considère le système d'équations de Lifshitz-Slyozov qui modélise l'immersion d'une population de macro-particules en interaction avec un bain de monomères. Ce modèle développe en temps long un comportement dépendant d'une manière très particulière de l'état initial et ses spécificités techniques en font un véritable challenge pour la simulation numérique. On introduit un nouveau schéma numérique de type volumes finis basé sur une stratégie anti-dissipative ; ce schéma parvient à capturer les profils asymptotiques attendus par la théorie et dépasse en performances les méthodes utilisées jusqu'alors. L'investigation numérique est poursuivie en prenant en compte dans le modèle des phénomènes de coalescence entre macro-particules à travers l'opérateur de Smoluchowski. La question est de déterminer par l'expérimentation numérique comment ces phénomènes influencent le comportement asymptotique. On envisage aussi une extension du modèle classique de Lifshitz-Slyozov qui prend en compte des effets spatiaux via la diffusion des monomères. On établit l'existence et l'unicité des solutions du système couplé hyperbolique-parabolique correspondant.

La seconde partie de ce mémoire aborde des modèles d'agrégation-fragmentation issus de la biologie. On s'intéresse en effet à des équations décrivant les phénomènes de croissance et de division pour une population de cellules caractérisée par sa densité de répartition en taille. Le comportement asymptotique de cette densité de répartition est accessible à l'expérience et peut être établi théoriquement. L'enjeu biologique consiste, à partir de données mesurées de la densité cellulaire, à estimer le taux de division cellulaire qui, lui, n'est pas expérimentalement mesurable. Ainsi, retrouver ce taux de division cellulaire fait appel à l'étude d'un problème inverse que nous abordons théoriquement et numériquement par des techniques de régularisations par quasi-reversibilité et par filtrage.

La troisième partie de ce travail de thèse est consacrée à des systèmes couplés décrivant des interactions fluide-particules, avec des termes de coagulation–fragmentation, de type Becker–Döring. On étudie les propriétés de stabilité du modèle et on présente des résultats d'asymptotiques correspondant à des régimes de forte friction.

Mots-clés: Analyse asymptotique, Problèmes hyperboliques-paraboliques, Modèles d'agrégation–fragmentation, Équations de Lifshitz-Slyozov, Modèles collisionnels, Modèle de Smoluchowski, Modèle de Becker-Döring, Schémas volumes finis, Schémas anti–dissipatifs, Problème inverse, Interactions fluide-particules.

Abstract

This thesis concerns the mathematical and numerical analysis of the asymptotic behavior of some coagulation-fragmentation type models arising in physics or in biology. In the first part we consider the Lifshitz-Slyozov system that models the dumping of a population of macro-particles in interaction with a bath of monomers. This model develops in long time a behavior depending in a very particular way on the initial data and its technical specificities make a real challenge for the numerical simulation. We introduce a new numerical finite volume type scheme based on an anti-dissipative strategy ; this scheme succeeds in capturing the asymptotic profiles waited by the theory and exceeds in performances the methods used before. The numerical investigation is pursued by taking into account in the model the phenomena of coalescence between macro-particles through the Smoluchowski operator. The question is to find by numerical experiment how these phenomena influence the asymptotic behavior. We also consider an extension of the classical Lifshitz-Slyozov model which takes into account the spatial effects via the diffusion of monomers. We establish the existence and the uniqueness of the solutions of the corresponding hyperbolic-parabolic coupled system.

The second part of this thesis deals with approaches coagulation-fragmentation models stemming from biology. Indeed, we are interest in equations describing the phenomena of growth and division for a cells population caracterised by its size density repartition. The asymptotic behavior of this size density repartition is accessible to the experiment and can be established in theory. The biological stake consists, from measured data of the cellular density, to estimate the cellular division rate which is not experimentally measurable. So, to find this cellular division rate requires the study of an inverse problem which we approach numerically and theoretically by techniques of regularizations by quasi-reversibility and by filtering.

The third part of this thesis work is devoted to coupled systems describing fluid-particles interactions with coagulation-fragmentation terms of Becker-Döring type. We study the stability properties of the model and we present some asymptotic results corresponding to the regime with strong friction force.

Keywords: Asymptotic analysis, Hyperbolic-parabolic problems, Aggregation-fragmentation models, Lifshitz-Slyozov equations, Encounters models, Smoluchowski model, Becker-Döring model, Finite volumes schemes, Anti-dissipative schemes, Inverse problem, fluid-particles interactions.

Remerciements

Un grand merci du fond du coeur à Thierry Goudon, mon directeur de thèse, d'avoir accepté de m'encadrer durant ces trois années d'initiation à la recherche. Sa disponibilité, son talent scientifique, sa patience et son humanité ont facilités mon intégration et mon travail d'apprentissage à la recherche. Un grand merci aussi à mes co-encadrants Mamadou Sy et Frédéric Lagoutière avec qui les échanges scientifiques et les conseils rigoureux ont été un bonheur constant.

J'adresse ma profonde reconnaissance à toute l'équipe SIMPAF (INRIA Lille) au sein de laquelle j'ai effectué mes travaux de thèse durant tout mon séjour en France. Que des moments de plaisirs et aussi de follies surtout en compagnie de mon frère Martin Parisot avec son "woukoulélé", de Anne Devys à qui je témoigne toute ma profonde gratitude, de Bénedicte Aguer "miss frittes" avec sa joie constante de vivre, de Chang Yang mon ami chinois à qui je dis "xièxie" , de Benjamin Boutin "le mignon" d'une gentillesse hors paire, de Aliou Diouf, le sénégalais avec ses points de vues dures mais pas méchants sur la France, de Yuan Penel pour toutes les discussions et conseils durant les pauses déjeuners.

Mes remerciements vont aussi à l'endroit de l'équipe projet BANG et je pense déjà à Marie Doumic pour sa collaboration franche et fructueuse qui m'a donné goût aux mathématiques appliquées à la biologie. J'en profite pour adresser mes remerciements à Benoît Perthame et toute son équipe thésarde de Paris 6 à savoir Alexis Blasselle, Sép Ideh, Alexandre et surtout Pierre Gabriel avec qui j'ai effectué un réel plaisir d'initiation aux mathématiques biologiques durant le Cemracs 2009. Merci aussi à Eleo pour sa gentillesse et son hospitalité.

À tous mes amis que j'ai connu à Lille, je vous dis merci pour tous les bons moments passés ensemble. J'ai une pensée pieuse pour les amis de la résidence Robespierre, également une pensée pour Jovana Deravel, Antoine Ndione, Mame coumba Faye, Paul aziz Fall, Joe Sadio, Abdou K. Tine, Tati, Pauline "ma petite soeur", Marie Noël Diokh, Albinou Ndecky, Pamella, Christophe Calvès, Russel Nzekwa, Paul Koropogui "l'international guinéen", Aly, Kader, Mouty, Steve etc. Un merci à tous les amis de la résidence Pont de bois pour tous les moments de plaisir et de vie commune à la résidence, je pense spécilement à Yvan et Annie, à Aurélien, à Nico, à Florine, à Oritcha Sourou et à la martiniquaise Naomy Lafleur "ho ! la petite c'est comment ?".

À toute l'univerité Gaston Berger de Saint-Louis je dis merci. Un merci spécial au laboratoire LANI qui m'a offert l'opportunité de faire de la recherche à travers la bourse de coopération franco-sénégalaise et j'en profite également pour lancer un grand remerciement au Service de Coopération et d'Action Culturelle de l' ambassade de France à Dakar. Merci à toute ma promotion de DEA à savoir Lamine Diagne, Ben Mansour Dia, Samsydine Goudiaby, ect.

Ces derniers mots de remerciement sont adressés à mes parents, toute cette grande famille Tine de Thiès Nones. Merci à "Dé" Anna et tonton Alain Masselot pour m'avoir acheté mon premier livre de mathématiques "Fractale T.S". Merci à "Pa" Henry de m'avoir donné en un moment le goût des études par les petites récompenses financières qui me faisaient tant plaisir.

Table des matières

Introduction Générale

Ce manuscrit est le fruit de mon travail de thèse mené en co-tutelle entre l'Université des Sciences et Technologies de Lille 1 (France) et l'Université Gaston Berger de Saint-Louis (Sénégal). Ce travail a été réalisée en partie au sein de l'équipe SIMPAF du centre de recherche INRIA Lille Nord Europe. Il développe un ensemble de résultats obtenus sur l'analyse mathématique et la simulation numérique de divers problèmes liés aux phénomènes de coagulation et fragmentation.

Les phénomènes de coagulation et fragmentation interviennent de façon naturelle dans plusieurs processus physiques (aérosols, fumées, formation de gouttelettes, cristallisation et fabrication d'alliages métalliques), chimiques (polymérisation), biologiques (division cellulaire), astrophysiques (formation des planètes et galaxies), etc. Ils permettent de décrire la dynamique d'évolution d'une population de particules ou de cellules subissant des changements d'états par collisions et agrégation ou par divisions. La modélisation de ces phénomènes de coagulation et fragmentation peut se faire à différentes échelles :

Microscopique : où l'on s'intéresse à chaque individu de la population de particules ou de cellules en supposant que le processus par lequel deux individus coalescent est aléatoire. Un premier modèle de ce type a été proposé par Smoluchowski [168], puis d'autres modèles furent établis par A. Marcus [127], A. Lushnikov [126], D.J. Aldous et J. Pitman [3] et J.F.C. Kingman [109].

Mésoscopique : on ne s'intéresse plus à une description individuelle, mais on étudie plutôt l'évolution collective de groupes d'individus de la population considérée, chaque groupe étant caractérisé par une variable de taille et éventuellement par sa position.

Macroscopique : au niveau macroscopique on modélise typiquement l'évolution de la moyenne d'une certaine quantité liée à la population considérée ; par exemple il peut s'agir de la taille moyenne des individus ou de leur vitesse moyenne d'évolution.

Dans ce présent mémoire, nous nous focalisons sur une modélisation à l'échelle mésoscopique des phénomènes de coagulation-fragmentation intervenant dans les processus étudiés. Ce choix conduit à étudier la dynamique d'évolution de la population de particules ou de cellules considérée par sa densité de répartition (par exemple en taille). Les phénomènes de coagulation-fragmentation sont alors modélisés mathématiquement, par exemple, par les équations de coagulation de Smoluchowski ou par les équations de Becker-Döring.

Modèle discret des équations de coagulation-fragmentation

En 1917, Smoluchowski adopte un point de vue discret pour décrire les phénomènes de coagulation, [169] ; il aboutit au système (infini) d'équations différentielles ordinaires suivant

$$\begin{aligned}\frac{d}{\mathrm{d}t}f_i &= \sum_{j=1}^{i-1}\kappa_{j,i-j}f_jf_{i-j} - \sum_{j=1}^{\infty}\kappa_{i,j}f_if_j \quad \forall\, i\geq 1,\\ &= Q_i^+ - Q_i^-\end{aligned}$$

où $f_i(t)$ représente la densité des individus (particules ou cellules) de taille $\{i\} \in \mathbb{N}\setminus\{0\}$ à l'instant t. La quantité $\kappa_{i,j} \geq 0$ pour i, j entiers non nuls peut être reliée à la probabilité de coagulation par unité de temps entre individus de taille $\{i\}$ et individus de taille $\{j\}$ suivant le schéma

$$\{i\} + \{j\} \longrightarrow \{i+j\}$$

le résultat de cette réaction étant la formation d'une particule de taille $i + j$. L'hypothèse de symétrie

$$\kappa_{i,j} = \kappa_{j,i} \geq 0$$

apparaît ainsi naturelle. Le terme Q_i^+ représente le gain en individus de taille $\{i\}$ dû aux coagulations de deux individus de tailles plus petites $\{j\}$ et $\{i-j\}$, avec $1 \leq j < i$. Le terme Q_i^- représente quant à lui la perte en individus de taille $\{i\}$ par coagulation avec un individu de taille quelconque $\{j\} \geq 1$. Le modèle de Becker-Döring, établi en 1935 [16], est une variante de ce système où seuls le gain ou la perte de monomères, c'est-à-dire d'individus de taille $j = 1$, sont autorisés. Plus généralement, un modèle discret prenant en compte à la fois les phénomènes de coagulation et de fragmentation s'écrit comme suit :

$$\begin{cases}\dfrac{d}{\mathrm{d}t}f_i = Q_i(f), \qquad \forall i \geq 1,\\[2ex] f_i(0) = f_i^0\end{cases} \tag{1}$$

où l'opérateur $Q_i = \big(Q_{1,i} - Q_{2,i}\big) - \big(Q_{3,i} - Q_{4,i}\big)$ est de la forme

$$\begin{aligned}Q_{1,i}(f) &= \frac{1}{2}\sum_{j=1}^{i-1}\kappa_{j,i-j}f_jf_{i-j} \quad \text{gain en individus de taille } \{i\} \text{ par coagulation}\\ Q_{2,i}(f) &= \sum_{j=1}^{\infty}\kappa_{i,j}f_if_j \quad \text{perte en individus de taille } \{i\} \text{ par coagulation}\\ Q_{3,i}(f) &= \frac{1}{2}\sum_{j=1}^{i-1}\beta_{j,i-j}f_i \quad \text{perte en individus de taille } \{i\} \text{ par fragmentation}\\ Q_{4,i}(f) &= \sum_{j=1}^{\infty}\beta_{i,j}f_{i+j} \quad \text{gain en individus de taille } \{i\} \text{ par fragmentation}\end{aligned}$$

et $\beta_{i,j}$ est le noyau de fragmentation lorsqu'un individu de taille $\{i + j\}$ se fragmente en deux individus de tailles $\{i\}$ et $\{j\}$.

Notion de solution faible du modèle discret de coagulation-fragmentation

L'analyse des équations de coagulation-fragmentation discrètes exploite la définition suivante.

Définition .1. *Soit la donnée initiale $f_i^0 \geq 0$ vérifiant $\sum_{i=1}^{\infty} i f_i^0 < \infty$. On appelle solution faible du modèle discret* (1) *une fonction $t \mapsto f(t) = (f_i(t))_{i\geq 1} \in \mathcal{M}$ où $\mathcal{M}$ désigne l'ensemble*

$$\mathcal{M} = \left\{ (h_i)_{i\geq 1} \in \mathbb{R},\ h_i \geq 0,\ \sum_{i=1}^{\infty} i h_i < \infty \right\}$$

telle que $Q_i(f)$ soit localement sommable en temps et vérifie de plus :

- $\displaystyle\sum_{i=1}^{\infty} i f_i \leq \sum_{i=1}^{\infty} i f_i^0,$
- $\displaystyle\frac{\mathrm{d}}{\mathrm{d}t} \sum_{i=1}^{\infty} f_i \phi_i = \sum_{i=1}^{\infty} Q_i(f)\phi_i,$

pour toute suite $(\phi_i)_{i\geq 1}$ tendant vers 0 «suffisamment vite».

Notons que, d'un point de vue physique, la quantité $\sum_{i=1}^{\infty} i f_i$ est proportionnelle à la masse totale du système de particules. Il est donc naturel de supposer cette quantité finie. L'existence de solution du modèle discret de coagulation-fragmentation (1) peut s'obtenir par deux approches fonctionnelles différentes. Par exemple P. Dubovskiĭ et I. Stewart [70] en 1996 utilisent un argument de point fixe dans l'espace $\mathcal{M}$, alors que J. Ball, J. Carr et O. Penrose [10] en 1986 raisonnent par compacité (au sens fort et faible) dans l'espace

$$X = \left\{ h \geq 0, \sum_{i=1}^{\infty} i h_i < \infty \right\}.$$

Cette dernière approche conduit à mettre en évidence le principe de stabilité suivant.

Principe de stabilité. Soit $(f^n)_{n\geq 1}$ une suite d'approximations du modèle discret de coagulation-fragmentation (par exemple obtenue par troncature en ne considérant qu'un nombre fini de tailles). Si pour tout $0 \leq t \leq T < \infty$, $f^n(t)$ et $Q_i(f^n)(t)$ appartiennent à un sous-ensemble faiblement compact de X et l'application $t \longrightarrow \sum_{i=1}^{\infty} f_i^n(t)\phi_i$ appartient à un sous-ensemble fortement compact de $L^1(0,T)$ pour toute suite $(\phi_i)_{i\geq 1}$ à décroissance assez rapide, alors il existe une sous-suite qu'on persiste à désigner par f^n et une fonction f tel que $f^n(t) \rightharpoonup f(t)$ et $Q(f^n)(t) \rightharpoonup Q(f)(t)$ dans X, pour presque tout $0 \leq t \leq T$.

Ces arguments permettent d'établir l'existence de solutions aux équations de coagulation-fragmentation, pour une large classe de noyaux $k_{i,j}$ et $\beta_{i,j}$ vérifiant certaines hypothèses de croissance. Par ailleurs les phénomènes de coagulation-fragmentation n'affectent pas en général le bilan de masse au sens où

$$\sum_{i=1}^{\infty} i Q_i(f) = 0.$$

La question consiste donc à déterminer si les solutions obtenues ont la même masse pour tout temps. On impose l'hypothèse de croissance suivante sur les noyaux :

$$\sup_{i\leq N} \frac{\kappa_{i,j}}{j} \longrightarrow 0, \qquad \sup_{i\leq N} \frac{\beta_{i,j}}{j} \longrightarrow 0 \quad \text{lorsque } j \to \infty.$$

Sous cette hypothèse il y a bien conservation de la masse. Lorsque cette hypothèse de croissance est violée, il y a possibilité de perte de masse en temps fini et de formation d'un individu de taille infinie, c'est le phénomène de gélation. On se réferera à la synthèse de M. Escobedo, S. Mischler, B. Perthame [77] pour une analyse fouillée de cette question. L'unicité de solution pour des modèles discrets généraux (1) est étudiée par P. Laurençot et S. Mischler [115].

Modèle continu des équations de coagulation-fragmentation

On peut aussi s'intéresser à des modèles continus, où la variable de taille décrit toute la demi–droite $x \geq 0$. La version continue des équations de coagulation-fragmentation prend la forme d'une équation intégro-différentiellle

$$\begin{cases} \dfrac{d}{\mathrm{d}t} f = Q(f), & (t,x) \in]0,\infty[\times[0,\infty[, \\ \\ f^0(x) = f(t=0,x) \geq 0, & x \in [0,\infty[, \end{cases} \tag{2}$$

où $f(t,x)$ est la densité de répartition des individus (particules ou cellules) de taille ou de volume x à l'instant t et l'opérateur $Q(f)$ se décompose en $\big(Q_1(f) - Q_2(f)\big) - \big(Q_3(f) - Q_4(f)\big)$ avec l'interprétation

$$\begin{aligned} Q_1(f)(t,x) &= \frac{1}{2}\int_0^x \kappa(y,x-y) f(t,y) f(t,x-y)\,\mathrm{d}y \quad \text{gain en individus de taille } x \\ &\qquad\qquad\qquad\qquad\qquad\qquad\qquad\qquad\qquad\qquad \text{par coagulation} \\ Q_2(f)(t,x) &= \int_0^\infty \kappa(x,y) f(t,x) f(t,y)\,\mathrm{d}y \quad \text{perte en individus de taille } x \text{ par coagulation} \\ Q_3(f)(t,x) &= \frac{1}{2}\int_0^x \beta(y,x-y) f(t,x)\,\mathrm{d}y \quad \text{perte en individus de taille } x \text{ par fragmentation} \\ Q_4(f)(t,x) &= \int_0^\infty \beta(x,y) f(t,x+y)\,\mathrm{d}y \quad \text{gain en individus de taille } x \text{ par fragmentation.} \end{aligned}$$

Les paramètres $\kappa \geq 0$ et $\beta \geq 0$ sont respectivement les noyaux de coagulation et de fragmentation et sont supposés symétriques.

Notion de solution faible du modèle continu de coagulation-fragmentation

Comme pour le cas discret on introduit une notion de solution faible adéquate.

Définition .2. *Soit la donnée initiale $f^0 \geq 0$ vérifiant $\int_0^\infty (1+x) f^0(x)\,\mathrm{d}x < \infty$, et soit $\phi \in \mathcal{D}(\mathbb{R}_+)$. On appelle solution faible du modèle continu* (2) *toute fonction f satisfaisant à*

$$\begin{aligned} &\frac{\mathrm{d}}{\mathrm{d}t}\int_0^\infty f\phi\,\mathrm{d}x \\ &\quad = \frac{1}{2}\int_0^\infty\int_0^\infty \Big(\kappa(x,y) f(t,x) f(t,y) - \beta(x,y) f(t,x+y)\Big)\Big(\phi(x+y) - \phi(x) - \phi(y)\Big)\,\mathrm{d}x\,\mathrm{d}y. \end{aligned}$$

Comme dans le modèle discret, l'existence de solution du modèle continu s'obtient soit par l'approche de P. Dubovskiĭ et I. Stewart [70] dans l'ensemble $L^1_1 = \big\{f \geq 0, (1+x)f \in L^1(\mathbb{R}_+)\big\}$ soit par l'approche de J. Ball, J. Carr et O. Penrose [10] dans l'espace $L^1(\mathbb{R}_+)$. La conservation de la masse réclame encore une hypothèse de croissance sur les noyaux de coagulation et de fragmentation. On trouvera de nombreux détails et références dans le travail de P. Laurençot et

S. Mischler [115].
Le lien entre les modèles discret et continu de coagulation-fragmentation a été étudié par certains auteurs comme R. L. Drake [69] et M. Aizenman, T. A. Bak [2]. Le passage du modèle discret au modèle continu avec des hypothèses générales sur les noyaux de coagulation et fragmentation est établi de façon rigoureuse par P. Laurençot et S. Mischler [114]. La simulation numérique des équations de coagulation-fragmentation soulève des questions spécifiques, notamment liées à la nécessaire troncature de la variable de taille, et reproduire avec acuité le phénomène de gélation ou au contraire préserver la masse sont des problématiques sources de difficultés. F. Filbet et P. Laurençot [82] ont développé des méthodes performantes et originales pour aborder ces problèmes et ces techniques seront reprises dans ce mémoire de thèse.

Dans cette thèse on aborde des problèmatiques d'ordres mathématique et numérique faisant intervenir des phénomènes de coagulation et fragmentation, avec des applications principalement motivées par la physique et la biologie. Ainsi dans la première partie on s'intéresse au système d'équations de Lifshitz-Slyozov, une variante continue du système de Becker-Döring, dont le comportement asymptotique des solutions est particulièrement inhabituel. Dans le premier chapitre on introduit un nouveau schéma de type volumes finis à stratégie anti-dissipative pour simuler numériquement les équations de Lifshitz-Slyozov. En s'inspirant des travaux de F. Filbet et P. Laurençot [82], on met en évidence par des expérimentations numériques le rôle des collisions entre particules dans le processus de sélection du profil asymptotique. Le second chapitre prend en compte la diffusion spatiale des monomères et détaille l'analyse mathématique du modèle de Lifshitz–Slyozov correspondant, qui prend la forme d'un système d'EDPs couplées de types hyperbolique et parabolique. La deuxième partie du manuscrit considère des questions issues des applications en biologie et médecine. En biologie, la compréhension et le contrôle de l'évolution d'une population de cellules structurée en taille et subissant des phénomènes de croissance, de division et de mort constituent des enjeux majeurs, par exemple dans l'étude des maladies neurodégénératives. Par des techniques de mesures biologiques, par exemple par flux cytométrique, on peut déterminer la densité de la population cellulaire au bout d'un temps T donné ; mais on n'a pas accés au taux de division cellulaire. On développe donc des techniques de problème inverse pour fournir des méthodes mathématiques permettant d'estimer ce taux de division ; c'est l'objet du premier chapitre de la seconde partie de ce mémoire de thèse. Le second chapitre traite d'un modèle spécifique de polymérisation avec coalescence pour le prion (**Pr**oteinaceous **i**nfectious **on**ly). Dans la troisième partie du manuscrit nous abordons un modèle de couplage microscopique-macroscopique d'interaction fluide-particules où des phénomènes de coagulation-fragmentation sont pris en compte par un terme de type Becker-Döring. Nous nous intéressons à l'étude de stabilité et l'analyse asymptotique de ce modèle d'interaction fluide-particules.

1 Système d'équations de Lifshitz-Slyozov

1.1 Simulation numérique du modèle de Lifshitz-Slyozov standard

Contexte général

Historiquement, le système d'équations de Lifshitz-Slyozov est un modèle physique établi par E. Lifshitz et V. Slyozov [124] en 1916 pour modéliser la cinétique de formation de grains par précipitation dans une solution solide super-saturée. Il s'agit d'un modèle très couramment utilisé en métallurgie, pour décrire la formation de certains alliages. La dynamique d'évolution peut être vue comme l'interaction entre macro-particules, décrites par une fonction de densité $f(t,x)$, $x \geq 0$ étant la variable de taille, et des monomères dont la densité est notée $c(t)$. Mathématiquement,

en notant par $a(x) \geq 0$ et $b(x) \geq 0$ respectivement les taux en gain et perte de monomères par les macro-particules, le modèle s'écrit comme une équation de transport

$$\begin{cases} \partial_t f(t,x) + \partial_x(V(t,x)f(t,x)) = 0, \quad t \in [0,\infty[,\ x \in [0,\infty[, \\ \\ V(t,x) = a(x)c(t) - b(x), \end{cases}$$

couplée à une équation intégrale décrivant la conservation de la masse totale

$$c(t) + \int_0^\infty x f(t,x)\,\mathrm{d}x = \rho,$$

avec ρ la masse totale initiale.

Malgré son apparence simpliste, ce couplage continue d'intriguer un bon nombre d'auteurs, notamment en ce qui concerne l'étude du comportement asymptotique en temps des solutions. En effet Lifshitz et Slyozov avaient émis la conjecture suivant laquelle les solutions suivent en temps grand un profil universel, indépendant à un facteur d'échelle près de l'état initial. Une suite de résultats d'analyse et d'expérimentations numériques, établis par B. Niethammer et R. Pego [145] en 2000, J. A. Carrillo et T. Goudon [35] en 2003, M. Hermann, B. Niethammer et J. J. L Velàzquez [104] en 2008, ont montré que cette conjecture n'était pas vraie. Contrairement aux conjectures de Lifshitz et Slyozov, il existe une famille de profils asymptotiques et, en partant d'une donnée initiale à support compact, la dynamique choisit le profil ayant le même comportement que la donnée initiale au bord du support. L'analyse de ce comportement asymptotique étrange est délicate et requiert l'introduction de notions de stabilité nouvelles. Parvenir à capturer numériquement le profil correct est un challenge difficile, la diffusion numérique ayant tendance à lisser artificiellement le profil des solutions et à conduire de façon erronée vers le profil, régulier, prédit par Lifshitz et Slyozov. L'étude numérique effectuée par J. A. Carrillo et T. Goudon repose sur un schéma WENO (Weighted Essentially Non–Oscillatory) d'ordre 5. Numériquement ils obtiennent les profils asymptotiques donnés à la figure 1 pour la solution f du modèle de Lifshitz–Slyozov en partant de deux données initiales différentes avec le choix $a(x) = x^{1/3}$ et $b(x) = 1$.

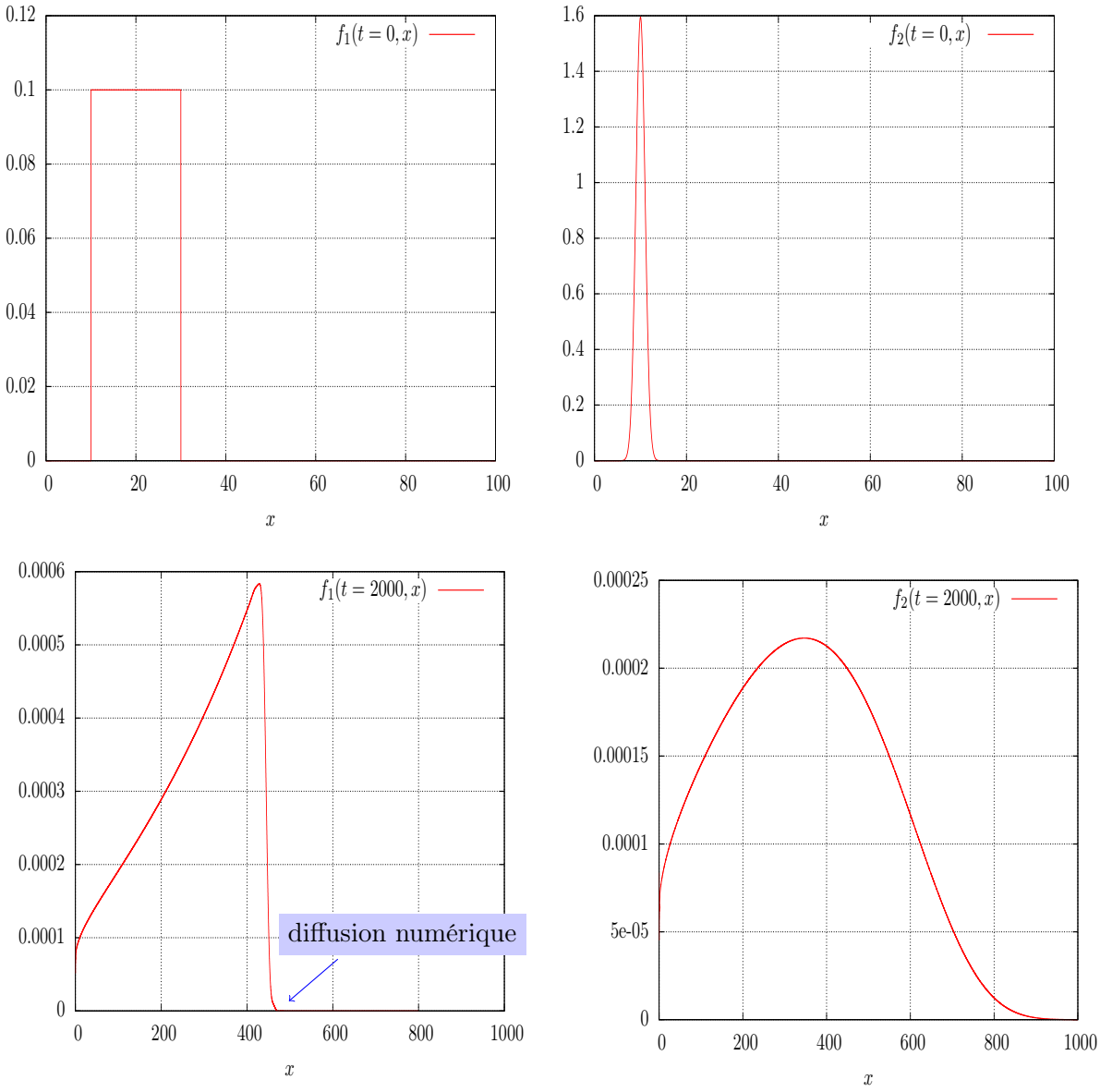

Figure 1 – Reconstruction numérique avec WENO 5 du profil asymptotique suivant deux données initiales différentes.

Bien que le schéma WENO soit d'ordre élevé, on remarque que ce dernier développe une certaine diffusion numérique, comme le montre la figure 1. Bien que celle-ci soit réduite, et en général tout à fait tolérable pour la plupart des applications et simulations de lois de conservation, elle conduit ici à perdre pour des temps de simulation grands le profil asymptotique attendu. Il est très probable que des conclusions trompeuses aient été déduites de ce type de phénomènes, bien plus sensibles avec des schémas moins performants que WENO (voir [35] pour des illustrations utilisant des schémas comme Upwind ou de Lax–Friedrichs).

Modèle de Lifshitz-Slyozov en variables auto–similaires

L'étude du comportement asymptotique du modèle de Lifshitz-Slyozov repose sur un changement de variables adapté :

$$\begin{cases} f(t,x) = \dfrac{1}{(1+t)^2} g(\ln(1+t), \dfrac{x}{1+t}), \\ \\ \tau = \ln(1+t),\ y = \dfrac{x}{1+t},\ d(\tau) = (1+t)^{1/3} c(t), \\ \\ W(\tau, y) = y^{1/3} d(\tau) - 1 - y. \end{cases}$$

En supposant que $\lim_{\tau\to\infty} d(\tau) = K$, ce qui correspond à la conjecture de Lifshitz–Slyozov suivant laquelle le rayon moyen des particules évolue comme $t^{1/3}$, et en posant $W_K(y) = y^{1/3}K - 1 - y$, on obtient le modèle de Lifshitz-Slyozov mis à l'échelle suivant

$$\begin{cases} \partial_\tau g(\tau, y) + \partial_y \Big(W_K(y) g(\tau, y) \Big) = g(\tau, y), \\ \displaystyle\int_0^\infty y g(\tau, y)\, \mathrm{d}y = \rho. \end{cases} \tag{3}$$

L'analyse de l'équation (3) montre l'existence d'une *famille* de profils asymptotiques paramétrée par K. De façon plus précise il est prouvé que :

- Pour $K < K_{LS} = \frac{3}{2^{2/3}}$ aucune solution stationnaire M_K n'est admissible.
- Pour $K = K_{LS}$ on obtient la solution stationnaire M_K prédite par Lifshitz et Slyozov

$$M_{K_{LS}}(y) = \begin{cases} \dfrac{\exp\Big(-\dfrac{(2y)^{1/3}}{1-(2y)^{1/3}} \Big)}{\Big(1-(2y)^{1/3}\Big)^{11/3} \Big(1+1/2(2y)^{1/3}\Big)^{7/3}}, & 0 \le y < y_0 = 1/2, \\ \\ 0, & y \ge y_0. \end{cases}$$

- Pour $K > K_{LS}$ on obtient comme profil admissible

$$M_K(y) = \begin{cases} \Big(y_0\ y_-\ y_+\Big)^{1/3} \dfrac{\Big(1-(y/y_0)^{1/3}\Big)^{p-1}}{\Big(1-(y/y_-)^{1/3}\Big)^{1-q} \Big(1-(y/y_+)^{1/3}\Big)^{1-r}}, & 0 \le y \le y_0 = 1/2, \\ \\ 0, & y > y_0, \end{cases}$$

avec les paramètres $p \ge 0$, q, r dépendants de K (voir [35]) ; en particulier on a $K = \dfrac{3(p+1)}{(2p+1)^{2/3} p^{1/3}}$.

On trace sur la figure 2 les différents profils correspondant à K_{LS} ($p = \infty$), $K = 9 \times 7^{-2/3} \times 2^{-1/3}$ (p=2) et $K = 6 \times 5^{-2/3}$ ($p = 1$). Le profil de $M_{K_{LS}}$ est très régulier tandis que plus K est petit,

moins le profil M_K est régulier.

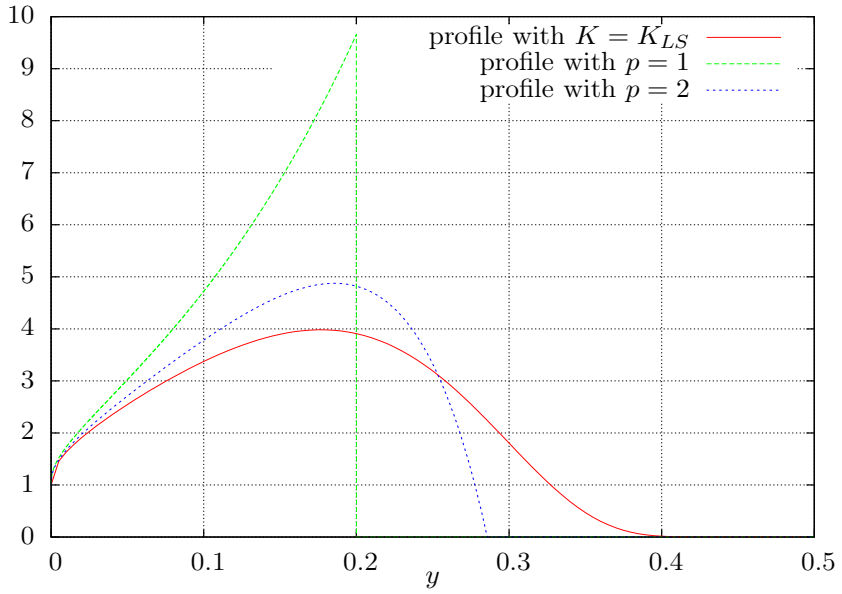

Figure 2 – Plusieurs profils asymptotiques M_K admissibles.

On remarque sur la Figure 2 que pour $p = 1$ la solution stationnaire M_K présente un front raide, comme une fonction indicatrice. Ainsi en partant des conditions initiales suivantes

$$g(x) = \begin{cases} 0.1, & x \in [10, 30] \\ 0, & \text{sinon} \end{cases} \quad ; \quad d^0 = d(\tau = 0) = 1 \quad \rho = 41, \tag{4}$$

les simulations numériques réalisées dans [35] à l'aide d'un schéma WENO d'ordre 5 ont montré que la solution se comportait pour de «grands» τ comme le profil M_K correspondant à $p = 1$. Toutefois, plus on augmente le temps de simulation, plus il est difficile de préserver le front de la solution : la diffusion numérique lisse le profil. La figure 3 présente au temps $\tau = 20$ (c'est-à-dire $t = e^{20}$ en variables originales), le résultat d'une simulation avec le schéma WENO du système de Lifshitz-Slyozov en variables (τ, y) avec la donnée (4) sur une longueur de domaine $[0, 40]$ avec 1000 points par unité de longueur.
Pour de tels temps de simulation, l'effet de la diffusion numérique, en dépit des qualités du schéma WENO, n'est pas négligeable et éloigne la solution du profil attendu. On peut en effet comparer le profil obtenu à celui correspondant à une donnée régulière, comme dans la figure 4. Ces résultats illustrent à la fois la difficulté d'ordre numérique pour préserver en temps long le profil asymptotique correct, mais aussi combien les notions de stabilité à introduire pour analyser ces phénomènes sont délicates.

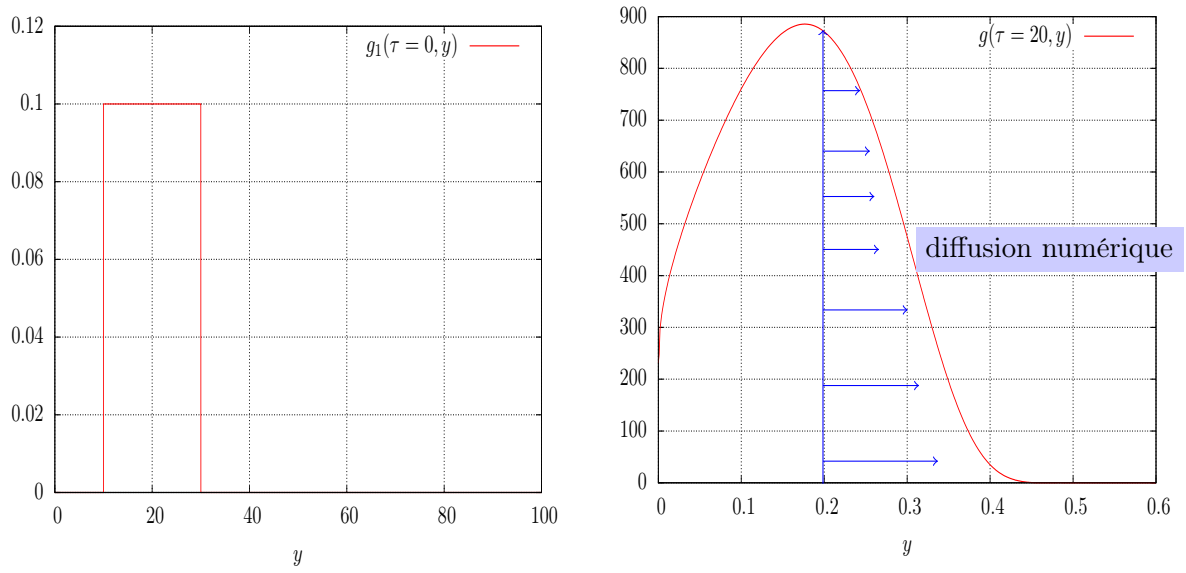

Figure 3 – Effet de la diffusion numérique sur le profil asymptotique en variables auto–similaires avec le schéma WENO 5.

Contribution

L'étude du comportement asymptotique en temps long du sytème de Lifshitz–Slyozov se révèle donc être un cas-test redoutable pour les schémas numériques développés pour les lois de conservation, en dépit de la simplicité apparente du problème. Au chapitre 1, nous proposons un nouveau schéma de type volumes finis pour simuler les équations de Lifshitz–Slyozov. Ce schéma repose sur une stratégie anti-dissipative basée sur une technique de «décentrage aval avec contrainte amont», dans l'esprit des méthodes introduites par B. Després et F. Lagoutière [57]. Il s'avère très performant pour capturer les profils asymptotiques corrects de Lifshitz–Slyozov, permettant d'atteindre des temps de simulation bien plus élevés qu'avec WENO (et à temps de simulation égal, pour un coût moindre). En fait, le schéma s'applique à toute équation de transport de la forme :

$$\partial_t f(t,x) + \partial_x(V(t,x)f(t,x)) = 0, \quad t \geq 0, x \geq 0$$

où $V(t,x)$ représente le champ de vitesse.
On considère un maillage régulier de pas d'espace $\Delta x > 0$: $[x_{k-1/2}, x_{k+1/2}]$, $k \in \mathbb{N}$ avec $x_{-1/2} = 0$, $x_{k+1/2} = (k+1)\Delta x$. On pose $\Delta t^{(n)}$ le pas de temps à la $n$ième itération, contraint par une condition de stabilité de type *Courant-Friedrichs-Lewy (CFL)*. L'inconnue numérique f_k^n s'interprète comme une approximation de $\frac{1}{\Delta x}\int_{x_{k-1/2}}^{x_{k+1/2}} f(n\Delta t, z)\,\mathrm{d}z$. On définit le schéma par la relation

$$f_k^{n+1} = f_k^n - \frac{\Delta t}{\Delta x}\left(f_{k+1/2}^n V_{k+1/2}^n - f_{k-1/2}^n V_{k-1/2}^n\right)$$

où le point clef réside dans la définition du flux numérique $f_{k\pm1/2}^n$ permettant d'avoir le caractère anti-dissipatif grâce à des contraintes de stabilité et de consistance sur les paramètres numériques. On impose que ce flux numérique vérifie

$$\begin{cases} \min(f_k^n, f_{k+1}^n) \leq f_{k+1/2}^n \leq \max(f_k^n, f_{k+1}^n) & \text{contrainte de consistance,} \\ b_{k+1/2}^n \leq f_{k+1/2}^n \leq B_{k+1/2}^n & \text{contrainte de stabilité,} \end{cases} \tag{5}$$

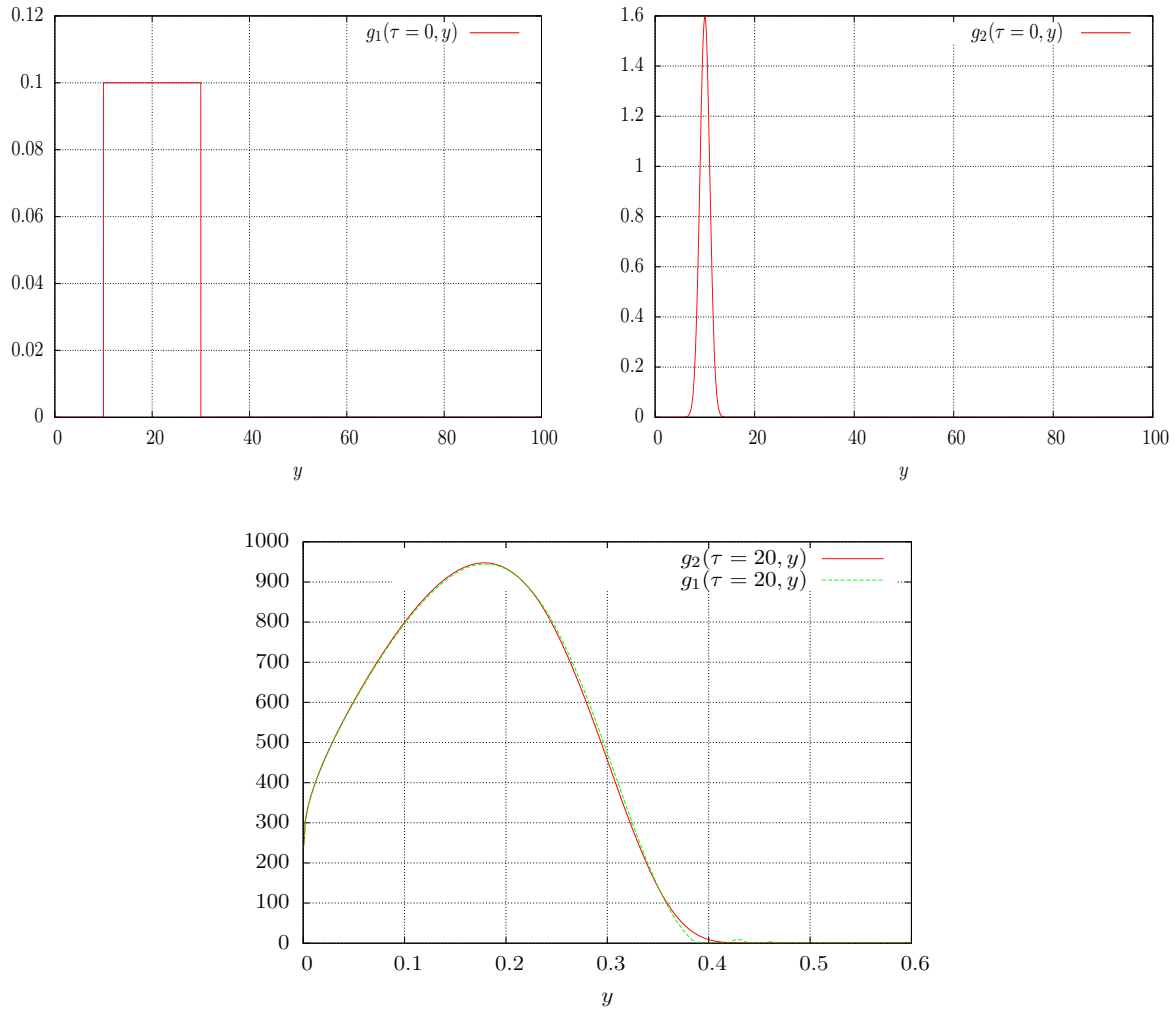

Figure 4 – Effet régularisant de la diffusion numérique due au schéma WENO sur le profil asymptotique en variables auto–similaires.

avec

$$b^n_{k+1/2} = \frac{1}{\nu^n V^n_k}\big(f^n_k - \max(f^n_k, f^n_{k-1})\big) + \max(f^n_k, f^n_{k-1}),$$

$$B^n_{k+1/2} = \frac{1}{\nu^n V^n_k}\big(f^n_k - \min(f^n_k, f^n_{k-1})\big) + \min(f^n_k, f^n_{k-1}),$$

où $\nu^n = \frac{\Delta t^{(n)}}{\Delta x}$ tand que $V^n_k \neq 0$.
On établit que ce schéma est TVD (Variation Totale Décroissante), qu'il vérifie un principe du maximum, qu'il est stable et consistant. On désigne ce schéma par ADM (Anti-Dissipative Method). Pour le modèle de Lifshitz-Slyozov, la figure 5 montre les solutions obtenues au temps $t = 2000$ en variables originales pour des données de type créneau ou régulière.
La figure 6 donne le résultat d'une simulation avec le schéma ADM en variables auto–similaires (τ, y), sous les mêmes conditions que celles de la figure 4, pour une fonction initiale en créneau. On observe cette fois que le profil raide est bien préservé.

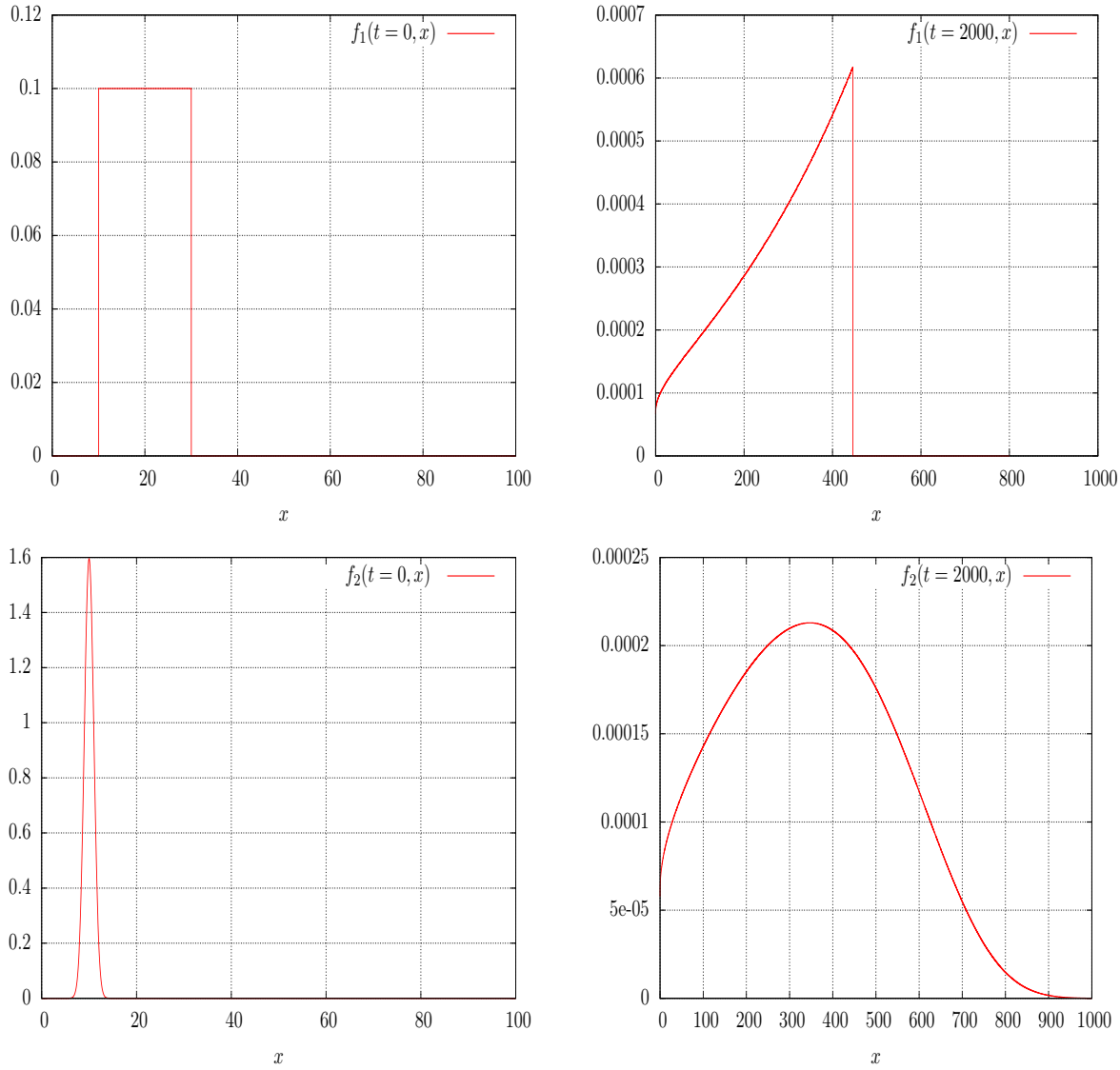

Figure 5 – Reconstruction numérique avec ADM du profil asymptotique suivant deux données initiales différentes en variables originales.

L'article original de Lifshitz et Slyozov suggère de modifier l'équation originale en y incorporant un terme de coagulation. En effet, puisque la dynamique forme des agrégats de taille de plus en plus grande, pour des temps longs on ne peut plus négliger les interactions directes entre macro-particules qui conduisent à des phénomènes de coagulation, la rencontre d'agrégats de tailles respectives x et y produisant une nouvelle particule de taille $x + y$. Ces collisions

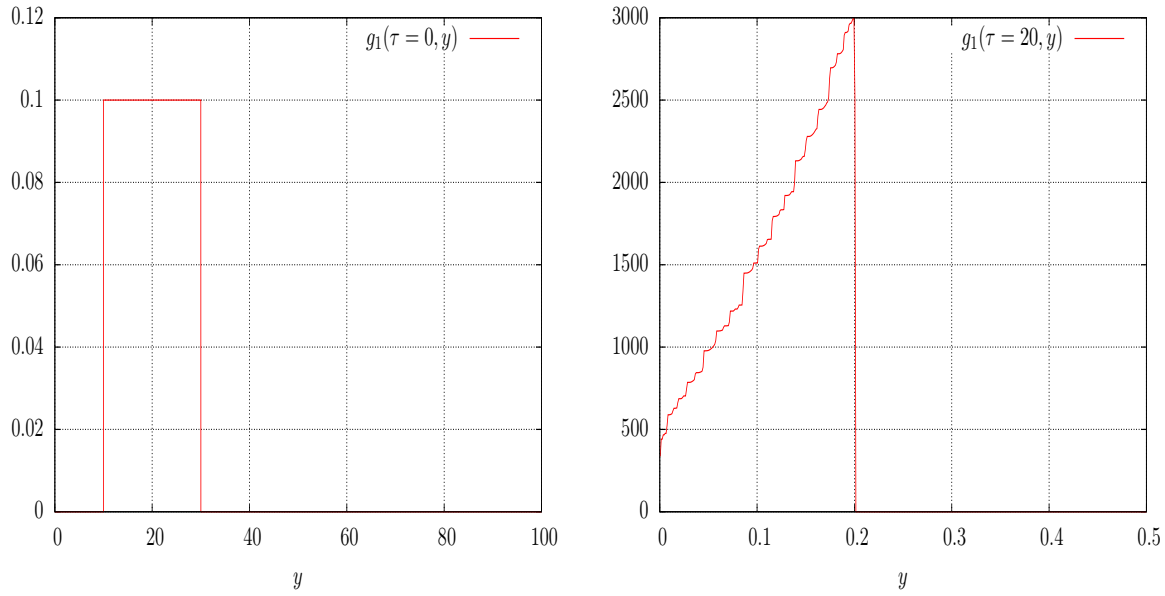

Figure 6 – Reconstruction numérique avec ADM de l'advection d'une donnée initiale de type créneau en variables auto–semblables.

apparaissent dans le modèle à travers l'opérateur de coagulation de Smoluchowski comme suit :

$$\begin{cases} \partial_t f(t,x) + \partial_x(V(t,x)f(t,x)) = \lambda Q_{coag}(f)(t,x), \quad t \in [0,\infty[,\ x \in [0,\infty[, \\ V(t,x) = a(x)c(t) - b(x); \quad \lambda > 0, \\ Q_{coag}(f)(t,x) = \dfrac{1}{2}\displaystyle\int_0^x f(t,x-y)f(t,y)\,\mathrm{d}y - \int_0^\infty f(t,x)f(t,y)\,\mathrm{d}y = Q^+_{coag}(f) - Q^-_{coag}(f), \\ c(t) + \displaystyle\int_0^\infty x f(t,x)\,\mathrm{d}x = \rho. \end{cases} \tag{6}$$

Le terme $Q^+_{coag}(f)$ représente le gain en particules de taille x résultant de la coagulation des particules de tailles $0 \leq y \leq x$ et $x - y$ tandis que le terme $Q^-_{coag}(f)$ représente la perte en particules de tailles x lorsque cette dernière entre en collision avec une autre particule de taille $y \geq 0$. L'opérateur de coagulation Q_{coag} satisfait d'une part à la propriété de conservation de la masse

$$\int_{\mathbb{R}_+} x\, Q_{coag}(f)(t,x)\,\mathrm{d}x = 0$$

et d'autre part à la propriété de diminution du nombre total de particules

$$\int_{\mathbb{R}_+} Q_{coag}(f)(t,x)\,\mathrm{d}x \leq 0.$$

Les arguments développés par Lifshitz et Slyozov indiquent que ces processus de coagulation pourraient jouer un rôle dans la sélection des profils asymptotiques. L'analyse mathématique de ce modèle «corrigé» est encore balbutiante, un premier pas étant du à M. Herrmann, B. Niethammer et J. Velázquez [104]. Le chapitre 1 se donne pour objectif d'étudier numériquement

l'influence de ce terme de collisions sur le comportement asymptotique des solutions du système de Lifshitz–Slyozov. La simulation numérique de ce modèle (6) de Lifshitz-Slyozov avec coagulation repose sur l'équation de transport

$$\partial_t f + \partial_x(V(t,x)f) = \lambda Q_{coag}(f)$$

que l'on décompose en deux parties «schéma de splitting». En premier, on résout l'équation de transport

$$\partial_t f + \partial_x(V(t,x)f) = 0$$

avec le schéma ADM, ce qui permet d'obtenir l'approximation

$$f_k^{n+1/2} = f_k^n - \frac{\Delta t}{\Delta x}\big((Vf)_{k+1/2}^n - (Vf)_{k-1/2}^n\big).$$

En second, on résout l'équation

$$\partial_t f = \lambda Q_{coag}(f). \tag{7}$$

À cette fin, on propose deux approches. Une première approche dite «naïve » consiste à réécrire l'équation (7) sous la forme

$$\partial_t f + \lambda L(f) \times f = \lambda Q_{coag}^+(f), \quad Q_{coag}^-(f) = f \times L(f), \quad L(f) = \int_0^\infty f(t,y)\,\mathrm{d}y.$$

Ainsi en adoptant un point de vue semi-implicite on écrit l'équation précédente comme suit

$$\frac{d}{\mathrm{d}t}\Big[f\exp(\lambda L\,t)\Big] = \exp(\lambda L\,t)\lambda Q_{coag}^+(f).$$

On intègre sur l'intervalle d'un pas de temps en supposant que $Q_{coag}^+(f)$ et $L(f)$ restent constants, ce qui conduit à l'approximation

$$f_k^{n+1} = \exp(-l_k^{n+1/2}\Delta t) f_k^{n+1/2} + q_k^{n+1/2}\left(\frac{1-\exp(-l_k^{n+1/2}\Delta t)}{l_k^{n+1/2}}\right)$$

où $q_k^{n+1/2}$ et $l_k^{n+1/2}$ sont respectivement les approximations discrètes des quantités $\lambda Q_{coag}^+(f_k^{n+1/2})$ et $\lambda L(f_k^{n+1/2})$. L'avantage de cette approche est qu'elle préserve naturellement la positivité des solutions. Cependant cette méthode s'avère coûteuse en temps CPU.
Une deuxième approche s'inspire de la méthode introduite par F. Filbet et P. Laurençot [82] évoquée plus haut. L'idée de cette méthode est d'écrire l'opérateur $Q_{coag}(f)$ comme la dérivée d'un certain flux J, ce qui permet de façon naturelle d'utiliser la méthode des volumes finis. Pour ce faire, l'équation (7) est réécrite comme suit

$$x\partial_t f = \lambda x\, Q_{coag}(f) = -\lambda\partial_x J(f)$$

avec

$$J(f)(t,x) = \int_0^x \int_{x-u}^\infty u f(t,u) f(t,v)\,\mathrm{d}v\,\mathrm{d}u.$$

L'approximation du flux J nécessite d'introduire un paramètre $0 < R < \infty$ de troncature pour évaluer l'intégrale du domaine infini. Ici, on privilégie l'approche «conservative»où l'expression de $J(f)$ est remplacée par

$$J_{cons}^R(f)(t,x) = \int_0^x \int_{x-u}^{R-u} u f(t,u) f(t,v)\,\mathrm{d}v\,\mathrm{d}u$$

pour $0 < x < R < \infty$. On remarque que $J^R_{cons}(f)(t,R) = J^R_{cons}(f)(t,0) = 0$ et par conséquent la solution f_R de l'équation

$$x\partial_t f_R = -\lambda \partial_x J^R_{cons}(f_R), \quad t \geq 0,\ 0 \leq x \leq R < \infty$$

conserve le moment d'ordre 1 :

$$\int_0^R x\, f_R(t,x)\,\mathrm{d}x = \int_0^R x f_R(0,x)\,\mathrm{d}x.$$

En effectuant le changement de variable $w = u + v$ on obtient

$$J^R_{cons}(f)(t,x) = \int_0^x \int_x^R u f(t,u) f(t,w-u)\,\mathrm{d}w\,\mathrm{d}u.$$

On en déduit l'approximation

$$(k\Delta x)\, f_k^{n+1} = (k\Delta x)\, f^{n+1/2} - \lambda \frac{\Delta t}{\Delta x}(J^n_{k+1/2} - J^n_{k-1/2})$$

où $J^n_{k+1/2}$ est le flux numérique approchant $J^R_{cons}(f^n_k)$. Cette approche, couplée au schéma ADM pour traiter la partie convective de l'équation, s'avère très performante.

La conclusion majeure de ce chapitre 1 est que la prise en compte des phénomènes de collisions entre macro-particules régularise les différents profils asymptotiques observés pour le modèle de Lifshitz–Slyozov standard vers un profil quasi-universel. En guise d'exemple nous montrons à la figure 7 les simulations obtenues avec différentes données initiales sous l'effet des collisions avec approche conservative. On se place sur une longueur de domaine $[0, 2200]$ avec 20 mailles par unité de longueur ; on considère que la concentration initiale des monomères vaut $c^0 = 1$, que la masse totale initiale $\rho = 41$ et on a $\lambda = 1/100$. Enfin, les simulations semblent indiquer qu'en faisant tendre le paramètre de collisions λ vers 0, les solutions en temps longs ressemblent au profil régulier de Lifshitz- -Slyozov.

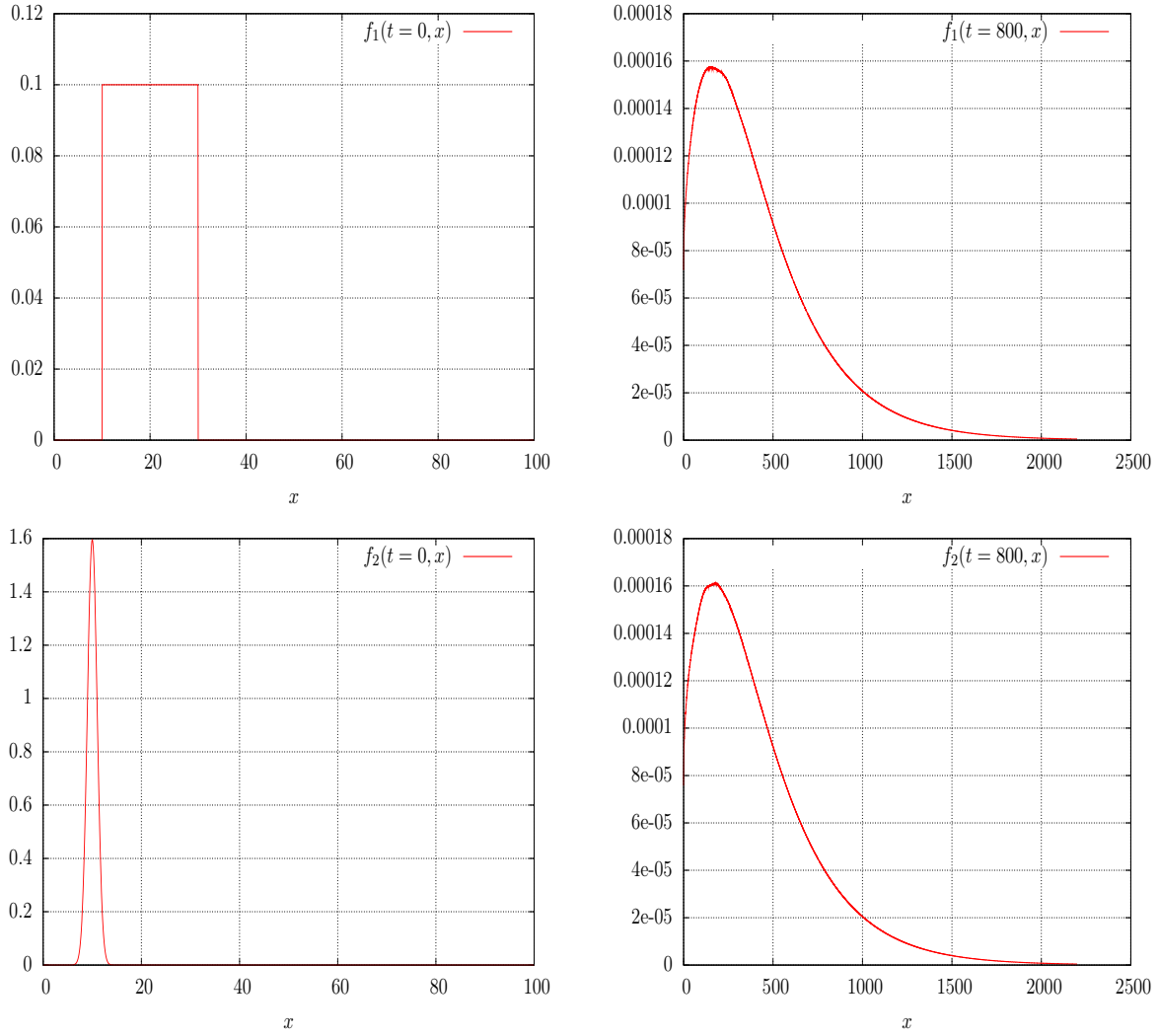

Figure 7 – Reconstruction du profil asymptotique avec le schéma ADM, plus approche conservative des collisions.

1.2 Équations de Lifshitz-Slyozov avec diffusion spatiale

Formalisme du couplage

Nous nous intéressons ensuite à une autre variante du modèle de Lifshitz–Slyozov, dans laquelle les monomères sont aussi soumis à une dynamique de diffusion spatiale. En notant maintenant $\xi \geq 0$ la variable de taille et $x \in \Omega \subset \mathbb{R}^N$ la variable d'espace, on est conduit au système suivant, qui couple des EDP de types hyperbolique et parabolique,

$$\begin{cases} \partial_t f(t,x,\xi) + \partial_\xi \Big((a(\xi)c(t,x) - b(\xi)) f(t,x,\xi) \Big) = 0, \quad t \geq 0,\ x \in \Omega,\ \xi \geq 0, \\ \partial_t \Big(c(t,x) + \displaystyle\int_0^\infty \xi f(t,x,\xi)\, \mathrm{d}\xi \Big) - \Delta_x c(t,x) = 0, \qquad t \geq 0,\ x \in \Omega. \end{cases} \tag{8}$$

Le chapitre 2 analyse ce système d'équations et en établit le caractère bien posé, pour une large classe de coefficients et de données initiales, physiquement pertinente. Nous présentons brièvement un schéma numérique pour simuler le comportement des solutions. Cependant il convient de noter que, si la densité f obéit toujours à une simple équation de transport, les coefficients de celle-ci sont maintenant paramétrés par la variable d'espace. Ceci rend les calculs rapidement lourds, tant en encombrement mémoire qu'en temps de calcul.

Contribution

Pour ce couplage hyperbolique-parabolique (8) nous avons considéré la condition aux bords de type Neumann homogène suivante

$$\partial_\nu c = \nabla c \cdot \nu = 0, \qquad \text{on } \partial\Omega$$

et les conditions initiales suivantes

$$c(0,x) = c_{init}(x) \geq 0, \qquad f(t,x,\xi) = f_{init}(x,\xi) \geq 0.$$

Nous avons adapté les différents résultats obtenus au cas où les conditions aux bords sont de type Dirichlet et aussi au cas où l'espace est $\mathbb{R}^N$ tout entier.
L'interprétation physique des mécanismes de transfert de masse conduisent aux hypothèses assez naturelles suivantes :

$$c_{init} \in L^\infty(\Omega), \qquad f_{init} \in L^\infty(\Omega; L^1(]0,\infty[, (1+\xi)\,\mathrm{d}\xi)).$$

Les coefficients cinétiques a et b vérifient

- $b = 1$,
- a est une fonction croissante avec $a(0) = 0$ et $a(+\infty) = +\infty$,
- $a \in \mathcal{C}^0\big([0,\infty[\big) \cap \mathcal{C}^1\big(]0,\infty[\big)$ et pour tout $\xi_0 > 0$, il existe $L_{a,0} > 0$ tel que $0 \leq a'(\xi) \leq L_{a,0}$ pour tout $\xi \geq \xi_0$.

Le résultat principal s'énonce sous la forme suivante.

Théorème .3 (Tine, Goudon, Lagoutière)**.** *Sous les hypothèses précédentes sur les données initiales et les coefficients cinétiques, il existe une unique solution faible (c,f) du système* (8) *telle que*

$$\forall\, 0 < T < \infty,\ c \in L^\infty\big(]0,T[\times\Omega\big) \cap L^2\big(]0,T[; H^1(\Omega)\big), \quad f \in L^\infty\big(]0,T[\times\Omega; L^1\big(]0,\infty[, (1+\xi)\,\mathrm{d}\xi\big)\big);$$

$$c \in \mathcal{C}^0\big([0,T]; L^2(\Omega) - \textit{faible}\big), \quad f \in \mathcal{C}^0\big([0,T]; L^1\big(\Omega\times]0,\infty[\big) - \textit{faible}\big).$$

De plus la solution du système couplé vérifie l'équation de conservation de masse totale suivante

$$\frac{d}{\mathrm{d}t}\left[\int_\Omega \int_0^\infty \xi f(t,x,\xi)\,\mathrm{d}\xi\,\mathrm{d}x + \int_\Omega c(t,x)\,\mathrm{d}x\right] = 0.$$

2 Modélisation en dynamique de population structurée en taille

La structuration d'une population d'individus (cellules) se fait en biologie à l'aide d'un marqueur x positif représentant soit leur taille, leur masse, leur volume, leur âge soit le contenu en nutriments ou parasites de chaque individu. Comprendre l'évolution d'une population d'individus structurée en x est un enjeu de taille d'une part dans l'étude des mécanismes de divisions cellulaires ou de polymérisations et d'autre part dans l'étude de la prolifération de certaines protéines telles les prions (**Pr**oteinaceous **i**nfectious **on**ly), responsables des Encélophalopathies Spongiformes Transmissibles (EST) qui sont des maladies neurodégénératives mortelles et infectieuses. Parmi ces maladies, on peut citer l'Encélophalopathie Spongiforme Bovine (ESB), cause de la crise de la «vache folle» chez l'animal dans les années 1990. On mentionne également le KURU apparu au cours du 20^e siècle chez l'homme et qui a ravagé presque toute une tribu en Papouasie-Nouvelle-Guinée, et aussi la maladie de Kreuzfeld-Jacob transmise par injection d'hormones de croissance et par transfusion sanguine. Face aux limites des expérimentations biologiques pour une compréhension complète de tous ces mécanismes, plusieurs modèles mathématiques ont été élaborés à des fins de prédiction. Deux types de descriptions ont été privilégiés : des modèles de populations structurées en âge connus sous le nom de modèles de MacKendrick-Von Foerster [7, 129, 174, 60] et des modèles de populations structurées en taille [60, 157, 137, 134]. Dans cette partie de thèse, on s'intéresse à l'évolution d'une population d'individus (cellules) structurée en taille $x > 0$ et on traite d'une part un problème inverse pour un modèle général d'agrégation-fragmentation et d'autre part on aborde un modèle spécifique de polymérisation avec coalescence pour le prion.

2.1 Problème inverse pour un modèle général d'agrégation-fragmentation

Plusieurs modèles mathématiques pour la modélisation des mécanismes de croissance et de division cellulaire existent [60, 59, 137, 135, 138, 157, 39, 8, 101, 100, 84, 161]. Plus particulièrement, pour les mécanismes de polymérisation nucléée, le modèle le plus utilisé aujourd'hui est celui de M. Masel [106] qui est constitué d'un nombre infini d'Équations Différentielles Ordinaires (EDO). Une version continue de ce modèle est due à J. Greer et *al.* [95]. En notant $n(t,x)$ la densité de répartition à l'instant t des cellules de taille x, on va s'intéresser au modèle suivant

$$\begin{cases} \partial_t n(t,x) + c\partial_x(g(x)n(t,x)) + B(x)n(t,x) = 2\displaystyle\int_0^\infty B(y)\kappa(x,y)n(t,y)\,\mathrm{d}y, \quad t>0,\ x>0, \\ \\ n(t=0,x) = n^0(x), \quad x \geq 0, \\ \\ g(x=0)n(t,x=0) = 0; \quad t \geq 0, \quad c>0. \end{cases} \tag{9}$$

Le paramètre $g(x)$ représente la vitesse de croissance des cellules de taille x par absorption de nutriments, par exemple avec un taux c. La fonction $B(x)$ représente le taux de division d'une cellule de taille x et κ le taux de formation d'une cellule de taille x à partir de la division d'une cellule de taille $y > x$.
L'étude du comportement asymptotique en temps d'un tel modèle d'agrégation-fragmentation joue un rôle majeur pour les applications, notamment par son caractère prédictif sur l'évolution de la population considérée. Les travaux menés sur ce sujet (voir par exemple [157, 135, 116, 63, 62]) conduisent à l'existence d'éléments propres principaux (λ_0, N, ϕ) solutions de l'équation

stationnaire

$$\begin{cases} c\partial_x(g(x)N(x)) + (B(x)+\lambda_0)N(x) = 2\displaystyle\int_0^\infty B(y)\kappa(x,y)N(y)\,\mathrm{d}y \quad x>0, \\ gN(x=0)=0; \quad N(x)\geq 0; \quad \displaystyle\int_0^\infty N(x)\,\mathrm{d}x = 1, \quad \lambda_0>0, \\ cg(x)\partial_x\phi(x) - (B(x)+\lambda_0)\phi(x) = -2B(x)\displaystyle\int_0^x \kappa(y,x)\phi(y)\,\mathrm{d}y, \\ \phi(x)\geq 0; \quad \displaystyle\int_0^\infty \phi(x)N(x)\,\mathrm{d}x = 1. \end{cases}$$

Ces éléments propres dirigent le comportement en temps long puisqu'on a

$$\int_0^\infty |n(t,x)\exp(-\lambda_0 t) - \rho_0 N(x)|\phi(x)\,\mathrm{d}x \xrightarrow{t\to\infty} 0$$

où $\rho_0 = \int_0^\infty n^0(x)\phi(x)\,\mathrm{d}x$.

Contribution

Les résultats théoriques sur le comportement asymptotique de la densité de répartition en taille de la population peuvent être confrontés à l'expérience. Par exemple la technologie du flux cytométrique permet de mesurer à chaque instant donné le nombre d'individus (cellules) de la population considérée. Cependant il n'existe aucune technique biologique permettant de mesurer le taux de division cellulaire $B(x)$ alors que le contrôle de cette quantité serait d'une importance cruciale dans l'étude de la prolifération de certaines protéines telles le prion. Ainsi, connaissant la densité de répartition N de la population et le coefficient malthusien λ_0, on étudie au chapitre 3, le problème inverse associé

$$2\int_0^\infty B(y)\kappa(x,y)N(y)\,\mathrm{d}y - B(x)N(x) = c\partial_x(g(x)N(x)) + \lambda_0 N(x). \tag{10}$$

dont l'inconnue est maintenant la fonction B. On cherche à reconstruire, à partir de données mesurées N_ε de N, le taux de division cellulaire B_ε, le paramètre ε évaluant l'erreur commise par les mesures sous une norme appropriée sur les données N.

Toutefois, B. Perthame et J. Zubelli ont montré dans [158], pour un cas particulier du modèle, que le problème inverse (10) est mal posé. Une des obstructions est qu'on a aucun moyen pour mesurer $\partial_x(g(x)N_\varepsilon(x))$ et donc reconstruire B_ε. On introduit donc des régularisations de l'équation (10) afin de définir un taux approchant le vrai taux de division cellulaire. À cette fin, on propose deux méthodes de régularisation. La première méthode, nommée quasi-réversible, consiste à chercher, sous certaines conditions, une solution $H_{\varepsilon,\alpha} = B_{\alpha,\varepsilon}N_\varepsilon$ du problème approché suivant

$$\begin{cases} \alpha x^{-k}\partial_x(x^{k+1}H_{\varepsilon,\alpha}(x)) + H_{\varepsilon,\alpha}(x) - 2\displaystyle\int_0^\infty \kappa(x,y)H_{\varepsilon,\alpha}(y)\,\mathrm{d}y = -c_{\alpha,\epsilon}\partial_x(g(x)N_\varepsilon(x)) - \lambda_\varepsilon N_\varepsilon(x), \\ H_{\varepsilon,\alpha}(0)=0; \quad 0<\alpha<1, \quad k\in\mathbb{R}_+, \end{cases} \tag{11}$$

où le paramètre de régularisation α est destiné à tendre vers 0.
Une deuxième méthode exploite une régularisation par filtrage : ceci consiste à chercher, sous certaines conditions, une solution $H_{\varepsilon,\alpha} = B_{\alpha,\varepsilon}N_\varepsilon$ du problème approché suivant

$$\begin{cases} H_{\varepsilon,\alpha}(x) - 2\displaystyle\int_0^\infty \kappa(x,y)H_{\varepsilon,\alpha}(y)\,\mathrm{d}y = \rho_\alpha * \Big(-c_{\alpha,\epsilon}\partial_x(g(x)N_\varepsilon(x)) - \lambda_\varepsilon N_\varepsilon(x)\Big), \\ H_{\varepsilon,\alpha}(0) = 0, \end{cases} \tag{12}$$

où ρ_α est une suite régularisante définie par

$$\rho_\alpha(x) = \frac{1}{\alpha}\rho(\frac{x}{\alpha}), \quad \rho \in \mathcal{C}_0^\infty(\mathbb{R}), \quad \int_0^\infty \rho(x)\,\mathrm{d}x = 1, \quad \rho \geq 0, \quad \mathrm{Supp}(\rho) \subset [0,1], \quad \alpha > 0.$$

L'énoncé principal sur ce sujet prend la forme suivante.

Théorème .4 (Doumic et Tine)**.** *Sous des hypothèses sur κ, g et B énoncées dans le chapitre 3, il existe une solution (en un sens faible) $H_{\varepsilon,\alpha} \in L^2(x^p,\,\mathrm{d}x)$, $p > 2$ du problème inverse* (11) *avec les estimations*

$$|c_{\varepsilon,\alpha} - c| \leq C(p,N)\varepsilon,$$
$$\|B_{\varepsilon,\alpha} - B\|_{L^2(x^p N_\varepsilon^2,\,\mathrm{d}x)} \leq C(p,N)(\alpha + \frac{\varepsilon}{\alpha})$$

où C dépend de p, λ_0, k, $\|BN\|_{H^1((1+x^{p+1}),\,\mathrm{d}x)}$, $\|gN\|_{L^1(\,\mathrm{d}x)}$, $\|N\|_{L^1((1+x+g(x))\,\mathrm{d}x)}$ et $\|N\|_{H^1((x^p+1),\,\mathrm{d}x)}$.

Par ailleurs, il existe une solution faible $H_{\varepsilon,\alpha} \in L^2(x^p,\,\mathrm{d}x)$, $p > 1$ du problème inverse (12) *avec les estimations*

$$|c_{\varepsilon,\alpha} - c| \leq C(p,\rho,N)(\alpha + \varepsilon),$$
$$\|B_{\varepsilon,\alpha} - B\|_{L^2(x^p N^2,\,\mathrm{d}x)} \leq C(p,\rho,N)(\alpha + \frac{\varepsilon}{\alpha})$$

où C une constante dépendant de p, des moments de ρ et $\partial_x\rho$, λ_0, $\|gN\|_{W^{1,1}(\,\mathrm{d}x)}$, $\|gN\|_{H^2(1+x^p,\,\mathrm{d}x)}$, $\|N\|_{H^1(1+x^p,\,\mathrm{d}x)}$ et $\|N\|_{L^1((1+x+g(x))\,\mathrm{d}x)}$.

Dans cette étude du problème inverse, on a aussi proposé des schémas pour la résolution numérique des problèmes (11) et (12) avec comme données d'entrée la solution stationnaire N obtenue en résolvant l'équation de croissance-fragmentation (9).

2.2 Modèle spécifique de polymérisation avec coalescence pour le prion

Dans le cas où la population d'individus considérée est une population de protéines prions, un mécanisme important à prendre en compte est d'une part la polymérisation ou agrégation entre deux protéines (polymères) et d'autre part la dépolymérisation qui correspond à la perte d'un monomère (protéine de taille négligeable) par détachement. En supposant l'absence de production et de dégradation de protéines, nous considérons pour cette partie dans le contexte *in vitro* un modèle prenant en compte ces mécanismes de polymérisation et de dépolymérisation. On note $V(t)$ la concentration des monomères et $u(t,x)$ la densité de répartition en taille des protéines et on obtient

$$\begin{cases} \dfrac{d}{dt}V(t) &= -\displaystyle\int_0^\infty \mathcal{T}\big(V(t),x\big)u(x,t)\,\mathrm{d}x, \\ \partial_t u(x,t) &= -\partial_x\big(\mathcal{T}\big(V(t),x\big)u(x,t)\big) + \mathcal{Q}(u)(x,t), \\ u(0,t) = 0, \quad u(x,0) = u_0(x) \geq 0 \quad \text{et} \quad V(0) = V_0 \geq 0. \end{cases} \tag{13}$$

Le terme de transport

$$\mathcal{T}\big(V(t),x\big) = V(t)k_{\rm on}(x) - k_{\rm off}(x)$$

fait apparaître une compétition entre le processus d'agrégation des monomères aux polymères avec un taux $k_{\rm on}(x) \geq 0$ et le processus de détachement des monomères des polymères avec un taux $k_{\rm off}(x)$. L'opérateur $\mathcal{Q}(u) = \mathcal{Q}_{\rm c}(u) - \mathcal{Q}_{\rm f}(u)$ représente l'opérateur de coagulation-fragmentation et s'exprime sous la forme

$$\mathcal{Q}_{\rm c}(u)(x) = \frac{1}{2}\int_0^x k_{\rm c}(y,x-y)\,u(y)u(x-y)\,dy - u(x)\int_0^\infty k_{\rm c}(x,y)\,u(y)\,dy,$$

et

$$\mathcal{Q}_{\rm f}(u)(x) = \frac{1}{2}u(x)\int_0^x k_{\rm f}(y,x-y)\,dy - \int_0^\infty k_{\rm f}(x,y)\,u(x+y)\,dy.$$

Deux polymères de tailles respectives x et y s'agrègent suivant le taux de coagulation $k_{\rm c}(x,y)$ pour fournir un polymère de taille $x+y$ et inversement suivant le taux de fragmentation $k_{\rm f}(y,x-y)$ un polymère de taille x se fragmente en deux polymères dont l'un de taille $y<x$ et l'autre de taille $x-y>0$.

L'absence de production et de dégradation de protéines induit la propriété de conservation de masse au cours du temps suivante

$$\frac{d}{dt}\left(V(t) + \int_0^\infty xu(t,x)\,{\rm d}x\right) = 0.$$

Au chapitre 4, on s'intéresse à la simulation numérique de cette équation de polymérisation avec coalescence. On développe un schéma d'ordre élevé avec un traitement spécial de l'opérateur de coagulation-fragmentation permettant au niveau discret de préserver la propriété de conservation de masse du modèle. En effet on écrit l'opérateur de coagulation–fragmentation sous une forme conservative introduite par P. Laurençot et F. Filbet [82] :

$$x\mathcal{Q}_{\rm c}(u)(x) = -\partial_x\mathcal{C}(u)(x) \qquad \text{et} \qquad x\mathcal{Q}_{\rm f}(u)(x) = -\partial_x\mathcal{F}(u)(x),$$

avec

$$\mathcal{C}(u)(x) := \int_0^x\int_{x-y}^\infty yk_{\rm c}(y,z)u(y)u(z)\,{\rm d}z\,{\rm d}y \qquad \text{et} \qquad \mathcal{F}(u)(x) := \int_0^x\int_{x-y}^\infty yk_{\rm f}(y,z)u(y+z)\,{\rm d}z\,{\rm d}y.$$

Ainsi l'équation de distribution en taille des protéines s'écrit

$$x\partial_t u(x,t) + \partial_x\Big(\mathcal{T}\big(V(t),x\big)xu(x,t) + \mathcal{C}(u)(t,x) + \mathcal{F}(u)(t,x)\Big) = \mathcal{T}\big(V(t),x\big)u(x,t).$$

La simulation de cette équation est faite par le schéma WENO d'ordre 5, qui est un schéma de type volumes finis très approprié pour le transport conservatif et avec la propriété d'être numériquement peu dissipatif. Ce schéma est utilisé pour évaluer les éléments propres caractérisant le comportement en temps long du système.

3 Interaction fluide/particules avec coagulation-fragmentation

3.1 Étude de stabilité et analyse asymptotique du modèle

Formalisme du couplage

La dispersion d'une densité de particules dans un fluide engendre des phénomènes d'interactions décrites d'une part par les équations d'Euler compressibles pour le fluide et d'autre part

par l'équation de Vlasov-Fokker-Planck pour le mouvement microscopique des particules. Le couplage de ces équations micro-macroscopiques se fait à travers la force de friction mutuelle entre fluide et particules. De plus les phases denses et disperses peuvent être soumises à des forces extérieures de type gravitationnel, centrifuge, électrique ou magnétique. Ce type de modèle de couplage fluide/particules a été présenté par R. Caflisch et G. Papanicolaou [28] et s'applique dans plusieurs domaines tels que l'étude de la formation des gouttelettes d'eau, le traitement des eaux usées, l'étude de processus de pollution [26, 172], la modélisation des moteurs Diesel [176, 175, 5] ou l'optimisation d'écoulements biomédicaux [13].
En posant $f(t,x,v)$ la densité d'un unique groupe de particules à l'instant t contenu dans un domaine infinitésimal centré en $(x,v) \in \mathbb{R}^3 \times \mathbb{R}^3$ et de volume $\mathrm{d}x\,\mathrm{d}v$ alors le modèle de couplage standard s'écrit comme suit [36, 37]

$$\begin{cases} \partial_t f + v\cdot\nabla_x f - \nabla_x\phi\cdot\nabla_v f = \dfrac{9\mu}{2a^2\rho_P}\nabla_v\cdot\left((v-u)f + \dfrac{k\theta}{\frac{4}{3}\pi a^3\rho_P}\nabla_v f\right), \\ \partial_t n + \nabla_x\cdot(n\,u) = 0, \\ \rho_F\partial_t(n\,u) + \rho_F Div_x(n\,u\otimes u) + \rho_F\alpha n\nabla_x\phi + \nabla_x p(n) = 6\pi\mu a\displaystyle\int_{\mathbb{R}^3}(v-u)f\,\mathrm{d}v - \mu_R\Delta_x u. \end{cases} \tag{14}$$

Le fluide est décrit par sa densité $n(t,x)$ et son champ de vitesse $u(t,x)$. La force de friction mutuelle entre fluide et particules est proportionnelle à la vitesse relative $u(t,x)-v$. De plus on suppose que les forces extérieures agissant sur le couplage sont d'intensité α et dérivent du potentiel ϕ indépendant du temps. Les paramètres $\rho_p > 0$ et $a > 0$ représentent respectivement la masse volumique et le rayon moyen des particules, tandis que $\rho_f > 0$ et μ représentent la masse volumique et la viscosité du fluide. En notant $\theta > 0$ la température du milieu environnant et par k la constante de Boltzmann alors l'agitation «Brownienne»des particules est prie en compte par le terme de diffusion en la variable v et le coefficient de diffusion s'obtient grâce à la formule d'Einstein [72]. Suivant le phénomène à observer, plusieurs variantes du modèle de couplage fluide-particules sont étudiées dans [87, 102, 98, 89, 88, 20] et les références qui y sont citées.

Dans notre étude, on traite au chapitre cinq une variante du modèle (14) en considérant non plus un unique groupe de particules mais plutôt une famille de groupes de particules dont chaque groupe est indexé par sa taille moyenne i. On s'intéresse donc aux densités de répartition $f_i(t,x,v)$ avec $i \in \mathbb{N}\setminus\{0\}$. D'autre part on prend en compte les phénomènes de collision entre particules à travers l'opérateur de coagulation-fragmentation. Ainsi la variante du modèle considérée s'écrit comme suit

$$\begin{cases} \partial_t f_i + v\cdot\nabla_x f_i - \nabla_x\phi\cdot\nabla_v f_i = \dfrac{9\mu}{2\rho_P a_i^2}\nabla_v\cdot\left((v-u)f_i + \dfrac{k\theta}{\frac{4}{3}\pi a_i^3\rho_P}\nabla_v f_i\right) + \dfrac{1}{\tau_c}Q_i(f), \\ \partial_t n + \nabla_x\cdot(n\,u) = 0, \\ \rho_F\partial_t(n\,u) + \rho_F Div_x(n\,u\otimes u) + \rho_F\alpha n\nabla_x\phi + \nabla_x p(n) = 6\pi\mu\displaystyle\sum_i\int_{\mathbb{R}^3}(v-u)f_i a_i\,\mathrm{d}v - \mu_R\Delta_x u, \end{cases}$$

où Q_i représente l'opérateur de coagulation-fragmentation de Smoluchowski avec τ_c le temps caractéristique correspondant.

$$Q_i(f) = \frac{1}{2}\sum_{j=1}^{i-1}\kappa_{j,i-j}f_j f_{i-j} - \sum_{j=1}^{\infty}\kappa_{i,j}f_i f_j + \sum_{j=i+1}^{\infty}\beta_{j-i,i}f_j - \frac{1}{2}\sum_{j=1}^{i-1}\beta_{j,i-j}f_i$$

avec d'une part $\kappa_{i,j}$ le taux de coagulation lorsque qu'une particule de taille i rencontre une autre de taille j pour donner naissance à une particule de taille $i+j$ et d'autre part $\beta_{i,j}$ le taux de fragmentation lorsqu'une particule de taille $i+j$ se fragmente en une de taille i et en une autre de taille j.
La prise en compte des phénomènes de coagulation et fragmentation réduit le nombre total de particules tout en conservant la masse totale ce qui se traduit par les hypothèses suivantes :

$$\sum_{i=1}^{\infty} Q_i(f) \leq 0, \qquad \sum_{i=1}^{\infty} iQ_i(f) = 0.$$

Contribution

Pour ce modèle d'interaction fluide-particules avec coagulation-fragmentation on dérive par des techniques de dimensionnalisation des propriétés de dissipation d'entropie conduisant d'une part à l'existence de solutions d'équilibre stable et d'autre part à des estimations nécessaires pour l'analyse du coupage.

La dissipation d'entropie liée à la coagulation-fragmentation est basée sur la fonctionnelle

$$\mathscr{L}(f) = \sum_{i=1}^{\infty} f_i\Big(\ln\Big(\frac{f_i}{\mathscr{M}_i}\Big) - 1\Big), \tag{15}$$

avec la suite $\{\mathscr{M}_1, \mathscr{M}_2, ...\}$ satisfaisant l'équation $Q_i(\mathscr{M}) = 0$ ce qui équivaut à résoudre

$$\kappa_{i,j}\mathscr{M}_i\mathscr{M}_j = \beta_{i,j}\mathscr{M}_{i+j} \qquad \text{for any } i,j \geq 1. \tag{16}$$

une solution de l'équation (16) si elle existe, est connue sous le nom «detailed balance equilibrium». La fonctionnelle $\mathscr{L}(f)$ joue le rôle d'une fonction de Lyapounov pour une équation de coagulation-fragmentation pure. Ainsi la dissipation d'entropie liée à la coagulation-fragmentation s'écrit sous la forme

$$\sum_{i=1}^{\infty} Q_i(f) \ln\Big(\frac{f_i}{\mathscr{M}_i}\Big) \leq 0,$$

et elle s'annule si et seulement si $f_i = \mathscr{M}_i$.

Concernant la dissipation d'entropie lié à l'interaction fluide-particules, on considère la fonction d'énergie totale du couplage $\mathcal{F}(f,n,u)$ comme somme des énergies libres associées respectivement aux particules et au fluide. Ainsi grâce à des hypothèses sur la pression du fluide et sur le ratio de densité ρ_P/ρ_F on prouve la relation de dissipation d'entropie générale suivante :

$$\begin{aligned}\frac{\mathrm{d}}{\mathrm{d}t}\mathcal{F}(f,n,u) + \mu\int_\Omega |\nabla_x u|^2\,\mathrm{d}x + \frac{1}{\varepsilon}\sum_{i=1}^{\infty}\int_\Omega\int_{\mathbb{R}^3}\Big|(v-\frac{1}{\beta}u)\sqrt{i^{1/3}f_i} + \frac{1}{i^{5/6}}\frac{\nabla_v f_i}{\sqrt{f_i}}\Big|^2\,\mathrm{d}v\,\mathrm{d}x \\ = \frac{1}{\tau_c}\sum_{i=1}^{\infty}\int_\Omega\int_{\mathbb{R}^3} Q_i(f)\ln\Big(\frac{f_i}{\mathscr{M}_i}\Big)\,\mathrm{d}v\,\mathrm{d}x \leq 0,\end{aligned} \tag{17}$$

avec le paramètre ε mesurant le rapport du temps de Stockes τ_1 par rapport au temps d'observation T et β mesurant la fluctuation de la vitesse par unité de vitesse d'observation.

En s'intéressant aux régimes hydrodynamiques lorsque $0 < \varepsilon \ll 1$, on devine à l'aide de la relation (17) que le comportement de la densité des particules prend la forme

$$f_i(t,x,v) \simeq \frac{\rho_i(t,x)}{(2\pi/i)^{3/2}} \exp\Big(- i\frac{|v-u(t,x)/\beta|^2}{2}\Big) \quad \text{lorsque } \varepsilon \to 0,$$

et dépend de la concentration macroscopique $\rho_i(t,x) = \displaystyle\int_{\mathbb{R}^3} f_i(t,x,v)\,\mathrm{d}v$, de la vitesse $u(t,x)$ et de la densité $n(t,x)$ du fluide.
Suivant la variation du paramètre ε on définie deux régimes qu'on appelle communément «flowing regime» et «bubbling regime» dont on montre les différents modèles caractérisant l'évolution des particules sous l'effet de l'écoulement du fluide et des forces extérieures.

Chapitre 1

Simulation des équations de Lifschitz-Slyozov avec coagulation

Ce chapitre est consacré à l'analyse numérique des équations de Lifshitz-Slyozov [124] modélisant la formation de grains par précipitation dans une solution solide super-saturée. Le comportement asymptotique en temps de la densité de répartition des grains est très intrigant de par sa dépendance ou non soit à la répartition initiale ou à la prise en compte des effets de collision entre grains. Suivant des notions de stabilité assez rigoureuses, nous proposons un nouveau schéma numérique de type volumes finis permettant de capturer grâce à sa propriété anti-dissipative, les différents profils asymptotiques possibles. On met aussi en évidence, en s'inspirant des travaux de F. Filbet et P. Laurençot [82], le rôle des collisions dans le processus de sélection du profil asymptotique quasi-universel.

Ce travail a été réalisé en collaboration avec Thierry Goudon et Frédéric Lagoutière et a été soumis pour publication sous le titre *Simulations of the Lifshitz-Slyozov equations : the role of the coagulation terms in the asymptotic behavior* [92].

1.1 Introduction

The Lifshitz-Slyozov system models the formation of grains in supersaturated solid solutions. The dynamics can be thought of as an interaction between macroparticles and momomers. The particles are described by their size-density $f(t,x)$, where the variable $x \geq 0$ is interpreted as the volume of the particle ; the momomers are described by their density $c(t)$. The evolution of the solution is governed by addition to or removal from clusters of monomers. We denote by $a(x) \geq 0$ and $b(x) \geq 0$ respectively, the rates characterizing these phenomena. Accordingly the density f obeys the following transport equation

$$\left\{ \begin{array}{ll} \partial_t f + \partial_x(Vf) = 0, & t \geq 0,\ x \geq 0, \\ V(t,x) = a(x)c(t) - b(x), & \end{array} \right. \tag{1.1}$$

associated with a non-negative initial value $f(0,x)$. It is coupled to the integral equation

$$c(t) + \int_0^\infty x f(t,x)\,\mathrm{d}x = \rho, \qquad t \geq 0, \tag{1.2}$$

which determines the monomers concentration $c(t)$ (the initial values are also assumed to satisfy $c(0) = \rho - \int_0^\infty x f(0,x)\,\mathrm{d}x \geq 0$). This relation is interpreted as a constraint of mass conservation. Indeed, $\int_0^\infty x f(t,x)\,\mathrm{d}x$ is (proportional to) the mass of material contained in the grains, thus adding $c(t)$, which is (proportional to) the mass of monomers, we obtain the total mass which remains constant. The dynamics depends on the precise dependence of the coefficients a, b with respect to the size variable. All the physics of the precipitation/dissolution process is embodied into these coefficients. Considering that mass transfer is driven by monomers diffusion, we obtain

$$a(x) = x^{1/3}, \qquad b(x) = 1. \tag{1.3}$$

For details on the model, we refer to the seminal paper of Lifshitz and Slyozov [124]. Further comments can be found in the treatise [123] or in [163]. More recently, this model has been derived from mean-field theory and homogenization arguments [143]. A derivation from the Becker-Döring system, a discrete model of coagulation-fragmentation, is proposed in [48]. We point out immediately two key features of the model :

- First, the rate of growth at $x = 0$, that is $a(0)c(t) - b(0)$, is naturally negative. Hence, neglecting any difficulty associated to the lack of regularity of the coefficients, the characteristics associated to $V(t,x)$ are outgoing on the boundary $x = 0$, which explains that we do not need a boundary condition.
- At any time, there exists a unique critical size $x_{crit}(t)$ where the growth rate changes sign. More precisely, any grain with size $0 \leq x \leq x_{crit}(t)$ shrinks, while grains larger than x_{crit} grow. This phenomenon where large grains are growing at the expense of the smaller ones is known as Ostwald ripening. For (1.3), we have $x_{crit}(t) = 1/c(t)^3$.

The system (1.1)-(1.3) together with non-negative initial conditions has been mathematically investigated, and we refer to the developments in [47, 112, 145, 147] for the existence theory in various functional frameworks. It turns out that the question of the large time behavior of the solutions, which is of central importance in physical chemistry, is highly intriguing and challenging. Based on physical arguments, the following conclusions have been proposed in [124] : as t goes to infinity,

- $c(t)$ tends to 0 and behaves like $K_{LS} t^{-1/3}$, where $K_{LS} > 0$ is a universal constant,
- The total number of macroparticles $M_0(t) = \int_0^\infty f(t,x)\,\mathrm{d}x$ behaves like $C_{LS} t^{-1}$ where C_{LS} depends on K_{LS} and ρ,
- The mean radius of the particles

$$R_{mean}(t) = \frac{1}{M_0(t)} \int_0^\infty x^{1/3} f(t,x)\,\mathrm{d}x$$

  goes to $+\infty$ like $t^{1/3}/K_{LS}$,
- The solution $f(t,x)$ behaves like a rescaled universal asymptotic profile, that we denote $M_{K_{LS}}$.

The analysis of the problem has motivated a series of papers [34, 49, 146, 144]. It turns out that the asymptotic behavior is much more rich and complicated. Investigating the large time behavior relies on the self-similarity properties of the equation. We can exhibit a one-parameter family of self-similar solutions : the parameter, that we denote K, characterizes the size of the support of the self-similar solution and its regularity. The LS profile corresponds to the unique infinitely smooth profile, which is also the solution with the largest support. The other solutions are infinitely smooth, but at the tip of their support where they behave as a power law. Hence we address the question of the selection of the asymptotic profile among the members of this family. The – highly surprising – answer is that the selected profile depends on the initial data, and more

precisely on its shape at the end of its support. The analysis of this unusual selection process is very intricate and suitable notions of stability need to be introduced. The influence of the tail of the initial data is pointed out in [25, 130] and we refer to [146, 144] for a sharp mathematical analysis of these phenomena. The numerical investigation proposed in [35] brings out the strange selection process. Furthermore, it also shows that the problem is highly challenging for numerics since fronts have to be preserved with accuracy on a long time range and spurious smoothing effects should be eliminated to preserve the correct asymptotic profile. Let us point out that the question is relevant for instance in metallurgy engineering where the design of certain alloys production processes are based on the Lifshitz-Slyozov predictions. Lifshitz-Slyozov's claim is also subject to controversy for experimentalists and quite recent micro-gravity investigations bring out the need of further analysis of the model [159].

Before detailing the aims and scopes of the present paper, it is worth mentioning that several modifications of the system (1.1)-(1.3) have been introduced in order to restore a more standard large time behavior. An interesting attempt consists in introducing diffusive corrections, derived from a discrete-to-continuous regime : we expect with such a reasoning to recover a behavior similar to what is known for the Becker-Döring system. This viewpoint is discussed, among others, in [53, 50, 48, 51, 155, 142, 119]. Going back to a more microscopic description and the mean-field derivation of the Lifshitz-Slyozov system, it can be shown that fluctuations of the particles distribution can also lead to diffusive corrections, as detailed in [150]. A different approach has been discussed in [124, Section 3] : since the precipitation/dissolution process produces larger and larger grains, the modeling assumption that the distance between clusters remains large so that they do not interact directly becomes questionable as time becomes large. Accordingly, encounters between particles should be taken into account and (1.1) is replaced by

$$\partial_t f + \partial_x(Vf) = \lambda Q_{coag}(f) \tag{1.4}$$

where $\lambda > 0$ and the coagulation operator $Q_{coag}(f)$ is given by

$$Q_{coag}(f)(t,x) = \frac{1}{2}\int_0^x f(t,x-y)f(t,y)\,\mathrm{d}y - \int_0^\infty f(t,x)f(t,y)\,\mathrm{d}y = Q^+_{coag}(f) - Q^-_{coag}(f). \tag{1.5}$$

The gain term $Q^+_{coag}(f)$ characterizes the gain of particles with size x produced by the coalescence of particles with size $0 \le y \le x$ and $x-y$; the loss term $Q^-_{coag}(f)$ characterizes the loss of particles with size x due to the collisions of such a particle x and another grain having size $y \ge 0$. The operator Q_{coag} satisfies the following mass conservation property

$$\int_0^\infty x Q_{coag}(f)\,\mathrm{d}x = 0$$

while it implies a decay of the the total number of particles since

$$\int_0^\infty Q_{coag}(f)(t,x)\,\mathrm{d}x \le 0.$$

As far as we are concerned with existence issues, the analysis of the modified model is discussed in [46, 111]. From the discussion in [124], where the family of self-similar solutions is already identified, it is expected that the collision term induces a selection process which in turn, in the limit of vanishing λ, makes the LS profile the most physically relevant. A breakthrough in this direction is due to [104] where the existence of a stationary solution for the model with collision is proved. The obtained solution decays exponentially fast and it is isolated in a suitable functional space. In this paper the question we address is two-fold.

– As pointed out in [35], capturing the correct asymptotic profile is numerically challenging : numerical diffusion smoothes out the fronts so that we can be artificially led to the LS profile. We also refer to the conclusions of the sharp investigations in [42]. The investigation of the coagulation-free problem in [35] uses the WENO scheme, see [107, 43], but for sharp profiles the problem is very stiff and the computational cost is high. On the other hand, a specific Finite Volume scheme is introduced in [82], but even if the scheme has nice analytical properties, it is not able to capture non-smooth profiles (see results and comments in [82, Section 5]). Therefore, we wish to design a specific scheme, with reduced numerical diffusion. Our approach is based on an adaptation of downwinding techniques, as developped in [57].
– In the same spirit as in [35], we wish to discuss on numerical grounds the effect of the coagulation term Q_{coag}. The method we propose relies on a time splitting where we first solve the transport part of the equation, and second the collisional part. To this end, we tested several methods to evaluate the collision operator. This revealed that it is performing to make use of the conservative Finite Volume method presented in [82].

The paper is organized as follows. In Section 1.2 we collect some basic material about the Lifshitz-Slyozov model. In particular, we describe a relevant rescaling of the equation and remind the derivation of the self-similar profiles. Section 1.3 is devoted to the presentation of the numerical scheme for (1.1)-(1.3). By contrast to the WENO scheme, which is a high order reconstruction flux method for the advection equation, we introduce a first order (explicit) scheme. However, the construction relies on an anti-dissipative approach which eliminates numerical diffusion and, in turn, we will be able to confirm the results of [35] for a reduced computational cost. We detail in Section 1.4 possible treatments of the coagulation operators, paying attention to the incorporation of the Finite Volume approach of [82] in our scheme for the Lifshitz-Slyozov model.

1.2 Basic results

Let us start with a few remarks concerning the model (1.2)-(1.5). We shall perform here some formal manipulations in order to bring out interesting properties. Due to the singularity of the kinetic coefficients at $x = 0$, the justification of these relations might need some technicalities, see [46, 49, 112]. Firstly, since $V(t,0) \leq 0$ and $\int_0^\infty Q_{coag}(f)\,\mathrm{d}x \leq 0$, we have

$$\frac{\mathrm{d}}{\mathrm{d}t}\int_0^\infty f(t,x)\,\mathrm{d}x = -\int_0^\infty \partial_x(Vf)(t,x)\,\mathrm{d}x + \lambda\int_0^\infty Q_{coag}(f)(t,x)\,\mathrm{d}x \leq 0.$$

Hence the total number of macroparticles is non increasing. Secondly, for the evolution of the monomers concentration, we have

$$\begin{aligned}\frac{\mathrm{d}}{\mathrm{d}t}c(t) &= -\int_0^\infty V(t,x)f(t,x)\,\mathrm{d}x - \lambda\int_0^\infty xQ_{coag}(f)(t,x)\,\mathrm{d}x \\ &= -\int_0^{x_{crit}(t)} V(t,x)f(t,x)\,\mathrm{d}x - \int_{x_{crit}(t)}^\infty V(t,x)f(t,x)\,\mathrm{d}x.\end{aligned}$$

Therefore $t \mapsto c(t)$ does not have a priori a monotone behavior. Nevertheless this relation shows that $c(t)$ remains positive for any time. Indeed if we assume the existence of $t_* > 0$ such that $c(t_*)$ vanishes, then the time derivative satisfies

$$\frac{\mathrm{d}}{\mathrm{d}t}c(t_*) = \int_0^\infty b(x)f(t_*,x)\,\mathrm{d}x > 0,$$

which leads to a contradiction. The final remark is concerned with a simplification of the model. As it is expected that the monomers concentration tends to 0, we replace, for large times, the mass conservation relation (1.2) by the constraint

$$\int_0^\infty x f(t,x)\,\mathrm{d}x = \rho.$$

Accordingly, in the growth rate, the definition of $c(t)$ is modified and we are finally led to consider the system

$$\begin{cases} \partial_t f + \partial_x(Vf) = \lambda Q_{coag}(f), \\ V(t,x) = a(x)c(t) - b(x), \\ c(t) = \displaystyle\int_0^\infty b(x)f(t,x)\,\mathrm{d}x \left(\int_0^\infty a(x)f(t,x)\,\mathrm{d}x\right)^{-1}. \end{cases}$$

In the specific case of coefficients (1.3), $c(t)$ is nothing but the inverse of the mean radius. It is referred to as the Lifshitz-Slyozov-Wagner (LSW) model ; it can be derived form the original model through suitable asymptotic arguments, see [113]. This is the model dealt with in [145] and [34] (the last one with the simplification $a(x) = x$, $b(x) = 1$).

For discussing the large time behavior of the solutions of (1.1)-(1.3), or the model with coagulation (1.2)-(1.5), it is convenient to consider the following rescaling, see [35] and the references therein : we set

$$\begin{cases} f(t,x) = \dfrac{1}{(1+t)^2} g\left(\ln(1+t), \dfrac{x}{1+t}\right), \\ \\ \tau = \ln(1+t), \qquad y = \dfrac{x}{1+t}, \qquad d(\tau) = (1+t)^{1/3} c(t). \end{cases}$$

As we shall see below, the rescaling is particularly important for numerics since it provides a natural way to reduce the computational domain. Indeed, since the dynamics tends to form infinitely large clusters as time becomes large, we would need a huge computational domain to evaluate the behavior of the solution on a large time range. Accordingly, the computational resources needed for the simulation would become prohibitive. In rescaled variables, most of the information remains in a bounded domain. In rescaled variables the Lifshitz-Slyozov system becomes

$$\begin{cases} \partial_\tau g(\tau,y) + \partial_y((y^{1/3}d(\tau) - 1 - y)g(\tau,y)) = g(\tau,y) + \lambda Q^r_{coag}(g)(\tau,y) \quad \tau \geq 0,\ y \geq 0, \\ \\ d(\tau)\exp(-\tau/3) + \displaystyle\int_0^\infty y g(\tau,y)\,\mathrm{d}y = \rho, \\ \\ g(0,y) = g^0(y), \quad y \in \mathbb{R}_+, \qquad d(0) = d^0. \end{cases} \tag{1.6}$$

The coagulation operator $Q^r_{coag}(g)$ reads

$$Q^r_{coag}(g)(\tau,y) = \frac{1}{2}\int_0^y g(\tau,y-u)g(\tau,u)\,\mathrm{d}u - \int_0^\infty g(\tau,y)g(\tau,u)\,\mathrm{d}u.$$

Notice that the homogeneity of the collision kernel is crucial in this manipulation (here we work with a constant collision kernel, but the reasoning applies for more general kernels as in [104]). As a matter of fact, we still have the conservation property

$$\int_0^\infty y Q^r_{coag}(g)(\tau,y)\,\mathrm{d}y = 0.$$

As time tends to $+\infty$, we expect that $c(t)t^{1/3}$ tends to a constant $K > 0$; in order words

$$\lim_{\tau\to\infty} d(\tau) = K.$$

Accordingly, $d(\tau)\exp(-\tau/3) \sim K\exp(-\tau/3)$ becomes negligible for large rescaled times τ. We are thus led to the following rescaled version of the LSW equation, for $\tau \geq 0$, $y \geq 0$

$$\begin{cases} \partial_\tau g + \partial_y(Wg) = g + \lambda\, Q^r_{coag}(g), \\ W(t,y) = Ky^{1/3} - 1 - y, \\ \displaystyle\int_0^\infty yg(\tau,y)\,\mathrm{d}y = \rho, \\ \displaystyle K = \int_0^\infty g(\tau,y)\,\mathrm{d}y\Big(\int_0^\infty y^{1/3}g(\tau,y)\,\mathrm{d}y\Big)^{-1}. \end{cases}$$

We are interested in stationary solutions, that is, we search for $y \mapsto M_K(y)$ verifying

$$\partial_y((y^{1/3}K - 1 - y)M_K) = M_K + \lambda\, Q^r_{coag}(M_K), \qquad \int_0^\infty yM_K(y)\,\mathrm{d}y = \rho. \tag{1.7}$$

Equation (1.7) can be seen as an ODE with the term Q^r_{coag} as a perturbation.

Let us first discuss the coagulation-free equation

$$\partial_y((y^{1/3}K - 1 - y)M_K) = M_K.$$

We obtain

$$M_K(y) = -\frac{\mathrm{d}}{\mathrm{d}y}\left[\exp\left(\int_0^y \frac{\mathrm{d}\sigma}{\sigma^{1/3}K - 1 - \sigma}\right)\right]. \tag{1.8}$$

The question is now to identify parameters K that make the solution M_K admissible. The discussion relies on the properties of the function $T_K(z) = Kz - 1 - z^3$. We observe that $\frac{\mathrm{d}^2}{\mathrm{d}z^2}T_K(z) \leq 0$ for any $z \geq 0$; thus T_K is concave, and it reaches its maximum at $z = \sqrt{K/3}$: for any $z \geq 0$

$$T_K(z) \leq T_K^{max} = 2\left(\frac{K}{3}\right)^{3/2} - 1.$$

The function $K \mapsto T_K^{max}$ is increasing from $[0, +\infty[$ to $[-1, +\infty[$ and it vanishes at $K_{LS} = \frac{3}{2^{2/3}}$. We are thus led to the following cases :

$\underline{K < K_{LS}}$ The solution M_K is not admissible since its first moment blows up. Indeed, noting $t_K(\sigma) = T_K(\sigma^{1/3})$, we have $t_K(\sigma) < 0$ for any $\sigma \geq 0$ and we remark that

$$(1+y)\exp\left(\int_0^y \frac{d\sigma}{t_K(\sigma)}\right) = \exp\left(\int_0^y \frac{K\sigma^{1/3}\,\mathrm{d}\sigma}{(1+\sigma)(t_K(\sigma))}\right).$$

But $\frac{K\sigma^{1/3}d\sigma}{(1+\sigma)(t_K(\sigma))} \sim_{\sigma\to\infty} -K\sigma^{-5/3}$ which is integrable at infinity. Therefore,

$$\lim_{y\to+\infty}(1+y)\exp\left(\int_0^y \frac{d\sigma}{t_K(\sigma)}\right) = l > 0,$$

and we deduce that

$$yM_K(y) = \frac{y}{-t_K(y)}(1+y)\exp\left(\int_0^y \frac{d\sigma}{t_K(\sigma)}\right)\frac{1}{1+y} \geq \frac{l}{4}\frac{1}{1+y}$$

holds for $y \geq Y > 0$ large enough. Consequently $yM_K(y) \notin L^1(\mathbb{R}_+)$ for $K < K_{LS}$.

$\underline{K = K_{LS}}$ The point $z_0 = 2^{-1/3}$ is a double root of $T_{K_{LS}}(z)$ and then we can write $T_{K_{LS}}(z) = -(z - 2^{-1/3})^2(z + 2^{2/3})$. It allows to compute $M_{K_{LS}}$: we arrive at

$$M_{K_{LS}}(y) = \begin{cases} \dfrac{\exp\Big(-\dfrac{(2y)^{1/3}}{1-(2y)^{1/3}}\Big)}{\Big(1-(2y)^{1/3}\Big)^{11/3}\Big(1+1/2(2y)^{1/3}\Big)^{7/3}}, & 0 \le y < y_0 = 1/2, \\ \\ 0, & y \ge y_0. \end{cases}$$

$\underline{K > K_{LS}}$ The polynomial $T_K(z)$ admits three distinct roots that we denote z_-, z_0, z_+, with $z_- < 0 < z_0 < \sqrt{\frac{K}{3}} < z_+$. We set

$$\begin{cases} -T_K(z) = (z - z_0)(z - z_+)(z - z_-), \\ \\ z_\pm = 1/2\Big(-z_0 \pm \sqrt{4K - 3z_0^2}\Big), \\ \\ p = \dfrac{3z_0^2}{(z_0 - z_-)(z_+ - z_0)}, \qquad q = \dfrac{-3z_-^2}{(z_0 - z_-)(z_+ - z_-)}, \qquad r = \dfrac{-3z_+^2}{(z_+ - z_0)(z_+ - z_-)}, \end{cases}$$

and we are finally led to the following expression, see [35]

$$M_K(y) = \begin{cases} \Big(y_0\, y_-\, y_+\Big)^{1/3} \dfrac{\Big(1-(y/y_0)^{1/3}\Big)^{p-1}}{\Big(1-(y/y_-)^{1/3}\Big)^{1-q}\Big(1-(y/y_+)^{1/3}\Big)^{1-r}} & 0 \le y \le y_0 = 1/2, \\ \\ 0 & y > y_0, \end{cases}$$

with the relation

$$K = \frac{3(p+1)}{(2p+3)^{2/3}p^{1/3}}. \tag{1.9}$$

We plot in Fig. 1.1 the functions M_K corresponding to $K_{LS} = 3/(2^{2/3})$ ($p = \infty$), $K = 9 \times 7^{-2/3} \times 2^{-1/3} > K_{LS}$ ($p = 2$) and $K = 6 \times 5^{-2/3} > K_{LS}$ ($p = 1$). The profile $M_{K_{LS}}$ is infinitely smooth, while the smaller K, the less regular the profile M_K. Similarly, letting K decrease reduces the size of the support of the profile M_K.

Coming back to the evolution problem (1.1)-(1.3) we expect that

$$f(t,x) \sim_{t\to\infty} \frac{A_\rho}{(1+t)^2}\, M_K\Big(\frac{x}{1+t}\Big)$$

where $A_\rho = \rho\big(\int_0^\infty y M_K(y)\,\mathrm{d}y\big)^{-1}$ is a normalizing constant related to mass conservation. Of course, it remains to precise the selection of the parameter K in the asymptotic behavior. The conjecture of Lifshitz and Slyozov [124] is that the solution of (1.1)-(1.3) behaves for large time as the smooth profile $M_{K_{LS}}$, whatever the shape of the initial data is. However, both numerical

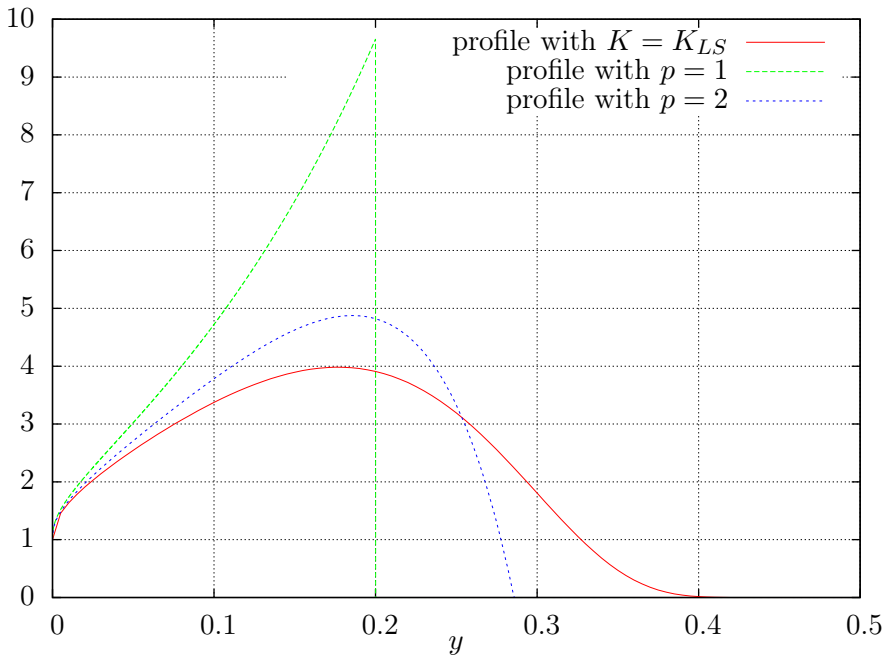

Figure 1.1 – Plot of asymptotic profiles M_K for $p = 1$, $p = 2$, $p = \infty$.

simulations [35] and mathematical analysis [144, 146, 149] have shown that the selection of the profile is much more amazing : considering a data with compact support, the large time behavior selects K according to the shape of the initial data at the tip of the support ! Such a phenomenon is highly unusual and it has motivated the introduction of sharp notions to describe the behavior of a function at the end of its support, and for numerics it requires performing schemes with as reduced as possible numerical diffusion.

Of course, dealing with the equation (1.7) containing the non linear collision term is certainly much more difficult. It could be quite natural to think of the solution as a fixed point of the mapping $\tilde{g} \mapsto g$, with g solution of

$$\partial_y((y^{1/3}K - 1 - y)g) = g + \lambda Q^r_{coag}(\tilde{g}), \qquad \int_0^\infty yg(y)\,\mathrm{d}y = \rho. \tag{1.10}$$

This iterative process is already described in [124]. This viewpoint is further developped in [104] to prove the existence, for λ small enough, of a stationary solution close to $M_{K_{LS}}$. Our goal here is to propose a numerical scheme to treat the Lifshitz-Slyozov equation with coagulation and to investigate numerically the influence of these encounters on the large time asymptotics.
What we observe based on the numerical simulations is the regularization effect of the collisions. Considering different initial data leading to different asymptotic profiles in the coagulation-free case, the numerical large time solutions become similar with collisions. Furthermore as the parameter λ in front of the coagulation operator tends to zero, the large time profile looks like the smooth $M_{K_{LS}}$ profile. Of course further analysis will be necessary to decide whether this effect is due to the numerical approximation or really to the effect of encounters. However, the use of a specific non-dissipative scheme reduces the numerical diffusion, at least for the transport part, and the scheme is validated by performing simulation of the coagulation-free problem.

1.3 An anti-diffusive Finite Volume scheme for the Lifshitz-Slyozov system

In this part we set up a new numerical scheme for the (collisionless) Lifshitz-Slyozov system (1.1)-(1.3). The scheme we propose is a Finite Volume scheme, with a flux reconstruction that cancels out the numerical diffusion. The method is first-order accurate, but in comparison to the 5th-order WENO scheme used in [35], it allows simulations of the solutions with a given accuracy for a reduced computational cost, and furthermore it allows to capture the large time behavior far beyond the capabilities of the WENO scheme. We point out again that reducing the numerical diffusion is crucial to capture the correct asymptotic profile. Even if WENO is very performing in preserving fronts, the problem becomes so stiff that the computations can be quite long when dealing with non smooth data, as reported in [35]. We start by describing how downwinding techniques taken from [57] apply for the conservative transport equation. Then, we detail the splitting scheme we use for solving (1.1)-(1.3). Finally, we compare numerical results with those obtained with the WENO scheme.

1.3.1 A scheme for the transport equation

In this section we are concerned with the simple transport equation

$$\partial_t f(t,x) + \partial_x\big(V(t,x)f(t,x)\big) = 0, \tag{1.11}$$

where $V(t,x)$ is a given smooth velocity field. We neglect any difficulties due to truncation of the computational domain, and we consider the problem set on $t \geq 0$, $x \geq 0$, assuming that $V(t,0) < 0$. We introduce a regular mesh, with constant step $\Delta x > 0$: the cells are the intervals $[x_{k-1/2}, x_{k+1/2}]$, $k \in \mathbb{N}$ with $x_{-1/2} = 0$, $x_{k+1/2} = (k+1)\Delta x$, and we denote by x_k the midpoint of the cell : $x_k = (k+1/2)\Delta x$. We denote by f_k^n the numerical unknown, which is intended to be an approximation of $\frac{1}{\Delta x}\int_{x_{k-1/2}}^{x_{k+1/2}} f(t^{(n)},z)\,\mathrm{d}z$, where $t^{(0)} = 0 < t^{(1)} < ... < t^{(n)} < t^{(n+1)}$ defines a time-discretization, with possibly variable step $\Delta t^{(n)} = t^{(n+1)} - t^{(n)}$ in order to adapt to the time variation of V. We denote by V_k^n the approximation of the velocity *in* the cells (meaning that the approximation is piecewise constant) and by $V_{k-1/2}^n$ the velocity *at* the cell interfaces : namely, we set

$$\begin{aligned} V_k^n &= V(t^{(n)}, x_k), && n \in \mathbb{N}, k \in \mathbb{N}, \\ V_{k-1/2}^n &= V(t^{(n)}, x_{k-1/2}), && n \in \mathbb{N}, k \in \mathbb{N}. \end{aligned}$$

The scheme is defined by the relation

$$f_k^{n+1} = f_k^n - \frac{\Delta t^{(n)}}{\Delta x}\big(V_{k+1/2}^n f_{k+1/2}^n - V_{k-1/2}^n f_{k-1/2}^n\big). \tag{1.12}$$

It remains to define the interface fluxes $f_{k+1/2}^n$. To this end it is convenient to rewrite (1.12) as follows :

$$\begin{aligned} f_k^{n+1} &= f_k^n - \frac{\Delta t^{(n)}}{\Delta x} V_k^n\big(f_{k+1/2}^n - f_{k-1/2}^n\big) \\ &\quad - \frac{\Delta t^{(n)}}{\Delta x}\big(f_{k+1/2}^n(V_{k+1/2}^n - V_k^n) + f_{k-1/2}^n(V_k^n - V_{k-1/2}^n)\big). \end{aligned}$$

The last term is an approximation of $f\partial_x V(t^{(n)}, x_k)$ and the definition of the fluxes will be driven by anti-diffusive strategies for the advection equation

$$\partial_t f + V\partial_x f = 0. \tag{1.13}$$

Additionally to the anti-diffusive features, the construction of the fluxes will be requested to satisfy stability properties, that lead to some constraints on the numerical parameters. Let us introduce the following notation :

- $\nu^n = \frac{\Delta t^{(n)}}{\Delta x}$,
- $m^n_{k+1/2} = \min(f^n_k, f^n_{k+1})$, and $M^n_{k+1/2} = \max(f^n_k, f^n_{k+1})$,
- If $V^n_k, V^n_{k+1/2}, V^n_{k-1/2} > 0$:

$$b^n_{k+1/2} = \frac{1}{\nu^n V^n_k}\big(f^n_k - \max(f^n_k, f^n_{k-1})\big) + \max(f^n_k, f^n_{k-1}) = \frac{1}{\nu^n V^n_k}\big(f^n_k - M^n_{k-1/2}\big) + M^n_{k-1/2},$$

$$B^n_{k+1/2} = \frac{1}{\nu^n V^n_k}\big(f^n_k - \min(f^n_k, f^n_{k-1})\big) + \min(f^n_k, f^n_{k-1}) = \frac{1}{\nu^n V^n_k}\big(f^n_k - m^n_{k-1/2}\big) + m^n_{k-1/2},$$

$$\mathscr{B}^n_{k+1/2} = \begin{cases} \min\Big(B^n_{k+1/2}, m^n_{k-1/2}\dfrac{V^n_{k-1/2}}{V^n_{k+1/2}} + \dfrac{f^n_k}{\nu^n V^n_{k+1/2}}\Big) & \text{if } m^n_{k-1/2} \geq 0, \\ B^n_{k+1/2} & \text{otherwise,} \end{cases}$$

- If $V^n_k, V^n_{k+1/2}, V^n_{k-1/2} < 0$

$$b^n_{k-1/2} = \frac{1}{\nu^n |V^n_k|}\big(f^n_k - \max(f^n_k, f^n_{k+1})\big) + \max(f^n_k, f^n_{k+1}) = \frac{1}{\nu^n |V^n_k|}\big(f^n_k - M^n_{k+1/2}\big) + M^n_{k+1/2},$$

$$B^n_{k-1/2} = \frac{1}{\nu^n |V^n_k|}\big(f^n_k - \min(f^n_k, f^n_{k+1})\big) + \min(f^n_k, f^n_{k+1}) = \frac{1}{\nu^n |V^n_k|}\big(f^n_k - m^n_{k+1/2}\big) + m^n_{k+1/2},$$

$$\mathscr{B}^n_{k-1/2} = \begin{cases} \min\Big(B^n_{k-1/2}, m^n_{k+1/2}\dfrac{|V^n_{k+1/2}|}{|V^n_{k-1/2}|} + \dfrac{f^n_k}{\nu^n |V^n_{k-1/2}|}\Big) & \text{if } m^n_{k+1/2} \geq 0, \\ B^n_{k-1/2} & \text{otherwise,} \end{cases}$$

- If $V^n_k, V^n_{k+1/2}, V^n_{k-1/2}$ do not have the same sign, we set $b^n_{k+1/2} = \mathscr{B}^n_{k+1/2} = f^n_k$ if $V^n_{k+1/2} > 0$ and $b^n_{k+1/2} = \mathscr{B}^n_{k+1/2} = f^n_{k+1}$ if $V^n_{k+1/2} < 0$.
- $\mu^n_{k+1/2} = \max(m^n_{k+1/2}, b^n_{k+1/2})$, and $\mathscr{M}^n_{k+1/2} = \min(M^n_{k+1/2}, \mathscr{B}^n_{k+1/2})$.

The following statement makes the principles on which the construction of the fluxes is based clear.

Proposition 1.3.1. *We assume that the following standard Courant-Friedrichs-Lewy (CFL) stability condition*

$$\frac{\Delta t^{(n)}}{\Delta x} \max_k \big(|V^n_k|, |V^n_{k+1/2}|\big) \leq 1 \tag{1.14}$$

is satisfied. Then, for any k the set $[\mu^n_{k+1/2}, \mathscr{M}^n_{k+1/2}]$ is non-empty. Suppose that for any k the fluxes satisfy $f^n_{k+1/2} \in [\mu^n_{k+1/2}, \mathscr{M}^n_{k+1/2}]$. Then, the following assertions hold :

i) The scheme (1.12) *is consistent with* (1.11),

ii) If $f^n_k \geq 0$ for any k then $f^{n+1}_k \geq 0$ too, if Δx is sufficiently small (otherwise a restricted CFL condition is requested to ensure the non-negativity : $(\Delta t^{(n)}/\Delta x) \max_k \big(|V^n_{k+1/2}|\big) \leq 1/2$).

iii) Let us set

$$f^{n\star}_k = f^n_k - \frac{\Delta t^{(n)}}{\Delta x} V^n_k (f^n_{k+1/2} - f^n_{k-1/2}), \quad k \in \mathbb{N}.$$

Let $j \in \mathbb{N}$. If $V^n_j \geq 0$ then $m^n_{j-1/2} \leq f^{n\star}_j \leq M^n_{j-1/2}$, while if $V^n_j \leq 0$ then $m^n_{j+1/2} \leq f^{n\star}_j \leq M^n_{j+1/2}$.

Proof. To discuss the properties of the scheme, we first suppose that $V^n_{k-1/2} > 0$, $V^n_k > 0$ and $V^n_{k+1/2} > 0$. Owing to (1.14), we have

$$\frac{1}{\nu^n V^n_k} - 1 \geq 0$$

and thus

$$\big(\frac{1}{\nu^n V^n_k} - 1\big)\big(f^n_k - \min(f^n_k, f^n_{k-1})\big) \geq 0.$$

It follows that

$$\frac{1}{\nu^n V^n_k}\big(f^n_k - \min(f^n_k, f^n_{k-1})\big) + \min(f^n_k, f^n_{k-1}) \geq f^n_k. \tag{1.15}$$

On the same token, we have

$$\big(\frac{1}{\nu^n V^n_k} - 1\big)\big(f^n_k - \max(f^n_k, f^n_{k-1})\big) \leq 0,$$

that leads to

$$\frac{1}{\nu^n V^n_k}\big(f^n_k - \max(f^n_k, f^n_{k-1})\big) + \max(f^n_k, f^n_{k-1}) \leq f^n_k. \tag{1.16}$$

By definition $f^n_k \in [m^n_{k+1/2}, M^n_{k+1/2}]$ while (1.15) and (1.16) tell us $f^n_k \in [b^n_{k+1/2}, B^n_{k+1/2}]$. When $m^n_{k-1/2} \geq 0$, we also observe that (1.14) implies $m^n_{k-1/2}\frac{V^n_{k-1/2}}{V^n_{k+1/2}} + \frac{f^n_k}{\nu^n V^n_{k+1/2}} \geq \frac{f^n_k}{\nu^n V^n_{k+1/2}} \geq f^n_k$. Hence we have $f^n_k \in [b^n_{k+1/2}, \mathscr{B}^n_{k+1/2}]$. The argument adapts when V is locally negative (leading to $f^n_k \in [m^n_{k-1/2}, M^n_{k-1/2}] \cap [b^n_{k-1/2}, B^n_{k-1/2}]$) or changes sign (in which case the requirement $f^n_{k+1/2} \in [\mu^n_{k+1/2}, \mathscr{M}^n_{k+1/2}]$ implies that the scheme is the upwind scheme). The consistency of the scheme follows from the very definition of $m^n_{k+1/2}$ and $M^n_{k+1/2}$.

Let us now prove that f^{n+1}_k remains non-negative. The non-negativity $f^{n+1}_k \geq 0$ is equivalent to

$$\nu^n\big(V^n_{k+1/2} f^n_{k+1/2} - V^n_{k-1/2} f^n_{k-1/2}\big) \leq f^n_k.$$

Again, we start by assuming, for k fixed, $V^n_{k+1/2}, V^n_{k-1/2}, V^n_k > 0$. Then $f^{n+1}_k \geq 0$ is equivalent to

$$f^n_{k+1/2} \leq \frac{f^n_k}{\nu^n V^n_{k+1/2}} + f^n_{k-1/2}\frac{V^n_{k-1/2}}{V^n_{k+1/2}}.$$

Assuming $f^n_{k-1/2} \geq m^n_{k-1/2}$ yields the following sufficient condition for this relation to hold :

$$f^n_{k+1/2} \leq \frac{f^n_k}{\nu^n V^n_{k+1/2}} + m^n_{k-1/2}\frac{V^n_{k-1/2}}{V^n_{k+1/2}}$$

which justifies the definition of $\mathscr{B}^n_{k+1/2}$.

In the case $V^n_{k+1/2}, V^n_{k-1/2}, V^n_k < 0$ we obtain the following analog condition

$$f^n_{k-1/2} \leq \frac{f^n_k}{-\nu^n V^n_{k-1/2}} + m^n_{k+1/2}\frac{-V^n_{k+1/2}}{-V^n_{k-1/2}}.$$

In the other cases we just choose the standard upwind flux, which is known to ensure the non-negativity *under the restricted CFL condition*

$$\frac{\Delta t^{(n)}}{\Delta x}\max_k\left(|V^n_{k+1/2}|\right)\leq 1/2.$$

Let us analyze this case in detail. In the case where $V^n_{k+1/2}<0$ and $V^n_{k-1/2}>0$, the non-negativity of f^{n+1}_k is ensured without any condition on the time step. The only problematic case is when $V^n_{k+1/2}>0$ and $V^n_{k-1/2}<0$ (where the cell can be "emptied" from the two sides). In this case, choosing the upwind fluxes leads to

$$f^{n+1}_k=f^n_k\left(1-\frac{\Delta t^{(n)}}{\Delta x}\left(V^n_{k+1/2}-V^n_{k-1/2}\right)\right).$$

Thus the non-negativity condition is

$$\frac{\Delta t^{(n)}}{\Delta x}\left(V^n_{k+1/2}-V^n_{k-1/2}\right)\leq 1$$

(which explains the CFL condition restriction by a factor $1/2$ in general). But now, assume that the velocity is Lipschitz with coefficient L. Then one has $V^n_{k+1/2}-V^n_{k-1/2}\leq L\Delta x$ and a sufficient condition on the time step becomes

$$\Delta t^{(n)}\leq 1/L.$$

Asymptotically when Δx tends to 0, this is automatically satisfied when the CFL condition of the proposition is satisfied, that is why we retain only this classical condition.

We finally turn to the proof of iii) which relies on the discretization of the advection equation (1.13). The construction is taken out from [57] and is based on the requirements to preserve the L^∞ norm and to satisfy the Total Variation Diminishing (TVD) property. We have already seen that, in the case $V^n_{k-1/2}>0$, $V^n_k>0$, $V^n_{k+1/2}>0$,

$$f^n_k\in[m^n_{k+1/2},M^n_{k+1/2}]\cap[b^n_{k+1/2},B^n_{k+1/2}]\neq\emptyset.$$

Now, we require that the numerical flux $f^n_{k+1/2}$ fulfills the same constraints

$$\begin{cases} m^n_{k+1/2}\leq f^n_{k+1/2}\leq M^n_{k+1/2} & \text{consistency constraint,}\\ b^n_{k+1/2}\leq f^n_{k+1/2}\leq B^n_{k+1/2} & \text{stability constraint.}\end{cases}\tag{1.17}$$

Combining the stability constraint in (1.17) to the consistency constraint $m^n_{k-1/2}\leq f^n_{k-1/2}\leq M^n_{k-1/2}$ we obtain

$$\frac{1}{\nu^nV^n_k}\left(f^n_k-M^n_{k-1/2}\right)+f^n_{k-1/2}\leq f^n_{k+1/2}\leq\frac{1}{\nu^nV^n_k}\left(f^n_k-m^n_{k-1/2}\right)+f^n_{k-1/2}.$$

Therefore, we deduce that

$$m^n_{k-1/2}\leq f^{n\star}_k=f^n_k-\nu^nV^n_k(f^n_{k+1/2}-f^n_{k-1/2})\leq M^n_{k-1/2}\tag{1.18}$$

holds. We conclude that the discrete solution satisfies the following maximum principle

$$\begin{cases}\max\limits_{k\in\mathbb{N}}(f^{n\star}_k)\leq\max\limits_{k\in\mathbb{N}}(f^n_k)\\ \min\limits_{k\in\mathbb{N}}(f^{n\star}_k)\geq\min\limits_{k\in\mathbb{N}}(f^n_k).\end{cases}$$

The TVD property is also insured, it follows from LeRoux and Harten's incremental analysis [99, 121]. The same can be done when the velocity is negative or changes sign : this ends the proof. □

The point now consists in defining $f^n_{k+1/2}$ so that on the one hand, Proposition 1.3.1 holds, and on the other hand the numerical diffusion is as reduced as possible : to this end we adopt a *downwinding* approach. When $V^n_{k-1/2} > 0$, $V^n_k > 0$ and $V^n_{k+1/2} > 0$, we choose the closest value to f^n_{k+1} that fulfills the requirements of Proposition 1.3.1. Namely $f^n_{k+1/2}$ will be the solution of the following problem

$$\begin{array}{l} \text{To minimize } |f^n_{k+1/2} - f^n_{k+1}| \\ \text{under the constraint } \ f^n_{k+1/2} \in [\mu^n_{k+1/2}, \mathscr{M}^n_{k+1/2}]. \end{array}$$

This minimization problem leads to the following three cases (again assuming that $V^n_{k-1/2} > 0$, $V^n_k > 0$ and $V^n_{k+1/2} > 0$)

$$\left\{ \begin{array}{ll} f^n_{k+1/2} = \mu^n_{k+1/2} & \text{if } f^n_{k+1} \leq \mu^n_{k+1/2} \\ f^n_{k+1/2} = f^n_{k+1} & \text{if } \mu^n_{k+1/2} \leq f^n_{k+1} \leq \mathscr{M}^n_{k+1/2} \\ f^n_{k+1/2} = \mathscr{M}^n_{k+1/2} & \text{if } f^n_{k+1} \geq \mathscr{M}^n_{k+1/2} \end{array} \right. \tag{1.19}$$

When the velocity is locally positive, we note that the stability constraint involves f^n_{k-1} and f^n_k only that are upwind values for $f^n_{k+1/2}$; it justifies the naming of downwind flux under upwind constraint.

1.3.2 Simulation of (1.1)-(1.3)

Let us explain the derivation of the anti-dissipative scheme for the conservative equation (1.1) based on the idea developed in section 1.3.1 by using a time splitting

- First, we solve the transport equation (1.1). Here, we know the discrete density f^n_k and the concentration c^n, approximation of the average of $f(t^{(n)}, \cdot)$ on the kth cell and $c(t^{(n)})$. The concentration is assumed constant during the time step, and thus the velocity field $V(t,x)$ is replaced by the given quantity $x^{1/3}c^n - 1$. The equation has the form (1.11) and we apply the scheme designed in the previous section. It defines f^{n+1}. Note that by construction the solution is non-negative.
- Second, we update the monomers concentration by setting :

$$c^{n+1} = \rho - \Delta x \sum_{k \in \mathbb{N}} x_k f^{n+1}_k$$

(recall that x_k is defined as the center of the kth cell : $x_k = (k+1/2)\Delta x$ for any $k \in \mathbb{N}$). In the algorithm, the time step $\Delta t^{(n)}$ is evaluated at each iteration, it is computed so that the scheme satisfies the CFL condition (1.14).

Simulations of the Lifshitz-Slyozov system : comparison with a fifth order WENO scheme.

To validate the scheme, we compare the simulations with those in [35]. The domain is $[0, 800]$ with 80 points by length unit. We set $\rho = 41$. As an initial condition we set

$$f^0(x) = \left\{ \begin{array}{ll} 0.1 & \text{for } x \in [10, 30], \\ 0 & \text{otherwise.} \end{array} \right. \tag{1.20}$$

This is a step function and the corresponding profile M_K is determined by $K = 6 \times 5^{-2/3}$ (that is $p = 1$, see Section 1.2). This is the hardest case dealt with in [35]. We perform the simulation with a Courant number $\nu^n \max |V_k^n, V_{k+1/2}^n| = 1/2$ (the maximum of the velocities is actually computed on the domain $[0, 800]$). The scheme detailed above is referred to as ADM (Anti-Dissipative Method) and we compare in Fig. 1.2 with results provided by the 5th order WENO scheme developed and used in [35]. The evolution of the monomers concentration is basically the same. However, the interesting point is the discrepancies observed at the final time $t = 2000$ in the particles distribution profile. At such a large time we observe the smearing in the WENO simulation, and numerical diffusion is sensible. By contrast, the ADM scheme preserves accurately the shape of the expected profile. Furthermore, while we use the same mesh size, of course, the ADM run is faster by a factor 3/4 than the WENO simulation. The smoothing effect is confirmed by the movie of the time evolution in Fig. 2.2 : the numerical diffusion in the WENO simulation becomes visible after 1000 time units. The maximum is damped and the shape of the solution, in particular at the tip of the support, is smoothed. The effect increases as time grows.

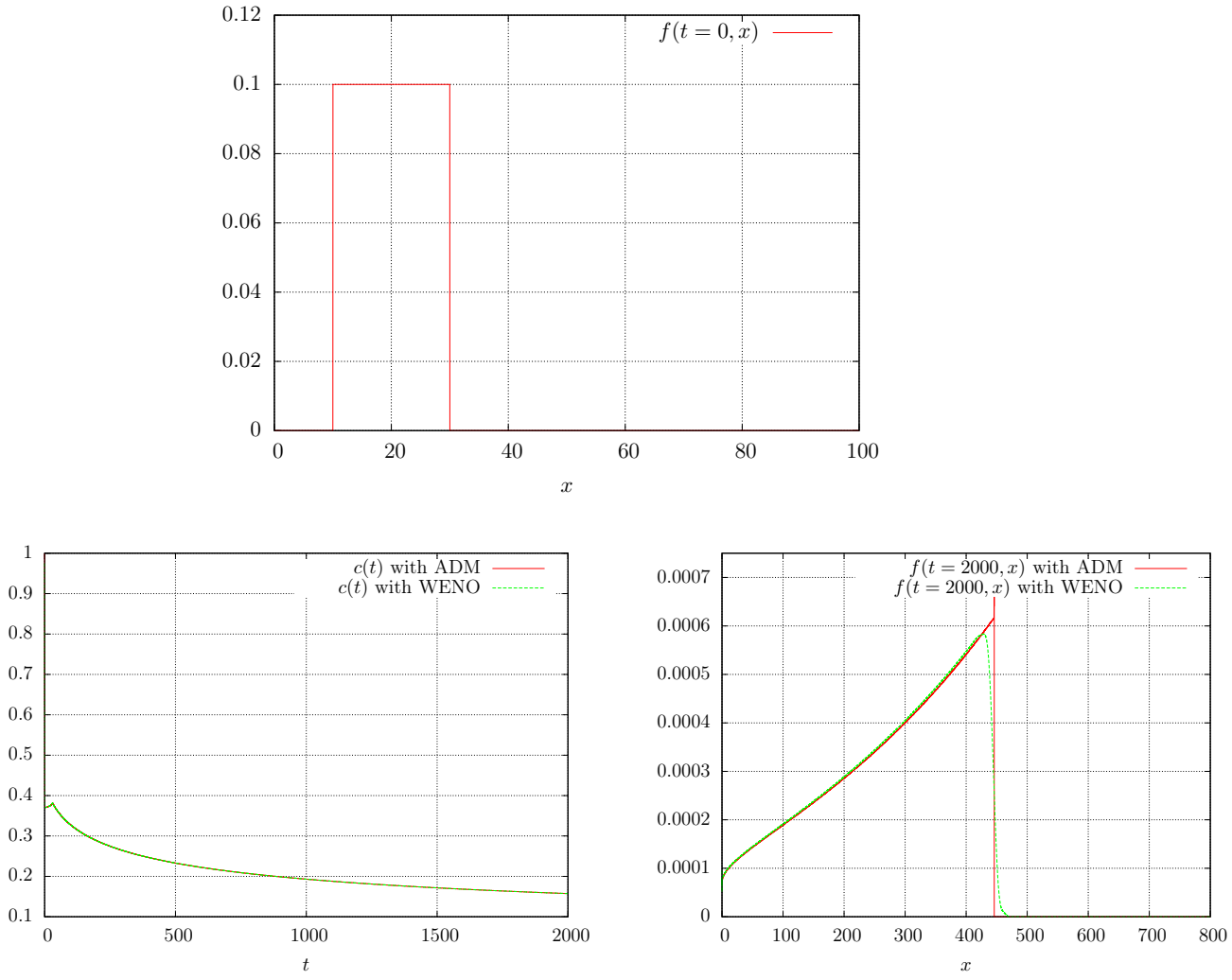

Figure 1.2 – Comparison WENO vs. ADM schemes. Top : step initial function. Down left : evolution of the monomers concentration. Down right : final solution at $t = 2000$.

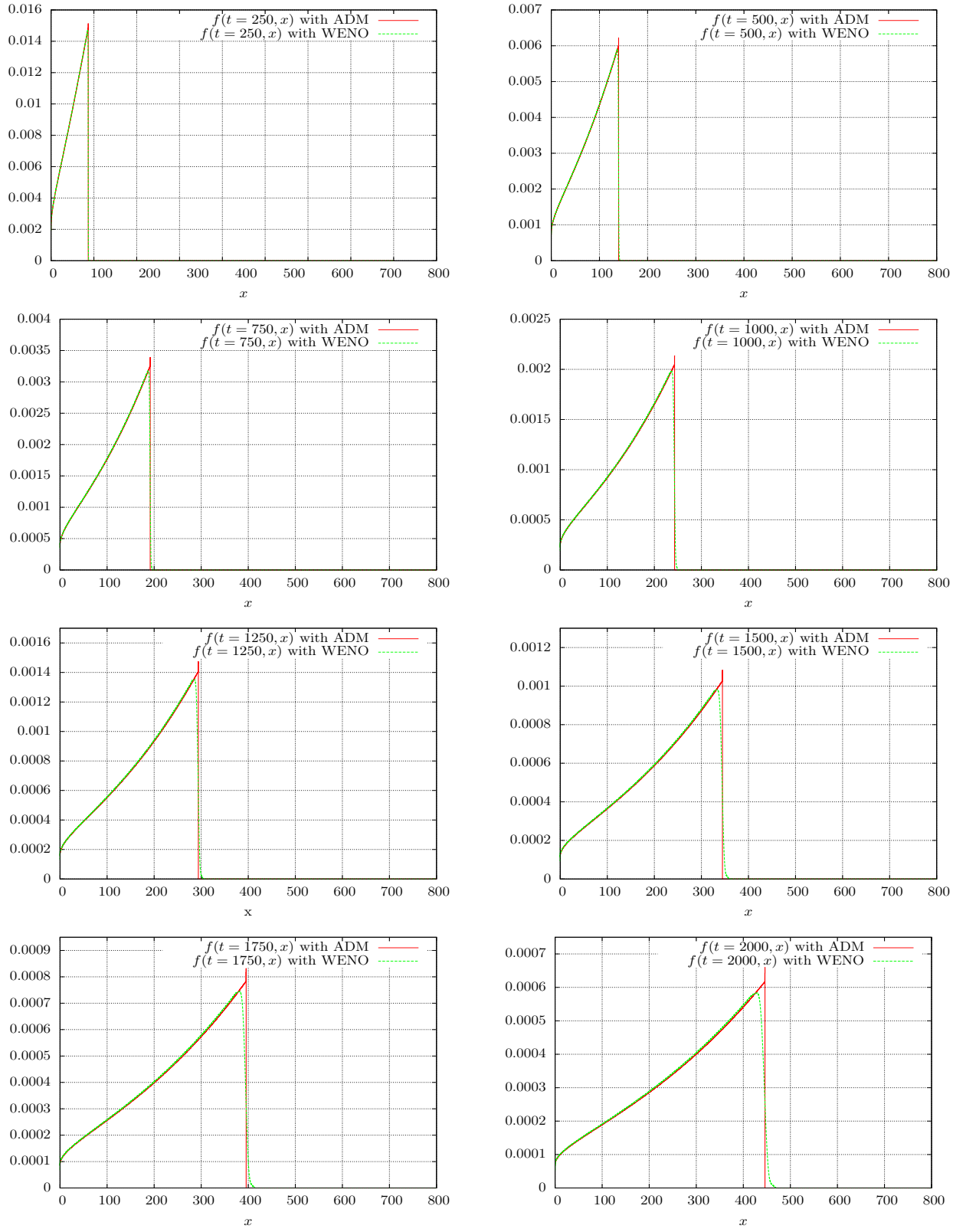

Figure 1.3 – Comparison WENO vs. ADM schemes. Evolution of the solution all 250 time units.

1.3.3 Simulation of the Lifshitz-Slyozov equation in rescaled variables

As detailed in Section 1.2, in rescaled variables the Lifshitz-Slyozov system becomes

$$\begin{cases} \partial_\tau g(\tau,y) + \partial_y(W(\tau,y)g(\tau,y)) = g(\tau,y), & \tau \geq 0,\ y \geq 0, \\ W(\tau,y) = y^{1/3}d(\tau) - 1 - y, & \tau \geq 0,\ y \geq 0, \\ d(\tau)\exp(-\tau/3) + \displaystyle\int_0^\infty y g(\tau,y)\,\mathrm{d}y = \rho, \quad \text{(constant)} & \tau \geq 0, \\ g(0,y) = g^0(y), & y \geq 0. \end{cases}$$

The advantage now is that the solution is expected to converge for large τ to a compactly supported profile, while in original variables the mean radius goes to $+\infty$. Therefore, for the rescaled problem we considerably reduce difficulties related to the truncation of the computational domain. However, as remarked in [35], the price to be paid is to increase significantly the stiffness of the problem. In practice, it requires for the WENO scheme some restrictions on the CFL number to prevent the apparition of spurious oscillations and smoothing effects.

The notations here are straightforwardly extended from the one of the discretization in the original variables. We again make use of a time-splitting :

– First, we solve the advection equation

$$\partial_\tau g(\tau,y) + \partial_y\big(W(\tau,y)g(\tau,y)\big) = g(\tau,y).$$

Knowing d^n and g^n approximations of the rescaled monomers concentration d and particles distribution g at time $\tau^{(n)}$, respectively, we use the ADM scheme to determine

$$g_k^{n+1} = g_k^n - \frac{\Delta\tau^{(n)}}{\Delta y}\big(W_{k+1/2}^n g_{k+1/2}^n - W_{k-1/2}^n g_{k-1/2}^n\big) + \Delta\tau^{(n)} g_k^n.$$

The only modification is to take into account the zeroth order term, but it is straightforward to adapt the scheme and Proposition 1.3.1 to this situation.

– Finally, we update the monomers concentration with

$$d(\tau)\exp(-\tau/3) + \int_0^\infty y g(\tau,y)\,\mathrm{d}y = \rho.$$

For the discrete unknowns, it yields

$$d^{n+1} = \left(\rho - \sum_{k=0}^{K} y_k\, g_k^{n+1}\,\Delta y\right)\exp((n+1)\Delta\tau/3), \quad \text{with } y_k = (k+1/2)\Delta y.$$

Using the scheme in this way we observe the apparition of spurious oscillations. In fact, in rescaled variables it seems that additional stability constraints need to be considered in the definition of the monomers concentration d. A rough derivation of a criterion that prevents the formation of oscillations works as follows. We have

$$\frac{\mathrm{d}}{\mathrm{d}\tau}d(\tau) = e^{\tau/3}\Big(\frac{\rho}{3} - \frac{4}{3}\int_0^\infty y g(\tau,y)\,\mathrm{d}y - \int_0^\infty W(y,\tau)g(\tau,y)\,\mathrm{d}y\Big).$$

From this relation we deduce that $\frac{\mathrm{d}}{\mathrm{d}\tau}d$ can be estimated by $\mathscr{O}(e^{\tau/3})$. By analogy with the basic theory of numerical integration of ODE, this estimate suggests to impose $\Delta\tau \leq Ce^{-\tau/3}$ as a stability criterion. Of course, as time increases this becomes much more restrictive than the CFL

condition (1.14) associated to the transport equation. We are not able to propose a complete analysis, nevertheless this condition turns out to be efficient. From our numerical experiences it seems also difficult to relax it.

Again we compare the results with the ADM and WENO schemes. The data are defined as follows :

- the domain is $[0, 40]$ with 1000 points by unit length,
- the initial data is : $g^0(y) = \begin{cases} 0.1 & y \in [10, 30], \\ 0 & \text{otherwise}, \end{cases}$
- the total initial mass, $\rho = 41$, is such that the initial monomers concentration is $d^0 = 1$.

Results are displayed in Fig. 1.4 at the final time $\tau = 20$. We also show the time evolution of the particles distribution in Fig. 1.5. We remind, see the comments in [35], that the rescaled problem is highly stiff and sensible to numerical diffusion. The non-dissipative character of the ADM scheme is definitely an asset to capture with accuracy the correct profile. Indeed, with the chosen numerical conditions, the effects of numerical dissipation appear sensitively at time $\tau = 7.5$ with the WENO scheme. Since this time, the smoothing effect propagates and, continuing the simulation, the asymptotic profile we obtain looks like the smooth LS profile (see Fig. 1.6 for simulations starting from a Maxwellian initial state). This is confirmed by looking at the behavior of the monomers concentration d : the ADM method keeps d close to the expected value ($K = 2.05197$), while with WENO it decays to $K_{LS} = 1.88988$.

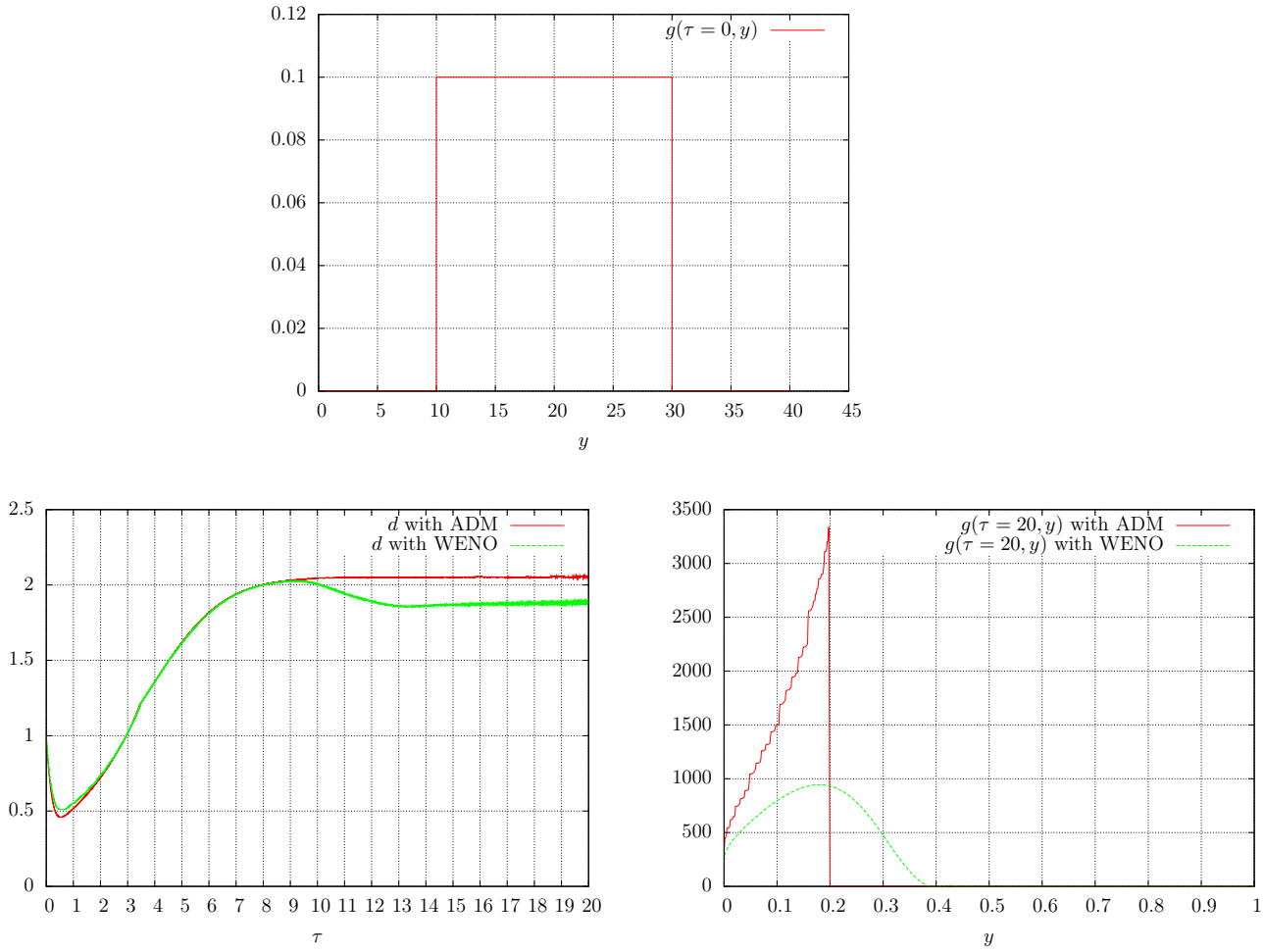

Figure 1.4 – Comparison WENO vs. ADM on the rescaled equation. Top : step initial function. Down left : evolution of rescaled monomers concentration. Down right : final rescaled solution.

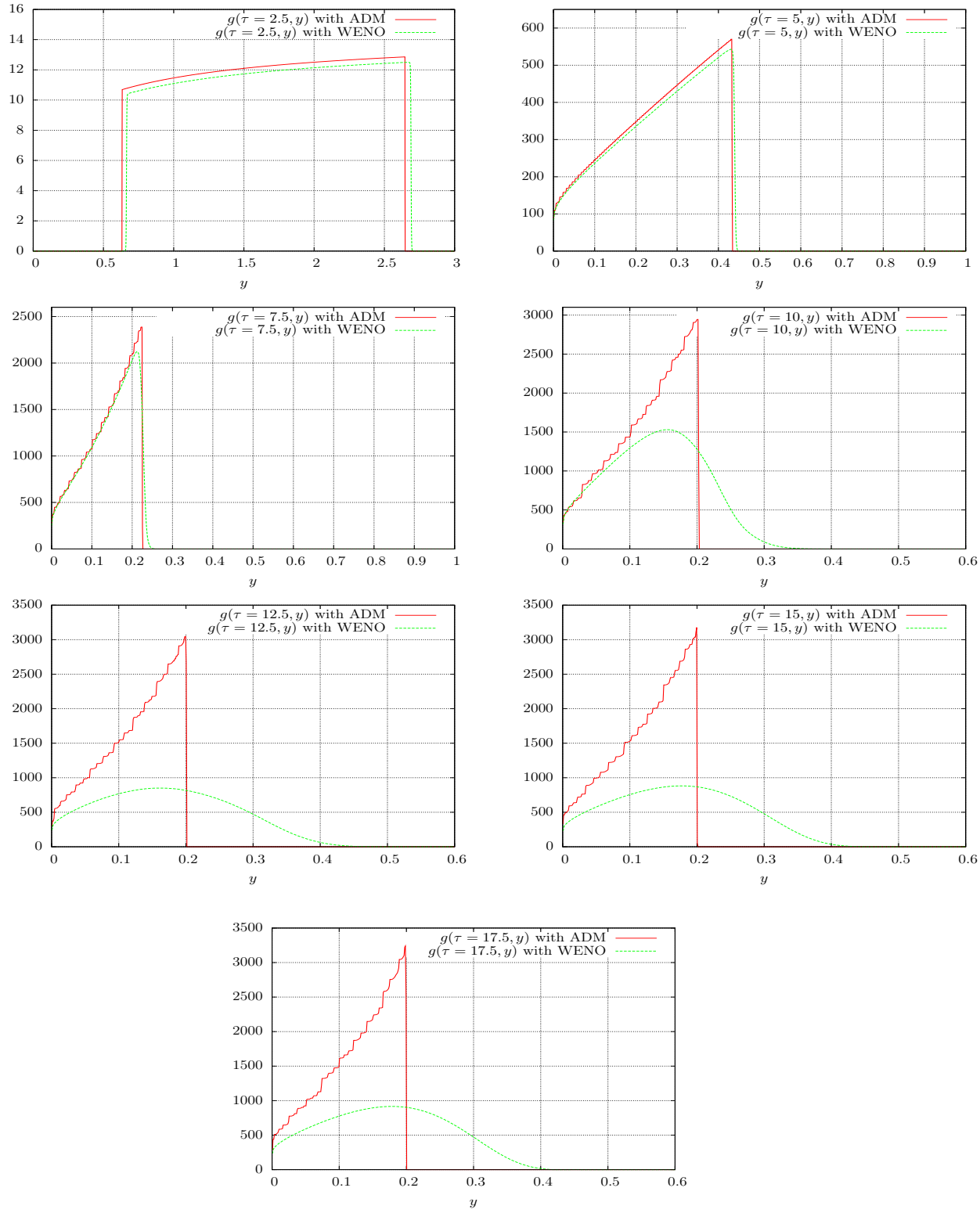

Figure 1.5 – Comparison WENO vs. ADM on the rescaled equation. Evolution of the rescaled solution all 2.5 time units.

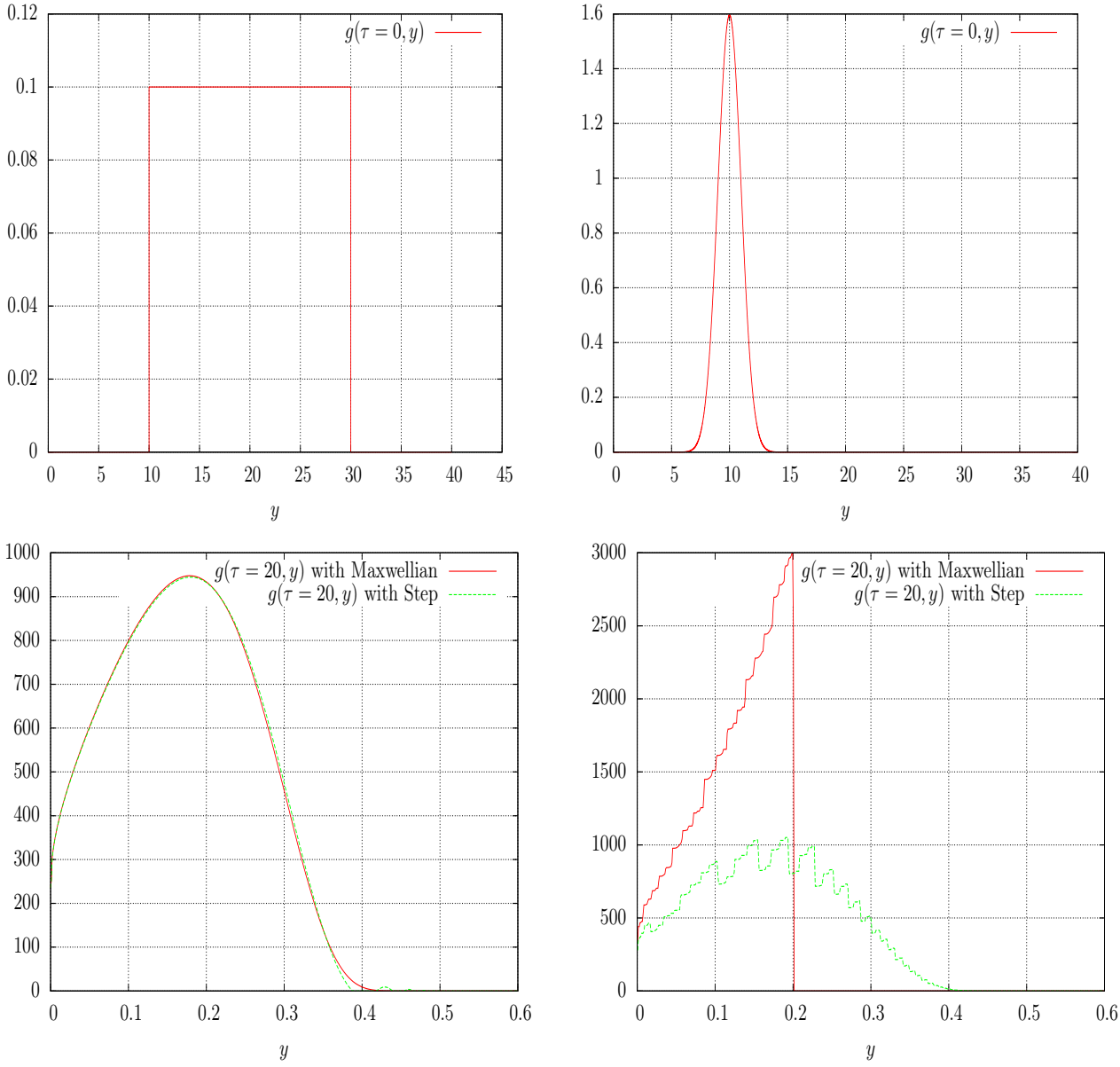

Figure 1.6 – Top left : Step initial function. Top right : Maxwellian initial function. Down left WENO5 : final rescaled solution with these two initial functions. Down right ADM : final rescaled solution with these two initial functions.

Furthermore, this simulation in rescaled variables, goes twice faster with the ADM scheme than with the WENO scheme (using the same CFL parameter as in [35]) despite the restriction imposed by the exponential stability condition.

Finally, we end the validation of the ADM scheme by imposing the analytic asymptotic profile (here with $p = 1$ see Fig.1.1) as initial condition and $d(\tau) = 2.05197$. The result reported in Fig. 1.7 shows that the solution is well-preserved by the scheme.

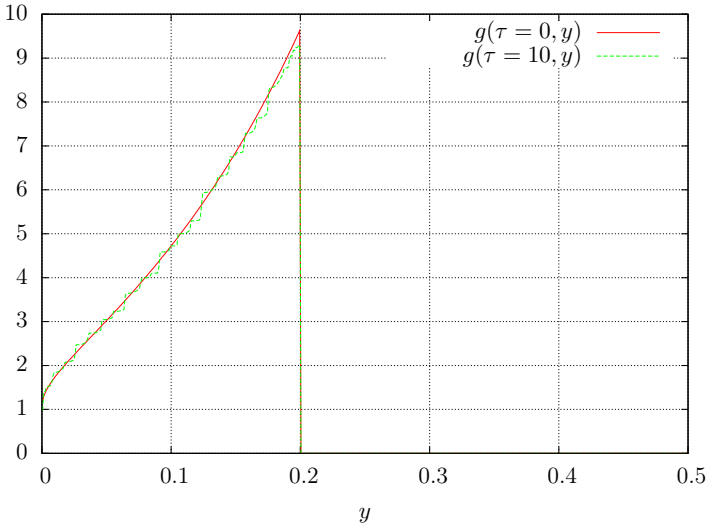

Figure 1.7 – ADM : behavior of the rescaled solution by starting with the analytic asymptotic profile for $p = 1$.

1.4 Treatment of the coagulation operator

In this Section we wish to investigate numerically how the coagulation term Q_{coag} modifies the asymptotic behavior of the solutions. To this end we need to incorporate in the time-splitting algorithm the treatment of the collision term. We first propose a "naive" approach where the integral operator is evaluated directly. As we shall see the computational cost of this method is quite heavy. Therefore, we adapt the treatment of coagulation terms introduced by F. Filbet and P. Laurençot [82]. The idea is to make from Q_{coag} the derivative of a flux $\partial_x J$ appear, which, in turn, can be naturally treated in a Finite Volume framework.

1.4.1 Direct evaluation of the coagulation term

We remind that $Q_{coag}(f) = Q^+_{coag}(f) - Q^-_{coag}(f)$ where

$$Q^-_{coag}(f) = f \times L(f), \qquad L(f) = \int_0^\infty f(t,y)\,\mathrm{d}y.$$

The PDE governing the size density is

$$\partial_t f + \partial_x(Vf) = \lambda Q^+_{coag}(f) - f \times \lambda L(f)$$

Then, the scheme splits into the following steps

– First, we solve the transport equation

$$\partial_t f + \partial_x(V(t,x)f) = 0.$$

Here, we assume that the monomers concentration does not change : $c(t)$ is replaced by c^n and we make use of either the WENO or the ADM scheme. It defines $f^{n+1/2}$. We write $f_k^{n+1/2} = f_k^n - \frac{\Delta t^{(n)}}{\Delta x}\left(V^n_{k+1/2} f^n_{k+1/2} - V^n_{k-1/2} f^n_{k-1/2}\right)$, and the fluxes $f^n_{k+1/2}$ are chosen according to the anti-dissipative method or the WENO scheme.

– Second we solve

$$\partial_t f(t,x) + \lambda L(f) \times f = \lambda Q^+_{coag}(f).$$

We adopt a semi-implicit viewpoint. We rewrite this equation as

$$\frac{\mathrm{d}}{\mathrm{d}t}\left[f \exp\left(\lambda \int_0^t L(f)(s)\,\mathrm{d}s\right)\right] = \exp\left(\lambda \int_0^t L(f)(s)\,\mathrm{d}s\right)\lambda Q^+_{coag}(f).$$

We integrate over a time step, assuming that $Q^+_{coag}(f)$ and $L(f)$ do not change on $(t^{(n)}, t^{(n+1)})$. We are led to the following formula

$$f_k^{n+1} = \exp\big(-\ell^{n+1/2}\Delta t^{(n)}\big) f_k^{n+1/2} + q_k^{n+1/2}\left(\frac{1-\exp(-\ell^{n+1/2}\Delta t^{(n)})}{\ell^{n+1/2}}\right)$$

where $q_k^{n+1/2}$ and $\ell^{n+1/2}$ correspond to the discrete version of the integral operators $\lambda Q^+_{coag}(f^{n+1/2})$ and $\lambda L(f^{n+1/2})$, the monomers concentration being still determined by c^n. The advantage of such a formula is that it naturally preserves the non non-negativity of the solution.

– We update the monomers concentration with

$$c(t) + \int_0^\infty x f(t,x)\,\mathrm{d}x = \rho.$$

We thus set

$$c^{n+1} = \rho - \Delta x \sum_{k\in\mathbb{N}} x_k f_k^{n+1}.$$

For the simulations, the data are given as follows

– the domain $[0, 2200]$ with 20 points by length unit,

– the initial function is

$$f^0(x) = \begin{cases} 0.1, & x \in [10,30], \\ 0, & \text{otherwise}, \end{cases} \tag{1.21}$$

– the total initial mass is $\rho = 41$ so that the initial monomers concentration is $c^0 = 1$.

We show in Fig. 1.8 and 1.9 a comparison between the ADM and 5th order WENO schemes ("asymptotic" profiles at the final time $t = 800$, and pictures of the evolution of the particles concentration each 75 time units). Here we have set $\lambda = 1/100$. We observe a remarkable agreement between the two methods. However, the ADM run is faster by a factor 2. Then we do not observe any numerical interference between the discretization of the transport term and the treatment of the coagulation term. Since the ADM scheme has better performances, we shall use it for further simulations.

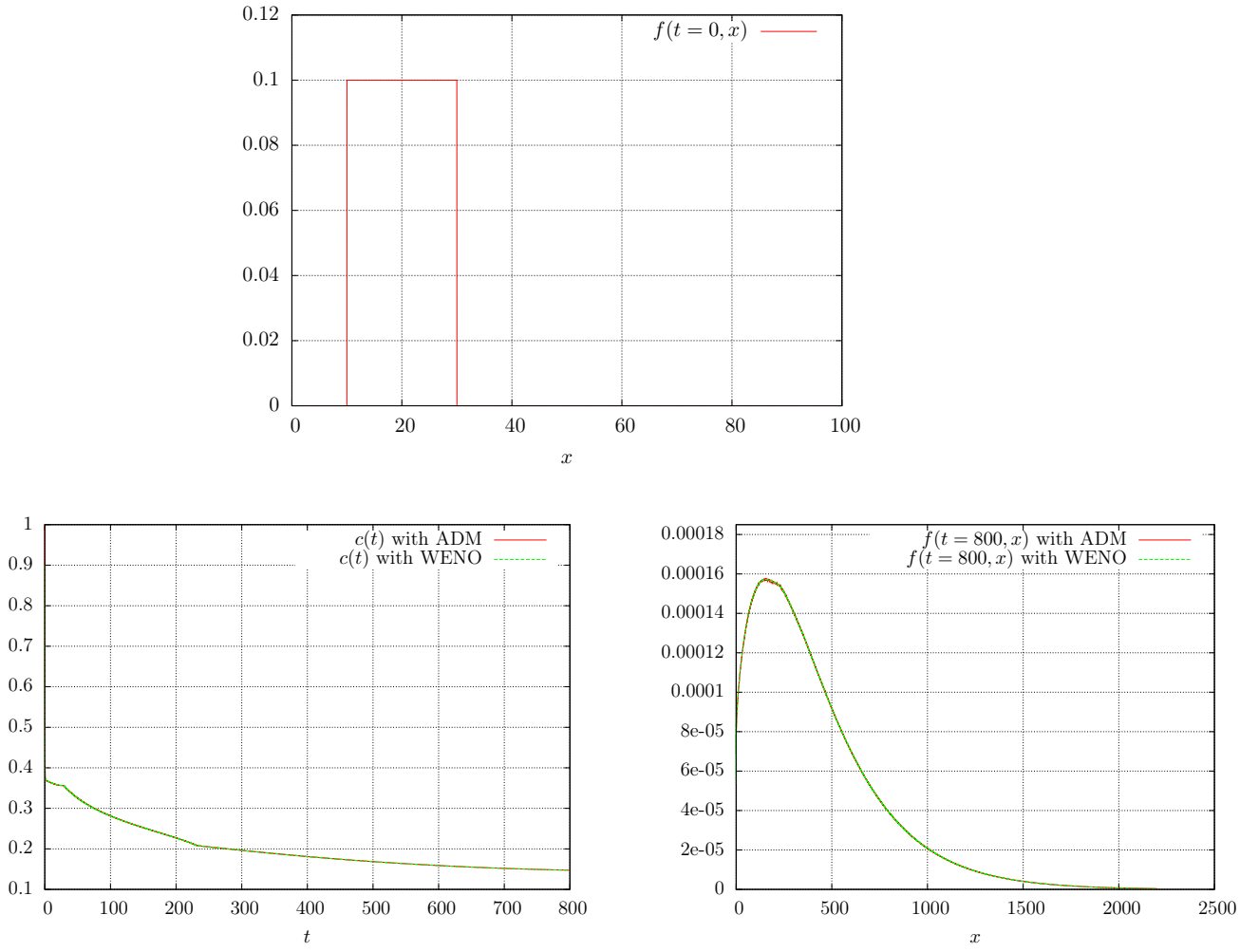

Figure 1.8 – Comparison WENO vs. ADM on the equation with encounters. Top : step initial function. Down left : evolution of monomers concentration. Down right : final solution at time $t = 800$ with $\lambda = 1/100$.

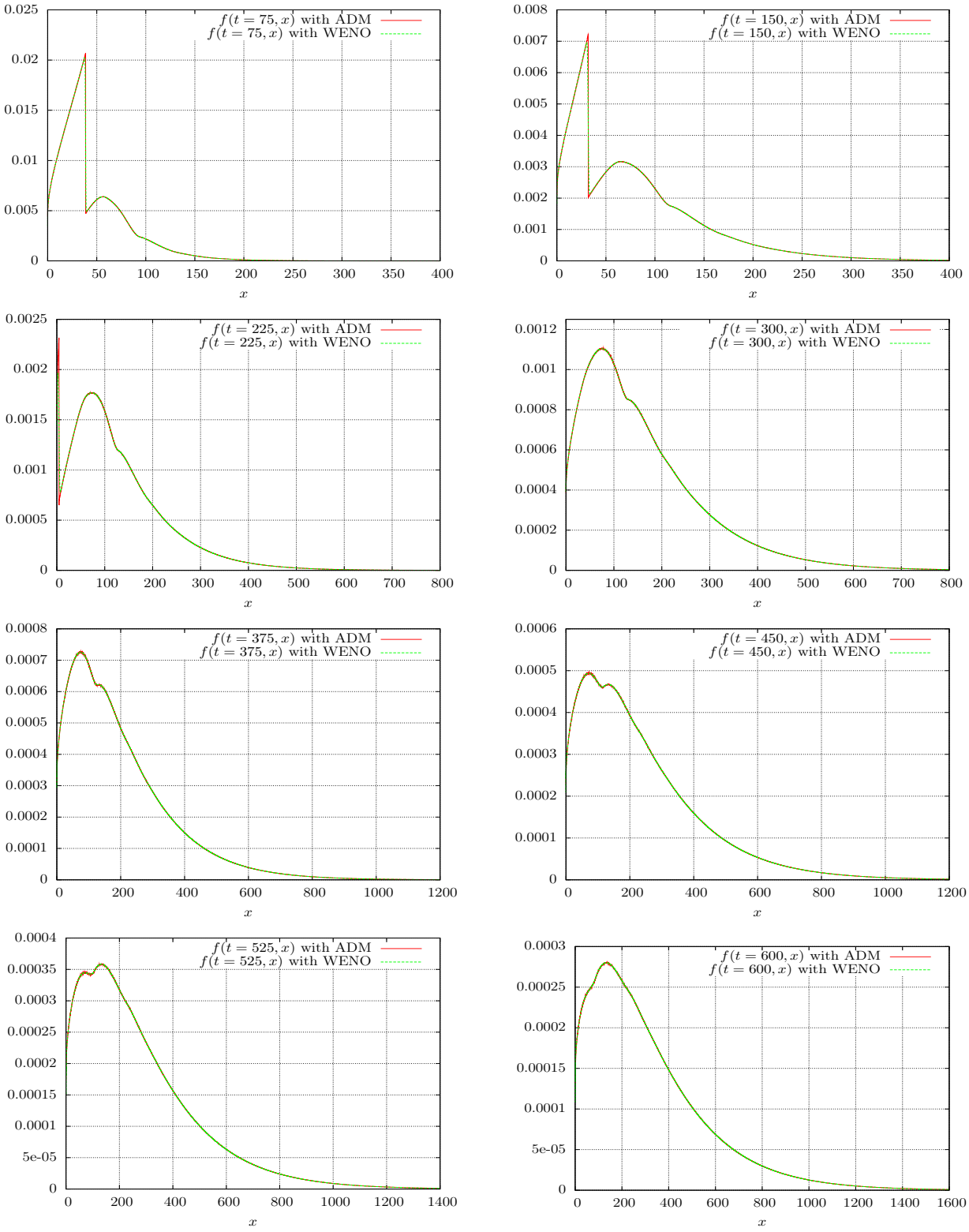

Figure 1.9 – Comparison WENO vs. ADM on the equation with encounters. Evolution of the solution all 75 time units with $\lambda = 1/100$.

Next, we compare the evolution when we start from different initial data : we consider the step function and the following Maxwellian distribution

$$f^0(x) = \frac{4}{\sqrt{2\pi}} \exp\left(-\frac{(x-10)^2}{2}\right). \tag{1.22}$$

All the other parameters are kept the same, and we work with the ADM scheme. Results are displayed in Fig. 1.10. The noticeable point is that now the shapes of the solutions look equally smooth after 800 time units. Comparing the time evolution in Fig. 1.9 (step function) we can see that the regularizing effects come from the largest particles and propagate to smooth out the front.

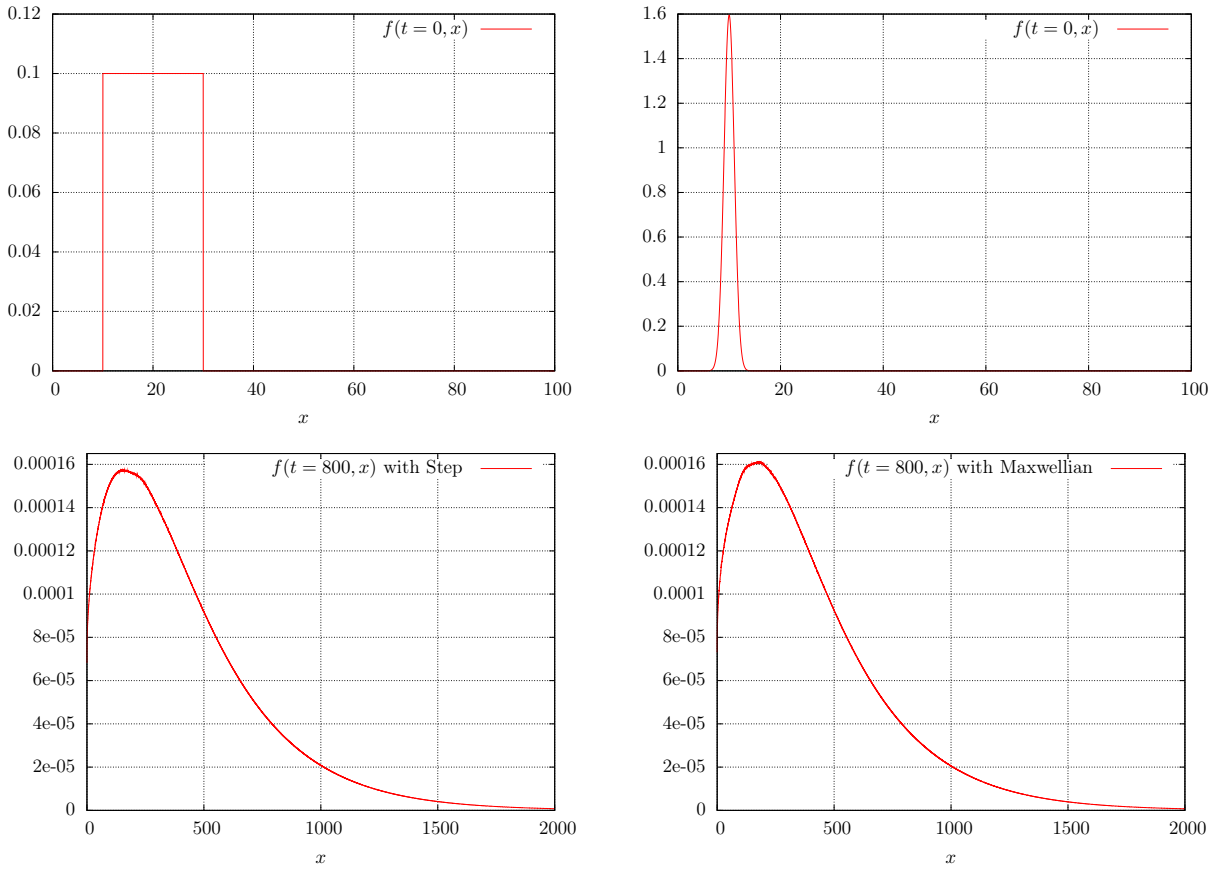

Figure 1.10 – ADM scheme for the equation with encounters for $\lambda = 1/100$: Top left : step initial function. Top right : Maxwellian initial function. Down left : solution corresponding to the step initial function. Down right : solution corresponding to the Maxwellian initial function.

Finally, we make the parameter λ vary : as it increases, the influence of the coagulation is more important. As λ becomes close to 1 we need a extended computational domain to keep accurate simulations : indeed, due to the convolution operator, the support of the solution spreads out and larger particles have to be considered as λ increases. For example with $\lambda = 1/10$ we work with the domain $[0, 6000]$ and 10 points by unit length, see Fig. 1.11 and 1.12. The rate of convergence towards the asymptotic profile seems to be highly dependent on the coefficient λ : the larger λ, the faster the convergence.

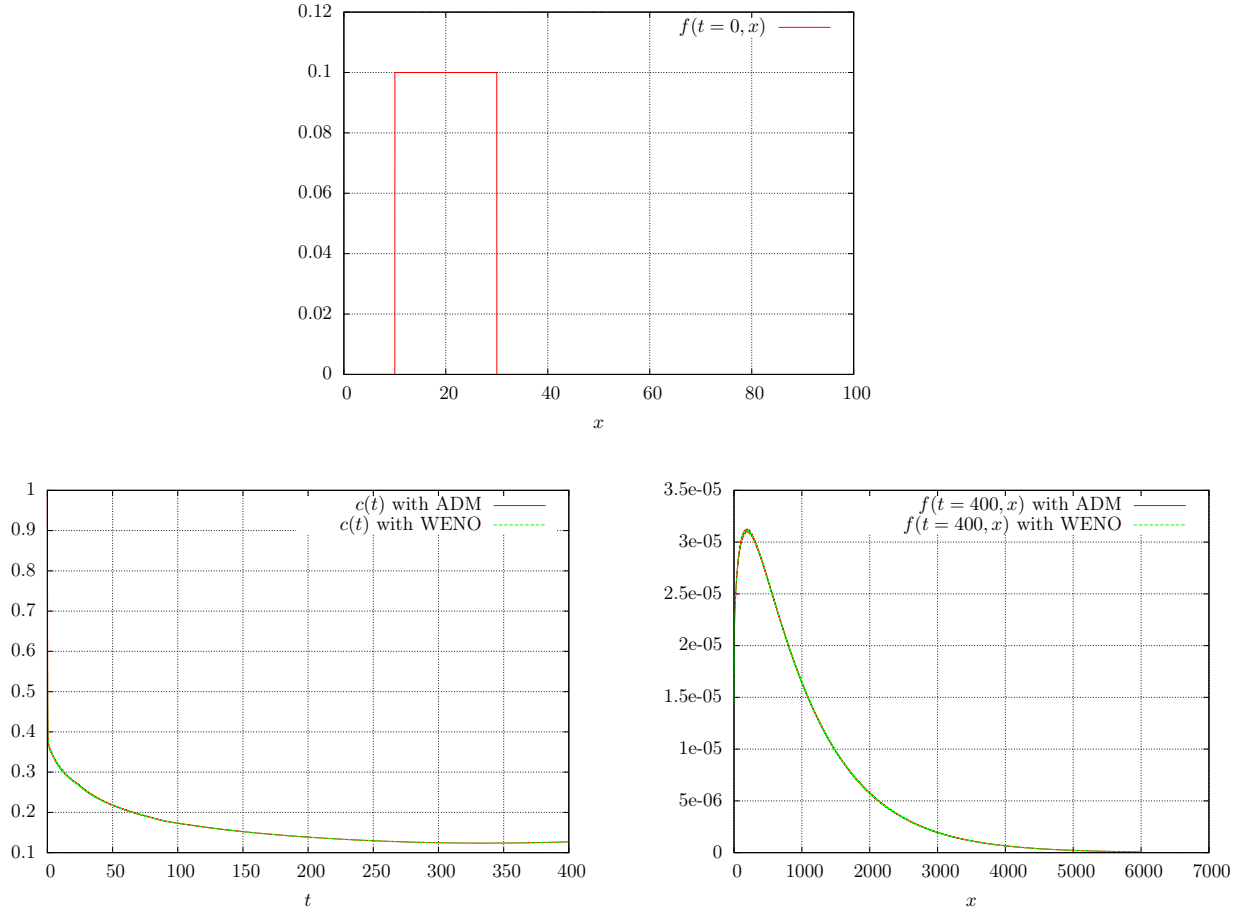

Figure 1.11 – Comparison WENO vs. ADM on the equation with encounters. Top : step initial function. Down left : evolution of monomers concentration. Down right : final solution at time $t = 800$ with $\lambda = 1/10$.

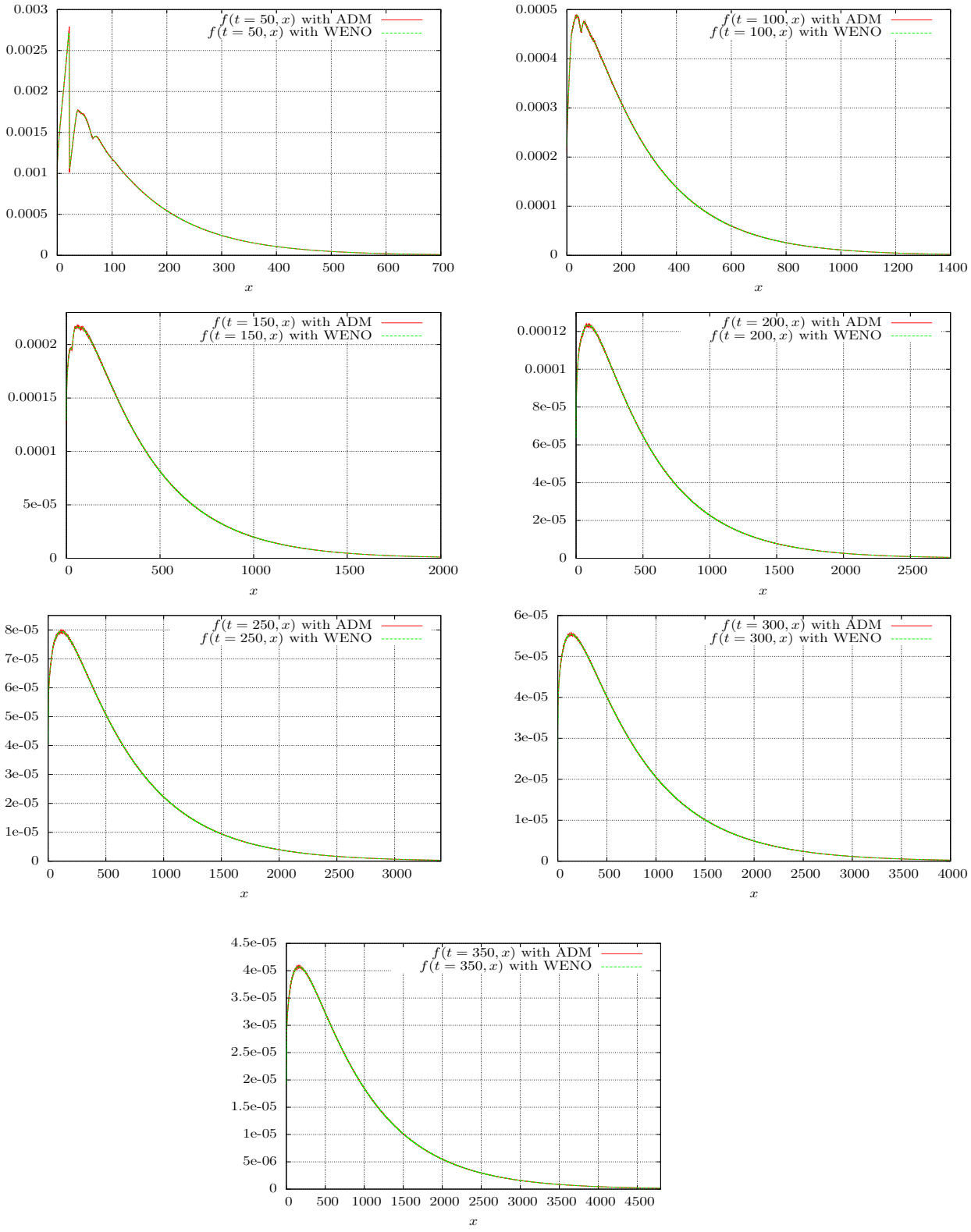

Figure 1.12 – Comparison WENO vs. ADM on the equation with encounters. Evolution of the solution all 50 time units with $\lambda = 1/10$.

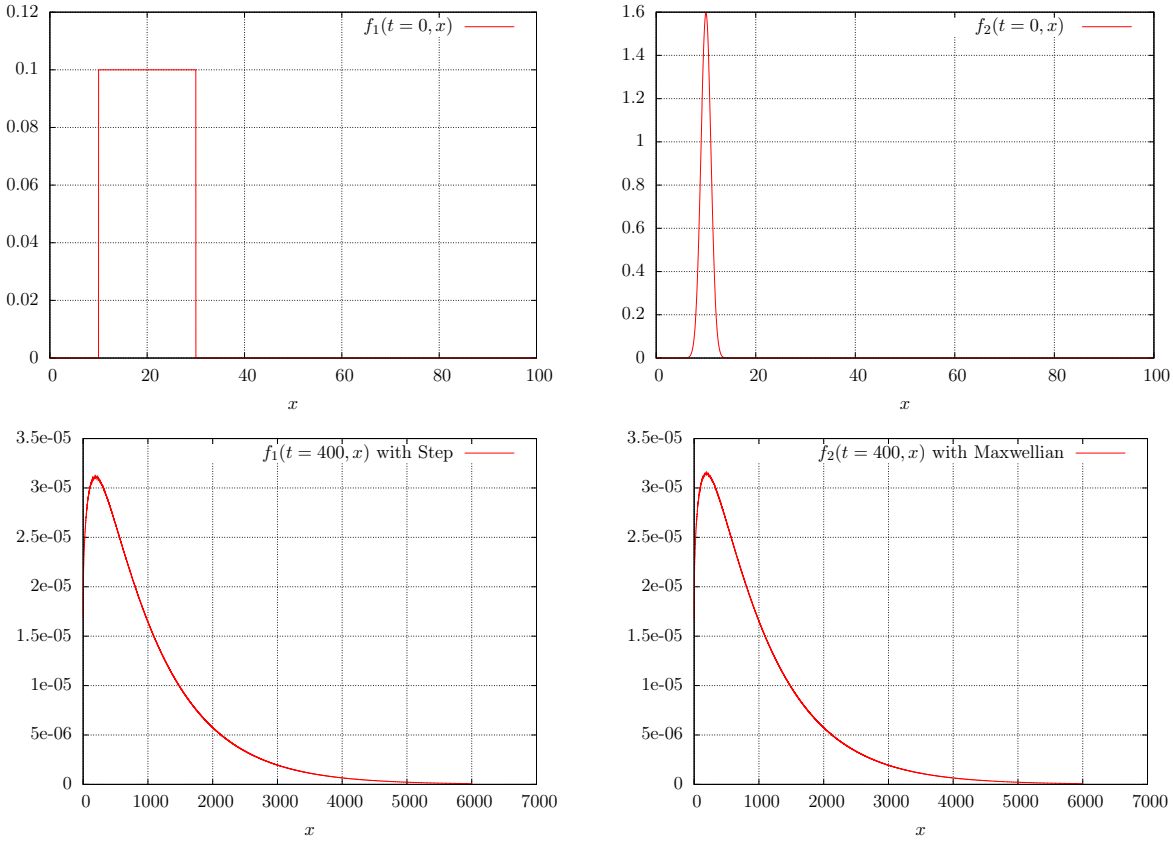

Figure 1.13 – ADM scheme for the equation with encounters for $\lambda = 1/10$: Top left : step initial function. Top right : Maxwellian initial function. Down left : solution corresponding to the step initial function. Down right : solution corresponding to the Maxwellian initial function.

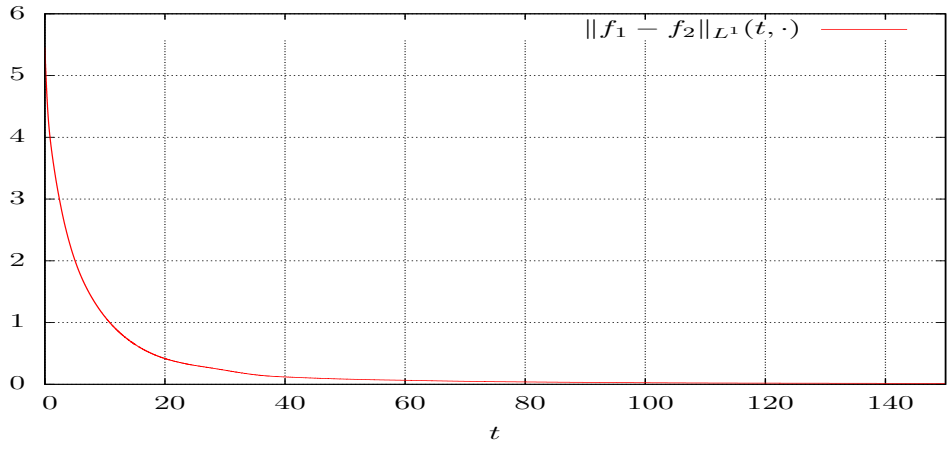

Figure 1.14 – Relaxation velocity : L^1 norm of the time evolution of the two solutions f_1 and f_2 for $\lambda = 1/10$. It behaves like $5.13\exp(-\frac{x^{3/4}}{4})$.

Simulation of the model with encounters in rescaled variables
We switch to the system (1.6) written in rescaled coordinates. Hence, the time-splitting adapts as follows

– First, we solve

$$\partial_\tau g + \partial_y(Wg) = g,$$

with fixed monomers concentration d^n. We use the ADM scheme and it defines $g^{n+1/2}$ as follows

$$g_k^{n+1/2} = (1+\Delta\tau^{(n)})g_k^n - \frac{\Delta\tau^{(n)}}{\Delta x}\big(W_{k+1/2}^n g_{k+1/2}^n - W_{k-1/2}^n g_{k-1/2}^n\big)$$

– Second, we consider the collision terms which leads to consider the following ODE

$$\partial_\tau g(\tau,y) + \lambda L^r(g)g(\tau,y) = \lambda Q_{coag}^{r+}(g)(\tau,y)$$

where

$$L^r(g) = \int_0^\infty g(y)\,\mathrm{d}y \quad \textit{and} \quad Q_{coag}^{r+}(g) = \frac{1}{2}\int_0^y g(y-u)g(u)\,\mathrm{d}u.$$

We adopt a semi-implicit viewpoint to solve

$$\partial_\tau g(\tau,y) + \ell^r g = q^r,$$

or, in other words, we set

$$g_k^{n+1} = g_k^{n+1/2}\exp(-\ell^{r,n+1/2}\Delta\tau^{(n)}) + q_k^{r,n+1/2}\left(\frac{1-\exp(-\ell^{r,n+1/2})\Delta\tau^{(n)})}{\ell^{r,n+1/2}}\right)$$

where $q_k^{r,n+1/2}$ and $\ell^{r,n+1/2}$ correspond to the approximation of $\lambda Q_{coag}^{r+}(g)$ and $\lambda L^r(g)$ respectively, defined with $g^{n+1/2}$ and d^n.

– Finally, we use the mass constraint

$$d(\tau)\exp(-\tau/3) + \int_0^\infty y g(\tau,y)\,\mathrm{d}y = \rho,$$

which yields

$$d^{n+1} = \Big(\rho - \sum_{k=0}^{K} y_k\, g_k^{n+1}\,\Delta y\Big)\exp\big(t^n/3\big).$$

We perform the simulation of the rescaled equation with encounters considering the following data :

– We bear in mind that considering the coagulation terms, we lose the support property of the solution in rescaled variables. Indeed, Q^+ and L are integral operators and they act like a convolution so that the support of the stationary solution is expected to fill the whole line $y \geq 0$: the main part of the information is likely contained in a bounded domain but the effect of the tail can be important, see [124, 104]. Accordingly, the definition of the computational domain is very sensitive, as already shown in original variables, to the value of the parameter λ. Then we choose the domain $[0, 100]$ with 200 points by unit length for $\lambda = 1/100$ and for $\lambda = 1/10$ we choose the domain $[0, 150]$ with 200 points by unit length.
– the total initial mass $\rho = 41$ is chosen so that the initial monomers concentration is $d^0 = 1$.

In figure Fig. 1.15 we compare the solutions associated to a Maxwellian initial data or a step function with $\lambda = 1/100$. Of course the remarkable fact is that $d(\tau)$ tends to the same constant, which however differs from $K_{LS} \simeq 1.88988$, while the solutions have a very similar profile at $\tau = 12$. We can expect that the stationary solution has an infinite support and we indeed observe that large particles should be considered compared to the compactly supported profiles of the collisionless equation. We see on Fig. 1.15 and 1.16 the time evolution of the particles distributions, where we can observe the regularizing effects due to the collision term and the spreading of the support. All these effects appear similarly when we make λ vary, see for instance Fig. 1.16. We remark that the asympotic value of d depends on λ. However our numerical investigation shows that letting λ go to 0, the large time value of $d(\tau)$ tends to K_{LS}.

1.4.2 (Conservative) Finite Volume approximation of the coagulation term

In this Section we propose another method to evaluate the coagulation operator, inspired from [82]. Let us remind how the scheme of F. Filbet and P. Laurençot [82] works when dealing with

$$\partial_t f = \lambda Q_{coag}(f).$$

The starting point of the method consists in rewriting the problem as follows

$$x\partial_t f(t,x) = \lambda\, xQ_{coag}(f)(t,x) = -\lambda \partial_x J(f),$$

where

$$J(f)(t,x) = \int_0^x \int_{x-u}^{\infty} uf(t,u)f(t,v)\,\mathrm{d}v\,\mathrm{d}u.$$

The next step relies on the approximation of the integrals that define $J(f)$ and the necessary truncation, embodied into a parameter $0 < R < \infty$, of the infinite integration domain. In [82] two approaches are designed :

– The "conservative method", which consists in replacing $J(f)$ by

$$J^R_{coag}(f)(t,x) = \int_0^x \int_{x-u}^{R-u} uf(t,u)f(t,v)\,\mathrm{d}v\,\mathrm{d}u$$

for $0 < x < R < \infty$. We remark that $J^R_{coag}(f)(t,R) = J^R_{coag}(f)(t,0) = 0$. Consequently, the solution f_R of

$$x\partial_t f_R(t,x) = -\lambda \partial_x J^R_{coag}(f_R) \qquad t \geq 0,\ 0 \leq x \leq R < \infty$$

satisfies the preservation of the first order moment :

$$\int_0^R x f_R(t,x)\,\mathrm{d}x = \int_0^R x f_R(0,x)\,\mathrm{d}x.$$

– The "non-conservative method" where we set

$$J^R_{nc}(f)(t,x) = \int_0^x \int_{x-u}^{R} uf(t,u)f(t,v)\,\mathrm{d}v\,\mathrm{d}u,$$

for $0 < x < R < \infty$. Again, we have

$$x\partial_t f_R(t,x) = -\lambda \partial_x J^R_{nc}(f_R)$$

but now the first moment of f_R is non increasing.

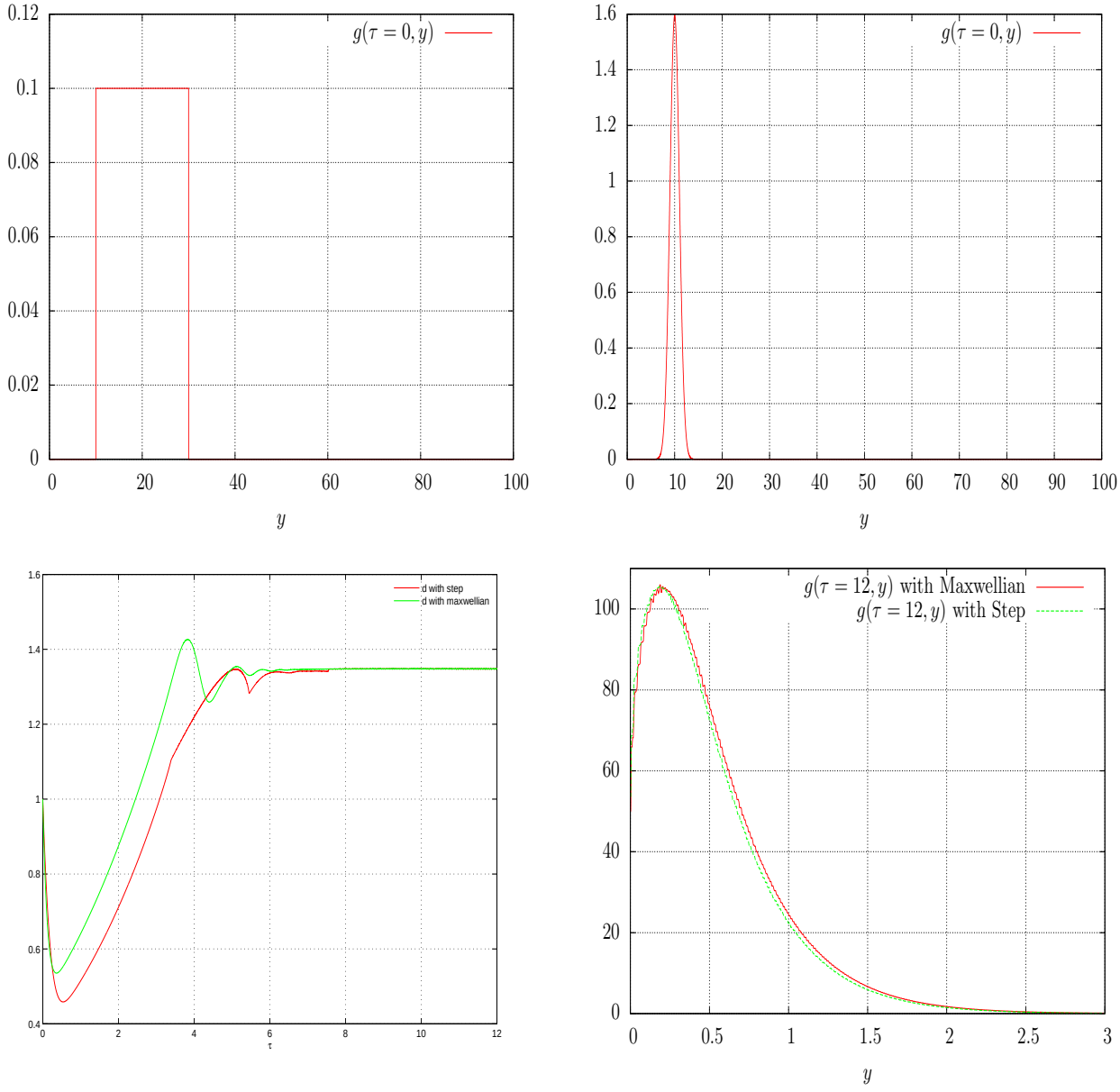

Figure 1.15 – ADM scheme for the equation with encounters for $\lambda = 1/100$: Top left : step initial function. Top right : Maxwellian initial function. Down left : evolution of $d(\tau)$. Down right : evolution of the density of particles.

We refer to [82] for a thorough analysis of the method and in particular for convergence analysis as $R \to \infty$, which typically holds under sublinear growth assumption on the coagulation kernel (see also [70, 131]). The problem addressed in [82] is essentially concerned with the capture of the gelation phenomenon, that is a loss of mass in finite time, a typical feature of certain coagulation equations. Here, the situation is different and it turns out that the conservation of the first moment by the encounters process is crucial for the accuracy of the scheme and the evaluation of the monomers concentration in the last step of the splitting. For this reason, we work here with the conservative method.

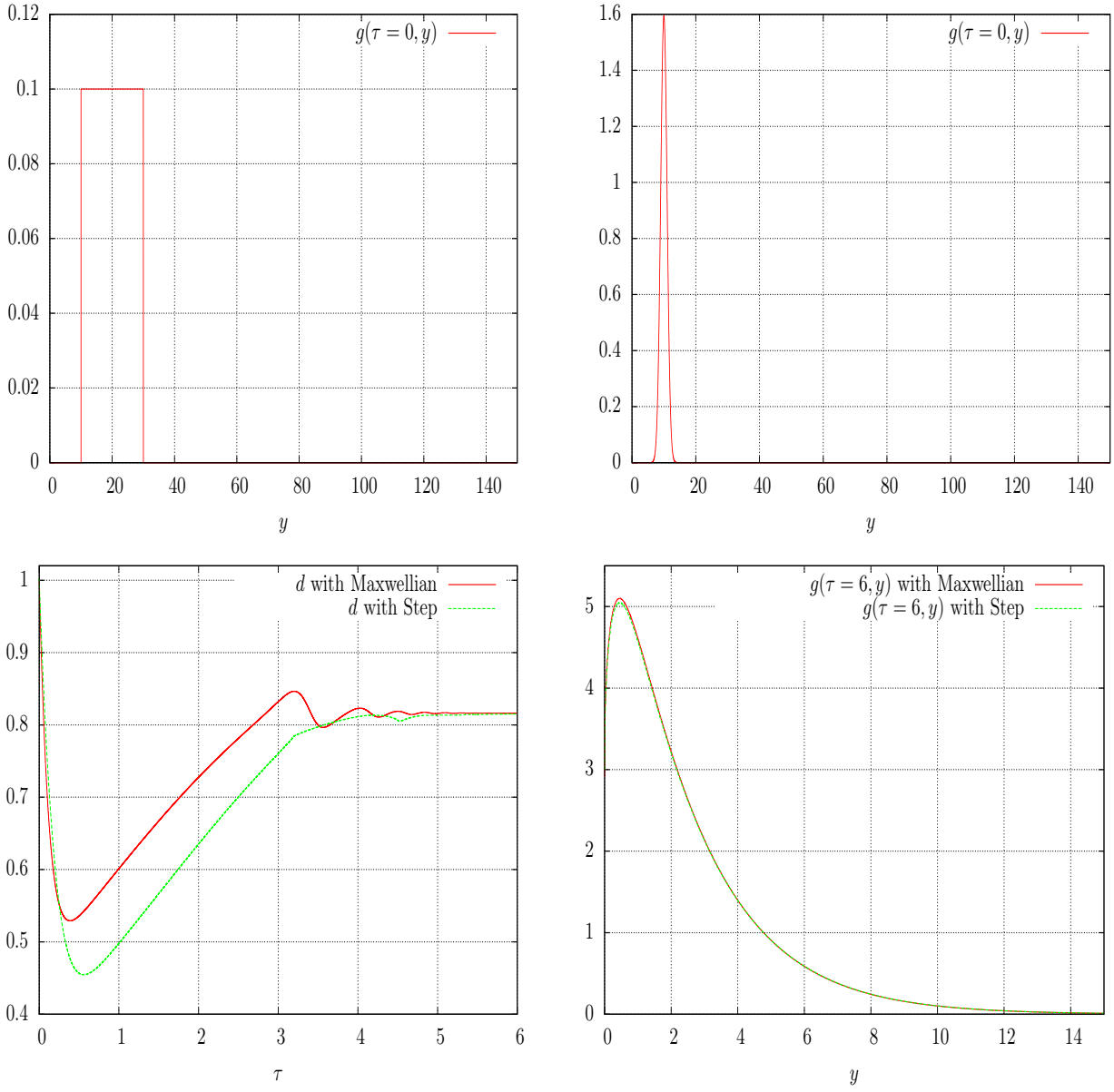

Figure 1.16 – ADM scheme for the equation with encounters for $\lambda = 1/10$: Top left : step initial function. Top right : Maxwellian initial function. Down left : evolution of $d(\tau)$. Down right : evolution of the density of particles.

To obtain the discrete expression of the operator J^R_{coag} it is convenient to introduce the change of variables $w = u + v$ so that J^R_{coag} recasts as

$$J^R_{coag}(f)(t,x) = \int_0^x \int_x^R u f(t,u) f(t,w-u)\,\mathrm{d}w\,\mathrm{d}u.$$

Recall that $x_k = (k+1/2)\Delta x$, for $k \in \{0,..,k_M-1\}$ where $k_M = R/\Delta x$ is the number of cells. We use the following approximation

$$J^R_{coag}(f)^n_{k+1/2} = \sum_{j=0}^{k}\sum_{l=k}^{K} x_j f^n_j \, f^n_{l-j} \, \Delta x^2 \tag{1.23}$$

with the boundary condition $J^R_{coag}(f)^n_{1/2} = J^R_{coag}(f)^n_{k_M-1/2} = 0$. Then, the time-splitting is organized as follows :

– First, we solve on a time step

$$\partial_t f + \partial_x(Vf) = 0.$$

To this end, we make use of the ADM scheme by assuming that the monomers concentration does not change : $c(t)$ is replaced by c^n. It defines $f^{n+1/2}_k$ as follows

$$f^{n+1/2}_k = f^n_k - \frac{\Delta t^{(n)}}{\Delta x}\big(V^n_{k+1/2} f^n_{k+1/2} - V^n_{k-1/2} f^n_{k-1/2}\big).$$

– Second, we solve

$$\partial_t(xf) = -\lambda \partial_x J^R_{coag}(f)$$

We are led to the following formula

$$x_k f^{n+1}_k = x_k f^{n+1/2}_k - \lambda \frac{\Delta t^{(n)}}{\Delta x}\big(J^{n+1/2}_{k+1/2} - J^{n+1/2}_{k-1/2}\big)$$

where the numerical flux $J^n_{k+1/2}$ is the approximation $J^R_{coag}(f)^n_{k+1/2}$.

– We update the monomers concentration by $\quad c^{n+1} = \rho - \sum_{k=0}^{K} x_k f^{n+1}_k \Delta x.$

We consider the same data as when dealing with the "naive" approach for the problem with coagulation in original variables. It allows to compare the two methods. The decisive advantage for the conservative Finite Volume approximation of the coagulation term relies on the fact that it does not need a very large computational domain. In turn, the computation is definitely less costly.

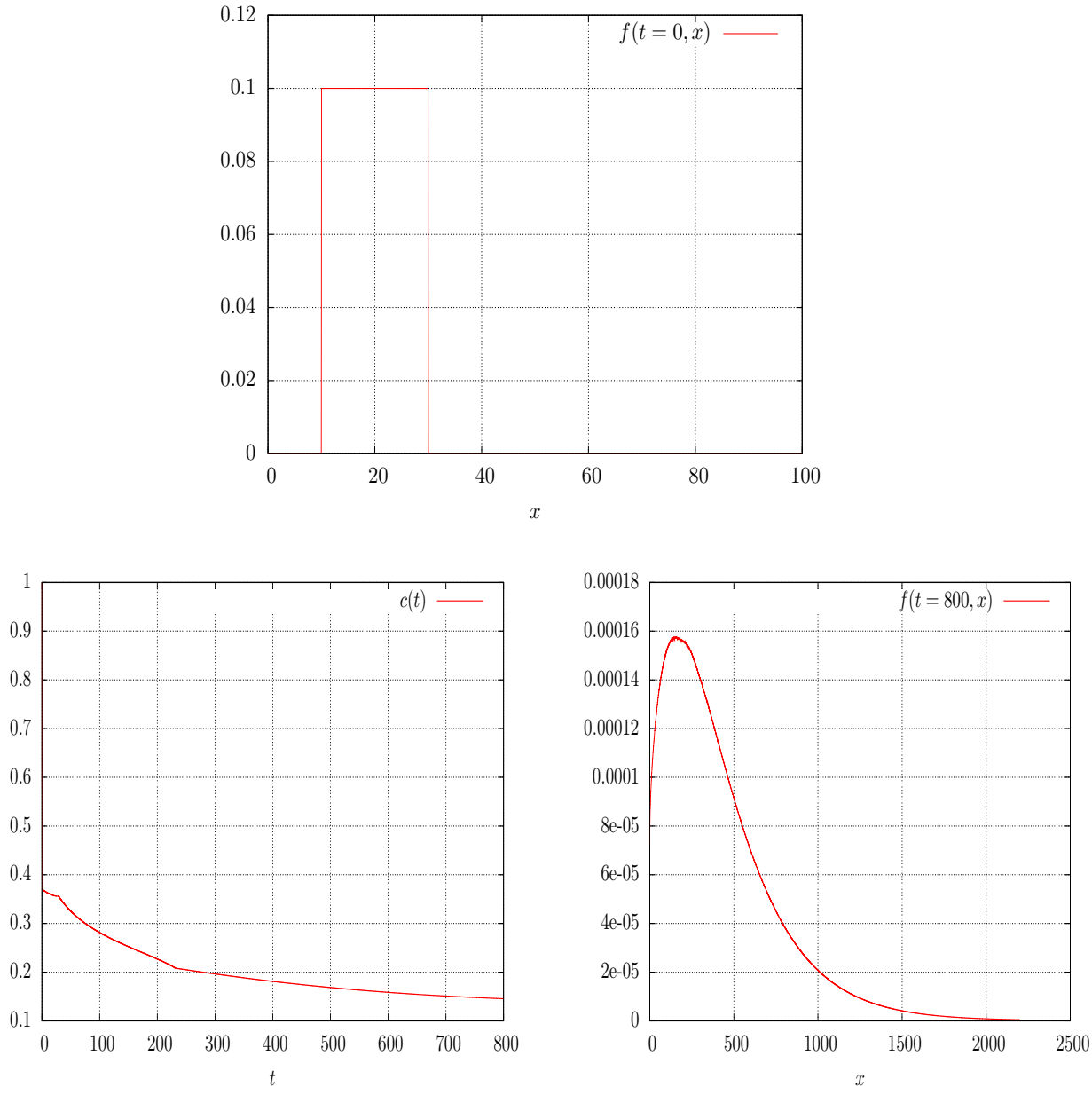

Figure 1.17 – ADM+Filbet-Laurençot approach for encounters with $\lambda = 1/100$. Top : step initial function. Down left : evolution of monomers concentration. Down right : final solution at time $t = 800$.

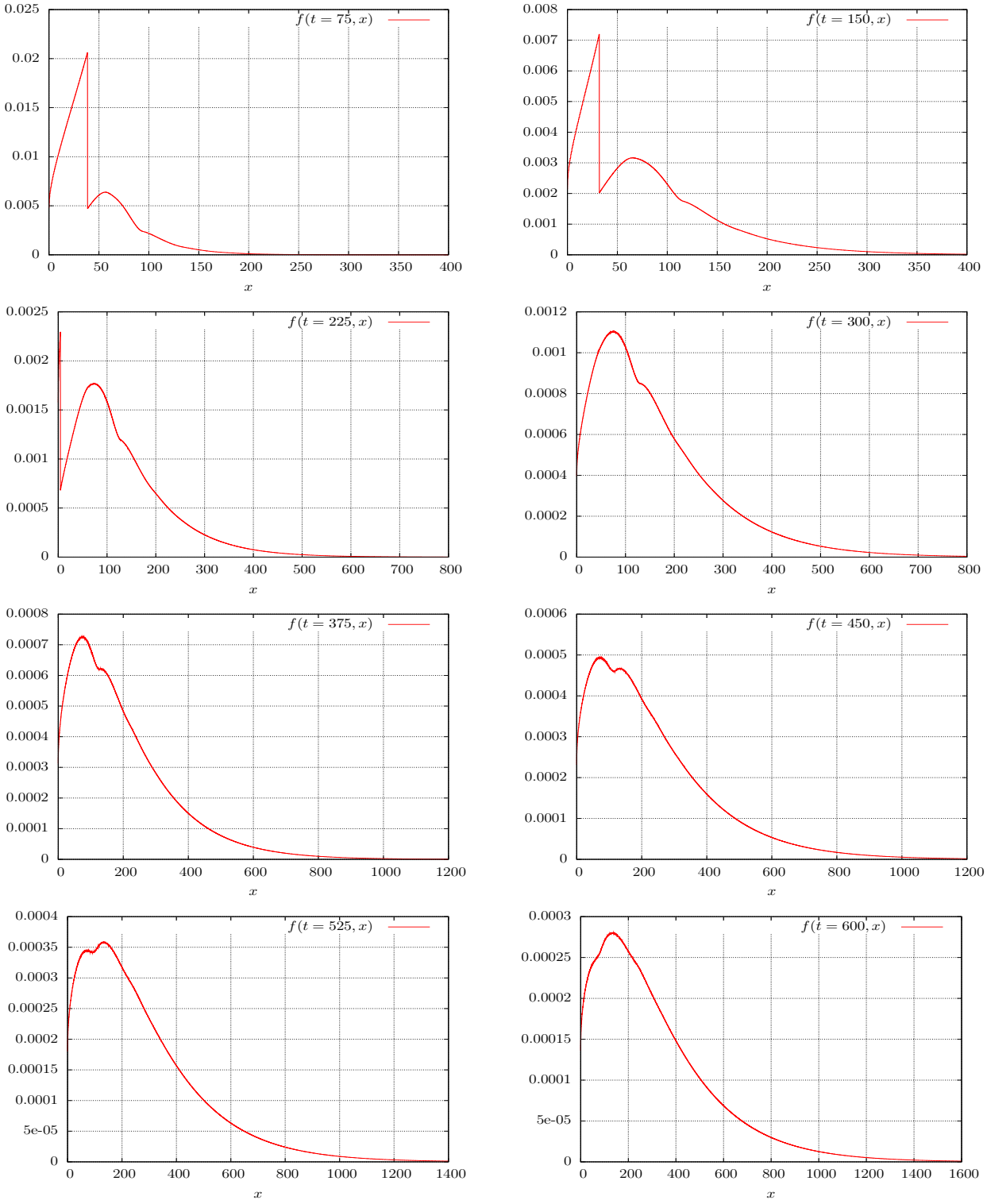

Figure 1.18 – ADM+Filbet-Laurençot approach for encounters with $\lambda = 1/100$. Evolution of the solution all 75 time units.

The numerical results obtained with the Filbet -Laurençot approach in Fig.1.17, 1.18 are very close to the corresponding results based on the "naive" approach in Fig. 1.8 and 1.9. The numerical results show again the regularizing effect of the encounters in the asymptotic behavior of the model. For instance, Fig. 1.20 compares the solutions starting form the step and the Maxwellian initial data, as in Fig.1.11.

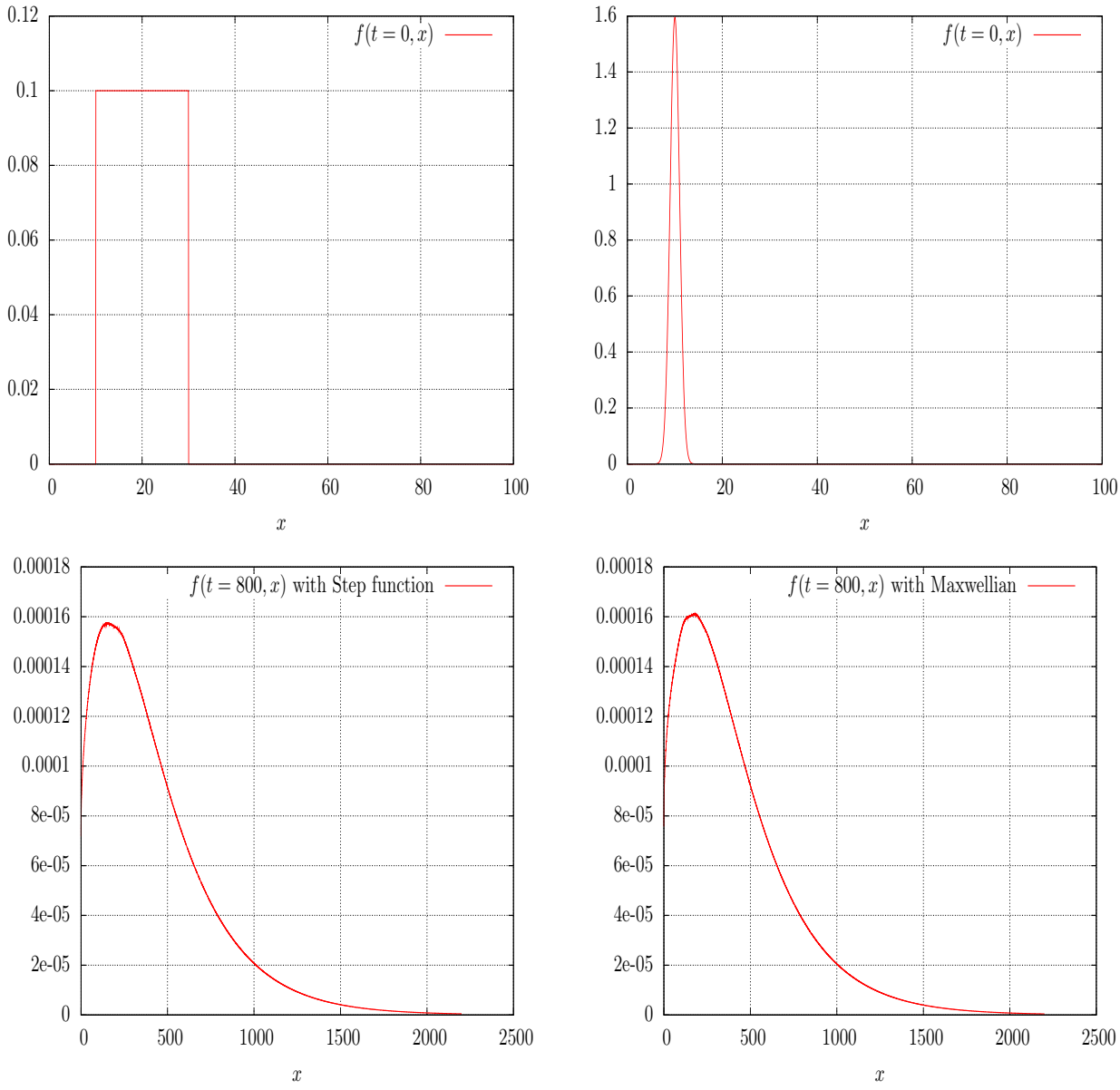

Figure 1.19 – ADM+Filbet-Laurençot approach for encounters with $\lambda = 1/100$. Top left : step initial function. Top right : Maxwellian initial function Down left : solution corresponding to the step initial function. Down right : solution corresponding to the Maxwellian initial function.

Numerical study in rescaled variables with coagulation operator in conservative form

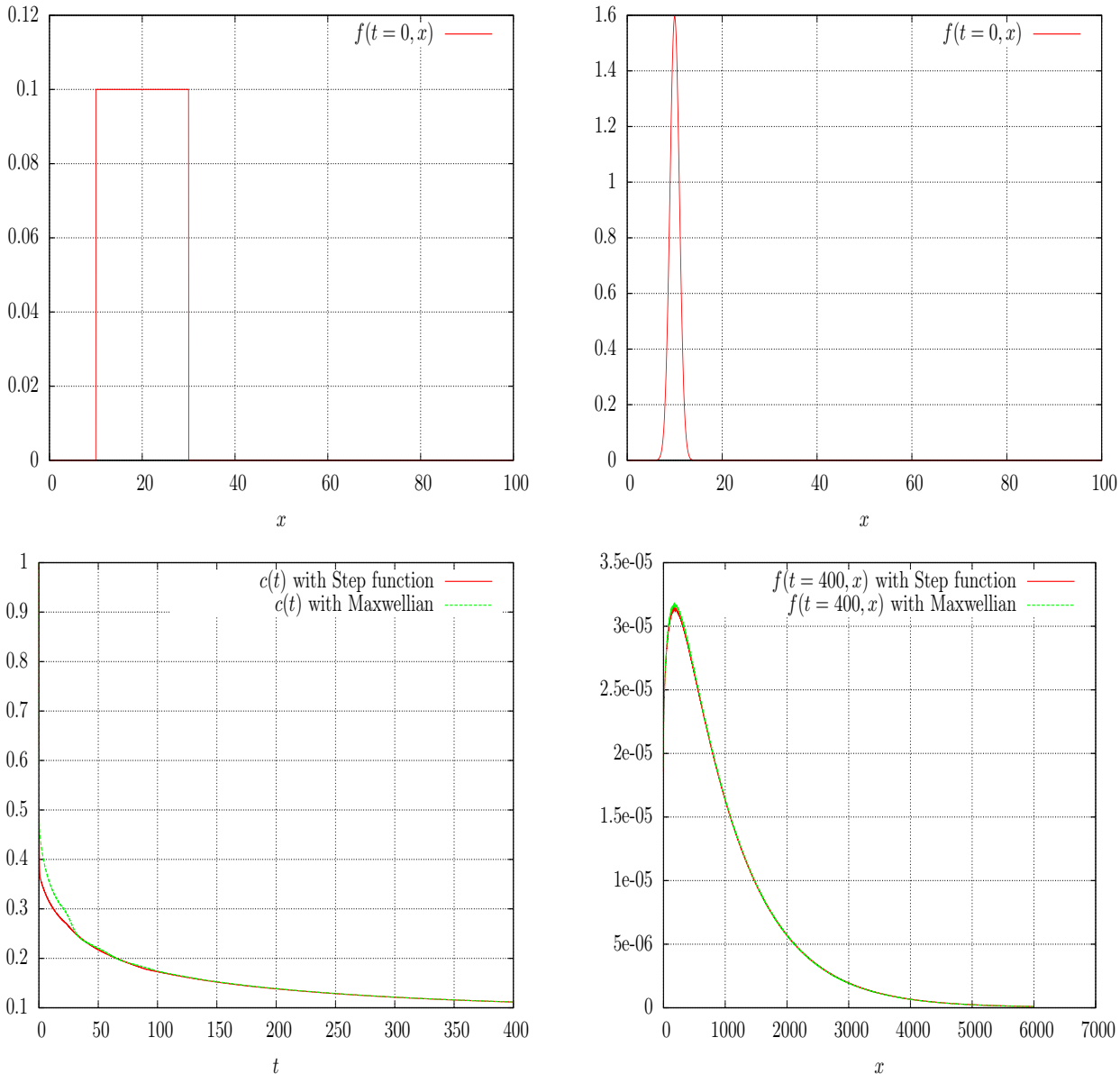

Figure 1.20 – ADM+Filbet-Laurençot approach for encounters with $\lambda = 1/10$. Top left : step initial function. Top right : Maxwellian initial function Down left : evolution of monomers concentration with the two initial functions. Down right : final solution at time $t = 400$ with the two initial functions.

In rescaled variables the system reads

$$\begin{cases} \partial_\tau g + \partial_y(Wg) = g(\tau, y) + \lambda Q^r_{coag}(g), & \tau \geq 0,\ y \geq 0, \\ d(\tau)\exp(-\tau/3) + \displaystyle\int_0^\infty y g(\tau, y)\,\mathrm{d}y = \rho, & \tau \geq 0, \\ g(0, y) = g^0(y),\ y \geq 0; \qquad W(\tau, y) = y^{1/3} d(\tau) - 1 - y, & \tau \geq 0,\ y \geq 0, \end{cases}$$

where ρ is a constant. We proceed as previously with the following time splitting :
- $\partial_\tau g + \partial_y(Wg) = g(\tau, y)$,
- $\partial_\tau g = \lambda Q^r_{coag}(g)$.

The fundamental point consists in transforming this last equation in the conservative flux form as above. As it is straightforward and we omit the details.

Simulation in rescaled variables with coagulation operator in conservative form
The data are defined as follows :
- The length domain is $[0, 40]$ with 1000 points by unit length what means $\Delta x = 4.10^{-2}$.
- The initial function is
$$g^0(x) = \begin{cases} 0.1 & x \in [10, 30], \\ 0 & x > 30. \end{cases}$$
- The total initial mass $\rho = 41$ is chosen so that the initial monomers rescaled concentration is $d^0 = 1$.

Results are displayed in Fig. 1.21 for the parameter $\lambda = 1/100$ and in Fig. 1.22 for $\lambda = 1/10$.

The results confirm what has been said above. Using the conservative approach for the coagulation term allows to keep a reduced computational domain, and thus preserves the computational cost. The effect of the coagulation term is again to smooth out the profile.

1.5 Conclusion

We discuss on numerical grounds several aspects of the Lifshitz-Slyozov system. To this end, we introduce a new scheme for the the colisionless model : based on anti-diffusive strategies, the scheme captures the singular profiles exhibited by the system in large times, and it outperforms other methods used to address the problem. Next, we investigate the effects of the addition of a coagulation term in the equation. Results should be considered cautiously and they have a purely experimental status but the preliminary study indicates that the coagulation operator can have a regularizing effect, which in turn can dictate the selection of the smooth profile predicted by Lifshitz-Slyozov. We wish this work will be a source of inspiration for further analysis of this challenging problem.

Acknowledgements

We thank J. A. Carrillo for many advices on the WENO code used in [35]. We are also gratefully indebted to P. Lafitte who pointed to our attention ref. [82] and for warm and constant encouragements.

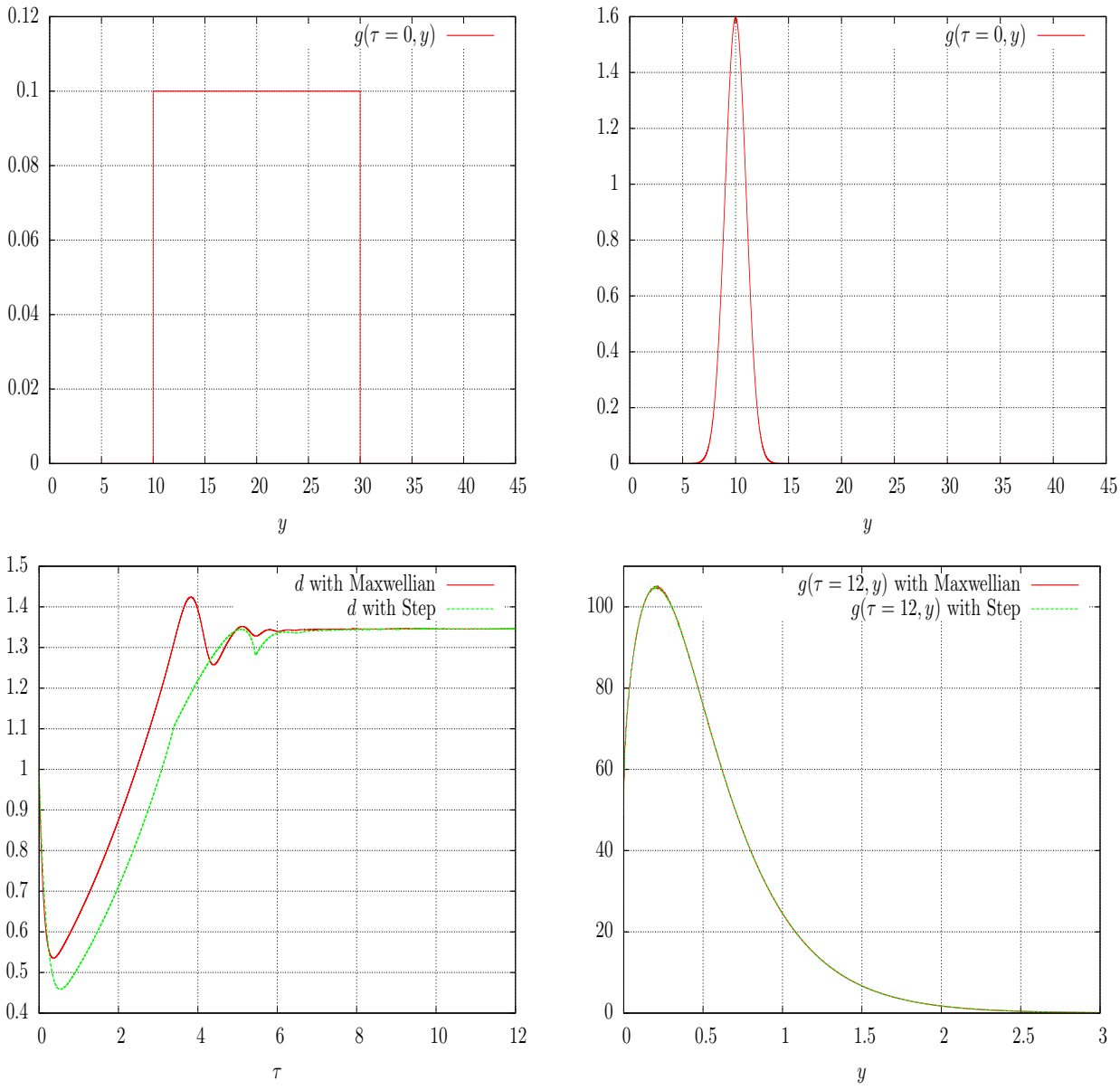

Figure 1.21 – ADM+Filbet-Laurençot approach for encounters in rescaled variables with $\lambda = 1/100$. Top left : step initial function. Top right : Maxwellian initial function. Down left : evolution of $d(\tau)$. Down right : evolution of the density of particles, at time $\tau = 12$.

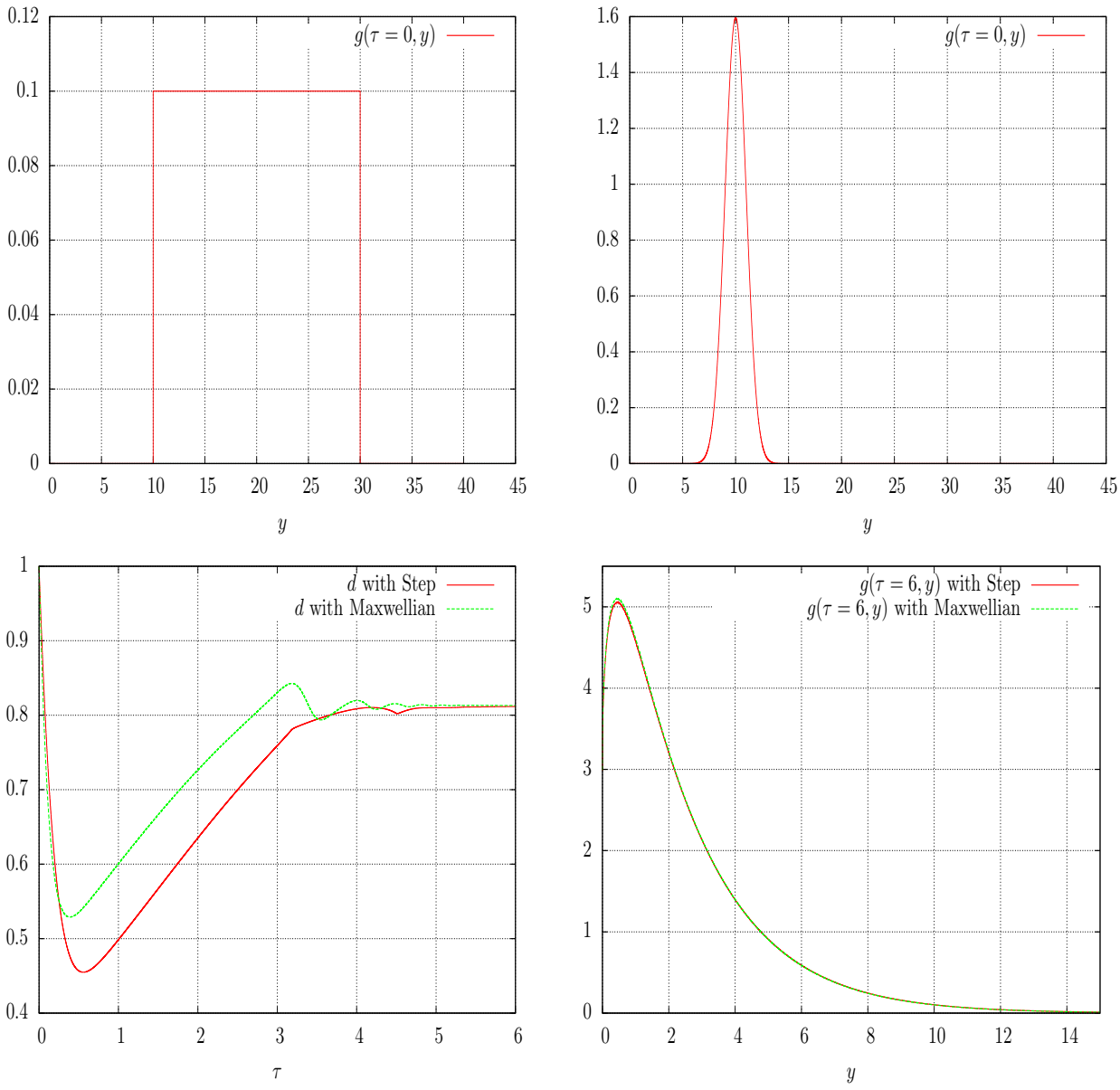

Figure 1.22 – ADM+Filbet-Laurençot approach for encounters in rescaled variables with $\lambda = 1/10$. Top left : step initial function. Top right : Maxwellian initial function. Down left : evolution of $d(\tau)$. Down right : evolution of the density of particles.

Chapitre 2

Équations de Lifshitz-Slyozov avec diffusion spatiale des monomères

Dans le chapitre précédent nous avons étudié le système d'équations de Lifshitz-Slyozov standard modélisant de façon spécifique l'immersion d'une population structurée en taille de macro-particules dans un bain de monomères caractérisé par sa concentration. Dans ce présent chapitre, nous proposons une extension de ce modèle standard à un modèle plus général prenant en compte la dimension d'espace en supposant que les monomères suivent une diffusion spatiale. Ainsi on obtient un nouveau modèle se présentant sous forme d'EDPs couplées de type hyperbolique et parabolique dont nous montrons, sous des hypothèses physiquement réalistes, l'existence et l'unicité de la solution.

Le travail présenté dans ce chapitre a été réalisé en collaboration avec Thierry Goudon et Frédéric Lagoutière et a été soumis pour publication sous le titre *The Lifshitz-Slyozov equation with space–diffusion of monomers* [91].

2.1 Introduction

We are interested in the mathematical modeling of the late stage of the precipitation kinetics in supersaturated metastable solid solutions. The problem is for instance motivated by the design of industrial processes for producing metallic alloys (stainless steel, a mixture of iron, nickel, and chromium, or gold and nickel alloys used in jewelry to name a few), based on theoretical and numerical predictions. The supersaturated alloys under consideration are made of two phases : solute monomers and coarsening precipitates. Existing models phrase the time–evolution of the solution in terms of a PDEs system for the monomers concentration and the distribution function of the precipitate in size space. The latter gives the concentration of solute clusters of a given size. The kinetic equations for cluster concentrations are driven by the rates at which clusters absorb and lose a solute atom. The attachment and detachment processes are actually governed by basic principles of overall reduction of the interface energy, where volume effects, which favor growth, compete with surface effects, which favor dissolution. It turns out that minimizing the total interfacial surface energy of the system leads to the growth of larger particles at the expense of smaller particles, which are thus assigned to become still smaller and the overall process results in an increase in the average particle radius, a phenomenon referred to as Ostwald ripening.

The Lifschitz–Slyozov equations are commonly used in an effort to understand ripening from a theoretical perspective.
The standard Lifschitz-Slyozov system, as introduced in [123, 124], describes the evolution of a solution of polymers. In this model, macro-particles, or polymers, interact with free particles, or monomers. The macro-particles are described by their size distribution function $f(t,\xi)$, with $t \geq 0$ and $\xi \geq 0$ the time and size variables respectively, while the monomers are described by their concentration $c(t)$. Therefore $\int_\zeta^{\zeta'} f(t,\xi)\,\mathrm{d}\xi$ is interpreted as the number of polymers having at time t their size between ζ and ζ' while $\int_\zeta^{\zeta'} \xi f(t,\xi)\,\mathrm{d}\xi$ is proportional to the corresponding mass. The dynamics is governed by the growth rate

$$V(t,\xi) = a(\xi)c(t) - b(\xi)$$

with a, b given non negative functions : these kinetic coefficients represent the rates at which monomers are added to or removed from the macro-particles with size ξ. The precise expression of the coefficient relies on the modeling of the precipitation/dissolution processes ; in [124], assuming that mass transfer is based on monomer diffusion, the following expression is proposed

$$a(\xi) = \xi^{1/3}, \qquad b(\xi) = 1. \tag{2.1}$$

We refer to [163] for other relevant formulae for the kinetic coefficients. In this paper we shall assume the following

Hypothesis 2.1.1. *The kinetic coefficients a, b are required to satisfy :*
i) $b = 1$,
ii) a is non decreasing with $a(0) = 0$ and $a(+\infty) = +\infty$,
iii) $a \in C^0([0,\infty)) \cap C^1((0,\infty))$ and for any $\xi_0 > 0$ there exists $L_{a,0} > 0$ such that $0 \leq a'(\xi) \leq L_{a,0}$ for $\xi \geq \xi_0 > 0$.

Note that these assumptions cover the case of the Lifschitz–Slyozov coefficients (2.1). As a matter of fact we remark that at any time $t \geq 0$ the size space splits into two parts : $0 \leq \xi \leq \xi_c(t)$ and $\xi \geq \xi_c(t)$ where $\xi_c(t)$ is the unique positive number verifying $a(\xi_c(t)) = 1/c(t)$. It agrees with the basic principle of ripening where larger particles grow and smaller particles shrink. In this model, direct collisions of clusters are not considered. Therefore, the dynamics of the precipitation process is embodied into the transport equation

$$\partial_t f + \partial_\xi (Vf) = 0 \tag{2.2}$$

coupled to the mass conservation relation

$$c(t) + \int_0^\infty \xi f(t,\xi)\,\mathrm{d}\xi = \rho \tag{2.3}$$

a given positive constant. Eq. (2.2) is a conservation law for the polymer concentration in size space, while (2.3) expresses the fact that the total mass is conserved, the solute material being accounted for either as dissolved particles or as macro-particles. We point out that for $\xi = 0$, the growth rate $V(t,0) = -1$ is negative so that we do not need a boundary condition.

Despite its apparent simplicity the Lifschitz-Slyozov system is quite intriguing for the mathematical analysis, and some aspects remain unclear even for physicists. We refer to [47, 112, 111, 145, 147] for existence-uniqueness results in various functional frameworks (bounded, integrable or measure–valued solutions). While crucial for the applications, the understanding of

the large time behavior is highly challenging, definitely far from the asymptotic trend to a universal profile, as derived in [124]. The Lifschitz–Slyozov system admits a family of self-similar solutions for the clusters distribution function. All of the profiles have compact support and can be parameterized by the value of the logarithmic derivative at the edge of the support which determines the asymptotic value of the (rescaled) monomers concentration. The selection of the correct self-similar solution which defines the profile for large time associated to a given initial data is highly non–trivial : it is precisely determined by the behavior of the data at the tip of its support ! We refer on these questions to the analysis performed in [49, 144, 146] and the numerical simulations in [35, 42, 92]. These results are in apparent contradiction to most of experimental results which appear to show strong selection, insensitive to initial conditions. However, recent microgravity experiments have also revived the controversy from a practical perspective and have shown that the subject deserves thorough investigation [159]. Finding selection principles appeals to go beyond the classical Lifschitz–Slyozov model.

To this end, modifications of the Lifschitz-Slyozov system (2.2)–(2.3) have been discussed in the literature. The addition of a coagulation operator is suggested in [124, 164] to account for possible coalescence of large clusters formed on the late stages of the process. Analysis of the Lifschitz-Slyozov equation with such a coagulation term can be found in [46, 111]. The impact of the coalescence terms on the selection of the asymptotic profile is analyzed in [104] ; we also refer to the numerical experiments in [92]. Other variants of the Lifschitz-Slyozov system (2.2)–(2.3) are obtained by introducing parabolic corrections. Such corrections can be motivated through suitable asymptotic arguments, deriving the Lifschitz-Slyozov model from the Becker-Döring system, an infinite system of ODEs where clusters' size is a discrete variable. The corrected model is intended to share more basic features with the discrete Becker-Döring model, in particular concerning selection mechanisms of the large time asymptotics. This aspect has been detailed in various ways by many authors, for instance we can refer to [48, 51, 53, 50, 142]. Another diffusive correction is discussed in [150], based on a deep mean field analysis.

In this paper we wish to discuss another relevant version of the Lifschitz-Slyozov equations by assuming that monomers are also subject to space diffusion. The model we wish to investigate is derived in details in [124, Section 4], with the formation of vacancies (which are the clusters in this framework) in a crystal as a specific application, in connection to the description of sintering processes. It is likely that considering diffusion of monomers induce spatial correlations in the Lifschitz–Slyozov model, which in turn can modify the asymptotic trend. This question is beyond the scope of the paper. Here, as a preliminary step, we restrict to investigate the well–posedness issues, dealing with physically relevant functional spaces, while the preliminary numerical study we propose gives some hints on the qualitative behavior of the solutions. Let $\Omega \subset \mathbb{R}^N$ be a smooth bounded domain, with boundary $\partial\Omega$; given $x \in \partial\Omega$ we denote $\nu(x)$ the outward unit normal vector at point x. Then, we are interested in the following variant of (2.2)–(2.3), where now the unknowns also depend on the space variable and monomers are subject to diffusion :

$$\begin{cases} \partial_t f(t,x,\xi) + \partial_\xi((a(\xi)c(t,x) - 1)f(t,x,\xi)) = 0 \quad t \geq 0,\, x \in \Omega,\, \xi \geq 0 \\ \\ \partial_t\Big(c(t,x) + \displaystyle\int_0^\infty \xi f(t,x,\xi)\,\mathrm{d}\xi\Big) - \Delta_x c(t,x) = 0 \quad t \geq 0,\, x \in \Omega. \end{cases} \tag{2.4}$$

To start with, the diffusion equation is endowed with homogeneous Neumann boundary condition

$$\partial_\nu c = \nabla c \cdot \nu = 0, \qquad \text{on } \partial\Omega, \tag{2.5}$$

but we will detail below adaptations to Dirichlet conditions (see Section 2.4.4) and to the free-space problem (Section 2.4.5). Finally, the problem is completed by initial conditions

$$c(0,x) = c_{\text{init}}(x) \geq 0, \qquad f(0,x,\xi) = f_{\text{init}}(x,\xi) \geq 0. \tag{2.6}$$

In view of the physical interpretation it appears quite natural to assume

Hypothesis 2.1.2. *The data satisfy*
- $c_{\text{init}} \in L^\infty(\Omega)$,
- $f_{\text{init}} \in L^\infty(\Omega; L^1((0,\infty),(1+\xi)\,\mathrm{d}\xi))$.

By using the conservation equation for f and integrating by parts, we observe that

$$\partial_t \int_0^\infty \xi f(t,x,\xi)\,\mathrm{d}\xi = \int_0^\infty a(\xi)c(t,x)f(t,x,\xi)\,\mathrm{d}\xi - \int_0^\infty f(t,x,\xi)\,\mathrm{d}\xi. \tag{2.7}$$

It allows to rewrite the equation for the monomers concentration in the more familiar fashion

$$\partial_t c + c\int_0^\infty a(\xi)f(t,x,\xi)\,\mathrm{d}\xi = \Delta_x c + \int_0^\infty f(t,x,\xi)\,\mathrm{d}\xi. \tag{2.8}$$

Owing to (2.5), the system preserves the total mass : we have

$$\frac{\mathrm{d}}{\mathrm{d}t}\left[\int_\Omega \int_0^\infty \xi f(t,x,\xi)\,\mathrm{d}\xi\,\mathrm{d}x + \int_\Omega c(t,x)\,\mathrm{d}x\right] = 0.$$

We point out that a coupling with the stationary diffusion equation is derived in [143] through homogenization arguments, the model being further analyzed in [148]. In this paper we shall establish the following well-posedness statement for the system (2.4)–(2.6).

Theorem 2.1.1. *Suppose that Hypotheses 2.1.1 and 2.1.2 are fulfilled. Then, there exists a weak solution (c,f) of (2.4)–(2.6) with, for any $0<T<\infty$, $c \in L^\infty((0,T)\times\Omega) \cap L^2(0,T;H^1(\Omega))$, $f \in L^\infty((0,T)\times\Omega; L^1((0,\infty),(1+\xi)\,\mathrm{d}\xi))$, $c \in C^0([0,T];L^2(\Omega)-\text{weak})$, $f \in C^0([0,T];L^1(\Omega\times(0,\infty))-\text{weak})$.*

The difficulty of course arises from the non-linear coupling which involves PDEs of different types acting on different variables. This work is organized as follows. In Section 2.2, we briefly set up the necessary material on transport and diffusion equations. Then, in Section 2.3 we make use of a fixed point strategy to obtain the existence-uniqueness of solutions associated to bounded initial data when the kinetic coefficients are globally Lipschitz. Section 2.4 extends the result in several directions : more general data, singular coefficients, Dirichlet boundary conditions and free–space problem can be dealt with as well. Finally, in Section 2.5 we introduce a numerical scheme for the simulation of (2.4)–(2.6) and we conclude with some commented numerical experiments.

2.2 Basic results on diffusion and transport equations

In this Section we collect some statements on diffusion and transport equations which will be useful for our purposes. We start with the following claim.

Proposition 2.2.1. *Let $0 < T < +\infty$. Let A and B be non negative functions in $L^\infty((0,T)\times\Omega)$. Suppose that $0 \le B(t,x) \le C_0 < \infty$ for almost every (t,x). Then, for any $c_{\rm init} \in L^2(\Omega)$, there exists a unique $c \in L^2(0,T;H^1(\Omega)) \cap C([0,T];L^2(\Omega))$ with $\partial_t c \in L^2(0,T;(H^1(\Omega))')$ solution of*

$$\partial_t c + Ac - \Delta_x c = B \quad \text{in } (0,T)\times\Omega, \qquad \partial_\nu c = 0 \quad \text{on } \partial\Omega,$$

with initial data $c(t=0,x) = c_{\rm init}(x)$. Furthermore if $c_{\rm init} \ge 0$ belongs to $L^\infty(\Omega)$, then the solution c satisfies $0 \le c(t,x) \le K_T$ with K_T a constant depending on C_0, $\|c_{\rm init}\|_\infty$ and T. We also have for $0 \le t \le T < \infty$

$$\int_\Omega |c(t,x)|^2 \,\mathrm{d}x \le C_T, \qquad \int_0^t \int_\Omega |\nabla_x c(s,x)|^2 \,\mathrm{d}x\,\mathrm{d}s \le C_T$$

for some constant C_T depending on C_0, T, Ω and $\|c_{\rm init}\|_{L^2(\Omega)}$.

Proof. The existence result is a direct consequence of a general statement on parabolic equation. Indeed, the bilinear form

$$\mathbb{A}(t;c,\bar c) = \int_\Omega \nabla_x c \cdot \nabla_x \bar c \, dx + \int_\Omega A\, c \cdot \bar c \,\mathrm{d}x$$

is well defined on $H^1(\Omega)\times H^1(\Omega)$ and it verifies the continuity estimate :

$$\big|\mathbb{A}(t;c,\bar c)\big| \le \big(1 + \|A\|_{L^\infty((0,T)\times\Omega)}\big)\ \|c\|_{H^1(\Omega)}\ \|\bar c\|_{H^1(\Omega)}.$$

Furthermore, we also have the coercivity property

$$\mathbb{A}(t;c,c) = \int_\Omega |\nabla_x c|^2 \,\mathrm{d}x + \int_\Omega Ac^2 \,\mathrm{d}x \ge \|c\|^2_{H^1(\Omega)} - \|c\|^2_{L^2(\Omega)}.$$

We can therefore apply the analog of the Lax-Milgram theorem for parabolic equations, see e. g. [24, Theorem X.9, p. 218], and we get the existence uniqueness statement in Proposition 2.2.1.

In order to prove the uniform estimate, we proceed as follows. Consider a function $G \in C^1(\mathbb{R}_+)$ such that

- There exists $M_0 > 0$ such that $|G'(s)| \le M_0$ for any $s \in \mathbb{R}$;
- The function $s \mapsto G(s)$ is increasing on $(0,+\infty)$;
- $G(s) = 0$ on $(-\infty, 0]$.

We start by checking that $c(t,x) \ge 0$. We set

$$s \in \mathbb{R} \longmapsto H(s) = \int_0^s G(\sigma)\,\mathrm{d}\sigma \qquad \text{and} \qquad t \in [0,T] \longmapsto \varphi(t) = \int_\Omega H\big(-c(t,x)\big)\,\mathrm{d}x \ge 0.$$

In particular, we observe that

$$\varphi(0) = \int_\Omega H\big(-c_{\rm init}(x)\big)\,\mathrm{d}x = 0$$

since $c_{\rm init}(x) \ge 0$. Next, we compute

$$\begin{aligned}\varphi'(t) = &-\int_\Omega G\big(-c(t,x)\big)B(t,x)\,\mathrm{d}x - \int_\Omega G'\big(-c(t,x)\big)\big|\nabla_x c(t,x)\big|^2\,\mathrm{d}x \\ &+ \int_\Omega G\big(-c(t,x)\big)A(t,x)c(t,x)\,\mathrm{d}x \le 0,\end{aligned}$$

since $tG(t) \geq 0$ and $G'(t) \geq 0$. We conclude that $\varphi(t) = 0$ and thus $H(-c(t,x)) = 0$ for a.e. (t,x) It implies $c(t,x) \geq 0$ a.e.
Next, we prove the bound from above. To this end, we set

$$K(t) = \|c_{\text{init}}\|_{L^\infty(\Omega)} + C_0 t$$

and

$$H(s) = \int_0^s G(\sigma)\,\mathrm{d}\sigma, \qquad \varphi(t) = \int_\Omega H\big(c(t,x) - K(t)\big)\,\mathrm{d}x \geq 0.$$

We have $\varphi(0) = 0$ and

$$\varphi'(t) = \int_\Omega G\big(c(t,x) - K(t)\big)\ \big(B(t,x) - C_0\big)\,\mathrm{d}x - \int_\Omega G'\big(c(t,x) - K(t)\big)\ \big|\nabla_x c(t,x)\big|^2\,\mathrm{d}x$$
$$- \int_\Omega G\big(c(t,x) - K(t)\big)\ A(t,x)c(t,x)\,\mathrm{d}x \leq 0.$$

It follows that $\varphi(t) = 0$ and thus $H\big(c(t,x) - K(t)\big) = 0$ for a. e. $t \geq 0,\ x \in \Omega$ which implies $0 \leq c(t,x) \leq K(T)$ a.e. on $(0,T) \times \Omega$. The last estimate follows from standard energy estimates and application of the Grönwall lemma. □

Let us now recall a few facts about transport equations. For the time being we neglect the space variable which appears only as a parameter in the equation for the size density. Thus, we are concerned with the problem

$$\begin{cases} \partial_t f + \partial_\xi (Vf) = 0, \\ f(0,\xi) = f_{\text{init}}(\xi) \end{cases} \tag{2.9}$$

on $t \geq 0$ and $\xi \geq 0$ where the function $(t,\xi) \mapsto V(t,\xi)$ is required to satisfy

Hypothesis 2.2.1. *We have $V(t,\xi) = a(\xi)c(t) - b(\xi)$ with continuous and non negative functions a, b, c, such that $a(0) = 0$, $b(0) > 0$. We suppose that c is locally bounded while a' and b' belong to $L^\infty(\mathbb{R})$. Accordingly, for any $0 \leq t \leq T < \infty$, there exists M_T such that for any $\xi, \xi' \geq 0$, we have*

- $V(t,0) \leq 0$,
- $V(t,\xi) \leq M_T \xi$ *and* $|V(t,\xi)| \leq M_T(1+\xi)$
- $|V(t,\xi) - V(t,\xi')| \leq M_T|\xi - \xi'|$.

Remark that $V(t,x,\xi) = a(\xi)c(t,x) - 1$ satisfies the requirements in Hypothesis 2.2.1, uniformly with respect to the parameter $x \in \Omega$, as far as the kinetic coefficient a has a globally bounded derivative (see Hypothesis 2.3.1 below, $||a'||_\infty \leq L_a$) and satisfies $a(0) = 0$, and the monomers concentration satisfies the L^∞ estimate $0 \leq c(t,x) \leq K_T$ (with $M_T = L_a K_T$).

Owing to Hypothesis 2.2.1, we can solve (2.9) by means of integration along characteristics. Indeed, we can define the characteristic curves solutions to the ODE

$$\begin{cases} \dfrac{\mathrm{d}}{\mathrm{d}s}\Xi(s;t,\xi) = V\big(s, \Xi(s;t,\xi)\big), \quad s \in \mathbb{R}, \\ \\ \Xi(t;t,\xi) = \xi. \end{cases} \tag{2.10}$$

Then, (2.9) recasts as

$$\frac{\mathrm{d}}{\mathrm{d}s}\Big[f\big(s, \Xi(s;t,\xi)\big)\Big] = -\partial_\xi V\big(s, \Xi(s;t,\xi)\big)\ f\big(s, \Xi(s;t,\xi)\big).$$

It yields

$$f(t,\xi) = f_{\text{init}}(\Xi(0;t,\xi))\ J(0;t,\xi) \tag{2.11}$$

with

$$J(s;t,\xi) = \partial_\xi \Xi(s;t,\xi) = \exp\Big(-\int_s^t \partial_\xi V(\sigma,\Xi(\sigma;t,\xi))\,\mathrm{d}\sigma\Big) \geq 0, \tag{2.12}$$

the Jacobian of the change of variables $\xi \mapsto \zeta = \Xi(s;t,\xi)$. The fundamental properties on the characteristics that are needed for our analysis are summarized in the following claim. (We refer to [47] for similar considerations and details.)

Lemma 2.2.2. *Let Hypothesis 2.2.1 be fulfilled. Then, we have*
i) for any $t \geq 0$, $\Xi(0;t,0) \geq 0$,
ii) for any $t \geq 0$, $\lim_{\xi\to\infty} \Xi(0;t,\xi) = \infty$,
iii) for any $0 \leq t \leq T < \infty$ and $\xi \geq 0$, there exists $L_T > 0$ such that $\Xi(t;0,\xi) \leq L_T\ \xi$.

Proof. Derivating with respect to the initial time, we obtain

$$\partial_t \Xi(s;t,\xi) = -V(t,\xi) J(s;t,\xi).$$

Since $J \geq 0$ and $V(t,0) \leq 0$, we deduce that $t \mapsto \Xi(0;t,0)$ is non decreasing and thus i) holds. Next, we have

$$\Xi(s_2;t,\xi) - \Xi(s_1;t,\xi) = \int_{s_1}^{s_2} V\big(\sigma,\Xi(\sigma;t,\xi)\big)\,\mathrm{d}\sigma.$$

(Note that $\Xi(s_2;t,\xi) \geq 0$ for $s_2 \leq t$ owing to the fact that $V(t,0) \leq 0$.) Since $V(t,\xi) \leq M_T\xi$ we obtain for $0 \leq s_1 \leq s_2 \leq t \leq T$

$$0 \leq \Xi(s_2;t,\xi) \leq \Xi(s_1;t,\xi) + M_T \int_{s_1}^{s_2} \Xi(\sigma;t,\xi)\,\mathrm{d}\sigma$$

and the Grönwall lemma yields

$$0 \leq \Xi(s_2;t,\xi) \leq e^{M_T(s_2-s_1)}\Xi(s_1;t,\xi).$$

With $s_2 = t$ we have $e^{M_T(s_1-t)}\ \xi \leq \Xi(s_1;t,\xi)$ which allows to conclude for ii) by letting ξ go to ∞. The third item is a direct consequence of the Grönwall lemma. □

Proposition 2.2.3. *Let Hypothesis 2.2.1 be fulfilled. Let f be the solution of (2.9), as given by (2.11). Then, the following assertions hold*
i) If $f_{\text{init}} \in L^1((0,\infty))$ with $\xi f_{\text{init}} \in L^1((0,\infty))$, then for any $t \geq 0$, $\xi \mapsto f(t,\xi)$ and $\xi \mapsto \xi f(t,\xi)$ are integrable. More precisely, we have $f \in C^0([0,T];L^1((0,\infty))$ and the following estimates hold for any $t \geq 0$

$$\int_0^\infty |f(t,\xi)|\,\mathrm{d}\xi \leq \int_0^\infty |f_{\text{init}}(\xi)|\,\mathrm{d}\xi, \tag{2.13}$$

and, for any $0 \leq t \leq T < \infty$

$$\int_0^\infty \xi\ |f(t,\xi)|\,\mathrm{d}\xi \leq L_T \int_0^\infty \xi\ |f_{\text{init}}(\xi)|\,\mathrm{d}\xi, \tag{2.14}$$

with L_T depending on M_T in Hypothesis 2.2.1.
ii) If $f_{\text{init}} \geq 0$, then $f(t,\xi) \geq 0$ too.

iii) We assume furthermore that $\partial_\xi V(t,\xi) \geq 0$ *for any* $t, \xi \geq 0$*, then if* $f_{\rm init}$ *belongs to* $L^\infty((0,\infty))$*, we have* $f \in L^\infty((0,\infty)\times(0,\infty))$ *with*

$$||f||_\infty \leq \|f_{\rm init}\|_\infty.$$

Proof. We simply integrate (2.11) and use Lemma 2.2.2 to obtain

$$\int_0^\infty |f(t,\xi)|\,\mathrm{d}\xi = \int_{\Xi(0;t,0)}^\infty |f_{\rm init}(\xi)|\,\mathrm{d}\xi \leq \int_0^\infty |f_{\rm init}(\xi)|\,\mathrm{d}\xi.$$

Similarly, we have

$$\int_0^\infty \xi|f(t,\xi)|\,\mathrm{d}\xi = \int_{\Xi(0;t,0)}^\infty \Xi(t;0,\xi)\ |f_{\rm init}(\xi)|\,\mathrm{d}\xi \leq L_T \int_0^\infty \xi\ |f_{\rm init}(\xi)|\,\mathrm{d}\xi.$$

When $\partial_\xi V \geq 0$, we observe that $0 \leq J(s;t,\xi) \leq 1$ holds when $s \leq t$. Therefore we obtain

$$|f(t,\xi)| = \big|f_{\rm init}\big(\Xi(0;t,\xi)\big)\big|\ J(0;t,\xi) \leq \|f_{\rm init}\|_\infty$$

for almost every (t,ξ). □

2.3 Existence-uniqueness for bounded data and smooth coefficients

In this Section, we restrict to the case where the data are bounded and the coefficients are globally Lipschitz. To be more specific we strengthen Hypotheses 2.1.1 and 2.1.2 as follows

Hypothesis 2.3.1. *Additionally to the requirements in Hypotheses 2.1.1 and 2.1.2 we suppose*
a) $a \in C^1([0,\infty))$ *and there exists a constant* $L_a > 0$ *such that* $0 \leq a'(\xi) \leq L_a$ *for any* $\xi \geq 0$*,*
b) $f_{\rm init} \in L^\infty(\Omega\times(0,\infty))$*.*

We wish to prove the well-posedness of the non homogeneous Lifschitz-Slyozov equation in this framework.

Theorem 2.3.1. *Suppose that Hypothesis 2.3.1 is fulfilled. Then, there exists a unique weak solution* (c,f) *of* (2.4)–(2.6) *with, for any* $0 < T < \infty$*,*

$$\begin{array}{l} c \in L^\infty((0,T)\times\Omega) \cap L^2(0,T;H^1(\Omega)),\\ f \in L^\infty(((0,T)\times\Omega\times(0,\infty)) \cap L^\infty((0,T)\times\Omega; L^1((0,\infty),(1+\xi)\,\mathrm{d}\xi)),\\ c \in C^0([0,T];L^2(\Omega) - \textit{weak}),\\ f \in C^0([0,T];L^1(\Omega\times(0,\infty)) - \textit{weak}). \end{array}$$

The proof uses the Schauder fixed point theorem, see [71, Corollary 3.6.2]. We set $\mathscr{Q}_T = [0,T]\times\Omega$ for a fixed $0 < T < \infty$. Let us denote

$$C_0 = \sup_{x\in\Omega} \int_0^\infty f_{\rm init}(x,\xi)\,\mathrm{d}\xi < \infty. \tag{2.15}$$

We associate to this quantity the constant K_T as defined in the proof of Proposition 2.2.1, $K_T = \|c_{\rm init}\|_\infty + C_0 T$. We introduce the set

$$\mathscr{C}_T = \big\{\tilde{c} \in L^2(\mathscr{Q}_T) \text{ such that } 0 \leq \tilde{c}(t,x) \leq K_T\big\}.$$

Then, we define the mapping

$$\begin{array}{rccc} \mathscr{T}: & \mathscr{C}_T & \longrightarrow & L^2(\mathscr{Q}_T) \\ & \tilde{c} & \longmapsto & \mathscr{T}(\tilde{c}) = c, \end{array}$$

with c solution of

$$\begin{cases} \partial_t c(t,x) - \Delta_x c(t,x) + A(t,x)c(t,x) = B(t,x) & \text{for } t \geq 0,\ x \in \Omega, \\ \partial_\nu c = 0 & \text{on } \partial\Omega, \\ c_{|t=0} = c_{\text{init}} & \text{on } \Omega, \end{cases}$$

where the coefficients A, B are given by

$$A(t,x) = \int_0^\infty a(\xi) f(t,x,\xi)\,\mathrm{d}\xi, \qquad B(t,x) = \int_0^\infty f(t,x,\xi)\,\mathrm{d}\xi,$$

f being solution of

$$\begin{cases} \partial_t f(t,x,\xi) + \partial_\xi\big((a(\xi)\tilde{c}(t,x) - 1) f(t,x,\xi)\big) = 0 & \text{for } t \geq 0,\ x \in \Omega,\ \xi \geq 0, \\ f_{|t=0} = f_{\text{init}} & \text{on } \Omega \times (0,\infty). \end{cases}$$

From now on we adopt the convention to denote by $L_T > 0$ a constant that depends on T, C_0, $\|c_{\text{init}}\|_\infty$, and on the Lipschitz constant L_a of a, even if the precise value of the constant might change from a line to another. Conversely, we will denote by C_T a constant which depends only on T, C_0 and $\|c_{\text{init}}\|_\infty$ but not on L_a (like K_T). According to Hypothesis 2.1.1, for any $\tilde{c} \in \mathscr{C}_T$, the rate $V(t,x,\xi) = a(\xi)\tilde{c}(t,x) - 1$, which is now parametrized by $x \in \Omega$, satisfies the estimates required in Hypothesis 2.2.1, uniformly with respect to $x \in \Omega$. (Namely M_T in Hypothesis 2.2.1 is $L_a K_T$.) Up to a slight abuse with regularity issues we can therefore appeal to the results established in Section 2.2. Indeed, within the functional framework adopted here, for fixed $x \in \Omega$, $t \mapsto \tilde{c}(t,x)$ cannot be considered as a continuous function of the time variable. The classical theory of characteristics with C^1 solutions of the ODE (2.10) does not apply. The alternative to circumvent the difficulty is as follows. The first option consists in dealing with a less regular notion of characteristics. The standard Picard iteration scheme actually shows that

$$\Xi(s;t,\xi) = \xi + \int_t^s V\big(\sigma, \Xi(\sigma;t,\xi)\big)\,\mathrm{d}\sigma$$

admits a continuous solution assuming only integrability of V with respect to the time variable and all the necessary estimates on Ξ hold in this framework (see [44, Theorem 1.1, p. 43] for an existence theorem without regularity in time). The second option consists in replacing $\tilde{c}$ in the convection term by $\zeta_\epsilon \star_{t,x} \tilde{c}$, with ζ_ϵ a convenient sequence of mollifiers. Again, all the necessary estimates are not affected by the regularization process and are uniform with respect to ϵ. Accordingly, the compactness arguments detailed below apply to pass to the limit as ϵ goes to 0. We do not detail further this issue, adopting the slight abuse of working with the characteristics Ξ, parametrized by the space variable x, without any further precision. Hence, we can apply Proposition 2.2.3 : f reads

$$f(t,x,\xi) = f_{\text{init}}(x, \Xi(0;t,x,\xi))\ J(0,t,x,\xi).$$

with Ξ and J defined by the characteristics equation associated to $\tilde{c}$. In particular, we have

$$\begin{cases} 0 \leq f(t,x,\xi) \leq \|f_{\text{init}}\|_\infty \quad a.e., \\ \sup\limits_{x\in\Omega} \displaystyle\int_0^\infty f(t,x,\xi)\,\mathrm{d}\xi \leq \sup_{x\in\Omega} \int_0^\infty f_{\text{init}}(x,\xi)\,\mathrm{d}\xi = C_0 < \infty, \\ \sup\limits_{x\in\Omega} \displaystyle\int_0^\infty \xi\ f(t,x,\xi)\,\mathrm{d}\xi \leq L_T\ \sup_{x\in\Omega} \int_0^\infty \xi\ f_{\text{init}}(x,\xi)\,\mathrm{d}\xi < \infty. \end{cases} \tag{2.16}$$

It follows that $A(t,x) \geq 0$ lies in $L^\infty((0,T)\times\Omega)$, and $0 \leq B(t,x) \leq C_0$. Coming back to Proposition 2.2.1 we conclude that $\mathscr{T}$ is well defined with $c = \mathscr{T}(\tilde{c}) \in L^2(0,T;H^1(\Omega)) \cap C([0,T];L^2(\Omega))$ and furthermore $0 \leq c(t,x) \leq K_T$. In other words $\mathscr{T}(\mathscr{C}_T) \subset \mathscr{C}_T$.

Let us now show that $\mathscr{T}(\mathscr{C}_T)$ is a compact set in $L^2(\mathscr{Q}_T)$. In fact Proposition 2.2.1 also shows that

$$c = \mathscr{T}(\tilde{c}) \text{ lies in a bounded set in } L^2(0,T;H^1(\Omega)).$$

The equation satisfied by c finally tells us that

$$\partial_t c \text{ is bounded } L^2(0,T;H^{-1}(\Omega)).$$

Since $H^1(\Omega)$ embeds compactly in $L^2(\Omega)$, we can therefore apply the compactness results in [166, Corollary 4] to conclude that $\mathscr{T}(\mathscr{C}_T)$ is a compact set in $L^2(\mathscr{Q}_T)$.

It remains to establish the continuity of $\mathscr{T}$ in the sense of the $L^2(\mathscr{Q}_T)$ norm. To this end, let us consider a sequence $\big(\tilde{c}_n\big)_{n\in\mathbb{N}}$ in $\mathscr{C}_T$ which converges to some $\tilde{c}$ (strongly) in $L^2(\mathscr{Q}_T)$. Clearly $\tilde{c} \in \mathscr{C}_T$. We define f_n and f as to be the solution of the transport equations

$$\begin{cases} \partial_t f_n(t,x,\xi) + \partial_\xi\big((a(\xi)\tilde{c}_n(t,x) - 1)f_n(t,x,\xi)\big) = 0 \\ \\ \partial_t f(t,x,\xi) + \partial_\xi\big((a(\xi)\tilde{c}(t,x) - 1)f(t,x,\xi)\big) = 0 \end{cases}$$

for $t \geq 0$, $x \in \Omega$ and $\xi \geq 0$, with the common initial data f_{init}. Using the characteristics

$$\begin{cases} \dfrac{\mathrm{d}}{\mathrm{d}s}\Xi_n(s;t,x,\xi) = a\big(\Xi_n(s;t,x,\xi)\big)\tilde{c}_n(t,x) - 1, \\ \Xi_n(t;t,x,\xi) = \Xi(t;t,x,\xi) = \xi \end{cases} \qquad \frac{\mathrm{d}}{\mathrm{d}s}\Xi(s;t,x,\xi) = a\big(\Xi(s;t,x,\xi)\big)\tilde{c}(t,x) - 1,$$

we write

$$\begin{cases} f_n(t,x,\xi) = f_{\text{init}}(x, \Xi_n(0;t,x,\xi))\ J_n(0;t,x,\xi), \\ \\ f(t,x,\xi) = f_{\text{init}}(x, \Xi(0;t,x,\xi))\ J(0;t,x,\xi) \end{cases}$$

with

$$J_n(s;t,x,\xi) = \exp\bigg(-\int_s^t a'\big(\Xi(\sigma;t,x,\xi)\big)\ \tilde{c}_n(\sigma;x)\,\mathrm{d}\sigma\bigg),$$
$$J(s;t,x,\xi) = \exp\bigg(-\int_s^t a'\big(\Xi(\sigma;t,x,\xi)\big)\ \tilde{c}(\sigma;x)\,\mathrm{d}\sigma\bigg).$$

The first step of the the proof consists in establishing the following claim

Lemma 2.3.2. *Let us set*

$$A_n(t,x) = \int_0^{+\infty} a(\xi)\ f_n(t,x,\xi)\,\mathrm{d}\xi, \quad A(t,x) = \int_0^{+\infty} a(\xi)\ f(t,x,\xi)\,\mathrm{d}\xi,$$
$$B_n(t,x) = \int_0^{+\infty} f_n(t,x,\xi)\,\mathrm{d}\xi, \qquad B(t,x) = \int_0^{+\infty} f(t,x,\xi)\,\mathrm{d}\xi.$$

Then, A_n and B_n tend to A and B, respectively, in $L^2(\mathscr{Q}_T)$.

In order to establish this property, we need an estimate on the distance between characteristic curves associated to different rates.

Lemma 2.3.3. *We assume that Hypothesis 2.3.1 is fulfilled. Let c_1 and c_2 in $\mathscr{C}_T$ and set $V_i(t,x,\xi) = a(\xi)c_i(t,x) - 1$, $i = 1,2$. We denote by Ξ_1 and Ξ_2 the associated characteristics. Then, we have for any $0 \le s,t \le T < \infty$*

$$|\Xi_1 - \Xi_2|(s;t,x,\xi) \le L_T\ (1+\xi)\ \left(\int_s^t |c_1 - c_2|^2(\sigma,x)\,\mathrm{d}\sigma\right)^{1/2}. \tag{2.17}$$

Proof. We detail the proof for the case $0 \le s \le t \le T$, the other situation follows by the same argument. By using the equation for the characteristics, we arrive at

$$\begin{aligned}
\big|\Xi_1(s;t,x,\xi) - \Xi_2(s;t,x,\xi)\big| &= \Big|\int_s^t \Big[a\big(\Xi_1(\sigma;t,x,\xi)\big)c_1(\sigma,x) - a\big(\Xi_2(\sigma;t,x,\xi)\big)c_2(\sigma,x)\Big]\,\mathrm{d}\sigma\Big| \\
&\le \int_s^t c_1(\sigma,x)\Big|a\big(\Xi_1(\sigma;t,x,\xi)\big) - a\big(\Xi_2(\sigma;t,x,\xi)\big)\Big|\,\mathrm{d}\sigma \\
&\quad + \int_s^t a\big(\Xi_2(\sigma;t,x,\xi)\big)\ \big|c_1 - c_2\big|(\sigma,x)\,\mathrm{d}\sigma \\
&\le K_T L_a \int_s^t \big|\Xi_1(\sigma;t,x,\xi) - \Xi_2(\sigma;t,x,\xi)\big|\,\mathrm{d}\sigma \\
&\quad + \left(\int_s^t \Big|a\big(\Xi_2(\sigma;t,x,\xi)\big)\Big|^2\,\mathrm{d}\sigma\right)^{1/2}\left(\int_s^t |c_1(\sigma,x) - c_2(\sigma,x)|\,\mathrm{d}\sigma\right)^{1/2}.
\end{aligned}$$

On the one hand, since $a(0) = 0$, we have

$$|a(\Xi)| = \Big|a(0) + \int_0^{\Xi} a'(\zeta)\,\mathrm{d}\zeta\Big| \le L_a|\Xi|.$$

On the other hand, we remark that

$$\begin{aligned}
\Big|\Xi_2(s;t,x,\xi)\Big| &= \Big|\xi + \int_t^s \Big(a\big(\Xi_2(\sigma;t,x,\xi)\big)c_2(\sigma,x) - 1\Big)\,\mathrm{d}\sigma\Big| \\
&\le \xi + \int_s^t \Big(1 + K_T L_a\big|\Xi_2(\sigma;t,x,\xi)\big|\Big)\,\mathrm{d}\sigma
\end{aligned}$$

holds. The Grönwall lemma then yields the estimate

$$\big|\Xi_2(s;t,x,\xi)\big| \le L_T(1+\xi).$$

It follows that

$$\big|a(\Xi_2(s;t,x,\xi))\big| \le L_T(1+\xi)$$

holds. Therefore, we obtain

$$\begin{aligned}
&\big|\Xi_1(s;t,x,\xi) - \Xi_2(s;t,x,\xi)\big| \\
&\quad \le L_T\left(\int_s^t \big|\Xi_1(\sigma;t,x,\xi) - \Xi_2(\sigma;t,x,\xi)\big|\,\mathrm{d}\sigma + (1+\xi)\left(\int_s^t |c_1(\sigma,x) - c_2(\sigma,x)|\,\mathrm{d}\sigma\right)^{1/2}\right).
\end{aligned}$$

Applying the Grönwall lemma again leads to (2.17). □

Proof of Lemma 2.3.2. By using the characteristics, we write

$$\begin{aligned}
(B_n - B)(t,x) &= \int_0^{\infty} f_{\mathrm{init}}(x, \Xi_n(0;t,x,\xi))J_n(0;t,x,\xi)\,\mathrm{d}\xi \\
&\qquad - \int_0^{+\infty} f_{\mathrm{init}}(x, \Xi(0;t,x,\xi))J(0;t,x,\xi)\,\mathrm{d}\xi \\
&= \int_{\Xi_n(0;t,x,0)}^{+\infty} f_{\mathrm{init}}(x,y)\,\mathrm{d}y - \int_{\Xi(0;t,x,0)}^{+\infty} f_{\mathrm{init}}(x,y)\,\mathrm{d}y.
\end{aligned}$$

It follows that

$$|B_n - B|(t,x) \leq \left| \int_{\Xi(0;t,x,0)}^{\Xi_n(0;t,x,0)} |f_{\rm init}(x,y)|\,\mathrm{d}y \right| \leq \|f_{\rm init}\|_{L^\infty(\Omega\times\mathbb{R}_+)} \big|\Xi_n - \Xi\big|(0;t,x,0),$$

and integrating over $x \in \Omega$ it yields

$$\|(B_n - B)(t,\cdot)\|^2_{L^2(\Omega)} \leq \|f_{\rm init}\|^2_{L^\infty(\Omega\times\mathbb{R}_+)} \int_\Omega \big|\Xi_n - \Xi\big|^2(0;t,x,0)\,\mathrm{d}x.$$

Hence, using Lemma 2.3.3, we get

$$\|(B_n - B)(t,\cdot)\|^2_{L^2(\Omega)} \leq L_T^2\ \|f_{\rm init}\|^2_{L^\infty(\Omega\times\mathbb{R}_+)} \int_0^t \int_\Omega \big|\tilde{c}_n - \tilde{c}\big|^2(\sigma,x)\,\mathrm{d}x\,\mathrm{d}\sigma.$$

We apply similar manipulations to evaluate

$$\begin{aligned} A_n(t,x) - A(t,x) &= \int_0^\infty a(\xi) f_n(t,x,\xi) d\xi - \int_0^\infty a(\xi) f(t,x,\xi)\,\mathrm{d}\xi \\ &= \int_{\Xi_n(0;t,x,0)}^\infty a(\Xi_n(t;0,x,y)) f_{\rm init}(x,y)\,\mathrm{d}y \\ &\qquad - \int_{\Xi(0;t,x,0)}^\infty a(\Xi(t;0,x,y)) f_{\rm init}(x,y)\,\mathrm{d}y. \end{aligned}$$

Indeed, we have

$$\begin{aligned} \big|A_n - A\big|(t,x) \ &\leq\ \Big| \int_{\Xi_n(0;t,x,0)}^{\Xi(0;t,x,0)} a(\Xi_n(t;0,x,y))\ f_{\rm init}(x,y)\,\mathrm{d}y \Big| \\ &\quad + \int_{\Xi(0;t,x,0)}^{+\infty} \big| a\big(\Xi_n(t;0,x,y)\big) - a\big(\Xi(t;0,x,y)\big)\big|\ f_{\rm init}(x,y)\,\mathrm{d}y \\ &\leq\ L_a \left(\Big| \int_{\Xi_n(0;t,x,0)}^{\Xi(0;t,x,0)} |\Xi_n(t;0,x,y)|\ f_{\rm init}(x,y)\,\mathrm{d}y \Big| \right. \\ &\quad \left. + \int_{\Xi(0;t,x,0)}^{+\infty} \big|\Xi_n(t;0,x,y) - \Xi(t;0,x,y)\big|\ f_{\rm init}(x,y)\,\mathrm{d}y \right). \end{aligned}$$

We observe that

$$\begin{aligned} \big|\Xi_n(t;0,x,y)\big| &= \big|\Xi_n(t;0,x,y) - \Xi_n(t;0,x,\Xi_n(0;t,x,0))\big| \\ &= \Big| \int_y^{\Xi_n(0;t,x,0)} \partial_\xi \Xi_n(t;0,x,\xi)\,\mathrm{d}\xi \Big| \\ &= \Big| \int_y^{\Xi_n(0;t,x,0)} \exp\Big(- \int_t^0 a'\big(\Xi_n(\sigma;t,x,\xi)\big)\ \tilde{c}_n(\sigma,x)\,\mathrm{d}\sigma \Big)\,\mathrm{d}\xi \Big| \\ &\leq L_T \big| y - \Xi_n(0;t,x,0)\big| \end{aligned}$$

by using Hypothesis 2.1.1. Since we are concerned with y restricted to the interval defined by $\Xi_n(0;t,x,0)$ and $\Xi(0;t,x,0)$ we have

$$\big|\Xi_n(t;0,x,y)\big| \leq L_T\ \big|\Xi - \Xi_n\big|(0;t,x,0).$$

It yields

$$\Big| \int_{\Xi_n(0;t,x,0)}^{\Xi(0;t,x,0)} a\big(\Xi_n(t;0,x,y)\big)\ f_{\text{init}}(x,y)\,\mathrm{d}y \Big| \ \leq L_T\ \big|\Xi - \Xi_n\big|(0;t,x,0)\ \int_0^{+\infty} f_{\text{init}}(x,y)\,\mathrm{d}y. \quad (2.18)$$

Moreover, Lemma 2.3.3 allows to estimate

$$\big|\Xi_n - \Xi\big|(t;0,x,y) \leq L_T\ (1+y)\ \Big(\int_0^t |\tilde{c}_n - \tilde{c}|^2(\sigma,x)\,\mathrm{d}\sigma\Big)^{1/2}. \quad (2.19)$$

Combining (2.18) et (2.19) we are led to

$$\begin{aligned}\big|(A_n - A)(t,x)\big| \leq L_T \Bigg(&\big|\Xi_n - \Xi\big|(0;t,x,0) \int_0^{+\infty} f_{\text{init}}(x,y)\,\mathrm{d}y \\ &+\Big(\int_0^t |\tilde{c}_n - \tilde{c}|^2(\sigma,x)\,\mathrm{d}\sigma\Big)^{1/2} \int_0^{+\infty} (1+y) f_{\text{init}}(x,y)\,\mathrm{d}y\Bigg).\end{aligned}$$

Therefore, we deduce that

$$\big\|A_n - A\big\|_{L^2(\mathscr{Q}_T)} \leq L_T \big\|\tilde{c}_n - \tilde{c}\big\|_{L^2(\mathscr{Q}_T)}.$$

It finishes the proof of Lemma 2.3.2. □

We are left with the task of proving that $c_n = \mathscr{T}(\tilde{c}_n)$ converges to $c = \mathscr{T}(\tilde{c})$ in $L^2(\mathscr{Q}_T)$. We remind that c_n and c are the solutions of

$$\begin{cases} \partial_t c_n(t,x) - \Delta_x c_n(t,x) + A_n(t,x) c_n(t,x) = B_n(t,x), \\ \\ \partial_t c(t,x) - \Delta_x c(t,x) + A(t,x) c(t,x) = B(t,x), \\ \\ \partial_\nu c_n = 0, \qquad \partial_\nu c = 0 \qquad \text{on } \partial\Omega, \\ \\ c_n(0,x) = c(0,x) = c_{\text{init}}(x). \end{cases}$$

We obtain the following energy estimate

$$\begin{aligned}&\frac{1}{2}\frac{\mathrm{d}}{\mathrm{d}t}\int_\Omega (c_n - c)^2(t,x)\,\mathrm{d}x + \int_\Omega \big|\nabla_x(c_n - c)\big|^2(t,x)\,\mathrm{d}x \\ &\quad = -\int_\Omega (c_n - c)(c_n A_n - cA)(t,x)\,\mathrm{d}x + \int_\Omega (c_n - c)(B_n - B)(t,x)\,\mathrm{d}x.\end{aligned}$$

It can be recast as

$$\begin{aligned}&\frac{1}{2}\frac{\mathrm{d}}{\mathrm{d}t}\int_\Omega (c_n - c)^2(t,x)\,\mathrm{d}x + \int_\Omega \big|\nabla_x(c_n - c)\big|^2(t,x)\,\mathrm{d}x + \int_\Omega A(c_n - c)^2(t,x)\,\mathrm{d}x \\ &\quad = -\int_\Omega c_n\ (c_n - c)\ (A_n - A)(t,x)\,\mathrm{d}x + \int_\Omega (c_n - c)\ (B_n - B)(t,x)\,\mathrm{d}x.\end{aligned}$$

We make use of the Cauchy-Schwarz and Young inequalities, together with the fact that $c_n \in \mathscr{C}_T$ to obtain

$$\begin{aligned}&\frac{1}{2}\frac{\mathrm{d}}{\mathrm{d}t}\int_\Omega (c_n - c)^2(t,x)\,\mathrm{d}x + \int_\Omega \big|\nabla_x(c_n - c)\big|^2(t,x)\,\mathrm{d}x + \int_\Omega A(c_n - c)^2(t,x)\,\mathrm{d}x \\ &\quad \leq \int_\Omega (c_n - c)^2(t,x)\,\mathrm{d}x + \frac{K_T^2}{2}\int_\Omega (A_n - A)^2(t,x)\,\mathrm{d}x + \frac{1}{2}\int_\Omega (B_n - B)^2(t,x)\,\mathrm{d}x.\end{aligned}$$

Eventually, an application of the Grönwall lemma yields

$$\int_\Omega (c_n - c)^2(t,x)\,\mathrm{d}x \le C_T \left(\int_{\mathscr{Q}_T} |B_n - B|^2(s,x)\,\mathrm{d}x\,\mathrm{d}s + \int_{\mathscr{Q}_T} |A_n - A|^2(s,x)\,\mathrm{d}x\,\mathrm{d}s \right)$$

on $0 \le t \le T < \infty$ where C_T depends only on T, C_0 and $\|c_{\mathrm{init}}\|_\infty$. Coming back to Lemma 2.3.2 we conclude that c_n tends to c in $L^2(\mathscr{Q}_T)$. □

Having established the properties of the mapping $\mathscr{T}$, we can apply the Schauder theorem which proves the existence of a fixed point $c = \mathscr{T}(c) \in \mathscr{C}_T$. The fixed point c then satisfies

$$\partial_t c + Ac = \Delta_x c + B \qquad \text{on } (0,T)\times\Omega,$$

endowed with $\partial_\nu c = 0$ on $\partial\Omega$ and the initial data $c_{|t=0} = c_{\mathrm{init}}$, where

$$A(t,x) = \int_0^\infty a(\xi) f(t,x,\xi)\,\mathrm{d}\xi, \qquad B(t,x) = \int_0^\infty f(t,x,\xi)\,\mathrm{d}\xi,$$

and

$$\partial_t f + \partial_\xi\big((a(\xi)c(t,x) - 1)f\big) = 0 \text{ on } (0,T)\times\Omega\times(0,\infty),$$

with initial data $f_{|t=0} = f_{\mathrm{init}}$. This ends the proof of the existence of solution to the system (2.4)–(2.6).

What we did can be used to justify the uniqueness of the solution as well. Indeed let us assume that (c_1, f_1) and (c_2, f_2) are solutions of (2.4)–(2.6) for the same initial data $(c_{\mathrm{init}}, f_{\mathrm{init}})$. Reproducing the arguments for proving the continuity of $\mathscr{T}$, we arrive at

$$\int_\Omega (c_1 - c_2)^2(t,x)\,\mathrm{d}x \le C_T \left(\int_0^t \int_\Omega \Big(|B_1 - B_2|^2 + |A_1 - A_2|^2 \Big)(s,x)\,\mathrm{d}x\,\mathrm{d}s \right).$$

Now, coming back to the proof of Lemma 2.3.2, we can estimate the right hand side so that

$$\int_\Omega (c_1 - c_2)^2(t,x)\,\mathrm{d}x \le L_T \int_0^t \int_\Omega |c_1 - c_2|^2(s,x)\,\mathrm{d}x\,\mathrm{d}s.$$

The Grönwall lemma then implies that $c_1 = c_2$. □

As a concluding remark of this section, we observe that

$$\frac{\mathrm{d}}{\mathrm{d}t}\int_0^\infty \xi f(t,x,\xi)\,\mathrm{d}\xi = \int_0^\infty \big(a(\xi)c(t,x) - 1\big) f(t,x,\xi)\,\mathrm{d}\xi = A(t,x)c(t,x) - B(t,x) \tag{2.20}$$

holds. (It follows by integrating by parts, we refer to [47, Lemma 3] for details.) Thus, with the Neumann boundary condition (2.5), the obtained solution satisfies the mass conservation relation

$$\int_\Omega c(t,x)\,\mathrm{d}x + \int_\Omega \int_0^\infty \xi f(t,x,\xi)\,\mathrm{d}\xi\,\mathrm{d}x = \int_\Omega c_{\mathrm{init}}(x)\,\mathrm{d}x + \int_\Omega \int_0^\infty \xi f_{\mathrm{init}}(x,\xi)\,\mathrm{d}\xi\,\mathrm{d}x. \tag{2.21}$$

2.4 Further existence–uniqueness results

2.4.1 Existence for general initial data

In this section we wish to relax the assumptions on the initial data, requiring only

$$f_{\mathrm{init}} \in L^\infty(\Omega; L^1((0,\infty), (1+\xi)\,\mathrm{d}\xi))$$

and removing the finiteness of the uniform norm of $f_{\rm init}$ which could be physically questionable. To justify the existence of solution in this framework, we appeal to approximation and compactness arguments. To this end, we consider a sequence $f^n_{\rm init}$ made of bounded functions which converge to $f_{\rm init}$ in $L^1(\Omega\times\mathbb{R}_+,(1+\xi)\,\mathrm{d}\xi\,\mathrm{d}x)$:

$$
\begin{aligned}
&0\le f^n_{\rm init}(x,\xi)\le C_n,\qquad 0\le f^n_{\rm init}(x,\xi)\le f_{\rm init}(x,\xi),\\
&\int_\Omega\int_0^\infty (1+\xi)|f^n_{\rm init}-f|(x,\xi)\,\mathrm{d}\xi\,\mathrm{d}x\xrightarrow[n\to\infty]{}0,\\
&\int_0^\infty f^n_{\rm init}(x,\xi)\,\mathrm{d}\xi\le\int_0^\infty f_{\rm init}(x,\xi)\,\mathrm{d}\xi\le C_0,\qquad \int_0^\infty \xi f^n_{\rm init}(x,\xi)\,\mathrm{d}\xi\le\int_0^\infty \xi f_{\rm init}(x,\xi)\,\mathrm{d}\xi.
\end{aligned}
$$

(with C_n possibly tending to $+\infty$; for instance we can set $f^n_{\rm init}(x,\xi)=\mathbf{1}_{0\le f_{\rm init}(x,\xi)\le n}f_{\rm init}(x,\xi)$). According to the previous Section we can associate to $f^n_{\rm init}$ the solution of the system

$$
\left\{\begin{array}{ll}
\partial_t f^n(t,x,\xi)+\partial_\xi((a(\xi)c^n(t,x)-1)f^n(t,x,\xi))=0 & t\ge0,\ x\in\Omega,\ \xi\ge0,\\
\\
\partial_t c^n(t,x)-\Delta_x c^n(t,x)+A^n(t,x)c^n(t,x)=B^n(t,x) & t\ge0,\ x\in\Omega,\\
\partial_\nu c^n=0 & \text{on }\partial\Omega,\\
A^n(t,x)=\displaystyle\int_0^\infty a(\xi)f^n(t,x\xi)\,\mathrm{d}\xi,\quad B^n(t,x)=\int_0^\infty f^n(t,x\xi)\,\mathrm{d}\xi, & \\
f^n_{|t=0}=f^n_{\rm init},\qquad c^n_{|t=0}=c_{\rm init}. &
\end{array}\right.
\tag{2.22}
$$

We can collect the following estimates, on $0\le t\le T<\infty$

$$
\begin{aligned}
&0\le c^n(t,x)\le K_T(=\|c_{\rm init}\|_\infty+C_0T),\\
&\int_0^\infty f^n(t,x,\xi)\,\mathrm{d}\xi\le C_0,\\
&\int_\Omega|c^n|^2(t,x)\,\mathrm{d}x+\int_0^t\int_\Omega|\nabla_x c^n|^2(s,x)\,\mathrm{d}x\,\mathrm{d}s\le C_T<\infty\\
&\int_\Omega\int_0^\infty\xi f^n\,\mathrm{d}\xi\,\mathrm{d}x\le\int_\Omega c^n(t,x)\,\mathrm{d}x+\int_\Omega\int_0^\infty\xi f^n(t,x,\xi)\,\mathrm{d}\xi\,\mathrm{d}x\\
&\qquad\le\int_\Omega c_{\rm init}(x)\,\mathrm{d}x+\int_\Omega\int_0^\infty\xi f^n_{\rm init}(x,\xi)\,\mathrm{d}\xi\,\mathrm{d}x\le\int_\Omega c_{\rm init}(x)\,\mathrm{d}x+\int_\Omega\int_0^\infty\xi f_{\rm init}(x,\xi)\,\mathrm{d}\xi\,\mathrm{d}x,
\end{aligned}
$$

with C_T a finite constant depending on $\|c_{\rm init}\|_{L^2(\Omega)}$, C_0 and T. Accordingly,

$$
A^n \text{ and } B^n \text{ are bounded in } L^\infty(\mathscr{Q}_T).
$$

Therefore, $\partial_t c^n$ is bounded in $L^2(0,T;H^{-1}(\Omega))$. We can apply the compactness statement in [166] which implies that, possibly at the price of extracting a subsequence,

$$
c^n\to c \text{ strongly in } L^2(\mathscr{Q}_T) \text{ and a. e.}
$$

We can also show that c^n converges to c in $C^0([0,T];L^2(\Omega)-\text{weak})$.

Next, we discuss further estimates on f^n. From the uniform integrability of $(f^n)_n$ and by using De La Vallée Poussin's lemma, see [55, p. 38], there exists a non negative function Φ satisfying

$$
\Phi(0)=0,\qquad \lim_{\tau\to+\infty}\frac{\Phi(\tau)}{\tau}=+\infty,\qquad \Phi \text{ is convex},
$$

and such that

$$
\sup_{n\in\mathbb{N}}\int_\Omega\int_0^\infty\Phi(f^n_{\rm init})\,\mathrm{d}\xi\,\mathrm{d}x\le C<\infty.
$$

Using characteristics, we show that the property extends to the solution f^n. Indeed, we have, with obvious notation,

$$f^n(t,x,\xi) = f^n_{\text{init}}\big(x, \Xi^n(0;t,x,\xi)\big)\ J^n(0;t,x,\xi).$$

Since $0 \le J^n(0;t,x,\xi) \le 1$ and $\Phi(0) = 0$, the convexity of Φ yields

$$\Phi\big(f^n(t,x,\xi)\big) \le \Phi\big(f^n_{\text{init}}\big(x, \Xi^n(0;t,x,\xi)\big)\big)\ J^n(0;t,x,\xi).$$

Integrating leads to the following uniform estimate

$$\begin{aligned}\int_\Omega \int_0^\infty \Phi\big(f^n(t,x,\xi)\big)\,\mathrm{d}\xi\,\mathrm{d}x &\le \int_\Omega \int_{\Xi^n(0;t,x,0)}^\infty \Phi\big(f^n_{\text{init}}(x,\xi)\big)\,\mathrm{d}\xi\,\mathrm{d}x \\ &\le \int_\Omega \int_0^\infty \Phi\big(f^n_{\text{init}}(x,\xi)\big)\,\mathrm{d}\xi\,\mathrm{d}x \le C < \infty.\end{aligned}$$

Since moreover the first moment with respect to ξ of f^n is controlled, the Dunford-Pettis theorem, see e. g. [71, Theorem 4.21.2], implies that f^n is relatively compact in $L^1((0,T)\times\Omega\times(0,\infty))$ for the weak topology. We can thus assume that

$$f^n \rightharpoonup f \text{ weakly in } L^1((0,T)\times\Omega\times(0,\infty)).$$

Furthermore, we can apply the De La Vallée Poussin Lemma again to exhibit a non negative function Ψ such that

$$\Psi(0) = 0, \qquad \lim_{\tau\to+\infty} \frac{\Psi(\tau)}{\tau} = +\infty, \qquad \Psi \text{ is convex},$$

and

$$\sup_{n\in\mathbb{N}} \int_\Omega \int_0^\infty \Psi(\xi)\ f^n_{\text{init}}\,\mathrm{d}\xi\,\mathrm{d}x \le \int_\Omega \int_0^\infty \Psi(\xi)\ f_{\text{init}}\,\mathrm{d}\xi\,\mathrm{d}x \le C < \infty.$$

This is the De La Vallée Poussin Lemma applied to the function $(\xi \mapsto \xi) \in L^1(\Omega\times(0,\infty), f_{\text{init}}\,\mathrm{d}\xi\,\mathrm{d}x)$. As remarked in [41, Proposition I.1.1], we can suppose moreover that $\Psi'(\tau) \ge 0$ and Ψ' is concave. Therefore we have (see [112, Lemma A.1])

$$\Psi(\xi) \le \xi\Psi'(\xi) \le 2\Psi(\xi).$$

Integrating the equation satisfied by f^n we get

$$\begin{aligned}\frac{\mathrm{d}}{\mathrm{d}t}\int_0^\infty \Psi(\xi)\ f^n(t,x,\xi)\,\mathrm{d}\xi &= \int_0^\infty \Psi'(\xi)\big(a(\xi)c^n(t,x) - 1\big)\ f^n(t,x,\xi)\,\mathrm{d}\xi \\ &\le K_T \int_0^\infty \Psi'(\xi)a(\xi)\ f^n(t,x,\xi)\,\mathrm{d}\xi.\end{aligned}$$

We evaluate the right hand side by separating small and large sizes : let $\xi_0 > 0$ and write

$$\begin{aligned}\int_0^\infty \Psi'(\xi)a(\xi)\ f^n(t,x,\xi)\,\mathrm{d}\xi &= \int_0^{\xi_0} \Psi'(\xi)a(\xi)\ f^n(t,x,\xi)\,\mathrm{d}\xi + \int_{\xi_0}^\infty \Psi'(\xi)a(\xi)\ f^n(t,x,\xi)\,\mathrm{d}\xi \\ &\le \sup_{0\le z\le\xi_0} \big(\Psi'(z)a(z)\big) \int_0^\infty f^n(t,x,\xi)\,\mathrm{d}\xi \\ &\qquad + L_{a,0}\int_0^\infty \Psi'(\xi)\xi f^n(t,x,\xi)\,\mathrm{d}\xi \\ &\le \sup_{0\le z\le\xi_0} \big(\Psi'(z)a(z)\big)C_0 + 2L_{a,0}\int_0^\infty \Psi(\xi)f^n(t,x,\xi)\,\mathrm{d}\xi\end{aligned}$$

where C_0 is defined in Equation (2.15). Hence applying the Grönwall lemma yields the uniform estimate

$$\int_\Omega \int_0^\infty \Psi(\xi)\ f^n(t,x,\xi)\,\mathrm{d}\xi\,\mathrm{d}x \le C_T$$

on $0 \le t \le T < \infty$ with $C_T > 0$ depending on C_0, ξ_0, Ω and T.

Therefore, for any function φ such that $|\varphi(\xi)| \le C(1+\xi)$, we can show that

$$\int_0^\infty \varphi(\xi) f^n(t,x,\xi)\,\mathrm{d}\xi \rightharpoonup \int_0^\infty \varphi(\xi) f(t,x,\xi)\,\mathrm{d}\xi \text{ weakly in } L^1((0,T)\times\Omega).$$

As a consequence A^n and B^n converge weakly to $A(t,x) = \int_0^\infty a(\xi) f(t,x,\xi)\,\mathrm{d}\xi$ and $B(t,x) = \int_0^\infty f(t,x,\xi)\,\mathrm{d}\xi$ in $L^1((0,T)\times\Omega)$, respectively. Since c^n is uniformly bounded and converges a.e. to c, a classical application of the Dunford-Pettis and Egoroff theorems proves that $c^n f^n$ converges weakly to cf in $L^1((0,T)\times\Omega\times(0,\infty))$. Similarly $A^n c^n$ converges weakly to Ac in $L^1((0,T)\times\Omega)$. Note also that $\partial_t f^n$ is bounded in $L^\infty((0,T)\times\Omega; W^{-1,1}(0,\infty))$[1], so that f^n is compact in $C^0([0,T]; L^1(\Omega\times(0,\infty)) - \text{weak})$. Finally, we can let n go to ∞ in (2.22) ; it shows that the pair (c,f) satisfies

$$\begin{cases} \partial_t f(t,x,\xi) + \partial_\xi((a(\xi)c(t,x)-1)f(t,x,\xi)) = 0 & t\ge 0,\ x\in\Omega,\ \xi\ge 0,\\ \partial_t c(t,x) - \Delta_x c(t,x) + A(t,x)c(t,x) = B(t,x) & t\ge 0,\ x\in\Omega,\\ \partial_\nu c = 0 & \text{on } \partial\Omega,\\ A(t,x) = \displaystyle\int_0^\infty a(\xi) f(t,x,\xi)\,\mathrm{d}\xi, \quad B(t,x) = \int_0^\infty f(t,x,\xi)\,\mathrm{d}\xi,\\ f_{|t=0} = f_{\text{init}}, \quad c_{|t=0} = c_{\text{init}}. \end{cases} \tag{2.23}$$

Note that we also get the mass conservation relation

$$\int_\Omega c(t,x)\,\mathrm{d}x + \int_\Omega\int_0^\infty \xi f(t,x,\xi)\,\mathrm{d}\xi\,\mathrm{d}x = \int_\Omega c_{\text{init}}(x)\,\mathrm{d}x + \int_\Omega\int_0^\infty \xi f_{\text{init}}(x,\xi)\,\mathrm{d}\xi\,\mathrm{d}x.$$

2.4.2 Existence for singular coefficients

We remark that in the arguments developed above, the estimates do not involve the Lipschitz constant L_a that appears in Hypothesis 2.3.1. Therefore, we can adapt straightforwardly the proof to deal with non smooth coefficients $a(\xi)$, as stated in Hypothesis 2.1.1, including the physical case $a(\xi) = \xi^{1/3}$. It suffices to consider a sequence of smooth coefficients which converges pointwise to $a(\xi)$. We prove that a subsequence extracted from the associated solutions converges to (c,f), solution with the coefficient a. We refer to [112] for such an extension in the context of the homogeneous Lifschitz-Slyozov equation.

2.4.3 Uniqueness

Let us consider $(c^{(1)}, f^{(1)})$ and $(c^{(2)}, f^{(2)})$ solution of (2.4) as obtained in the previous Section and let $0 < T < \infty$ be fixed once for all. We wish to prove that $c^{(1)} = c^{(2)}$ and $f^{(1)} = f^{(2)}$ for a.e $(t,x) \in (0,T)\times\Omega$ and $\xi \ge 0$ when the initial data coincide. We start by deriving an L^1 estimate

[1] Here, for $1 \le q \le \infty$, we denote by $W^{-1,q}(\Omega)$ the space of distributions which write as finite sums of zeroth and first order derivatives of functions belonging to $L^q(\Omega)$. Given $1 \le p < \infty$, for $1/p + 1/q = 1$, $W^{-1,q}(\Omega)$ identifies with the dual space of $W_0^{1,p}(\Omega)$, the closure of $C_c^\infty(\Omega)$ in $W^{1,p}(\Omega)$, see [171, Definition 31.3 & Proposition 31.3].

for the monomers concentration instead of the usual L^2 energy estimate. To this end, let $\eta > 0$ and introduce the function $S_\eta(z) = z/\sqrt{\eta + z^2}$ which approaches the sign function. Observe that $S_\eta \in C^1(\mathbb{R})$ with $S'_\eta(s) = \frac{\eta}{(s^2+\eta)^{3/2}} \geq 0$ so that by Stampacchia's theorem for $w \in H^1(\Omega)$, $S_\eta(w)$ belongs to $H^1(\Omega)$ too. Note also that $Z_\eta(z) = \int_0^z S_\eta(\tau)\, d\tau$ approaches $|s|$ as η goes to 0, with $0 \leq Z_\eta(z) \leq |z|$. We have

$$\big(\partial_t - \Delta_x + A^{(1)}\big)(c^{(1)} - c^{(2)}) = B^{(1)} - B^{(2)} + (A^{(2)} - A^{(1)})c^{(2)}.$$

It follows that

$$\begin{aligned}\frac{\mathrm{d}}{\mathrm{d}t}\int_\Omega Z_\eta(c^{(1)} - c^{(2)})\,\mathrm{d}x + \int_\Omega |\nabla_x(c^{(1)} - c^{(2)})|^2\ S'_\eta(c^{(1)} - c^{(2)})\,\mathrm{d}x \\ + \int_\Omega A^{(1)}(c^{(1)} - c^{(2)})S_\eta(c^{(1)} - c^{(2)})\,\mathrm{d}x \\ = \int_\Omega \big(B^{(1)} - B^{(2)} + (A^{(2)} - A^{(1)})c^{(2)}\big)S_\eta(c^{(1)} - c^{(2)})\,\mathrm{d}x.\end{aligned}$$

Since $|S_\eta(z)| \leq 1$, $S'_\eta(z) \geq 0$ and $zS_\eta(z) \geq 0$, we arrive at the following estimate

$$\begin{aligned}\int_\Omega Z_\eta(c^{(1)} - c^{(2)})(t,x)\,\mathrm{d}x \ \leq\ & \int_\Omega Z_\eta(c^{(1)}_{\mathrm{init}} - c^{(2)}_{\mathrm{init}})(t,x)\,\mathrm{d}x \\ & + \int_0^t\int_\Omega |B^{(1)} - B^{(2)}|(s,x)\,\mathrm{d}x\,\mathrm{d}s \\ & + K_T\int_0^t\int_\Omega |A^{(2)} - A^{(1)}|(s,x)\,\mathrm{d}x\,\mathrm{d}s.\end{aligned}$$

Letting $\eta \to 0$ yields

$$\begin{aligned}\int_\Omega |c^{(1)} - c^{(2)}|(t,x)\,\mathrm{d}x \ \leq\ & \int_\Omega |c^{(1)}_{\mathrm{init}} - c^{(2)}_{\mathrm{init}}|(t,x)\,\mathrm{d}x \\ & + \int_0^t\int_\Omega |B^{(1)} - B^{(2)}|(s,x)\,\mathrm{d}x\,\mathrm{d}s + K_T\int_0^t\int_\Omega |A^{(2)} - A^{(1)}|(s,x)\,\mathrm{d}x\,\mathrm{d}s.\end{aligned} \tag{2.24}$$

The next step of the proof of uniqueness relies on an adaptation of the reasoning and estimates in [112] for the homogeneous case. We associate to $f^{(k)}$ $(k = 1, 2)$ the repartition function

$$F^{(k)}(t,x,\xi) = \int_\xi^\infty f^{(k)}(t,x,\zeta)\,\mathrm{d}\zeta.$$

As a matter of fact, we have

$$\partial_\xi F^{(k)} = -f^{(k)},$$

and

$$F^{(k)}(t,x,0) = \int_0^\infty f^{(k)}(t,x,\xi)\,\mathrm{d}\xi = B^{(k)}(t,x), \qquad \int_0^\infty F^{(k)}(t,x,\xi)\,\mathrm{d}\xi = \int_0^\infty \xi\ f^{(k)}(t,x,\xi)\,\mathrm{d}\xi.$$

We need to introduce $\xi_T > 0$ such that for any $0 \leq \xi \leq \xi_T$, we have $a(\xi)K_T - 1 \leq a(\xi_T)K_T - 1 < 0$, which makes sense owing to Hypothesis 2.1.1. Furthermore, we can pick $r > 1$ large enough such that

$$K_T a(\xi) - 1 \leq -2\frac{K_T a(\xi_T) + 1}{r} < 0 \qquad \text{holds for any } 0 \leq \xi \leq \xi_T.$$

In what follows, $L_{a,T}$ will stand for the Lipschitz constant of a on $[\xi_T, \infty)$. We will use weighted L^1 estimate, which relies of defining the auxiliary function

$$W_T(\xi) = \begin{cases} \dfrac{1}{a(\xi_T) + 1 - a(\xi)} & \text{for } 0 \le \xi \le \xi_T, \\ 1 & \text{for } \xi \ge \xi_T. \end{cases}$$

Note that

$$0 < \frac{1}{a(\xi_T) + 1} \le W_T(\xi) \le 1.$$

We have

$$\partial_t(f^{(1)} - f^{(2)}) + \partial_\xi\big((ac^{(1)} - 1)(f^{(1)} - f^{(2)})\big) = \partial_\xi\big(a(c^{(2)} - c^{(1)})f^{(2)}\big),$$

and thus

$$\partial_t(F^{(1)} - F^{(2)}) + (ac^{(1)} - 1)\partial_\xi(F^{(1)} - F^{(2)}) = -a(c^{(2)} - c^{(1)})f^{(2)}.$$

Up to a regularization argument we deduce the following inequality (obtained formally by multiplying the previous relation by $|W_T(\xi)|^r \mathrm{sgn}(F^{(1)} - F^{(2)})$ and integrating over $\xi \in (0, \infty)$).

$$\begin{aligned} &\int_0^\infty |W_T(\xi)|^r \ |F^{(1)} - F^{(2)}|(t, x, \xi)\, \mathrm{d}\xi + \int_0^t |W_T(0)|^r \ |F^{(1)} - F^{(2)}|(s, x, 0)\, \mathrm{d}s \\ &\quad \le \int_0^\infty |W_T(\xi)|^r \ |F^{(1)}_{\text{init}} - F^{(2)}_{\text{init}}|(t, x, \xi)\, \mathrm{d}\xi + \int_0^t \int_0^\infty a(\xi) \ |c^{(2)} - c^{(1)}|(s, x) \ f^{(2)}(s, x, \xi)\, \mathrm{d}\xi\, \mathrm{d}s \\ &\qquad + \int_0^t \int_0^\infty \partial_\xi\big((a(\xi)c^{(1)}(s, x) - 1)|W_T(\xi)|^r\big)|F^{(1)} - F^{(2)}|(s, x, \xi)\, \mathrm{d}\xi\, \mathrm{d}s. \end{aligned}$$

The last integral in the right hand side can be recast as

$$\begin{aligned} &\int_0^t \int_0^{\xi_T} r a'(\xi)|W_T(\xi)|^{r+1}\Big(\frac{a(\xi_T) + 1 - a(\xi)}{r} c^{(1)}(s, x) + a(\xi)c^{(1)}(s, x) - 1\Big)|F^{(1)} - F^{(2)}|(s, x, \xi)\, \mathrm{d}\xi\, \mathrm{d}s \\ &\qquad + \int_0^t \int_{\xi_T}^\infty a'(\xi)c^{(1)}(s, x) \ |F^{(1)} - F^{(2)}|(s, x, \xi)\, \mathrm{d}\xi\, \mathrm{d}s. \end{aligned}$$

When $0 \le \xi \le \xi_T$, the integrand is dominated by

$$\begin{aligned} &r a'(\xi)|W_T(\xi)|^{r+1}\Big[K_T\Big(\frac{a(\xi_T) + 1}{r} + a(\xi)\Big) - 1\Big]|F^{(1)} - F^{(2)}|(s, x, \xi) \\ &\le -(K_T a(\xi_T) + 1)a'(\xi)|W_T(\xi)|^{r+1}|F^{(1)} - F^{(2)}|(s, x, \xi) \le 0 \end{aligned}$$

according to the definition of ξ_T and the choice of r. When $\xi \ge \xi_T$ we can simply use the fact that $a'(\xi)$ is bounded far away from $\xi = 0$. Note that we can also dominate, for some $\xi_0 > 0$,

$$\begin{aligned} &\int_0^t \int_0^\infty a(\xi) \ |c^{(2)} - c^{(1)}|(s, x) \ f^{(2)}(s, x, \xi)\, \mathrm{d}\xi\, \mathrm{d}s = \int_0^t \left(\int_0^{\xi_0} \ldots \mathrm{d}\xi + \int_{\xi_0}^\infty \ldots \mathrm{d}\xi\right) \mathrm{d}s \\ &\quad \le 2 \sup_{0 \le \xi \le \xi_0} \big(a(\xi)\big) \int_0^t \int_0^\infty |c^{(2)} - c^{(1)}|(s, x) \ f^{(2)}(s, x, \xi)\, \mathrm{d}\xi\, \mathrm{d}s \\ &\qquad + L_{a,0} \int_0^t \int_0^\infty |c^{(2)} - c^{(1)}|(s, x) \ \xi f^{(2)}(s, x, \xi)\, \mathrm{d}\xi\, \mathrm{d}s \\ &\quad \le \left(2 \sup_{0 \le \xi \le \xi_0} \big(a(\xi)\big) \ C_0 + L_{a,0} \ C_T\right) \int_0^t |c^{(2)} - c^{(1)}|(s, x)\, \mathrm{d}s. \end{aligned}$$

Finally, we are led to the following estimate

$$\begin{aligned}
&\int_0^\infty |W_T(\xi)|^r\ |F^{(1)}-F^{(2)}|(t,x,\xi)\,\mathrm{d}\xi \\
&\quad+\int_0^t |W_T(0)|^r\ |F^{(1)}-F^{(2)}|(s,x,0)\,\mathrm{d}s \\
&\quad+(K_T a(\xi_T)+1)\int_0^t\int_0^{\xi_T} |W_T(\xi)|^{r+1}\ a'(\xi)\ |F^{(1)}-F^{(2)}|(s,x,\xi)\,\mathrm{d}\xi\,\mathrm{d}s \\
&\qquad\le \int_0^\infty |W_T(\xi)|^r\ |F^{(1)}_{\mathrm{init}}-F^{(2)}_{\mathrm{init}}|(t,x,\xi)\,\mathrm{d}\xi \\
&\qquad\quad+\Big(2\sup_{0\le\xi\le\xi_0}\big(a(\xi)\big)\ C_0+L_{a,0}\ C_T\Big)\int_0^t |c^{(2)}-c^{(1)}|(s,x)\,\mathrm{d}s \\
&\qquad\quad+L_{a,T}\int_0^t\int_0^\infty |F^{(1)}-F^{(2)}|(s,x,\xi)\,\mathrm{d}\xi\,\mathrm{d}s,
\end{aligned} \tag{2.25}$$

where C_T is the bound on $\int_0^\infty \xi f^{(k)}(t,x,\xi)\,\mathrm{d}\xi$.

We combine the obtained relations, bearing in mind that W_T is bounded from below and above and that $B^{(k)}(t,x)=F^{(k)}(t,x,0)$. Let $\lambda>0$ to be precised. By using (2.24) and (2.25), we are led to

$$\begin{aligned}
&\frac{1}{(a(\xi_T)+1)^r}\int_\Omega\int_0^\infty |F^{(1)}-F^{(2)}|(t,x,\xi)\,\mathrm{d}\xi\,\mathrm{d}x+\lambda\int_\Omega |c^{(1)}-c^{(2)}|(t,x)\,\mathrm{d}x \\
&\quad+\Big(\frac{1}{(a(\xi_T)+1)^r}-\lambda\Big)\int_0^t\int_\Omega |B^{(1)}-B^{(2)}|(s,x)\,\mathrm{d}x\,\mathrm{d}s \\
&\quad+\frac{K_T a(\xi_T)+1}{(a(\xi_T)+1)^{r+1}}\int_0^t\int_\Omega\int_0^{\xi_T} a'(\xi)\ |F^{(1)}-F^{(2)}|(s,x,\xi)\,\mathrm{d}\xi\,\mathrm{d}x\,\mathrm{d}s \\
&\le\int_\Omega\int_0^\infty |F^{(1)}_{\mathrm{init}}-F^{(2)}_{\mathrm{init}}|(t,x,\xi)\,\mathrm{d}\xi\,\mathrm{d}x+\lambda\int_\Omega |c^{(1)}_{\mathrm{init}}-c^{(2)}_{\mathrm{init}}|(t,x)\,\mathrm{d}x \\
&\quad+\Big(2\sup_{0\le\xi\le\xi_0}\big(a(\xi)\big)\ C_0+L_{a,0}\ C_T\Big)\int_0^t\int_\Omega |c^{(1)}-c^{(2)}|(s,x)\,\mathrm{d}x\,\mathrm{d}s \\
&\quad+L_{a,T}\int_0^t\int_\Omega\int_0^\infty |F^{(1)}-F^{(2)}|(s,x,\xi)\,\mathrm{d}\xi\,\mathrm{d}s \\
&\quad+\lambda K_T\int_0^t\int_\Omega |A^{(2)}-A^{(1)}|(s,x)\,\mathrm{d}x\,\mathrm{d}s
\end{aligned}$$

on $0\le t\le T<\infty$. It remains to discuss the last integral of the right hand side. We split as follows

$$\begin{aligned}
|A^{(2)}-A^{(1)}|(s,x) &= \Big|\int_0^\infty a(\xi)(f^{(2)}-f^{(1)})(s,x,\xi)\,\mathrm{d}\xi\Big| = \Big|\int_0^\infty a(\xi)\partial_\xi(F^{(1)}-F^{(2)})(s,x,\xi)\,\mathrm{d}\xi\Big| \\
&= \Big|\int_0^\infty a'(\xi)(F^{(1)}-F^{(2)})(s,x,\xi)\,\mathrm{d}\xi\Big| = \Big|\int_0^{\xi_T}\ldots+\int_{\xi_T}^\infty\ldots\Big| \\
&\le \int_0^{\xi_T} a'(\xi)\ |F^{(1)}-F^{(2)}|(s,x,\xi)\,\mathrm{d}\xi+L_{a,T}\int_{\xi_T}^\infty |F^{(1)}-F^{(2)}|(s,x,\xi)\,\mathrm{d}\xi.
\end{aligned}$$

We now rearrange terms to obtain

$$\begin{aligned}
&\frac{1}{(a(\xi_T)+1)^r}\int_\Omega\int_0^\infty |F^{(1)}-F^{(2)}|(t,x,\xi)\,\mathrm{d}\xi\,\mathrm{d}x+\lambda\int_\Omega |c^{(1)}-c^{(2)}|(t,x)\,\mathrm{d}x\\
&\quad+\Big(\frac{1}{(a(\xi_T)+1)^r}-\lambda\Big)\int_0^t\int_\Omega |B^{(1)}-B^{(2)}|(s,x)\,\mathrm{d}x\,\mathrm{d}s\\
&\quad+\Big(\frac{K_T a(\xi_T)+1}{(a(\xi_T)+1)^{r+1}}-\lambda K_T\Big)\int_0^t\int_\Omega\int_0^{\xi_T} a'(\xi)\ |F^{(1)}-F^{(2)}|(s,x,\xi)\,\mathrm{d}\xi\,\mathrm{d}x\,\mathrm{d}s\\
&\le\int_\Omega\int_0^\infty |F^{(1)}_{\rm init}-F^{(2)}_{\rm init}|(t,x,\xi)\,\mathrm{d}\xi\,\mathrm{d}x+\lambda\int_\Omega |c^{(1)}_{\rm init}-c^{(2)}_{\rm init}|(t,x)\,\mathrm{d}x\\
&\quad+\Big(2\sup_{0\le\xi\le\xi_0}\big(a(\xi)\big)\ C_0+L_{a,0}\ C_T\Big)\int_0^t\int_\Omega |c^{(1)}-c^{(2)}|(s,x)\,\mathrm{d}x\,\mathrm{d}s\\
&\quad+L_{a,T}(1+\lambda K_T)\int_0^t\int_\Omega\int_0^\infty |F^{(1)}-F^{(2)}|(s,x,\xi)\,\mathrm{d}\xi\,\mathrm{d}x\,\mathrm{d}s.
\end{aligned}$$

Thus, we pick $\lambda>0$ so that

$$\frac{1}{(a(\xi_T)+1)^r}>\lambda>0\qquad\text{and}\qquad\frac{a(\xi_T)+1/K_T}{(a(\xi_T)+1)^{r+1}}>\lambda>0.$$

It suffices to apply the Grönwall lemma to conclude with a continuity estimate where

$$\int_\Omega\int_0^\infty |F^{(1)}-F^{(2)}|(t,x,\xi)\,\mathrm{d}\xi\,\mathrm{d}x\qquad\text{and}\qquad\int_\Omega |c^{(1)}-c^{(2)}|(t,x)\,\mathrm{d}x$$

are dominated on $0\le t\le T$ by

$$\Gamma_T\left(\int_\Omega\int_0^\infty |F^{(1)}_{\rm init}-F^{(2)}_{\rm init}|(x,\xi)\,\mathrm{d}\xi\,\mathrm{d}x+\int_\Omega |c^{(1)}_{\rm init}-c^{(2)}_{\rm init}|(x)\,\mathrm{d}x\right)$$

with a suitable constant $\Gamma_T>0$.

2.4.4 Dirichlet boundary condition

Let us consider the same problem, but we replace (2.5) by the Dirichlet condition

$$c_{|\partial\Omega}=0. \tag{2.26}$$

This is precisely the case presented in [124]. The total mass conservation does not hold because there is a diffusion current from the boundary. Nevertheless, the general strategy of proof can be adapted to this case. Let us indicate where the main modifications are, within the arguments. The discussion of Section 2.2 adapts readily using the space $H^1_0(\Omega)$ instead of $H^1(\Omega)$. Therefore, we can repeat the arguments of Section 2.3 ; the derivation of all the necessary estimates works exactly as before, except (2.21). However, (2.20) can still be used to estimate the first order moment of the cluster distribution, since we infer

$$0\le\int_0^\infty \xi f(t,x,\xi)\,\mathrm{d}\xi=\int_0^\infty \xi f_{\rm init}(x,\xi)\,\mathrm{d}\xi+\int_0^t (Ac-B)(s,x)\,\mathrm{d}s,$$

where

$$0\le B(t,x)=\int_0^\infty f(t,x,\xi)\,\mathrm{d}\xi\le\int_0^\infty f_{\rm init}(x,\xi)\,\mathrm{d}\xi$$

and, by using Hypothesis 2.1.1,

$$\begin{aligned} 0 \le A(t,x) &= \int_0^\infty a(\xi) f(t,x,\xi)\,\mathrm{d}\xi \\ &\le 2a(\xi_0)\int_0^\infty f(t,x,\xi)\,\mathrm{d}\xi + L_{a,0}\int_0^\infty \xi f(t,x,\xi)\,\mathrm{d}\xi. \end{aligned}$$

Applying the Grönwall lemma, we conclude again that

$$\int_0^\infty \xi f(t,x,\xi)\,\mathrm{d}\xi \le C_T$$

holds for $x \in \Omega$ and $0 \le t \le T < \infty$. This estimate, which does not require a global Lipschitz estimate on the kinetic coefficient a, allows to deal with general initial data and singular coefficients as we did in the previous subsections.

Theorem 2.4.1. *Suppose that Hypotheses 2.1.1 and 2.1.2 are fulfilled. Then, there exists a weak solution (c,f) of (2.4)–(2.6), where (2.26) replaces (2.5), with, for any $0 < T < \infty$, $c \in L^\infty((0,T)\times\Omega)\cap L^2(0,T;H_0^1(\Omega))$, $f \in L^\infty((0,T)\times\Omega;L^1((0,\infty),(1+\xi)\,\mathrm{d}\xi))$, $c \in C^0([0,T];L^2(\Omega)-$ weak$)$, $f \in C^0([0,T];L^1(\Omega\times(0,\infty)) -$ weak$)$.*

2.4.5 Free–space problem

It is finally worth to investigate the situation where Ω is replaced by the whole space $\mathbb{R}^N$ thus neglecting any boundary effect. Technically, it induces new difficulties because we are working in an unbounded domain and the compactness argument does not work directly. Hence, we need to establish some weighted estimates. In the context of Proposition 2.2.1, the estimates for the diffusion equation can be obtained as follows

$$\begin{aligned} &\frac{\mathrm{d}}{\mathrm{d}t}\int_{\mathbb{R}^N} |c(t,x)|^2\,\mathrm{d}x + 2\int_{\mathbb{R}^N} |\nabla_x c(t,x)|^2\,\mathrm{d}x + 2\int_{\mathbb{R}^N} A(t,x)\ |c(t,x)|^2\,\mathrm{d}x = 2\int_{\mathbb{R}^N} B(t,x)\ c(t,x)\,\mathrm{d}x \\ &\quad\le \int_{\mathbb{R}^N} |c(t,x)|^2\,\mathrm{d}x + \int_{\mathbb{R}^N} |B(t,x)|^2\,\mathrm{d}x \end{aligned}$$

together with

$$\begin{aligned} &\frac{\mathrm{d}}{\mathrm{d}t}\int_{\mathbb{R}^N} |x|^2\ |c(t,x)|^2\,\mathrm{d}x + 2\int_{\mathbb{R}^N} |x|^2\ |\nabla_x c(t,x)|^2\,\mathrm{d}x + 2\int_{\mathbb{R}^N} A(t,x)\ |x|^2|c(t,x)|^2\,\mathrm{d}x \\ &\quad= -\int_{\mathbb{R}^N} 4x\cdot\nabla_x\Big(\frac{c^2}{2}\Big)\,\mathrm{d}x + 2\int_{\mathbb{R}^N} |x|^2\ B(t,x)\ c(t,x)\,\mathrm{d}x \\ &\quad\le 2N\int_{\mathbb{R}^N} |c(t,x)|^2\,\mathrm{d}x + \int_{\mathbb{R}^N} |x|^2\ |c(t,x)|^2\,\mathrm{d}x + \int_{\mathbb{R}^N} |x|^2|B(t,x)|^2\,\mathrm{d}x. \end{aligned}$$

By using the Grönwall lemma and repeating the arguments of Section 2.2, we are thus led to the following analog to Proposition 2.2.1.

Proposition 2.4.2. *Let $0 < T < +\infty$. Let A and B be non negative functions in $L^\infty((0,T)\times\mathbb{R}^N)$, with furthermore $\sqrt{1+|x|^2}B \in L^\infty(0,T;L^2(\mathbb{R}^N))$. Suppose that $0 \le B(t,x) \le C_0 < \infty$ for almost every (t,x). Then, for any $c_{\mathrm{init}} \in L^2(\mathbb{R}^N)$ with $|x|c_{\mathrm{init}} \in L^2(\mathbb{R}^N)$, there exists a unique $c \in L^2(0,T;H^1(\mathbb{R}^N)) \cap C([0,T];L^2(\mathbb{R}^N))$ with $\partial_t c \in L^2(0,T;(H^1(\mathbb{R}^N))')$ solution of*

$$\partial_t c + Ac - \Delta_x c = B \quad \text{in } (0,T)\times\mathbb{R}^N,$$

with initial data $c(t=0,x) = c_{\rm init}(x)$. *Furthermore if* $c_{\rm init} \geq 0$ *belongs to* $L^\infty(\mathbb{R}^N)$, *then the solution* c *satisfies* $0 \leq c(t,x) \leq K_T$ *with* K_T *a constant depending on* C_0, $\|c_{\rm init}\|_\infty$ *and* T. *We also have*

$$\sup_{0\leq t\leq T}\int_{\mathbb{R}^N}(1+|x|^2)|c(t,x)|^2\,\mathrm{d}x \leq C_T \qquad \textit{and} \qquad \int_0^T\int_{\mathbb{R}^N}(1+|x|^2)|\nabla_x c(s,x)|^2\,\mathrm{d}x\,\mathrm{d}s \leq C_T.$$

for some constant C_T *depending on* C_0, T *and* $\|\sqrt{1+|x|^2}c_{\rm init}\|_{L^2(\mathbb{R}^N)}$.

The estimate on A and B can be deduced from the transport equation : since the space variable is only a parameter, we have (2.16) as well as

$$\sup_{0\leq t\leq T}\int_{\mathbb{R}^N}(1+|x|^2)\left(\int_0^\infty f(t,x,\xi)\,\mathrm{d}\xi\right)^2\mathrm{d}x \leq \int_{\mathbb{R}^N}(1+|x|^2)\left(\int_0^\infty f_{\rm init}(x,\xi)\,\mathrm{d}\xi\right)^2\mathrm{d}x.$$

It allows to apply the same reasoning as in Section 2.3 once it has been remarked that the set $\{\phi \in H^1(\mathbb{R}^N),\ |x|\phi \in L^2(\mathbb{R}^N)\}$ embeds compactly in $L^2(\mathbb{R}^N)$. Finally we can make use of the mass conservation to extend the result to unbounded data and singular coefficients, as we did in Section 2.4. The first order moment is bounded independently on the (global) Lipschitz constant of a, and we can show that the sequence of approximations f^n (resp. A^n and B^n) is weakly compact in $L^1((0,T)\times B(0,R)\times(0,\infty))$ (resp. $L^1((0,T)\times B(0,R))$ for any $0<T,R<\infty$. Details are left to the reader, which lead to the following statement.

Theorem 2.4.3. *Suppose that Hypotheses 2.1.1 and 2.1.2 are fulfilled (with* $\Omega = \mathbb{R}^N$*). Furtheremore, assume*

$$\int_{\mathbb{R}^N}(1+|x|^2)|c_{\rm init}(x)|^2\,\mathrm{d}x<\infty, \qquad \int_{\mathbb{R}^N}(1+|x|^2)\left(\int_0^\infty f_{\rm init}(x,\xi)\,\mathrm{d}\xi\right)^2\mathrm{d}x<\infty.$$

Then, there exists a weak solution (c,f) *of*(2.4) *associated to the initial condition* $(c_{\rm init}, f_{\rm init})$, *with, for any* $0<T<\infty$, $c \in L^\infty((0,T)\times\Omega)\cap L^2(0,T;H^1(\mathbb{R}^N))$, $f \in L^\infty((0,T)\times\Omega;L^1((0,\infty),(1+\xi)\,\mathrm{d}\xi))$, $c \in C^0([0,T];L^2(\mathbb{R}^N)-\textit{weak})$, $f \in C^0([0,T];L^1(\mathbb{R}^N\times(0,\infty))-\textit{weak})$.

2.5 Numerical simulations

In this Section we present a numerical scheme to simulate the behavior of the density of particles and monomers concentration, when monomers are subject to space diffusion, namely we design a scheme for (2.4). The construction of the scheme takes care of the mass conservation and we give some hints concerning stability issues. Note that adding the space variable considerably increases the computation cost in comparison to the homogeneous case. The scheme is satisfactory to investigate transient states, but, definitely, it seems difficult to expect relevant numerical experiments of the large time behavior. For the sake of simplicity we consider the problem set on the one-dimensional slab $x \in (0,L)$, but the extension to higher dimension is straightforward.

2.5.1 Presentation of the algorithm

We consider time, space and size steps $\Delta t>0$, $\Delta x>0$, and $\Delta\xi>0$, respectively. We define discrete time $t^n = n\Delta t$, discrete size $\xi_j = j\Delta\xi$, and position $x_i = i\Delta x$ for $n,i,j \in \mathbb{N}$. We consider the discrete cells $C_j = (\xi_{j-1/2},\xi_{j+1/2})$ centered on ξ_j. The discrete unknowns c_i^n and $f_{i,j}^n$ are intended to be approximations of $c(t^n,x_i)$ and $\frac{1}{\Delta\xi}\int_{C_j} f(t^n,x_i,\zeta)\,\mathrm{d}\zeta$, respectively. The scheme is based on the following time–splitting :

- The updating of the particles distribution follows by integrating the advection equation over the finite volume cells C_j ; for any fixed i, we set

$$f_{i,j}^{n+1} = f_{i,j}^n - \frac{\Delta t}{\Delta \xi}\Big((V\,f)_{i,j+1/2}^n - (V\,f)_{i,j-1/2}^n \Big) \quad \text{with } V(t,x,\xi) = a(\xi)c(t,x) - 1,$$

which requires a suitable definition of the numerical fluxes at the interfaces $\xi_{j\pm 1/2}$. In our simulation we use the Rusanov scheme where

$$(V\,f)_{i,j+1/2}^n = \frac{1}{2}\big[(V\,f)_{i,j}^n + (V\,f)_{i,j+1}^n\big] - \frac{L_i^n}{2}\big(f_{i,j+1}^n - f_{i,j}^n\big), \qquad L_i^n = \max_{j\in\mathbb{N}} |V_{i,j}^n|$$

for all fixed space indices i. Then we have the following approximation

$$f_{i,j}^{n+1} = \big(1 - L_i^n \frac{\Delta t}{\Delta \xi}\big) f_{i,j}^n - \frac{\Delta t}{2\Delta \xi}\Big(f_{i,j+1}^n \big(V_{i,j+1}^n - L_i^n\big) - f_{i,j-1}^n \big(V_{i,j-1}^n + L_i^n\big)\Big).$$

In practice, the index j spans a finite set $\{0, ..., j_{\max}\}$ and we need fictitious mesh points, where data and unknowns are defined as follows :

$$V_{i,j_{max+1}}^n = V_{i,j_{\max}}^n, \qquad V_{i,-1}^n = V_{i,0}^n, \qquad f_{i,j_{max+1}}^n = f_{i,j_{\max}}^n, \qquad f_{i,-1}^n = f_{i,0}^n.$$

The stability of the scheme is guaranteed by the CFL condition $\Delta t \leq \frac{\Delta x}{L_i^n}$. We point out that we tried other classical finite volume schemes like WENO (Weighted Essentially Non-Oscillatory method) or the ADM (Anti Dissipative Method) method described in [92] but we did not observe any substantial changes in the results (for short times).

- For updating the monomers concentration, we use the following numerical finite difference approximation

$$(E) \qquad \frac{c_i^{n+1} - c_i^n}{\Delta t} = \frac{c_{i+1}^n - 2c_i^n + c_{i-1}^n}{\Delta x^2} - \frac{\Delta \xi}{\Delta t}\sum_{j=0}^{j_{\max}} \xi_j \big(f_{i,j}^{n+1} - f_{i,j}^n\big) \quad \forall i \in \mathbb{N},$$

or the implicit version

$$(I) \qquad \frac{c_i^{n+1} - c_i^n}{\Delta t} = \frac{c_{i+1}^{n+1} - 2c_i^{n+1} + c_{i-1}^{n+1}}{\Delta x^2} - \frac{\Delta \xi}{\Delta t}\sum_{j=0}^{j_{\max}} \xi_j \big(f_{i,j}^{n+1} - f_{i,j}^n\big) \quad \forall i \in \mathbb{N}.$$

It can be written in matrix form

$$A_1 C^{n+1} = A_2 C^n - r^{n+1/2} \tag{2.27}$$

with $C^n = (c_i^n)_{i\in\{0,\dots,i_{\max}\}}$, $r^{n+1/2} = \big(\Delta\xi \sum_{j=0}^{j_{\max}} \xi_j (f_{i,j}^{n+1} - f_{i,j}^n)\big)_{i\in\{0,\dots,i_{\max}\}}$,

$$\mathbb{A} = \begin{pmatrix} -2 & 1 & 0 & ... & \\ 1 & -2 & 1 & 0 & ... \\ 0 & \ddots & \ddots & \ddots & \ddots \\ 0 & ... & 1 & -2 & 1 \\ 0 & ... & 0 & 1 & -2 \end{pmatrix}$$

and either $A_1 = \mathbb{I}$, the identity matrix, $A_2 = \frac{\Delta t}{\Delta x^2}\mathbb{A}$ for scheme (E) or $A_1 = \mathbb{I} - \frac{\Delta t}{\Delta x^2}\mathbb{A}$, $A_2 = \mathbb{I}$ for scheme (I). The stability of the explicit scheme (E) requires the CFL condition $\Delta t \leq \Delta x^2/2$. Since this condition is usually more restrictive than the one obtained at the previous step, it can be efficient to use a subcycling method where we perform one time step Δt_{adv} for f while several time steps $\Delta t_{\text{diff}} \ll \Delta t_{\text{adv}}$ for c. Anyway, the parabolic CFL condition leads to a prohibitive computational cost for multi-dimension simulations where the implicit scheme (I) will be preferred. It requires the inversion of the sparse positive definite matrix $\mathbb{I} - \frac{\Delta t}{\Delta x^2}\mathbb{A}$, that can be done by using performing algorithms like the conjugate gradient method. In numerical simulations we do not observe significant discrepancies between results obtained by either the explicit or the implicit scheme. The numerical results in the next section are provided by the explicit one. Owing to the Neumann boundary conditions, the discrete mass conservation relation

$$\Delta x \sum_i c_i^{n+1} + \Delta x \Delta\xi \sum_i \sum_j \xi_j f_{i,j}^{n+1} = \Delta x \sum_i c_i^n + \Delta x \Delta\xi \sum_i \sum_j \xi_j f_{i,j}^n \tag{2.28}$$

holds. We check numerically that this quantity is indeed exactly conserved.

2.5.2 Numerical results

The numerical simulations are performed in the slab $x \in [0, 100]$ with 10 points by length unit. The size variable is truncated to $\xi \in [0, 100]$ meshed with 20 points by size unit. The initial data are defined by

$$\begin{cases} c_{\text{init}}(x) = 0.5\ \mathbf{1}_{x\in[20,35]}, \\ \\ f_{\text{init}}(x,\xi) = 0.01\ \mathbf{1}_{x\in[20,35]} \times \mathbf{1}_{\xi\in[30,35]}. \end{cases} \tag{2.29}$$

Figure 3.2 shows the initial data $f_{\text{init}}(x, \xi)$. On Figure 2.2, the solution $f_{\text{init}}(T, x, \xi)$ at the final time $T = 20$ can be compared to the solution obtained by getting rid of the diffusion term in the monomers equation. We clearly observe the influence of the diffusion of monomers on the space repartition of the macro-particles.

The monomers concentration in the same situations is displayed in Figure 3.4 (diffusion case on the right, diffusion–free case on the left). As said above, the simulations also show a numerical evidence of the conservation of the total mass. The time evolution of the monomers concentration can be found in Figure 3.5. As expected the support of the concentration spreads as time increases, by contrast to the diffusion free case. Note however that the maximum of c seems unchanged between the two cases. Of course, since the space repartition of monomers is modified, it influences the dynamics of the whole system. In Figure 3.6 we show the time evolution of the mean value of c and f over space, that is compared to the usual solutions of the Lifschitz-Slyozov system. It clearly shows that, even considering only mean values, space diffusion changes the behavior of the solutions, for both the monomers concentration and the particles distribution function.

As explained in the Introduction, many questions arise with the large time behavior of the solutions of the Lifschitz-Slyozov equations (2.2)-(2.3), and capturing the correct asymptotic profile is numerically challenging. Similar questions can be addressed for the modified model with space diffusion of monomers. Like for the standard model a numerical difficulty comes from the formation of particles with large sizes. As time goes, the support of $f(t, x, \xi)$ might reach the largest size of the numerical domain, which then induces a fictitious loss of mass. Increasing the size domain leads to a considerable increase of the computational cost because f now also

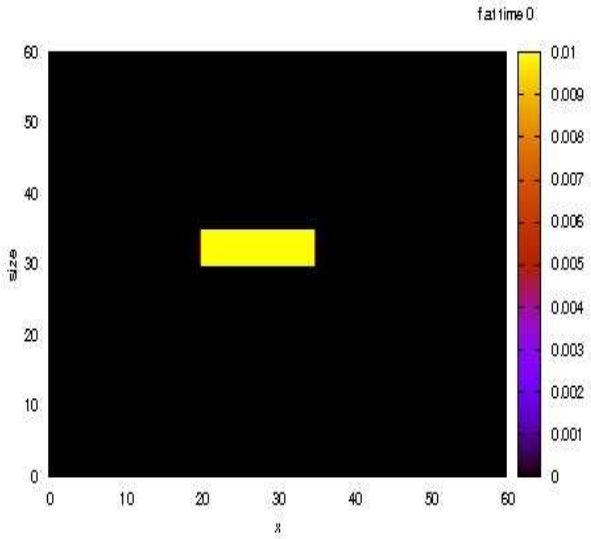

Figure 2.1 – initial density.

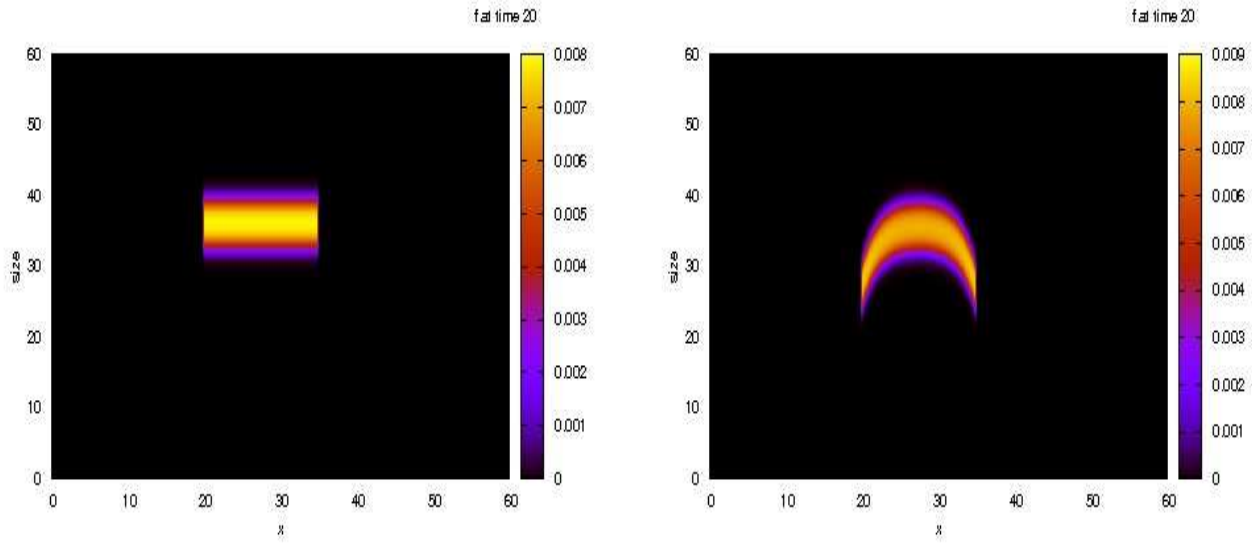

Figure 2.2 – left : density at time 20 without diffusion term ; right : density at time 20 with diffusion term.

depends on the space variable. Therefore, the present method is restricted to quite short times of simulations.

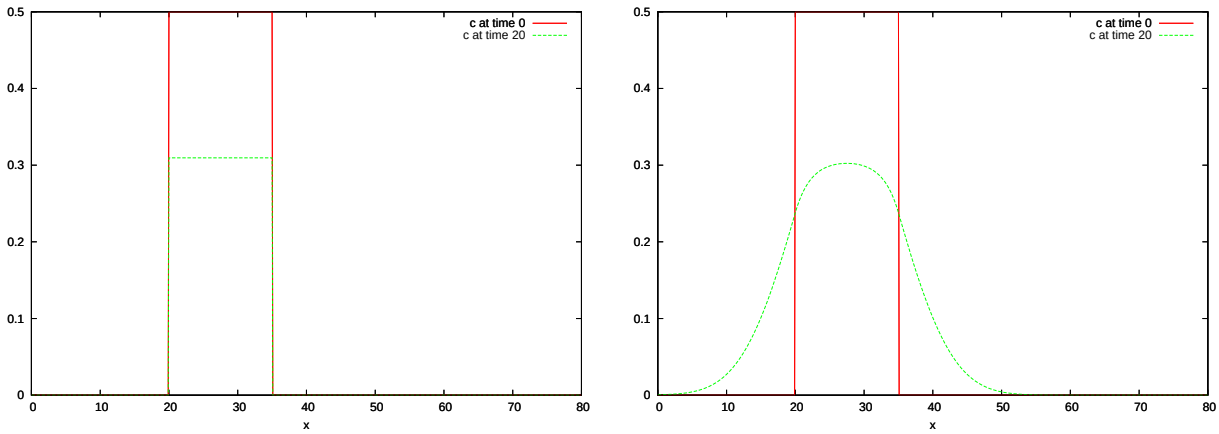

Figure 2.3 – left : evolution of the monomers concentration without diffusion ; right : evolution of the monomers concentration with diffusion.

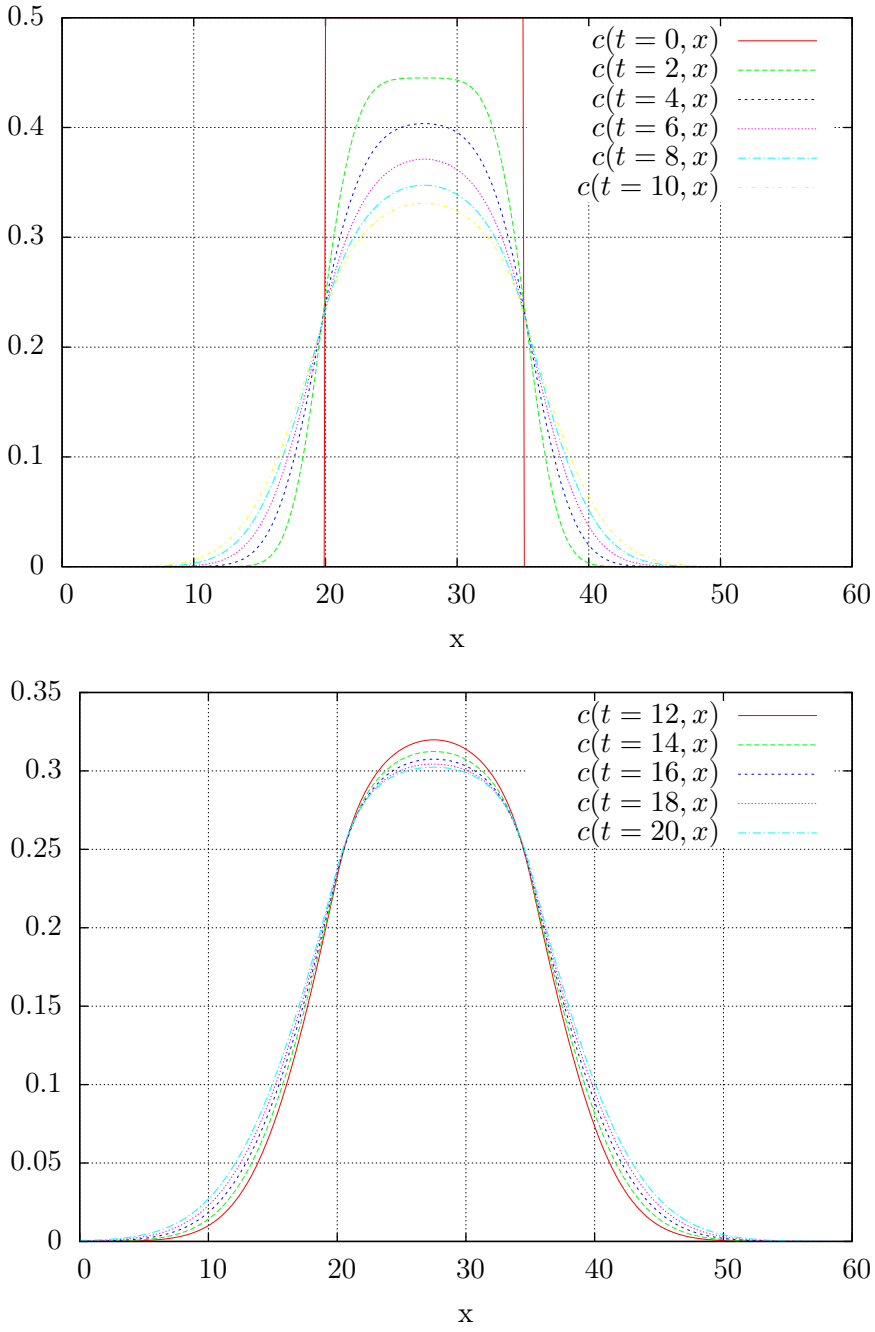

Figure 2.4 – Evolution of the monomers concentration all 2 time units with diffusion term.

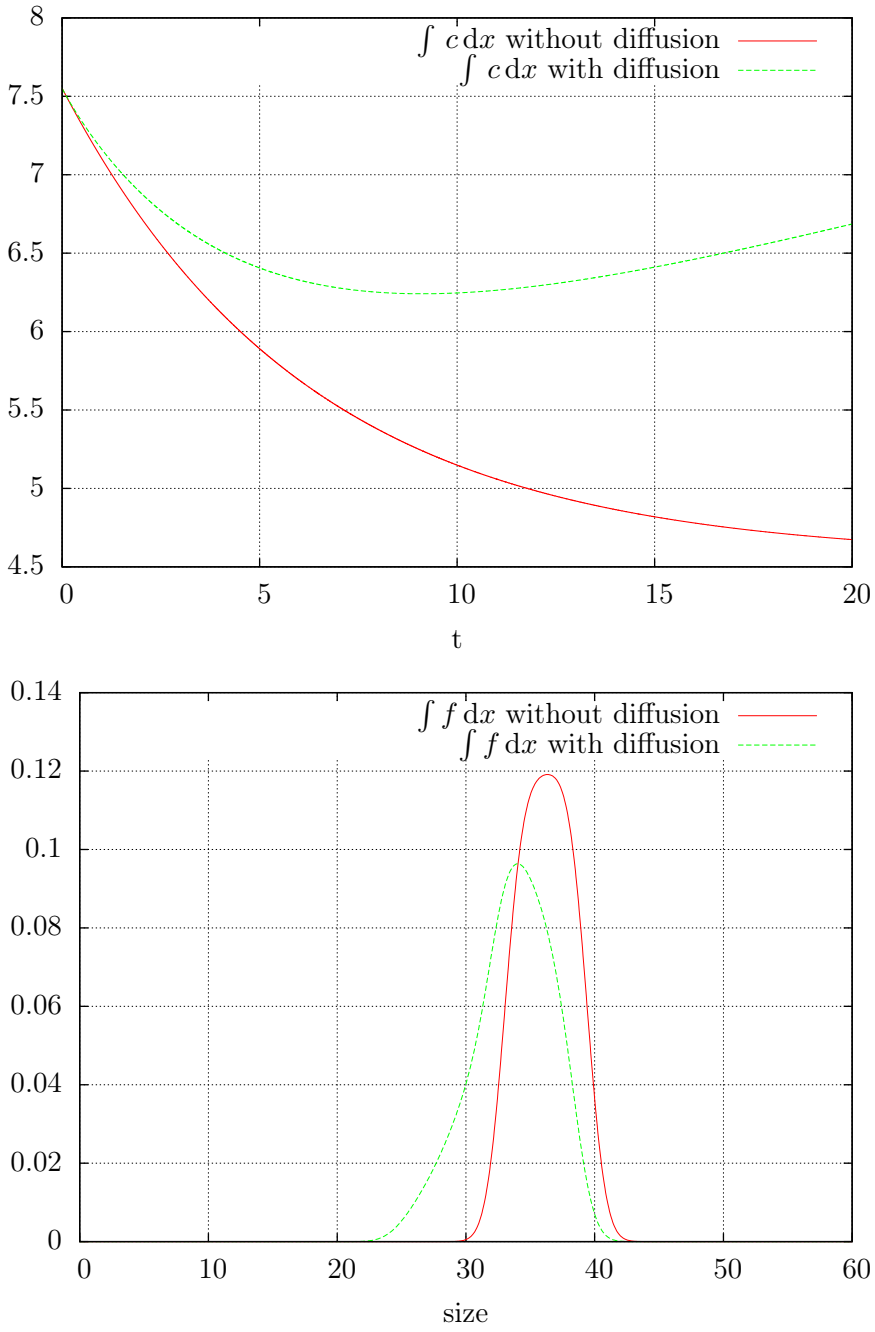

Figure 2.5 – Comparison of mean values of the unknowns (dashed line=diffusion case). Top : time evolution of $\int c(t,x)\,dx$; Bottom : size variation of $\int f(t=20,x,\xi)\,dx$.

Chapitre 3

Problème inverse pour un modèle général d'agrégation-fragmentation

Cet article étudie le problème inverse permettant de déterminer le taux de division cellulaire à partir d'une mesure en temps long de la densité de répartition pour une équation générale de type agrégation-fragmentation. Nous proposons des méthodes de régularisations de type quasi-réversible et filtrage permettant d'estimer le taux de division cellulaire pour un noyau de fragmentation et un taux de croissance assez généraux. Nous présentons également des résultats de simulations numériques sur la reconstruction de ce taux de division cellulaire à partir de données mesurées de la densité en temps long de la population cellulaire.

Le travail présenté dans ce chapitre a été réalisé en collaboration avec Marie Doumic et a été soumis pour publication [68].

Introduction

To model the behavior of a population where growth and division depend on a structuring quantity of the individuals such as size, the following mass-balance equation is currently used :

$$\begin{cases} \dfrac{\partial}{\partial_t} n(t,x) + c\dfrac{\partial}{\partial_x}(g(x)n(t,x)) + B(x)n(t,x) = 2\displaystyle\int_0^{+\infty} B(y)\kappa(x,y)n(t,y)\,\mathrm{d}y, \quad t>0,\ x>0, \\ n(t=0,x) = n^0(x), \quad x \geq 0, \\ g(x=0)n(t,x=0) = 0,\ t \geq 0, \quad c>0. \end{cases} \tag{3.1}$$

Here, n denotes the density of the individuals structured by the size variable x at time t; the growth rate is given by $g(x)$; the division rate $B(y)\kappa(x,y)$ represents the rate at which a given individual of size y gives birth to two individuals of size respectively x and $y-x$, whereas $B(y)$ is the total rate of division for individuals of size y. This physical interpretation of $\kappa(x,y)$ leads to the following assumptions :

$$\kappa(x,y) = 0 \ \ \forall x > y, \qquad \int_0^{\infty} \kappa(x,y)\,\mathrm{d}x = 1, \qquad \kappa(x,y) = \kappa(y-x,y). \tag{3.2}$$

By simple integration and symmetry, it leads to the following well-known relation, expressing the conservation of mass by the division process :

$$\int_0^\infty x\kappa(x,y)\,\mathrm{d}x = \frac{y}{2}.$$

Problem (3.1) or its variants arises in many different contexts, ranging from cell division, protein polymerization, telecommunication, neurosciences, and its mathematical study can provide useful information on the qualitative behavior of the phenomenon under consideration (see, among many others, [60, 156]). To be able to use it as a predictive model however, it is crucial to be able to estimate quantitatively its parameters g, B and κ.

A first step consists in the use of the asymptotic behavior of this equation, as first proposed in [158]. Indeed, by general relative entropy principle it is proven (see e.g [157, 136, 63]) that under suitable assumptions on κ, g and B one has

$$\int_0^\infty |n(t,x)e^{-\lambda_0 t} - \rho_0 N(x)|\phi(x)dx \underset{t\to\infty}{\longrightarrow} 0,$$

with $\rho_0 = \int n^0(x)\phi(x)dx$ and (λ_0, N, ϕ) is the unique eigenpair solution of the following problem :

$$\begin{cases} c\dfrac{\partial}{\partial_x}(g(x)N(x)) + (B(x)+\lambda_0)N(x) = 2\displaystyle\int_0^{+\infty} B(y)\kappa(x,y)N(y)\,\mathrm{d}y, \\ gN(x=0) = 0;\ N(x) \geq 0;\ \displaystyle\int_0^\infty N(x)\,\mathrm{d}x = 1, \quad \lambda_0 > 0, \\ cg(x)\dfrac{\partial}{\partial_x}\phi(x) - (B(x)+\lambda_0)\phi(x) = -2B(x)\displaystyle\int_0^x \kappa(y,x)\phi(y)\,\mathrm{d}y, \\ \phi(x) \geq 0;\ \displaystyle\int_0^\infty \phi(x)N(x)\,\mathrm{d}x = 1. \end{cases} \tag{3.3}$$

The use of this new problem allows to restrict the need for information to a non-temporal measure, and the problem becomes : How to recover information on g, B and κ from an experimental measurement of the asymptotic profile N and the global exponential rate of growth λ_0 of the population [2] ?

In the case when the equation models cell-division, direct measures of the growth rate $g(x)$ is possible. Direct measures of κ is also possible, by a study of the sizes of the two daughter cells born from a mother. The most delicate point is thus the measure of the division rate B, what implies to follow each cell from its birth to its division or death.

In [158] and [67], the problem of recovering the division rate from a measured N was addressed in the case when the growth rate is constant, *i.e* $g(x) \equiv 1$, and the daughter cells are twice smaller than their mother, *i.e.* when $\kappa(x,y) = \delta_{x=y/2}$. In this case, Problem (3.3) writes :

$$c\frac{\partial}{\partial_x}N + \big(B(x)+\lambda_0\big)N = 4B(2x)N(2x). \tag{3.4}$$

In this particular case, the inverse problem reads : How to recover $H = BN(x)$ solution of

$$\mathcal{L}(H) = F(N), \tag{3.5}$$

[2] Growth can naturally be balanced by death, by the addition for instance of a death term $d(x)N(x)$ on the left-hand side of the equation. This would lead to possible nonpositive rates λ_0, but our whole study would remain unchanged.

with $\mathcal{L}:\ H \to 4H(2x) - H(x)$, and $F(N) := c\partial_x N + \lambda_0 N$? The method used to solve Equation (3.5) [3] strongly uses the analytical study of the operator $\mathcal{L}$, and it was shown that the most efficient technique was then to view the problem as written in the variable $y = 2x$ rather than in x (see the discussion in [67]).

In this paper, we address the inverse problem of determining the cell division rate B when g and κ are known - or guessed - functions, but fully general ; hence, we cannot apply anymore the inversion of the operator $\mathcal{L}$ as done in [67], and new tools have to be designed.

We model the experimental measure of the distribution N by an approximation data N_ε of N satisfying $\|N - N_\varepsilon\| \leq \varepsilon$ for a suitable norm $\|\bullet\|$ [4]

The paper is organized as follows. We first study the regularity of the direct problem, what is a necessary step for a better understanding of the inverse problem. In a second part, we investigate the inverse problem of determining B by the Quasi-reversibility and Filtering methods proposed in [158] and [67] and properly adapted to our general context. In a third part we develop new numerical approaches in order to recover the rate B following the two regularization methods ; we give some numerical illustrations of our methods.

Main notations and assumptions

We use the following notations.

$$\mathbb{P} := \big\{ f \geq 0 \,:\, \exists\, \mu, \nu \geq 0,\ \limsup_{x\to\infty} x^{-\mu} f(x) < \infty,\ \liminf_{x\to\infty} x^{\nu} f(x) > 0 \big\}, \tag{3.6}$$

$$L_0^p := \big\{ f,\ \exists a > 0,\ f \in L^p(0,a) \big\}, \qquad L_p^2 := L^2(\mathbb{R}_+, x^p dx). \tag{3.7}$$

We work under the following technical assumptions, that guarantee well-posedness of Problem (3.3) as stated in [63] (we refer to that paper for a complete discussion and justification).

$$\exists\ 0 < c < \frac{1}{2}, \qquad \forall\ p \geq 2, \qquad \int_0^\infty \frac{x^p}{y^p} \kappa(x,y) dx \leq c < \frac{1}{2}. \tag{3.8}$$

$$B \in L^1_{loc}(\mathbb{R}_+^*) \cap \mathbb{P}, \quad \exists\ \alpha_0 \geq 0,\ g \in L^\infty_{loc}(\mathbb{R}_+, x^{\alpha_0} dx) \cap \mathbb{P} \tag{3.9}$$

$$\forall\, K \text{ compact in }]0, +\infty[,\ \exists\, m_k > 0 : g(x) \geq m_k\ \forall x \in K \tag{3.10}$$

$$\exists\, b \geq 0,\ supp B = [b, +\infty) \tag{3.11}$$

$$\exists\ C > 0,\ \gamma \geq 0, \frac{x^\gamma}{g(x)} \in L^1_0\ ;\ \int_0^x \kappa(z,y)\, \mathrm{d}z \leq \min\big(1, C(\frac{x}{y})^\gamma\big) \tag{3.12}$$

$$\frac{B(x)}{g(x)} \in L^1_0 \quad ;\ \frac{xB(x)}{g(x)} \xrightarrow[x\to+\infty]{} +\infty. \tag{3.13}$$

[3] the method was first developed in [158], then investigated deeper and solved numerically in [67] in a deterministic setting, and in [65] in a statistical setting. It was also successfully applied to experimental data in [66].

[4] A more precise model for the measured data, in a statistical setting, can be found in [65].

3.1 Regularity of the direct problem

Before studying the inverse problem, it is necessary to have a proper knowledge of the direct one, which states as follows : What is the regularity of the map $\Gamma : (c, B) \to (\lambda_0, N)$ solutions of Problem (3.3) ? How can we define a proper definition domain for Γ ?

In [67], Theorems 3.1. and 3.2 establish that the map $\Gamma_0 : B \to (\lambda_0, N)$ is Lipschitz-continuous for $c = 1$ fixed, $g = 1$, $\kappa = \frac{1}{2}\delta_{x=\frac{y}{2}}$ and division rates B such that $0 < B_m \leq B \leq B_M < \infty$; in other words, for division rates uniformly positive and uniformly bounded.

In this paper, we want to state such results for general growth rates g and division kernels κ, with division rates B not necessarily uniformly bounded. Our study is thus first based on the well-posedness of this general eigenvalue problem (3.3), as performed in [63].

Let us first settle a proper definition space for the division rates B. Theorem 1 of [63] states that, under Assumptions (3.2) and (3.8)-(3.13), there exists a unique eigenpair (λ_0, N, ϕ) solution of Problem (3.3). Hence, we first need that g and κ satisfy Assumptions (3.2), (3.8)–(3.10). Then, to study the regularity of the map $\Gamma : (c, B) \to (\lambda, N)$, one needs not only that such division rates B satisfy Assumptions (3.9), (3.11) and (3.13) but also that they satisfy them *uniformly*. This leads to the following definition.

Definition 3.1.1. *Let g, κ satisfying Assumptions* (3.2), (3.8)-(3.10). *For a constant $b \geq 0$ and functions $f_0 \in L^1_0$, $f_\infty \xrightarrow[x\to+\infty]{} \infty$, one defines the set*

$$\mathcal{D}(b, f_0, f_\infty) := \left\{ B \in L^\infty_{loc}(\mathbb{R}^*_+) \cap \mathbb{P}, \quad Supp(B) = [\tilde{b} \leq b, +\infty), \quad \frac{B}{g} \leq f_0, \quad \frac{xB}{g} \geq f_\infty \right\}.$$

In such a set, division rates B satisfy uniformly Assumption (3.13), what allows to use the powerful estimates proved in [63].

Under such assumptions, we also recall that we have the following results (see Theorem 1 in [63]) for the unique solution (λ_0, N, ϕ) to Problem (3.3) :

$$x^\alpha g N \in L^p(\mathbb{R}+) \ \forall\, \alpha \geq -\gamma, \ \forall\, 1 \leq p \leq +\infty \ ; \quad x^\alpha g N \in W^{1,1}(\mathbb{R}+) \ \forall \alpha \geq 0, \tag{3.14}$$

and

$$\exists\, k > 0, \ C > 0, \ \phi(x) \leq C(1 + x^k); \quad g\partial_x \phi \in L^\infty(\mathbb{R}+). \tag{3.15}$$

The two following fundamental estimates are straightfully obtained by integration on $[0, \infty[$ of Equation (3.3) or (3.3) multiplied by x :

$$\lambda_0 = \int_0^{+\infty} B(x) N(x)\, \mathrm{d}x, \tag{3.16}$$

$$\int_0^{+\infty} x N(x)\, \mathrm{d}x = \frac{c}{\lambda_0} \int_0^{+\infty} g(x) N(x)\, \mathrm{d}x. \tag{3.17}$$

We are now ready to state our regularity result.

Theorem 3.1.2. *Let parameters g and κ satisfy Assumptions* (3.8)-(3.10), *then*

i) The map $\Gamma : (c, B) \longmapsto (\lambda_0, N)$ *is :*

- *continuous in* (c, B) *under the* $L^\infty-$ *weak-*$*$*topology for* B *from any set* $\mathbb{R}_+^* \times \mathcal{D}(b, f_0, f_\infty)$ *to* $\mathbb{R}_+^* \times L^1 \cap L^\infty(\mathbb{R}_+)$.
- *injective.*

ii) Let moreover g *satisfy* $\dfrac{x^\gamma}{g} \in L^2_0$ *with* γ *defined in Assumption* (3.12). *Then the map* Γ *is Lipschitz-continuous under the strong topology of* $\mathbb{R}_+^* \times L^2 \cap \mathcal{D}(b, f_0, f_\infty)$. *More precisely, denoting* $\delta B = \bar{B} - B$, $\Delta = \|\bar{B} - B\|_{L^2(\mathbb{R}_+)}$, $\delta c = \bar{c} - c$, $\delta N = \bar{N} - N$, $\delta\lambda = \bar{\lambda_0} - \lambda_0$, *we have the following estimates, for* k *as in* (3.15) *:*

$$|\delta\lambda| \leq C_1(B, \bar{B})\Delta + C_2(B, \bar{B})|\delta c|, \quad \|\delta N\|_{L^2(\mathbb{R}_+)} \leq C_3(B, \bar{B})\Delta,$$

with

$$C_1 = C\|\frac{\phi}{1+x^k}\|_{L^\infty}\frac{\|(1+x^k)\bar{N}\|_{L^2}}{\int_0^\infty \bar{N}\phi\,\mathrm{d}x}, \quad C_2 = \frac{\lambda_0 + C}{c}\|(1+x^k)g\bar{N}\|_{L^1(\mathbb{R}_+)} + \|(1+x^k)g\bar{N}\|_{L^2}\|B\|_{L^2},$$

where $C > 0$ *is an absolute constant.*

Proof.

i) The continuity of the map Γ directly follows from the proof given in [63], Theorem 1. Therefore, we only sketch the main steps and let the reader refer to this article.
Let $c_n \to c > 0$ in $\mathbb{R}_+^*$ and $B_n \overset{*}{\rightharpoonup} B$ in $L^\infty(\mathbb{R}_+)$. Denoting (λ_n, N_n) the respective eigenpairs solutions of Problem (3.3) settled for (c_n, B_n), we can prove the same uniform estimates for N_n as in [63] due to the fact that since $B_n \in \mathcal{D}(b, f_0, f_\infty)$, Assumption (3.13) is uniformly verified. Such estimates give strong compactness in L^1 for N_n, and hence, up to a subsequence, we have a strong convergence of (λ_n, N_n) to (λ, N). Similarly, we prove $\lambda > 0$, and passing to the limit in the equations for N_n, we deduce that (λ, N) has to be the solution of Problem (3.3) settled for (c, B). Since such a solution is unique, the whole sequence (λ_n, N_n) converges to it.
Let us show by contradiction that Γ is an injection function.
Let $B_i \in L^1_{loc}(\mathbb{R}_+^*)$ and c_i positive constants $\forall i \in \{1, 2\}$ such that $(c_1, B_1) \neq (c_2, B_2)$ and $\Gamma(c_1, B_1) = \Gamma(c_2, B_2) = (\lambda_0, N)$.
We then integrate the two equations satisfied by (λ_0, N) against the weight x, to obtain

$$\int_0^\infty g(x)N(x)\,\mathrm{d}x = \frac{\lambda_0}{c_1}\int_0^\infty yN(y)\,\mathrm{d}y = \frac{\lambda_0}{c_2}\int_0^\infty yN(y)\,\mathrm{d}y,$$

what implies $c_1 = c_2$. By the contradiction assumption we get $B_1 \neq B_2$, so by making the difference between the fellowing Equations (3.18), (3.19) with consideration to the equality $c_1 = c_2$

$$c_1\frac{\partial}{\partial_x}(g(x)N(x)) + (B_1(x) + \lambda_0)N(x) = 2\int_0^\infty B_1(y)\kappa(x, y)N(y)\,\mathrm{d}y, \tag{3.18}$$

$$c_2\frac{\partial}{\partial_x}(g(x)N(x)) + (B_2(x) + \lambda_0)N(x) = 2\int_0^\infty B_2(y)\kappa(x, y)N(y)\,\mathrm{d}y, \tag{3.19}$$

we obtain after multiplying by x^p, $p \geq 2$ the following relation

$$x^p|B_1 - B_2|(x)N(x) \leq 2\int_0^\infty x^p|B_1 - B_2|(y)N(y)\kappa(x,y)\,\mathrm{d}y.$$

We integrate this relation on $(0,\infty)$ and due to Assumption (3.8) for $p \geq 2$ we deduce the following strict inequality :

$$\int_0^\infty x^p|B_1 - B_2|(x)N(x)\,\mathrm{d}x < \int_0^\infty x^p|B_1 - B_2|(x)N(x)\,\mathrm{d}x, \quad \forall p \geq 2$$

what is contradictory.

ii) First, the fact that $\dfrac{x^\gamma}{g} \in L^2_0$ implies that for all $p \geq 0$, $N \in L^2\big((1+x^p)\,\mathrm{d}x\big)$. Indeed, by (3.14) and since $g \in \mathbb{P}$, $\displaystyle\int_0^\infty N^2(x)(1+x^p)^2\,\mathrm{d}x < \infty$, and it only remains to bound $\displaystyle\int_0^\infty N^2(1+x^p)^2\,\mathrm{d}x$. This is given by writing $N^2(x) = (N^2g^2x^{-2\gamma})(\dfrac{x^{2\gamma}}{g^2})$, product of and L^∞ function with a L^1_0 function.
By making the sum between the two following equations

$$\phi(x)\bar{c}\frac{\partial}{\partial_x}(g(x)\bar{N}(x)) + \phi(x)(\bar{B}(x)+\bar{\lambda}_0)\bar{N}(x) = \phi(x)2\int_0^\infty \bar{B}(y)\kappa(x,y)\bar{N}(y)\,\mathrm{d}y$$

$$\bar{N}(x)cg(x)\frac{\partial}{\partial_x}\phi(x) - \bar{N}(x)(B(x)+\lambda_0)\phi(x) = -2\bar{N}(x)B(x)\int_0^x \kappa(y,x)\phi(y)\,\mathrm{d}y$$

we obtain

$$\delta c\,\phi\frac{\partial}{\partial_x}(g\bar{N}) + \frac{\partial}{\partial_x}\big(cg\bar{N}\phi\big)(x) + \big(\phi\bar{N}[\bar{B}+\bar{\lambda}_0 - B - \lambda_0]\big)(x) = 2\phi(x)\int_0^\infty \bar{B}(y)\kappa(x,y)\bar{N}(y)\,\mathrm{d}y$$
$$-2\bar{N}(x)B(x)\int_0^x \kappa(y,x)\phi(y)\,\mathrm{d}y$$

we then integrate this equation on $[0,\infty)$ that leads

$$\delta c\,\phi\frac{\partial}{\partial_x}(g\bar{N})dx + \delta\lambda\int_0^\infty \phi\bar{N}\,\mathrm{d}x + \int_0^\infty \phi\bar{N}\delta B\,\mathrm{d}x = 2\int_0^\infty \delta B(y)\bar{N}(y)\bigg(\int_0^\infty \phi(x)\kappa(x,y)\,\mathrm{d}x\bigg)\,\mathrm{d}y.$$

So

$$\delta\lambda\int_0^\infty \phi(x)\bar{N}(x)\,\mathrm{d}x = \int_0^\infty \delta B(x)\bar{N}(x)\bigg(2\int_0^\infty \phi(y)\kappa(y,x)\,\mathrm{d}y - \phi(x)\bigg)\,\mathrm{d}x + \delta c\int g\bar{N}\frac{\partial}{\partial_x}\phi\,\mathrm{d}x.$$

The first term of the left-hand side gives the term with $C_1(B,\bar{B})$ of the estimate on $\delta\lambda$ by using the fact that $\exists\, k > 0$, $\dfrac{\phi}{1+x^k} \in L^\infty(\mathbb{R}_+)$. For the second term, we use the equation for ϕ and write

$$\delta c\int g\bar{N}\frac{\partial}{\partial_x}\phi\,\mathrm{d}x = \frac{\delta c}{c}\int g\bar{N}\bigg((B+\lambda_0)\phi - 2B\int_0^x \kappa(y,x)\phi(y)\,\mathrm{d}y\bigg)dx,$$

and it provides the term with $C_2(B, \bar{B})$ in the estimate for $\delta\lambda$.

To prove the estimate on δN, we make the difference between the two following equations

$$c\frac{\partial}{\partial_x}(g(x)\bar{N}(x)) + (\bar{B}(x) + \bar{\lambda}_0)\bar{N}(x) = 2\int_0^\infty \bar{B}(y)\kappa(x,y)\bar{N}(y)\,\mathrm{d}y$$
$$c\frac{\partial}{\partial_x}(g(x)N(x)) + (B(x) + \lambda_0)N(x) = 2\int_0^\infty B(y)\kappa(x,y)N(y)\,\mathrm{d}y$$

we obtain

$$\begin{aligned}\delta c\frac{\partial}{\partial_x}(g\bar{N}) + c\frac{\partial}{\partial_x}(g\delta N) \quad &+ \quad \left((\bar{\lambda}_0 + \bar{B})\bar{N} - (\lambda_0 + B)N \pm (\lambda_0 + B)\bar{N}\right) \\ &= \quad 2\int_0^\infty \left(\bar{B}\bar{N} - BN \pm B\bar{N}\right)(y)\kappa(x,y)\,\mathrm{d}y.\end{aligned}$$

That implies

$$\begin{aligned}\delta c\frac{\partial}{\partial_x}(g\bar{N}) + c\frac{\partial}{\partial_x}(g\delta N) + (\lambda_0 + B)\delta N \quad &= \quad \left[2\int_0^\infty \bar{N}(y)\kappa(x,y)\delta B(y)\,\mathrm{d}y - (\delta\lambda + \delta B)\bar{N}\right] \\ &\quad +2\int_0^\infty B(y)\delta N(y)\kappa(x,y)\,\mathrm{d}y.\end{aligned}$$

We recast the previous equation as follows

$$c\frac{\partial}{\partial_x}(g(x)\delta N(x)) + (\lambda_0 + B(x))\delta N(x) = 2\int_0^\infty B(y)\delta N(y)\kappa(x,y)\,\mathrm{d}y + \delta R(x), \tag{3.20}$$

with

$$\delta R(x) = 2\int_0^\infty \bar{N}(y)\kappa(x,y)\delta B(y)\,\mathrm{d}y - (\delta\lambda + \delta B)\bar{N} - \delta c\frac{\partial}{\partial_x}(g\bar{N}) \tag{3.21}$$

We can bound $\|\delta R(x)\|_{L^2}$ as we previously bound $|\delta\lambda|$. The estimate on $\|\delta N\|_{L^2}$ thus follows from the following lemma.

Lemma 3.1.3. *Under the assumptions of Theorem 3.1.2 for g and κ, with δN defined as in Theorem 3.1.2 and δR defined by* (3.21)*, there exists $\nu(c, B) > 0$ a constant depending only on the eigenvalue problem* (3.3) *stated for given parameters $c > 0$ and $B \in L^2 \cap \mathcal{D}(b, f_0, f_\infty)$ such that, for all $\bar{c} \geq c_0 > 0$ and $\bar{B} \in L^2 \cap \mathcal{D}(b, f_0, f_\infty)$, one has*

$$\nu\|\delta N\|_{L^2(\mathbb{R}_+)} \leq \|\delta R\|_{L^2(\mathbb{R}_+)}.$$

Proof.
We argue by contradiction and assume that for a sequence $c_k \geq c_0 > 0$, $\bar{B}_k \in L^2 \cap \mathcal{D}(b, f_0, f_\infty)$, one has, for a vanishing sequence ν_k,

$$\nu_k\|\delta N_k\|_{L^2(\mathbb{R}_+)} \geq \|\delta R_k\|_{L^2(\mathbb{R}_+)},$$

with $\delta N_k = \bar{N}_k - N$, $\bar{N}_k$ solution of Problem (3.3) stated for $\bar{c}_k$ and $\bar{B}_k$, δR_k defined by (3.21) stated for δN_k.

As for the proof of continuity above, compactness arguments as done in [63] lead us to extract a converging subsequence $\bar{N}_k \to \bar{N}$ strongly in L^1, so $\delta N_k \to \delta N$ strongly in L^1. Moreover,

estimates as in [63] imply that $\bar{N}_k$ is uniformly bounded in L^2 (we write $\bar{N}_k^2 = x^{-2\gamma} g^2 N^2 \frac{x^{2\gamma}}{g^2}$ and use the assumption $\frac{x^\gamma}{g} \in L^2$ together with the result (3.14), result which is uniform for all $\bar{N}_k$), hence δN_k satisfy Equation (3.20) with $\|\delta R_k\|_{L^2} \to 0$. Passing to the limit, it implies that δN satisfies Equation (3.3), so by uniqueness of a solution we have $\delta N = CN$ for a given constant $C \in \mathbb{R}$. Since $\int N dx = \int \bar{N}_k dx = 1$, we have $\int \delta N dx = C = 0$: it is contradictory with our assumption on (ν_k). □

3.2 The inverse problem and its regularization

As in [66, 65], we consider the problem of recovering the cell division rate B and the constant c from the *a priori* knowledge of the shape of the growth rate $g(x)$ and the experimental measure of the asymptotic distribution N and exponential growth λ_0. To model this, we suppose that we have two given measurements $N_\varepsilon \in L^1 \cap L^\infty(\mathbb{R}_+)$ and $\lambda_\varepsilon > 0$ such that $||N - N_\varepsilon||_{L^2\left((1+x^p)\,\mathrm{d}x\right)} \leq \varepsilon$, $|\lambda_0 - \lambda_\varepsilon| \leq \varepsilon$.[5] The problem is : How to get estimates $(c_\varepsilon, B_\varepsilon)$ of (c, B) solutions of

$$c\frac{\partial}{\partial_x}(g(x)N(x)) + (B(x) + \lambda_0)N(x) = 2\int_0^\infty \kappa(x,y)B(y)N(y)\,\mathrm{d}y. \tag{3.22}$$

Firstly, one remarks that B cannot be recovered from Equation (3.22) when the distribution N vanishes : our inverse problem consists in recovering $H = BN$ rather than B directly. Our problem can now be viewed as : How to recover (c, H) solution of

$$\mathcal{L}_\kappa(H)(x) := H(x) - 2\int_0^\infty \kappa(x,y)H(y)\,\mathrm{d}y = -c\frac{\partial}{\partial_x}(g(x)N(x)) - \lambda_0 N(x) \tag{3.23}$$

when we have measurements $(\lambda_\varepsilon, N_\varepsilon)$ of (λ_0, N) ?

Secondly, since the measure N_ε is supposed to be in L^2, there is no way of controlling directly $\frac{\partial}{\partial_x}(gN_\varepsilon)$ even if g is known (see Section 2 of [158] for a discussion, or yet [74]).To come up this difficulty, two regularization methods were proposed in [158, 67] for the particular case of division into two equal cells, *i.e.* when $\kappa(x,y) = \delta_{x=y/2}$, a third method has also been proposed in [97], and a statistical treatment to estimate the derivative in [65]. Indeed, looking at the problem in terms of $H = BN$ and not in terms of B makes it *almost* linear in H; almost, because λ_0 being also measured, the term $\lambda_0 N$ can be viewed as quadratic. Hence, the classical tools designed to regularize linear inverse problems (see [74]) can be used, as illustrated by the three foreseen methods, as soon as the operator $\mathcal{L}_\kappa$ can be inverted.

This is the third and last difficulty : inverse the operator $\mathcal{L}_\kappa$ defined by Equation (3.23). None of the three regularization methods of [158, 67, 97] can be directly applied here : indeed, they strongly used the fact that for the kernel $\kappa = \delta_{x=\frac{y}{2}}$, the left-hand side of Equation (3.23) simplifies in $4BN(2x) - B(x)$, and can be viewed as an equation written in $y = 2x$. Then, a central point of the proofs in [158] as well as in [67] or [97] is the use of the Lax-Milgram theorem for the coercitive operator $\mathcal{L} : H \to 4H(y) - H(\frac{y}{2})$.

Nothing such as that can be written here, and the main difficulty, numerically as well as theoretically, is to deal with a nonlocal kernel $\int \kappa(x,y)H(y)dy$. The operator $\mathcal{L}$ is replaced by

[5] See [65] for a statistical viewpoint on the data $(N_\varepsilon, \lambda_\varepsilon)$: supposing that $N_\varepsilon \in L^2$ means that we deal with some preprocessed data. However, once the problem is solved in a deterministic setting, as we do in this article, it is immediate to apply the method of [65] to this general case.

$\mathcal{L}_\kappa$. For $\kappa = \delta_{x=\frac{y}{2}}$, $\mathcal{L}_\kappa$ has been proved in [67] (Proposition A.1. in the appendix) to be coercitive in $L^2(x^p dx)$ if $p > 3$, or in contrary $\mathcal{L}$ is coercitive if $p < 3$. Due to the nonlocal character of the kernel, it seems more natural now to look for cases when the first part of the operator $\mathcal{L}_\kappa$, *i.e.* identity, dominates the nonlocal part $2\int_x^\infty u(y)\kappa(x,y)\,\mathrm{d}y$. This is expressed by the following proposition.

Proposition 3.2.1. *Let κ satisfy Assumption* (3.2) *and $p \in \mathbb{R}$ satisfy the following assumption :*

$$C_p = \sup_x \int_x^\infty \frac{x^p}{y^p}\kappa(x,y)\,\mathrm{d}y < \frac{1}{4}. \tag{3.24}$$

Then for all $F \in L^2(\mathbb{R}_+, x^p\,\mathrm{d}x)$ there exists a unique solution $u \in L^2(x^p\,\mathrm{d}x)$ to the following problem :

$$u(x) - 2\int_x^\infty u(y)\kappa(x,y)\,\mathrm{d}y = F, \tag{3.25}$$

and we have the following estimate

$$||u||_{L^2(x^p\,\mathrm{d}x)} \leq \frac{1}{1-2\sqrt{C_p}}||F||_{L^2(x^p\,\mathrm{d}x)}.$$

Proof. We define the bilinear form

$$\mathcal{A}(u,v) = \int_0^{+\infty} u(x)v(x)x^p\,\mathrm{d}x - 2\int_0^{+\infty} u(x)\int_x^{+\infty}\kappa(x,y)v(y)\,\mathrm{d}y\,x^p\,\mathrm{d}x = < u, v >_{L^2(x^p\,\mathrm{d}x)} - 2\mathcal{B}(u,v),$$

where $<,>_{L^2}$ denotes the scalar product. We apply the Lax-Milgram theorem in $L^2(x^p\,\mathrm{d}x)$. Indeed, we have

$$\begin{aligned}
\mathcal{B}(u,v) &= \int_0^\infty\int_x^\infty \frac{x^p}{y^{\frac{p}{2}}}u(x)y^{\frac{p}{2}}v(y)\kappa(x,y)\,\mathrm{d}x\,\mathrm{d}y \\
&\leq \sqrt{\int_0^\infty\int_x^\infty \frac{x^{2p}}{y^p}u^2(x)\kappa(x,y)\,\mathrm{d}x\,\mathrm{d}y}\sqrt{\int_0^\infty\int_x^\infty y^p v^2(y)\kappa(x,y)\,\mathrm{d}x\,\mathrm{d}y} \\
&\leq \sqrt{\int_0^\infty\Big(\int_x^\infty \frac{x^p}{y^p}\kappa(x,y)\,\mathrm{d}y\Big)u^2(x)x^p\,\mathrm{d}x}\sqrt{\int_0^\infty y^p v^2(y)\Big(\int_0^y \kappa(x,y)\,\mathrm{d}x\Big)\,\mathrm{d}y} \\
&\leq \sqrt{\int_0^\infty x^p u^2(x)C_p\,\mathrm{d}x}\sqrt{\int_0^\infty y^p v^2(y)\,\mathrm{d}y} = \sqrt{C_p}||u||_{L^2(x^p\,\mathrm{d}x)}||v||_{L^2(x^p\,\mathrm{d}x)},
\end{aligned}$$

what proves the continuity of the bilinear forms $\mathcal{B}$ and $\mathcal{A}$. Moreover, it implies

$$\mathcal{A}(u,u) \geq (1-2\sqrt{C_p})||u||^2_{L^2(x^p\,\mathrm{d}x)} = \beta||u||^2_{L^2(x^p\,\mathrm{d}x)},$$

with $\beta = 1-2\sqrt{C_p} > 0$ under assumption (3.24). It ends the proof of Proposition 3.2.1.

Remark 3.2.2. *Assumption* (3.24) *can be linked to Assumption* (3.8). *One can easily check that for $\kappa(x,y) = \delta_{x=\frac{y}{2}}$, it is verified for $p > 3$: we recover part of the result of Proposition of [67]. It corresponds to the cases when the first part of the bilinear form (*i.e., $\int uvx^p\,\mathrm{d}x$*) dominates the*

second one ($\iint \kappa(x,y)u(x)v(y)x^p \,\mathrm{d}x\,\mathrm{d}y$). Solving it for smaller p, i.e. *prove in which cases the nonlocal part dominates the identity, remains an open problem.*

For the uniform kernel $\kappa(x,y) = \dfrac{1}{y}$ for $x \le y$, Assumption (3.24) *is verified* iff $p > 4$.

More generally, for homogeneous kernels $\kappa(x,y) = \dfrac{1}{y}k_0(\dfrac{x}{y})$ with $\displaystyle\int_0^1 k_0(z)dz = 1$, Assumption (3.24) *reads*

$$\int_0^1 z^{p-1}k_0(z)dz < \frac{1}{4}.$$

Since for $p = 2$, we have $\displaystyle\int k_0(z)z\,\mathrm{d}z = \frac{1}{2}$, Equation (3.24) *implies $p \ge 2$.*

3.2.1 Filtering method

This regularization method consists in looking for a solution $H_{\varepsilon,\alpha}$ of the following regularized problem

$$\mathcal{L}_\kappa(H_{\varepsilon,\alpha})(x) := H_{\varepsilon,\alpha}(x) - 2\int_0^{+\infty} \kappa(x,y)H_{\varepsilon,\alpha}(y)\,\mathrm{d}y = \rho_\alpha * \left(-c_{\varepsilon,\alpha}\frac{\partial}{\partial_x}\big(g(x)N_\varepsilon(x)\big) - \lambda_\varepsilon N_\varepsilon(x)\right), \tag{3.26}$$

where ρ_α is a mollifiers sequence defined by

$$\rho_\alpha(x) = \frac{1}{\alpha}\rho(\frac{x}{\alpha}), \quad \rho \in \mathbb{C}_c^\infty(\mathbb{R}), \quad \int_0^\infty \rho(x)\,\mathrm{d}x = 1, \quad \rho \ge 0, \quad Supp(\rho) \subset [0,1]. \tag{3.27}$$

One notices that $c_{\varepsilon,\alpha}$ is uniquely defined : indeed, integrating Equation (3.26) against the weight x leads to

$$c_{\varepsilon,\alpha} = \lambda_\varepsilon \frac{\displaystyle\int xN_\varepsilon\,\mathrm{d}x}{\displaystyle\int \rho_\alpha * (gN_\varepsilon)\,\mathrm{d}x}. \tag{3.28}$$

We want to study the well-posedness of this problem and estimate the distance between $B_{\varepsilon,\alpha} = \dfrac{H_{\varepsilon,\alpha}}{N_{\varepsilon,\alpha}}$ and B in order to choose an optimal approximation rate α. This is given by the following result.

Theorem 3.2.3. *Let g, B and κ satisfy Assumptions* (3.2) *and* (3.8)–(3.13)*, and moreover $\dfrac{x^\gamma}{g} \in L^2_0$ with γ defined in Assumption* (3.12)*. Let (λ_0, N) the unique eigenpair solution of Problem* (3.3) *(as stated in [63]). Let $p > 1$ satisfy Assumption* (3.24)*. Let $N_\varepsilon \in L^1 \cap L^\infty(\mathbb{R}_+)$ and $\lambda_\varepsilon > 0$ satisfy $\|g(N-N_\varepsilon)\|_{L^2(x^p\,\mathrm{d}x)} \le \varepsilon\|gN\|_{L^2(x^p\,\mathrm{d}x)}$, $|\lambda_\varepsilon - \lambda_0| \le \varepsilon\lambda_0$, $\|N-N_\varepsilon\|_{L^1\left((1+x+g(x))\,\mathrm{d}x\right)} \le \varepsilon\|N\|_{L^1\left((1+x+g(x))\,\mathrm{d}x\right)}$ and*
$\|N_\varepsilon - N\|_{L^2\left((x^p+1)\,\mathrm{d}x\right)} \le \varepsilon\|N\|_{L^2\left((x^p+1)\,\mathrm{d}x\right)}$.

Then there exists a unique solution $H_{\varepsilon,\alpha} \in L^2(x^p\,\mathrm{d}x)$ to Problem (3.26).

Defining $B_{\varepsilon,\alpha} := \chi_{N_{\varepsilon,\alpha}(x)\neq 0}H_{\varepsilon,\alpha}/N_{\varepsilon,\alpha}$ we have the following estimates :

$$|c_{\varepsilon,\alpha} - c| \le C(p,\rho,N)(\alpha+\varepsilon), \tag{3.29}$$

$$||B_{\varepsilon,\alpha} - B||_{L^2(x^p N^2\,\mathrm{d}x)} \leq C(p,\rho,N)(\alpha + \frac{\varepsilon}{\alpha}), \tag{3.30}$$

where C is a constant depending on p, moments of ρ and $\frac{\partial}{\partial_x}\rho$, λ_0, $\|gN\|_{H^2\left((1+x^p)\,\mathrm{d}x\right)}$, $\|N\|_{L^1\left((1+x+g(x))\,\mathrm{d}x\right)}$, $\|gN\|_{W^{1,1}(\,\mathrm{d}x)}$ and $\|N\|_{H^1\left((x^p+1)\,\mathrm{d}x\right)}$.

The estimate (3.34) of Theorem 3.2.3 relies, on the one hand, on the estimate of Proposition 3.2.1, and, on the other hand, on general approximation properties of the mollifiers, as expressed by Lemma 3.2.4 right above.

Lemma 3.2.4. *Let $p > 1$, $f \in L^2((x^p+1)\,\mathrm{d}x)$, ρ_α a mollifiers sequence defined by (3.27) and $0 < \alpha < 1$. Then we have the following estimates.*

1. $||f * \rho_\alpha||_{L^2(x^p\,\mathrm{d}x)} \leq C(p,\rho)||f||_{L^2\left((x^p+1)\,\mathrm{d}x\right)}$, *with $C(p,\rho)$ only depending on p and moments of ρ,*
2. $||\frac{\partial}{\partial x}(f * \rho_\alpha)||_{L^2(x^p\,\mathrm{d}x)} \leq \frac{1}{\alpha}C(p,\rho)||f||_{L^2\left((x^p+1)\,\mathrm{d}x\right)}$, *with $C(p,\rho)$ only depending on p and moments of ρ and $\frac{\partial}{\partial x}\rho$.*
3. $||f * \rho_\alpha - f||_{L^2(x^p\,\mathrm{d}x)} \leq C(\rho)\alpha||f||_{H^1(x^p\,\mathrm{d}x)}$ *if* $f \in H^1\left((1+x^p)\,\mathrm{d}x\right)$
4. $||f * \rho_\alpha - f||_{L^1} \leq C(\rho)\alpha||f||_{W^{1,1}}$
5. $||\rho_\alpha * f||_{L^1} \leq ||f||_{L^1}$.

Proof. The proof of this result is classical and relies on Minkowski inequality for convolution products ; we let it to the reader.

Proof of Theorem 3.2.3. We decompose the left-hand side of Estimate (3.34) as follows

$$\begin{aligned}
\|B_{\varepsilon,\alpha}N - BN\|_{L^2(x^p\,\mathrm{d}x)} &= \|B_{\varepsilon,\alpha}(N - N_\alpha + N_\alpha - N_{\varepsilon,\alpha}) + H_{\varepsilon,\alpha} - BN\|_{L^2(x^p\,\mathrm{d}x)} \\
&\leq \|B_{\varepsilon,\alpha}\|_{L^\infty}\Big(\|N - N_\alpha\|_{L^2(x^p\,\mathrm{d}x)} + \|N_\alpha - N_{\varepsilon,\alpha}\|_{L^2(x^p\,\mathrm{d}x)}\Big) \\
&\quad + \|H_{\varepsilon,\alpha} - BN\|_{L^2(x^p\,\mathrm{d}x)}
\end{aligned}$$

On the right-hand side, the first term is bounded by $C(p,\rho)\alpha\|N\|_{H^1\left((x^p+1)\,\mathrm{d}x\right)}$ due to Lemma 3.2.4, Estimate 3. The second term is bounded by $C(p,\rho)\varepsilon\|N\|_{L^2\left((x^p+1)dx\right)}$ due to Lemma 3.2.4, Estimate 1 applied to $f = N - N_\varepsilon$. For the third term, we apply Proposition 3.2.1 to $u = H_{\varepsilon,\alpha} - BN$ and $F = \rho_\alpha * \left(c_{\varepsilon,\alpha}\frac{\partial}{\partial_x}\big(gN_\varepsilon\big) + \lambda_\varepsilon N_\varepsilon\right) - \left(c\frac{\partial}{\partial_x}\big(g(x)N(x)\big) + \lambda_0 N\right)$. We treat these terms in a similar manner. Let us detail briefly the most binding term (with the notation $L^2_p = L^2(x^p\,\mathrm{d}x)$) :

$$\begin{aligned}
\|\rho_\alpha * c_{\varepsilon,\alpha}\frac{\partial}{\partial_x}\big(gN_\varepsilon\big) - c\frac{\partial}{\partial_x}\big(gN\big)\|_{L^2_p} \leq\ & c_{\varepsilon,\alpha}\Big(\|\frac{\partial}{\partial_x}\rho_\alpha * (gN_\varepsilon - gN)\|_{L^2_p} + \|\rho_\alpha * \frac{\partial}{\partial_x}\big(gN\big) - \frac{\partial}{\partial_x}\big(gN\big)\|_{L^2_p}\Big) \\
& + |c_{\varepsilon,\alpha} - c|\|\frac{\partial}{\partial_x}\big(gN\big)\|_{L^2_p}.
\end{aligned}$$

The first term is bounded by $C\frac{\varepsilon}{\alpha}\|gN\|_{L^2(x^p\,\mathrm{d}x)}$ by Lemma 3.2.4 Estimate 2, the second one by $C\alpha\|gN\|_{H^2(x^p\,\mathrm{d}x)}$ by Estimate 3. For the third term we write

$$\begin{aligned}
|c_{\varepsilon,\alpha}-c| &= |\lambda_\varepsilon\frac{\int xN_\varepsilon\,\mathrm{d}x}{\int \rho_\alpha * gN_\varepsilon\,\mathrm{d}x}-\lambda_0\frac{\int xN(x)\,\mathrm{d}x}{\int g(x)N(x)\,\mathrm{d}x}|\\
&= |\lambda_\varepsilon\frac{\int xN_\varepsilon}{\int \rho_\alpha * gN_\varepsilon\,\mathrm{d}x}\pm\lambda_\varepsilon\frac{\int xN\,\mathrm{d}x}{\int \rho_\alpha * gN_\varepsilon\,\mathrm{d}x}\pm\lambda_0\frac{\int xN\,\mathrm{d}x}{\int \rho_\alpha * gN_\varepsilon\,\mathrm{d}x}-\lambda_0\frac{\int xN\,\mathrm{d}x}{\int gN\,\mathrm{d}x}|\\
&\le |\lambda_\varepsilon\frac{\int xN_\varepsilon}{\int \rho_\alpha * gN_\varepsilon\,\mathrm{d}x}-\lambda_\varepsilon\frac{\int xN\,\mathrm{d}x}{\int \rho_\alpha * gN_\varepsilon\,\mathrm{d}x}|+|\lambda_\varepsilon\frac{\int xN\,\mathrm{d}x}{\int \rho_\alpha * gN_\varepsilon\,\mathrm{d}x}-\lambda_0\frac{\int xN\,\mathrm{d}x}{\int \rho_\alpha * gN_\varepsilon\,\mathrm{d}x}|\\
&\quad +|\lambda_0\frac{\int xN\,\mathrm{d}x}{\int \rho_\alpha * gN_\varepsilon\,\mathrm{d}x}-\lambda_0\frac{\int xN\,\mathrm{d}x}{\int gN\,\mathrm{d}x}|.
\end{aligned}$$

The assumptions of Theorem 3.2.3 together with Estimates 4 and 5 of Lemma 3.2.4 give the estimate for $|c_{\varepsilon,\alpha}-c|$ and ends the proof.

3.2.2 Quasi-Reversibility Method

To regularize the exact inverse problem (3.23), the so called *quasi-reversibility* method proposed in [158] for the case $\kappa=\delta_{x=\frac{y}{2}}$ consisted in adding a term derivative $\alpha\dfrac{\partial}{\partial_x}(BN(2x))$ with a small $\alpha>0$ to the right-hand side of Equation (3.22), viewed as an equation taken in the variable $y=2x$. The main difference is that we need here to take this term in the variable x and not $2x$ due to the general form of the nonlocal kernel κ. We choose to define, for $\alpha>0$ and $k\in\mathbb{R}$, the following regularised problem

$$\begin{cases}\mathcal{L}_k^\alpha(H_\varepsilon)(x):=\alpha x^{-k}\dfrac{\partial}{\partial_x}\big(x^{k+1}H_\varepsilon(x)\big)+H_\varepsilon(x)-2\displaystyle\int_0^\infty\kappa(x,y)H_\varepsilon(y)\,\mathrm{d}y=-c_{\alpha,\varepsilon}\dfrac{\partial}{\partial_x}\big(gN_\varepsilon(x)\big)-\lambda_\varepsilon N_\varepsilon(x),\\ H_\varepsilon(0)=0;\quad 0<\alpha<1,\quad k\in\mathbb{R}.\end{cases}\tag{3.31}$$

This equation has to be understood in a distribution sense in $\mathbb{R}_+$ undowed with the measure $x^p\,\mathrm{d}x$. We moreover assume that $Supp(N_\varepsilon)\subset\mathbb{R}_+^*$. Other adaptations would be possible, all consisting in adding a small term derivative of the form $\pm\alpha f_1(x)\dfrac{\partial}{\partial_x}(f_2(x)BN(x))$, with $\alpha>0$ and a boundary condition taken either in $x=0$ if $\alpha>0$ or $x=+\infty$ if $\alpha<0$. Numerically indeed, $\alpha<0$ proved to give better results (see below Section 3.3.3). The key point is to check that the regularised operator $\mathcal{L}_k^\alpha$ satisfies Proposition 3.2.6 below.

The choice of $c_{\alpha,\varepsilon}$ is not directly given by integration of the equation, contrarily to the case of [158]. Neglecting the regularisation terms involving α, we thus define, as for the exact equation (3.22) :

$$c_{\alpha,\varepsilon}=\frac{\lambda_\varepsilon\displaystyle\int xN_\varepsilon(x)\,\mathrm{d}x}{\displaystyle\int g(x)N_\varepsilon(x)\,\mathrm{d}x}.\tag{3.32}$$

Theorem 3.2.5. *Let g, B and κ satisfy Assumptions* (3.2) *and* (3.8)–(3.13)*, and moreover $\dfrac{x^\gamma}{g}\in L_0^2$ with γ defined in Assumption* (3.12)*. Let (λ_0,N) the unique eigenpair solution of Problem* (3.3) *(as stated in [63]). Let $p>2$ satisfy Assumption* (3.24)*. Let $N_\varepsilon\in L^1\cap L^\infty(\mathbb{R}_+)$,*

$Supp(N_\varepsilon) \subset \mathbb{R}_+^*$, and $\lambda_\varepsilon > 0$ satisfy $\|g(N-N_\varepsilon)\|_{L^2(x^p\,\mathrm{d}x)} \leq \varepsilon\|gN\|_{L^2(x^p\,\mathrm{d}x)}$, $|\lambda_\varepsilon - \lambda_0| \leq \varepsilon\lambda_0$, $\|N - N_\varepsilon\|_{L^1\left((1+x+g(x))\,\mathrm{d}x\right)} \leq \varepsilon\|N\|_{L^1\left((1+x+g(x))\,\mathrm{d}x\right)}$ and $\|N_\varepsilon - N\|_{L^2\left((x^p+1)\,\mathrm{d}x\right)} \leq \varepsilon\|N\|_{L^2\left((x^p+1)\,\mathrm{d}x\right)}$. Let $H_\varepsilon \in L^2(x^p\,\mathrm{d}x)$ be solution to Problem (3.31)(3.32).
Defining $B_{\varepsilon,\alpha} := \chi_{N_\varepsilon(x)\neq 0} H_\varepsilon/N_\varepsilon$ we have the following estimates :

$$|c_{\varepsilon,\alpha} - c| \leq C(p,N)\varepsilon, \tag{3.33}$$

$$||B_{\varepsilon,\alpha} - B||_{L^2(x^p N_\varepsilon^2\,\mathrm{d}x)} \leq C(p,N)(\alpha + \frac{\varepsilon}{\alpha}), \tag{3.34}$$

where C is a constant depending on p, k, λ_0, $\|BN\|_{H^1\left((1+x^{p+1})\,\mathrm{d}x\right)}$, $\|N\|_{L^1\left((1+x+g(x))\,\mathrm{d}x\right)}$, $\|gN\|_{L^1}$ and $\|N\|_{H^1\left((x^p+1)\,\mathrm{d}x\right)}$.

Proof. The estimate for $|c_{\varepsilon,\alpha} - c|$ is obtained in a similar manner as for the filtering method.

For the estimate for B, we first write

$$\|B_{\varepsilon,\alpha}N_\varepsilon - BN_\varepsilon\|_{L^2(x^p\,\mathrm{d}x)} \leq \|B_{\varepsilon,\alpha}N_\varepsilon - BN\|_{L^2(x^p\,\mathrm{d}x)} + \|BN - BN_\varepsilon\|_{L^2(x^p\,\mathrm{d}x)}.$$

The second term of the right-hand side is simply bounded by

$$\|B\|_{L^2(x^p\,\mathrm{d}x)}\|N - N_\varepsilon\|_{L^2(x^p\,\mathrm{d}x)} \leq \varepsilon\|B\|_{L^2(x^p\,\mathrm{d}x)}.$$

For the first term of the right-hand side, as for the filtering method, we decompose $H_\varepsilon - BN$, and for this we need to establish some regularity properties of the operator $\mathcal{L}_k^\alpha$ defined in Equation (3.31) and designed to approximate $\mathcal{L}_\kappa$. This is given by the following proposition, which is for the quasi-reversibility method the equivalent of Lemma 3.2.4 for the filtering method.

Proposition 3.2.6. *Let $p > 2$, $F = f_1 + \frac{\partial}{\partial_x} f_2$ with $f_1 \in L^1\big((1+x)\,\mathrm{d}x\big) \cap L^2(x^p\,\mathrm{d}x)$ and $f_2 \in H^1((1+x^p)\,\mathrm{d}x) \cap W^{1,1}(x\,\mathrm{d}x)$. Let κ, g, p satisfy the assumptions of Theorem 3.2.5. There exists $u \in L^1(x\,\mathrm{d}x)$ solution of the following problem, where $k \neq -2$ and $0 < \alpha \leq 1$:*

$$\mathcal{L}_k^\alpha(u)(x) := \alpha x^{-k}\frac{\partial}{\partial_x}\big(x^{k+1}u\big) + \mathcal{L}_\kappa(u) = F. \tag{3.35}$$

Moreover, we have the following estimates for a constant $C > 0$ only depending on g, κ, k and p :

1. $\|u\|_{L^2(x^p\,\mathrm{d}x)} \leq \dfrac{1}{1 - 2\sqrt{C_p}}\|F\|_{L^2(x^p\,\mathrm{d}x)}$,
2. $\|u\|_{L^2(x^p\,\mathrm{d}x)} \leq \dfrac{C}{\alpha}\|f_1 + f_2(1 + \dfrac{1}{x^2})\|_{L^2(x^p\,\mathrm{d}x)}$.

Proof. Let us first establish the existence of a solution in $L^1(x\,\mathrm{d}x)$. We rewrite (3.35) as follows

$$\begin{cases} \alpha x\dfrac{\partial}{\partial_x}(u(x)) + (\alpha(k+1)+1)u(x) = 2\displaystyle\int_x^\infty \kappa(x,y)u(y)\,\mathrm{d}y + F(x). \\ u(0) = 0, \quad p > 2. \end{cases} \tag{3.36}$$

We consider $v \in L^1(\mathbb{R}_+, x\,\mathrm{d}x)$ and define $u = T(v)$ the explicit solution of

$$\begin{cases} \alpha x\dfrac{\partial}{\partial_x}(u(x)) + (\alpha(k+1)+1)u(x) = 2\displaystyle\int_0^\infty v(y)\kappa(x,y)\,\mathrm{d}y - F(x), \\ u(0) = 0, \quad p > 2. \end{cases}$$

Let v_1 and v_2 two functions of $L^1(\mathbb{R}_+, x\,\mathrm{d}x)$ associated to u_1 and u_2 then by doing the difference between the two equations satisfied in the one hand by u_1, v_1 and in the other hand by u_2, v_2 we have

$$\alpha x\frac{\partial}{\partial_x}(\delta u(x))+(\alpha(k+1)+1)\delta u(x) = 2\int_0^\infty \delta v(y)\kappa(x,y)\,\mathrm{d}y, \quad \text{with } \delta u = u_1-u_2 \text{ and } \delta v = v_1-v_2, \tag{3.37}$$

what implies the inequality (see [156], prop.6.3 for instance)

$$\alpha x\frac{\partial}{\partial_x}|\delta u(x)| + (\alpha(k+1)+1)|\delta u(x)| \leq 2\int_0^\infty |\delta v(y)|\kappa(x,y)\,\mathrm{d}y.$$

Multiplying by x and integrating on $[0,\infty[$ we deduce the estimate

$$\int_0^\infty x|\delta u(x)|\,\mathrm{d}x \leq \frac{1}{\alpha(k-1)+1}\int_0^\infty y|\delta v(y)|\,\mathrm{d}y.$$

This proves that T is a Lipschitz function and we deduce the existence of a solution $u \in L^1(\mathbb{R}_+, x\,\mathrm{d}x)$ by the Schauder fixed point theorem.

For the first estimate, we multiply Equation (3.35) by $x^p u$ and integrate from 0 to x. Using that $ux^{p-k}\dfrac{\partial}{\partial_x}(x^{k+1}u) = (k+1)x^p u^2 + x^{p+1}\dfrac{\partial}{\partial_x}(\dfrac{u^2}{2})$, it gives

$$\int_0^x \alpha(k+1)x^p u^2(x)\,\mathrm{d}x + \frac{\alpha}{2}x^{p+1}u^2(x) + \int_0^x \mathcal{L}_\kappa(u)(x)u(x)x^p\,\mathrm{d}x = \int_0^x F(x)u(x)x^p\,\mathrm{d}x.$$

From this, we deduce

$$\int \mathcal{L}_\kappa(u)(x)u(x)x^p\,\mathrm{d}x \leq \int F(x)u(x)x^p\,\mathrm{d}x. \tag{3.38}$$

Applying the coercitivity on $L^2(x^p\,\mathrm{d}x)$ of the bilinear form $\mathcal{A}(u,v) = \displaystyle\int \mathcal{L}_\kappa(u)vx^p\,\mathrm{d}x$ we get immediately the first estimate.

For the second one, we integrate by part, on the right-hand side of Equation (3.35), the term with $\dfrac{\partial}{\partial_x}f_2$, and use the equation to express $\dfrac{\partial}{\partial_x}(u)$ with the other terms of the equation :

$$\begin{aligned}
\int (\frac{\partial}{\partial_x}f_2)ux^p\,\mathrm{d}x &= -\int f_2\frac{\partial}{\partial_x}(x^p u)\,\mathrm{d}x = -\int \frac{p}{x}f_2 ux^p\,\mathrm{d}x - \int f_2 x^p\frac{\partial}{\partial_x}(u)\,\mathrm{d}x \\
&= -\int \frac{p}{x}f_2 ux^p\,\mathrm{d}x + \int \frac{k+1}{x}f_2 ux^p\,\mathrm{d}x + \int \frac{1}{\alpha x}f_2\big(\mathcal{L}_\kappa(u)(x) - f_1(x) - \frac{\partial}{\partial_x}f_2\big)x^p\,\mathrm{d}x \\
&= \int \frac{k+1-p}{x}f_2 ux^p\,\mathrm{d}x + \frac{1}{\alpha}\bigg(\int \frac{1}{x}f_2\big(\mathcal{L}_\kappa(u)(x) - f_1(x)\big)x^p\,\mathrm{d}x + \frac{p-1}{2}\int f_2^2 x^{p-2}\,\mathrm{d}x\bigg) \\
&\leq \frac{C}{\alpha}\|f_2\|_{L^2((x^{p-1}+x^p)\,\mathrm{d}x)}\big(\|u\|_{L^2(x^p\,\mathrm{d}x)} + \|f_1\|_{L^2(x^p\,\mathrm{d}x)}\big) + \frac{p}{\alpha}\|f_2\|^2_{L^2(x^{p-2}\,\mathrm{d}x)}
\end{aligned}$$

Together with the first estimate, it provides the desired inequality.

We are now ready for the proof of Theorem 3.2.5. We see that H_ε can be viewed as solution of Equation (3.35) with $F = -c_{\alpha,\varepsilon}\dfrac{\partial}{\partial_x}\big(gN_\varepsilon(x)\big) - \lambda_\varepsilon N_\varepsilon(x)$, whereas $H = BN$ would be solution of (3.35) if $\alpha = 0$ and $F = -c\dfrac{\partial}{\partial_x}\big(gN(x)\big) - \lambda_0 N(x)$. To isolate in the error term the contribution due to the $\alpha-$regularization from the one due to the measurement error ε, we thus define an intermediate function H_α as the solution of Equation (3.35) with $F = -c\dfrac{\partial}{\partial_x}\big(gN(x)\big) - \lambda_0 N(x)$. We then write :

$$\|B_{\varepsilon,\alpha}N_\varepsilon - BN\|_{L^2(x^p\,\mathrm{d}x)} = \|H_\varepsilon - H\|_{L^2(x^p\,\mathrm{d}x)} \leq \|H_\varepsilon - H_\alpha\|_{L^2(x^p\,\mathrm{d}x)} + \|H_\alpha - H\|_{L^2(x^p\,\mathrm{d}x)}.$$

The function $H_\varepsilon - H_\alpha$ is solution of Equation (3.35) with

$$F_{\varepsilon,\alpha} = \frac{\partial}{\partial_x}\big(- c_{\alpha,\varepsilon}gN_\varepsilon(x) + cgN(x)\big) - \lambda_\varepsilon N_\varepsilon(x) + \lambda_0 N(x),$$

and we can use Estimate 2 of Proposition 3.2.6 to obtain an error term in the order of $\dfrac{\varepsilon}{\alpha}$. The difference $H_\alpha - H$ is solution of Equation (3.35) with $F = -\alpha x^{-k}\dfrac{\partial}{\partial_x}(x^{k+1}BN)$, and we can use Estimate 1 of Proposition 3.2.6 to obtain an error term bounded by $C\alpha\|BN\|_{H^1\left((1+x^{p+1})\,\mathrm{d}x\right)}$. It ends the proof of Theorem 3.2.5.

3.3 Numerical approach of the inverse problem

3.3.1 The direct problem

Assuming that the division rate B, the growth rate g and $c > 0$ are known, we solve the time-dependent problem (3.1) and look for a steady dynamics.
We choose to split the time evolution of the problem into its conservative advection part and into its gain and lost part by division as follows

$$\begin{cases} \dfrac{\partial}{\partial_t}n(t,x) + c\dfrac{\partial}{\partial_x}(g(x)n(t,x)) = 0 \\ \dfrac{\partial}{\partial_t}n(t,x) + B(x)n(t,x) = 2\displaystyle\int_x^\infty B(y)\kappa(x,y)n(t,y)\,\mathrm{d}y. \end{cases}$$

We use an upwind finite volume method with computation length domain L and grid number points ka : $x_i = i\Delta x,\ 0 \leq i \leq ka$ with $\Delta x = L/ka$

$$n_i^k = \frac{1}{\Delta x}\int_{x_{i-\frac{1}{2}}}^{x_{i+\frac{1}{2}}} n(k\Delta t, y)\,\mathrm{d}y, \quad \frac{1}{\Delta t}\int_0^{\Delta t} n(k\Delta t + s, x_i)\,\mathrm{d}s \approx n_i^{k+1}.$$

For the time discretization one can choose, thanks to the CFL (*Courant-Friedrichs-Lewy*) stability condition, the time step $\Delta t < \dfrac{1}{\max\limits_{i\in 1,\ldots,ka}(B_i + \dfrac{c}{\Delta x}g_i)}$ with the notation $g_i = g(i\Delta x)$ and $B_i = B(i\Delta x)$.
The numerical scheme is given for $i = 1, ..., ka$ by n_0^k and

- First for the conservative equation

$$n_i^{k+1/2} = n_i^k - c\frac{\Delta t}{\Delta x}\big((gn)_{i+1/2}^k - (gn)_{i-1/2}^k\big),$$

the interface fluxes $(gn)_{i\pm1/2}^k$ are defined by upwind method.

- Second for the gain and lost part by cellular division we compute

$$n_i^{k+1} = \big(1 - \Delta t\, B_i\big)n_i^{k+1/2} + 2\Delta t\, \mathcal{F}_i^k$$

where $\mathcal{F}_i^k \approx \displaystyle\int_{x_i}^{x_{ka}} B(y)n^{k+1/2}(y)\kappa(x_i, y)\,\mathrm{d}y$.

- At last we renormalize the discrete solution by

$$\tilde{n}^{k+1} = \frac{n^{k+1}}{\displaystyle\sum_{j=1}^{ka} n_j^{k+1}\Delta x}$$

what allows to have $\tilde{n}^{k+1} \xrightarrow[k\to\infty]{} N, \quad \displaystyle\sum_{i=1}^{ka} N_i\Delta x = 1, \quad N_i > 0$, where N is the dominant eigenvector for the discrete problem associated to the following steady equation

$$c\frac{\partial}{\partial_x}(g(x)N(x)) + (B(x) + \lambda_0)N(x) = 2\int_0^{+\infty} B(y)\kappa(x, y)N(y)\,\mathrm{d}y$$

with λ_0 the dominant eigenvalue associated to N.

3.3.2 The inverse problem without regularization

As illustrated in [67], solving numerically Equation (3.23) without regularization is unstable. Indeed this recovering naive method gives bad reconstructions of $H = BN$ as soon as the observed N_ε is irregular (see above the estimates and see also (3.23)). Here what we more over observe is that, at the neighborhood of $x = 0$, the solution explodes. As an example of this we consider a length domain $L = 25$ and the total number grid points $ka = 300$, then by an Upwind method we compute numerically the Equation (3.23) and compare the result with that obtained by solving the direct problem (D.P).

3.3.3 The inverse problem : Quasi-Reversibility discretization

In this section we numerically investigate the regularization of the inverse problem (3.23) by the Quasi-reversibility method based on Equation (3.31) that we rewrite, by dropping the index ε, as follows

$$\begin{cases} -\alpha x^{-k}\dfrac{\partial}{\partial_x}(x^{k+1}B_\alpha(x)N(x)) + c\dfrac{\partial}{\partial_x}(g(x)N(x)) + (B_\alpha(x) + \lambda_0)N(x) = 2\displaystyle\int_x^\infty \kappa(x, y)B_\alpha(y)N(y)\,\mathrm{d}y, \\ (B_\alpha N)(0) = 0, \quad (B_\alpha N)(\infty) = 0; \quad 0 < \alpha; \;\; k \in \mathbb{R}_+. \end{cases}$$

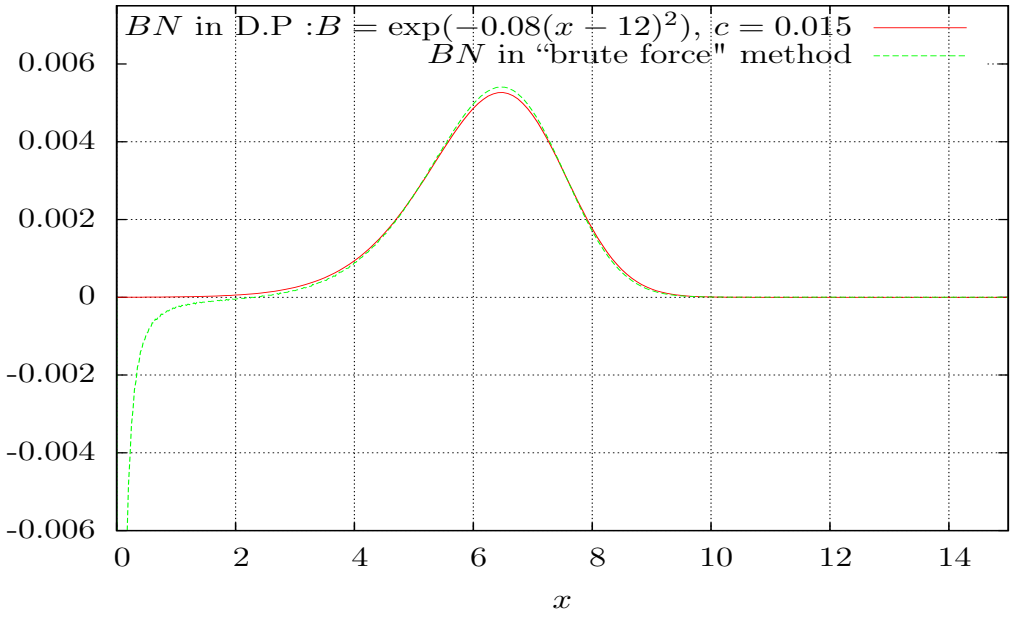

Figure 3.1 – Numerical reconstruction of BN by "brute force method" with the choice $g(x) = x$ and $\kappa(x,y) = \dfrac{1}{y}\mathbb{I}_{x<y}$.

Assuming that N and λ are measured, we first define c by (3.32) and then look for an estimate of the division rate B_α. For this, we put the notation

$$H_\alpha = B_\alpha N \text{ and } L = -c\frac{\partial}{\partial_x}(gN) - \lambda_0 N.$$

By a standart upwind method we obtain, when dropping the index α, the following discretization

$$\begin{cases} -\alpha x_i^{-k}\left(\dfrac{x_{i+1}^{k+1}H_{i+1} - x_i^{k+1}H_i}{\Delta x}\right) + H_i - 2\displaystyle\sum_{j=i}^{ka} H_j\kappa_{i,j}\Delta x = L_i \\ \text{with } L_i = -\lambda_0 N_i - c\left(\dfrac{g_{i+1}N_{i+1} - g_iN_i}{\Delta x}\right), \quad \forall\, i = 1,...,ka \\ H_0 = 0 \text{ and } H_l = 0, \quad \forall\, l > ka. \end{cases}$$

By developping this discrete equation we obtain

$$\left(-\alpha\frac{(i+1)^{k+1}}{i^k} - 2\kappa_{i,i+1}\Delta x\right)H_{i+1} + \left(1 + \alpha i - 2\kappa_{i,i}\Delta x\right)H_i - 2\sum_{j=i+2}^{ka} H_j\kappa_{i,j}\Delta x = L_i, \quad \forall\, i = 1,...,ka.$$

We rewrite it under matrix shape $A \times H = L$ with A the matrix of coeficients of size $ka \times ka$; H is the unknown vector of size ka and L is a known vector of size ka.
The matrix A being a upper triangular one, what allows to solve directly the linear system thanks to the following iterations

$$\begin{cases} H_{ka} = \dfrac{L_{ka}}{A_{ka,ka}}; \\ H_i = \dfrac{1}{A_{i,i}}\left(L_i - \displaystyle\sum_{j=i+1}^{ka} A_{i,j}H_j\right); \quad \forall\, i = ka-1,...,1. \end{cases}$$

The matrix A satisfying $A_{i,j} > 0$ for $j \geq i+1$, we can choose Δx small enough so that $A_{i,i} = 1 + \alpha i - 2\kappa_{i,i}\Delta x > 0$ for all i. This guarantees that no oscillations appear.

3.3.4 The inverse problem : Filtering discretization

This section is devoted to the numericall discretization of the inverse problem (3.23) by the Filtering method based on Equations (3.26)-(3.27). The aim is to numerically solve the Equation (3.26) that we rewrite when dropping the index ε as follows

$$\begin{cases} x^p c_\alpha \dfrac{\partial}{\partial_x}\big(g(x)N_\alpha(x)\big) + x^p(B_\alpha(x)+\lambda_\alpha)N_\alpha(x) = 2x^p \displaystyle\int_0^{+\infty} \kappa(x,y)B_\alpha(y)N_\alpha(y)\,\mathrm{d}y, \\ \big(B_\alpha N_\alpha\big)(0) = 0, \quad \alpha > 0, \end{cases}$$

with $N_\alpha = N * \rho_\alpha$ and ρ_α a sequence of mollifiers.
As previously, we want to estimate B_α from a measured density N and Malthus parameter λ. We first define c by (3.28). We then rewrite the regularised equation as follows

$$x^p B_\alpha(x)N_\alpha(x) - 2\int_x^\infty x^p \kappa(x,y)B(y)N_\alpha(y)\,\mathrm{d}y = -x^p c_\alpha \frac{\partial}{\partial_x}\big(g(x)N_\alpha(x)\big) - \lambda_\alpha x^p N_\alpha(x)$$

For the convolution terms arising in the previous equation we use the combination of the Fast Fourier Transform and its inverse which we respectively note by F and F^* then we define the mollifiers ρ_α by its Fourier transform : $\hat{\rho}_\alpha(\xi) = \dfrac{1}{\sqrt{1+\alpha^2\xi^2}}$.
This leads to the following approximations

$$N_\alpha \approx F^*\big(\hat{\rho}_\alpha(\xi)F(N)(\xi)\big); \quad \frac{\partial}{\partial_x}\big(gN_\alpha\big) \approx dGN_\alpha = F^*\big(i\xi\hat{\rho}_\alpha(\xi)F(gN)(\xi)\big).$$

For the discretization we put the notation

$$H_\alpha = B_\alpha N_\alpha \text{ and } \quad L_\alpha = -c_\alpha dGN_\alpha - \lambda_\alpha N_\alpha$$

then in each grid point $x_i = i\Delta x$ we obtain when dropping the index α :

$$\begin{cases} H_0 = 0 \\ x_i^p(1-2\kappa_{i,i}\Delta x)H_i - 2\displaystyle\sum_{j=i+1}^{ka} x_i^p H_j \kappa_{i,j}\Delta x = x_i^p L_i\,; \quad \forall\, i = 1,...,ka. \end{cases}$$

We rewrite this previous discrete equation under matrix shape $A \times H = L$ with A the matrix of coeficients which is an upper triangular one and of size $ka \times ka$.
The shape of the matrix A allows to use adequately the LU iterative numerical method, and then we deduce the following iteration

$$\begin{cases} H_{ka} = \dfrac{L_{ka}}{A_{ka,ka}} \\ H_i = \dfrac{1}{A_{i,i}}\Big(L_i - \displaystyle\sum_{j=i+1}^{ka} A_{i,j}H_j\Big)\,; \quad \forall\, i = ka-1,...,1 \end{cases}$$

3.4 Numerical Tests

For the numerical tests we use as input data the noisy one N_ε which correspond for $\varepsilon = 0$ to the eigenfunction N obtained by solving numerically the long time behavior of the direct problem in section 3.3.1. The direct problem is solved in the length domain $L = 25$ for $ka = 300$ number grid points with two differents initial data : a step initial data and a maxwellian one, as follows

$$\text{Step function} : \begin{cases} n^0(x) = 0.2 \quad 5 \leq x \leq 10, \\ n^0(x) = 0 \quad \text{other where} \end{cases} \quad \text{Maxwellian} : \begin{cases} n^0(x) = \dfrac{1}{\sqrt{0.4\pi}} \exp\left(-\dfrac{(x-10)^2}{0.4}\right), \\ \forall\, 0 \leq x \leq L \end{cases} \tag{3.39}$$

and the steady solution is taken when $\|n(t,x) - N(x)\|_{L^1} <= 10^{-10}$.

In order to show the unique asymptotic profile of the direct problem we plot in pictures Fig.3.2 the steady cellular density N related to the two previous initial data with different values of c, B and with the choice $g(x) = x^{1/2}$ and $\kappa(x,y) = \dfrac{1}{y}\,\mathbb{I}_{\{x<y\}}$.

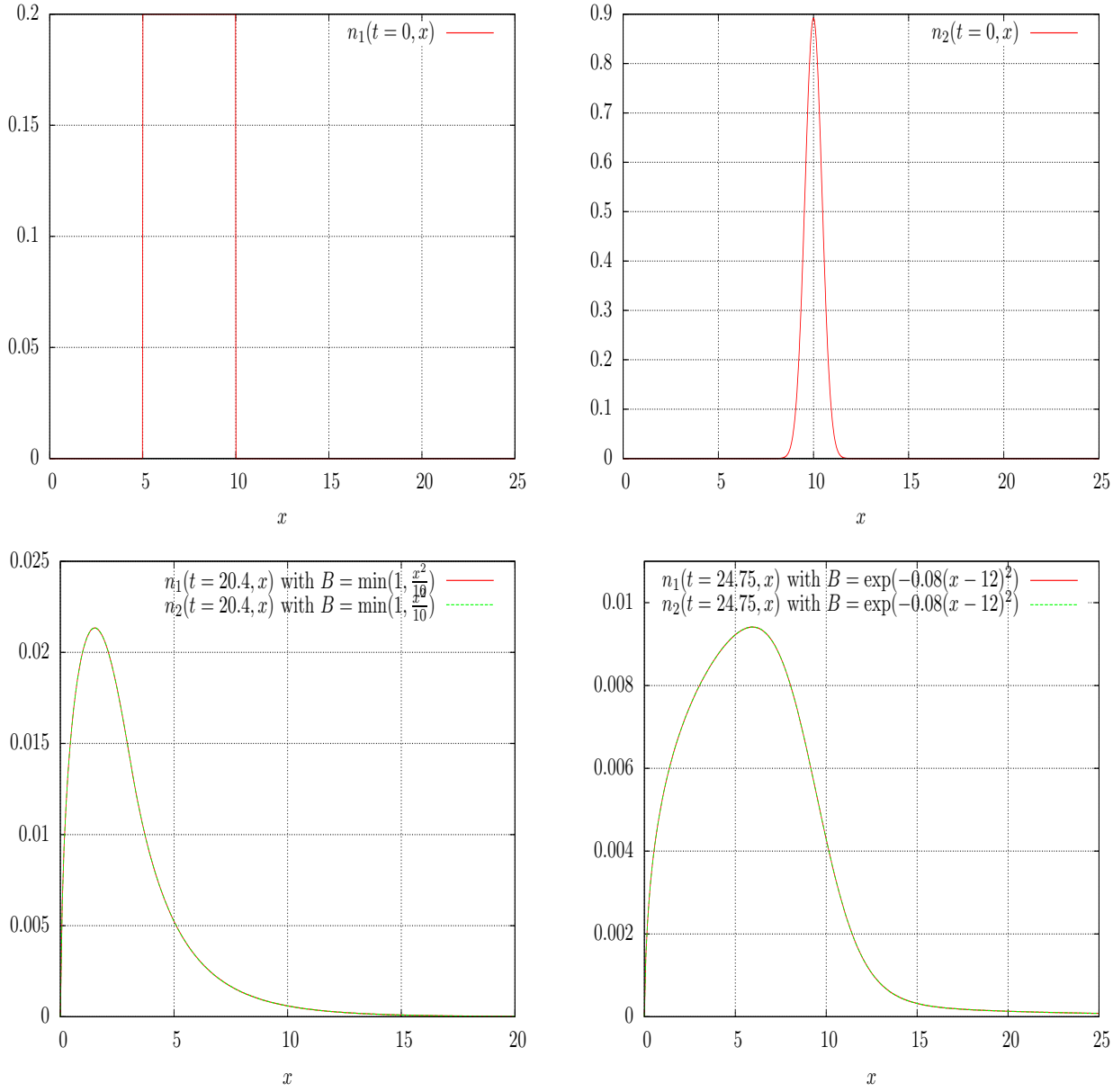

Figure 3.2 – Direct problem $g = x^{1/2}$: Top left : Step initial function. Top right :Maxwellian initial function. Down left : Steady solutions of cellular density with $c = 1$. Down right : Steady solutions of cellular density with $c = 0.5$.

3.4.1 Numerical reconstruction of BN in the noiseless case $\varepsilon = 0$

For the case where the input data are exactly known i.e. for $\varepsilon = 0$, we recover thanks to the Quasi-reversibility and Filtering methods the division rate B by computing numerically the value of BN with N obtained by solving the direct problem with high precision and for various choices of the division rate B as shows in figure Fig.3.3 below.

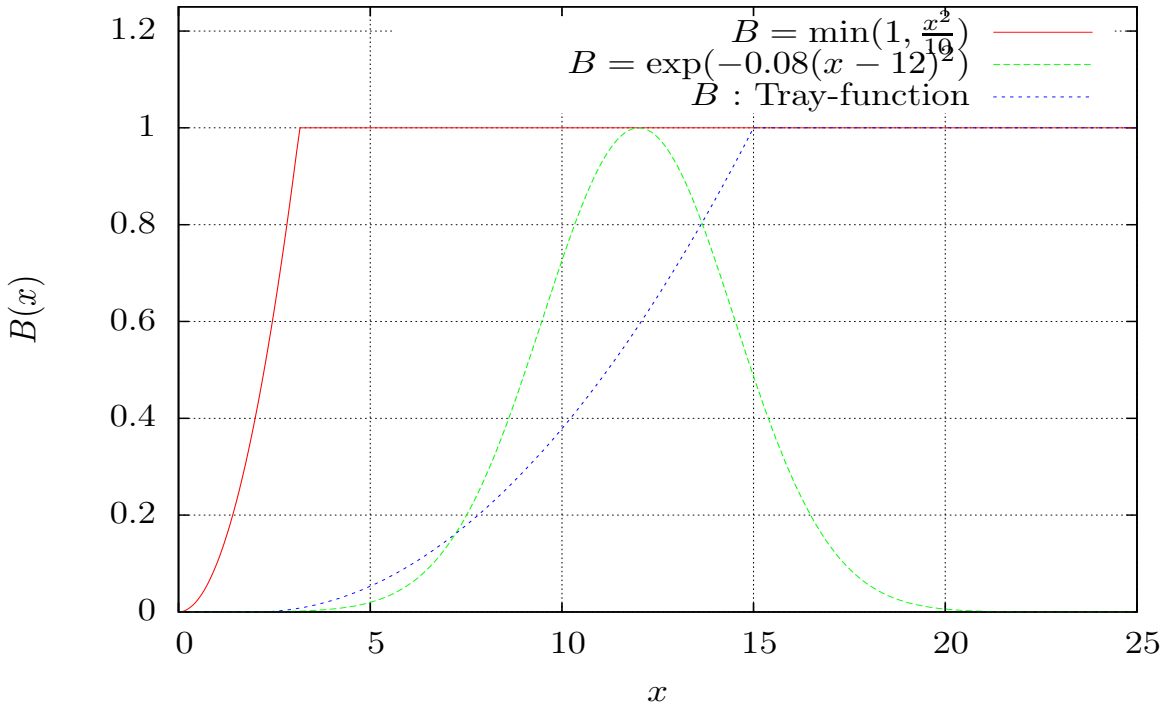

Figure 3.3 – Various choices of B to solve the direct problem .

In figure Fig.3.3, the Tray-function is defined as follow

$$B(x) = \begin{cases} 0, & \text{for } x < 2 \\ \dfrac{(x-2)^2}{13^2}, & \text{for } x \in [2, 15] \\ 1, & \text{for } x > 15. \end{cases}$$

Then with the notation D.P for the direct problem we obtain :

- **For the choice** $\kappa(x, y) = \dfrac{1}{y}\mathbb{I}_{\{x<y\}}$

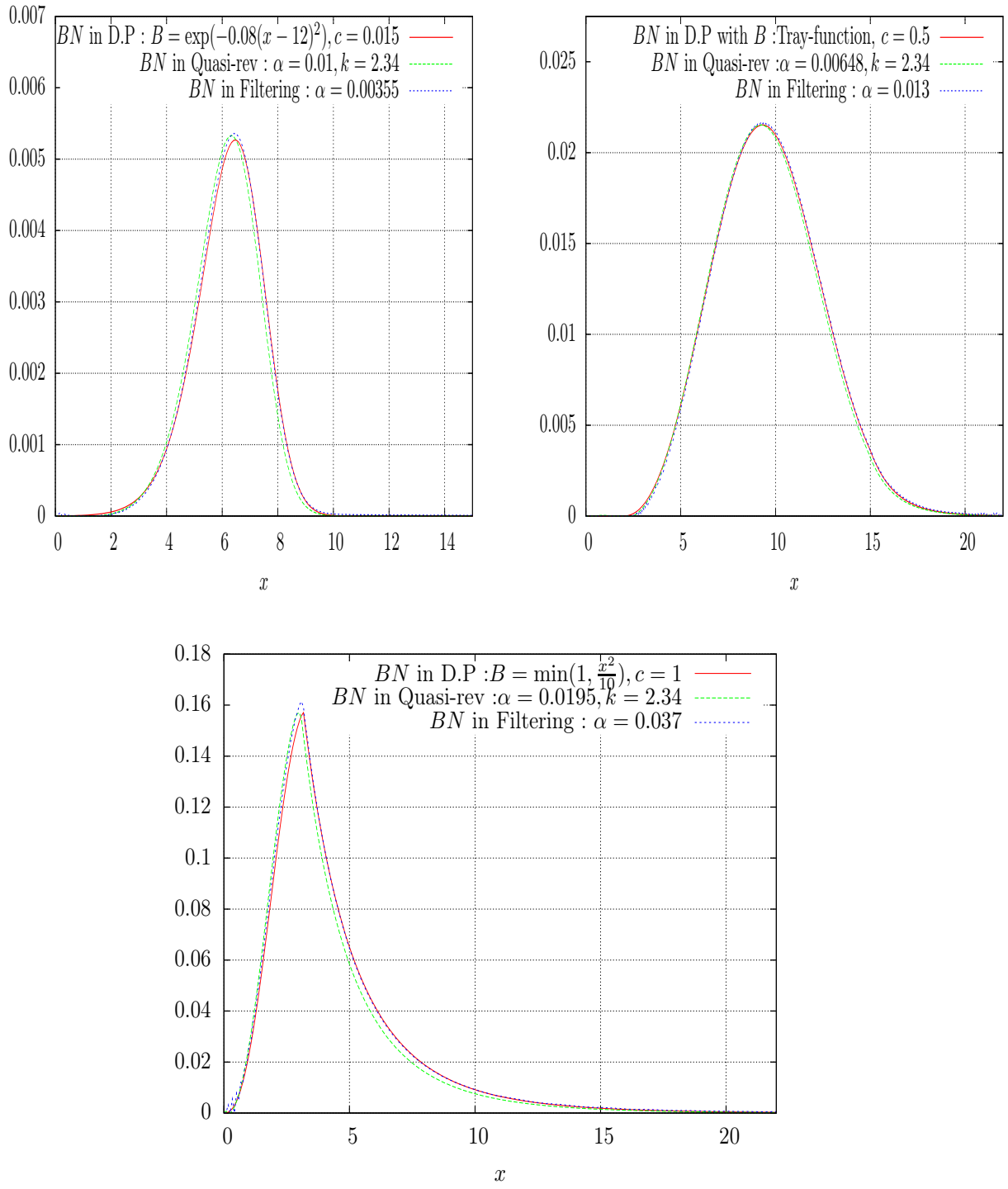

Figure 3.4 – Numerical reconstruction of BN for each regularization method in the case $\varepsilon = 0$. Top left :$g(x) = x$. Top right :$g(x) = x^{1/3}$. Down :$g(x) = x^{1/2}$.

We measure the relative error in L^2 norm by

$$error = \frac{\left\| BN - (BN)_{\varepsilon,\alpha} \right\|_{L^2}}{\left\| BN \right\|_{L^2}}, \tag{3.40}$$

where BN is the exact numerical solution of the direct problem and $(BN)_{\varepsilon,\alpha}$ represents the numerical reconstruction either by the Quasi-reversibility method or by the Filtering one. So we obtain for instance for the given parameters $g(x) = x^{1/3}$, $c = 0.5$ and $k = 2.34$ the following reconstruction error of the division rate as a function of α.

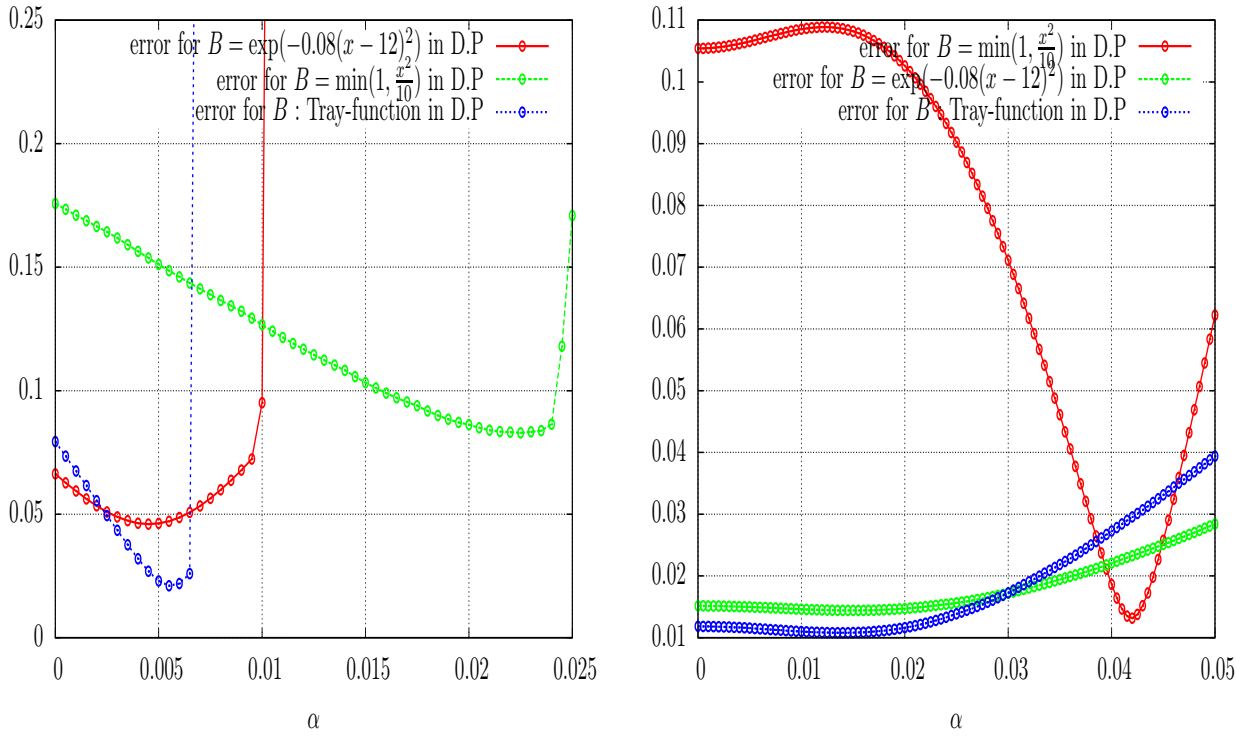

Figure 3.5 – Numerical errors for $\varepsilon = 0$ with different choices of B in the direct problem. Left : errors by Quasi-reversibility method. Right : errors by Filtering method.

- **For the choice** $\kappa(x,y) = \dfrac{1}{y}\kappa_0(\dfrac{x}{y})$ **with** $\kappa_0 \sim \mathcal{N}(\frac{1}{2}, \frac{1}{4})$

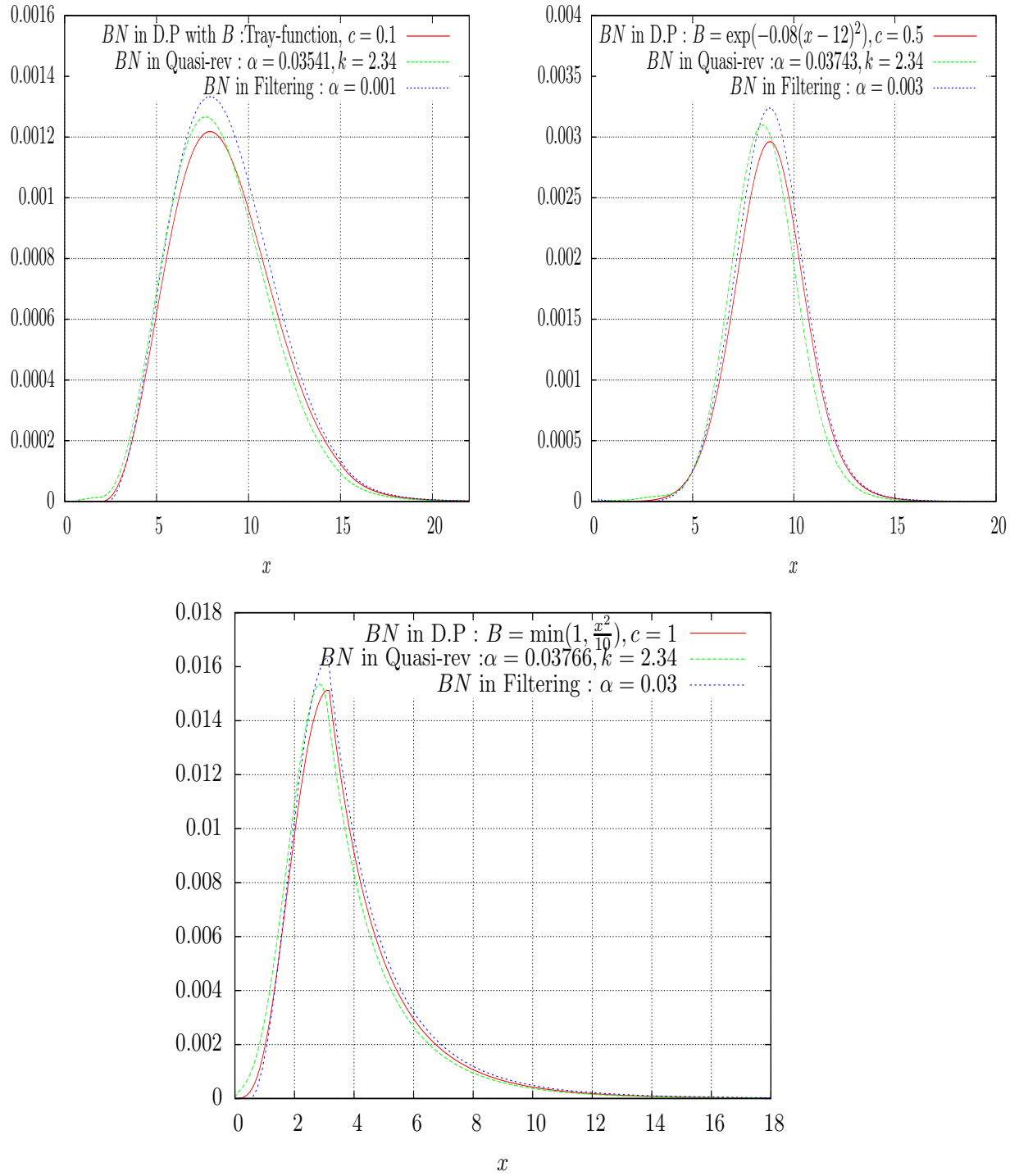

Figure 3.6 – Numerical reconstruction of BN for each regularization method in the case $\varepsilon = 0$. Top left :$g(x) = x$. Top right : $g(x) = x^{1/3}$. Down : $g = x^{1/2}$.

We measure the reconstruction error thanks to the relation (3.40) for the given parameters $g(x) = x^{1/3},\ c = 0.5,\ k = 2.34$ and we obtain the following representations

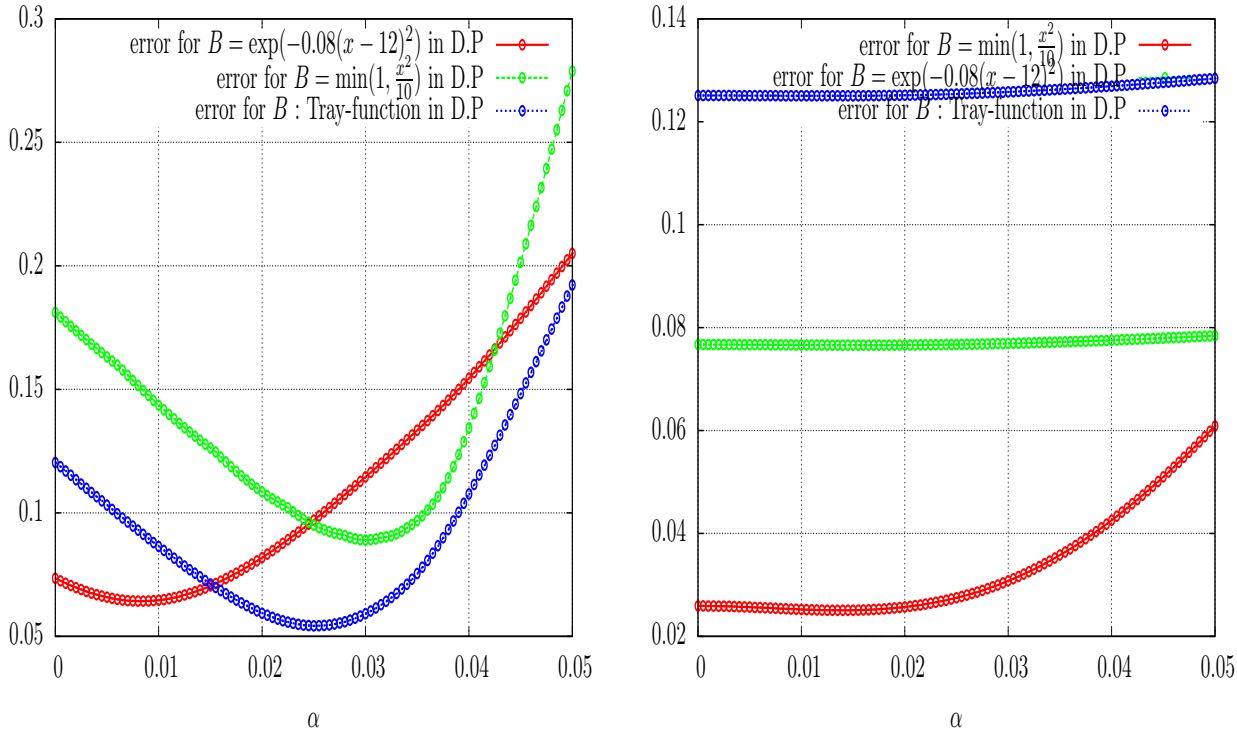

Figure 3.7 – Numerical errors for $\varepsilon = 0$ with different choices of B and c in the direct problem. Left : errors by Quasi-reversibility method ($k = 2.34$) . Right : errors by Filtering method.

3.4.2 Numerical reconstruction of BN in the noisy case $\varepsilon \neq 0$

For this case, we consider as input data the values of the solution N of the direct problem in which we add a multiplicative random noise uniformely distributed in $[\frac{-\varepsilon}{2}, \frac{\varepsilon}{2}]$ (see [65] for a more precise statistical setting of noisy informations). The nonnegativity of the data is insured by the choice

$$N_\varepsilon = \max(N(1 + l\varepsilon), 0), \quad l \in [-\frac{1}{2}, \frac{1}{2}],\ \varepsilon \in [0, 1].$$

Then with these noisy data we numerically obtain

- **For the case** $\kappa(x, y) = \frac{1}{y}\mathbb{I}_{\{x<y\}}$

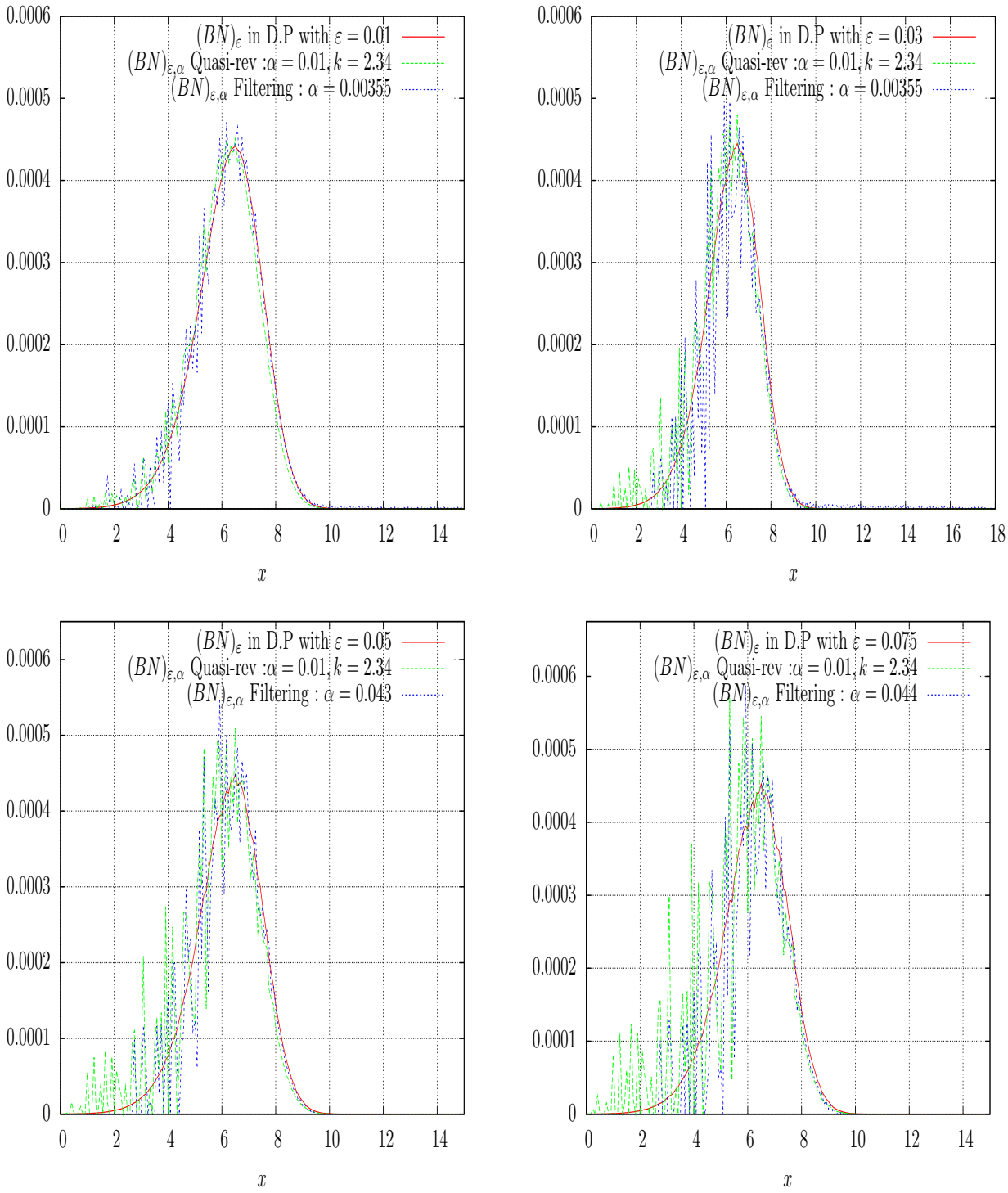

Figure 3.8 – Numerical reconstruction of BN by the measured data N_ε for different values of ε with the choice $B(x) = \exp(-0.08(x-12)^2)$, $c = 0.015$ and $g(x) = x$.

For various choice of the parameter ε we compute the relative error thanks to the relation (3.40) and obtain the following representations

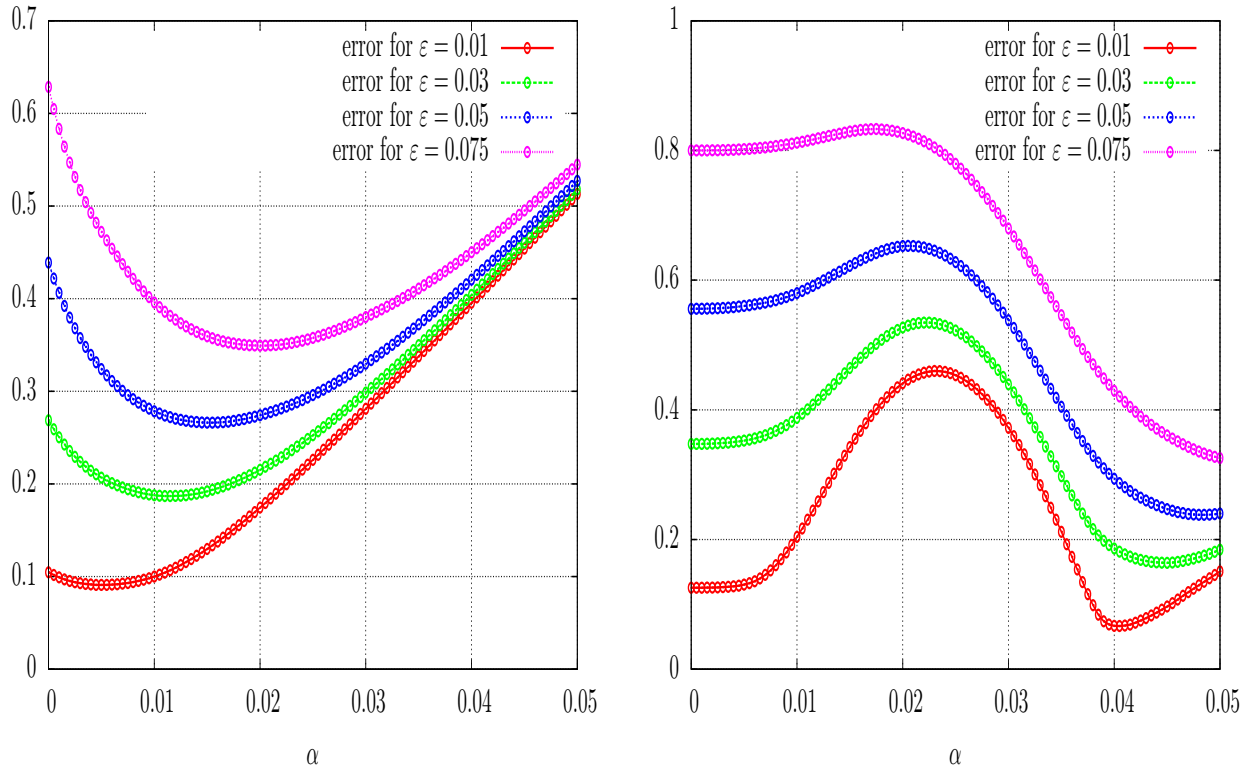

Figure 3.9 – Numerical errors for different values of $\varepsilon \neq 0$ with $B(x) = \exp(-0.08(x-12)^2)$, $c = 0.015$ and $g(x) = x$ in the direct problem. Left : errors by Quasi-reversibility method ($k = 2.34$) . Right : errors by Filtering method.

Remark 3.4.1. *Let us note that for data with high noise values i.e. $\varepsilon > 0.075$ the regularization by Quasi-reversibility method gives numerically better results than the Filtering one which creates big oscillations.*

- **For the choice $\kappa(x,y) = \frac{1}{y}\kappa_0(\frac{x}{y})$ with $\kappa_0 \sim \mathcal{N}(\frac{1}{2}, \frac{1}{4})$**

Discussion

As shown by the numerical illustrations above, and after that we tried many different shapes of regularization (trying for instance a wide variety of k and p, with $\pm\alpha$, in the quasi-reversibility method), our simulations still present some delicate points. Indeed, even if the regularization methods prove to give better result than the naive "brute force" method as shown by Figure 3.9, the gain remains relatively small, and the regularizing parameter α has also to remain small to avoid wrong reconstructions. Due to this small regularization, as shown by Figures 3.8, 3.10, the noise is filtered but not as much as we hoped first - especially for smaller x, that are farer from the departing point of the algorithm. Finally, the parameter α needs to stay in a confidence interval, selected, for a given growth rate $g(x)$, from a range of simulations carried out for various plausible birth rates (see for instance Figures 3.5, 3.7, 3.9).

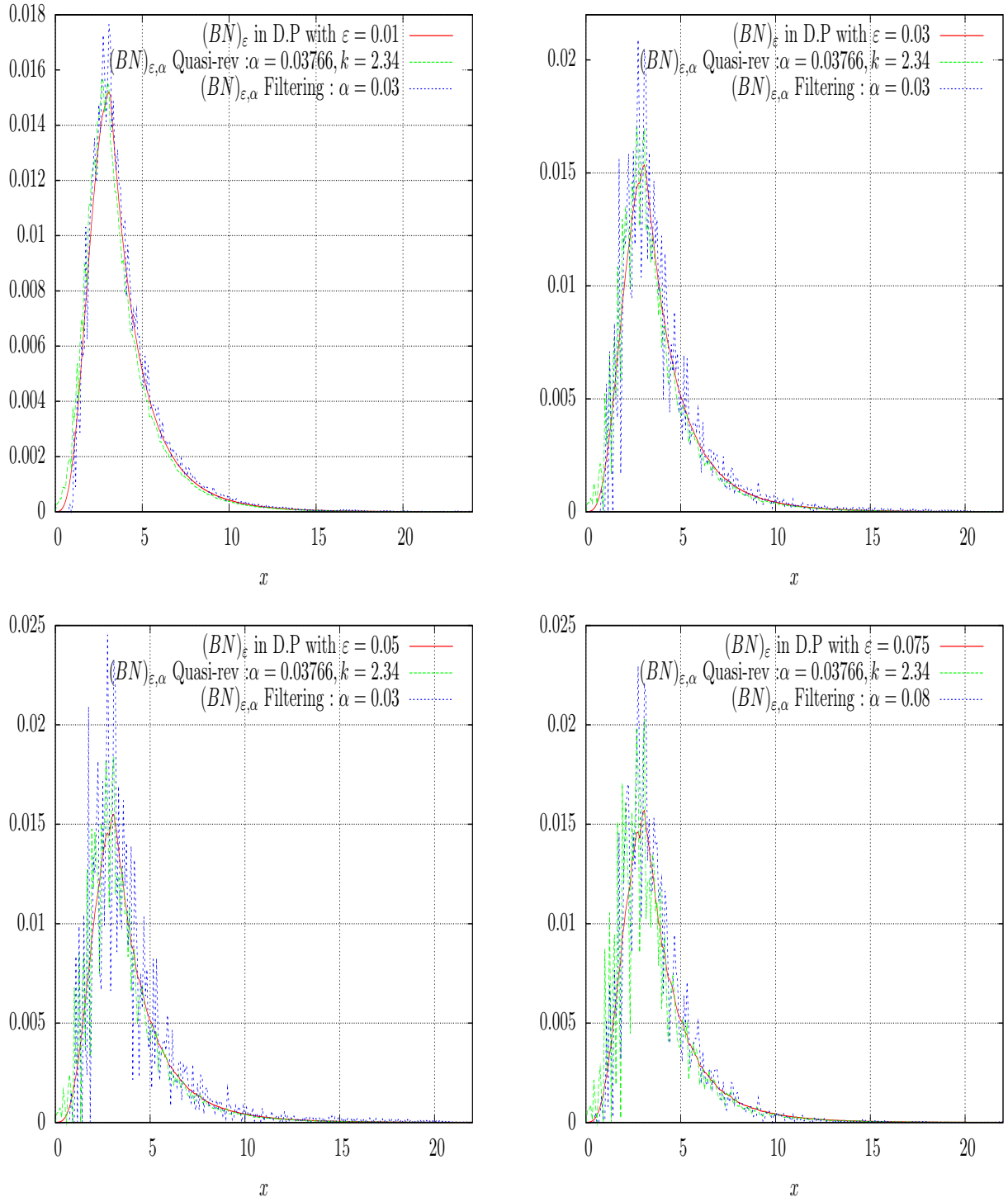

Figure 3.10 – Numerical reconstruction of BN by the measured data N_ε for different values of $\varepsilon \neq 0$ with the choice $B = \min(1, \frac{x^2}{10})$, $c = 1$ and $g(x) = x^{1/2}$.

3.5 Conclusion

We have addressed here the problem of recovering a birth rate B of a size-structured population from measurements of the time-asymptotic profile of its density, in the general case when a

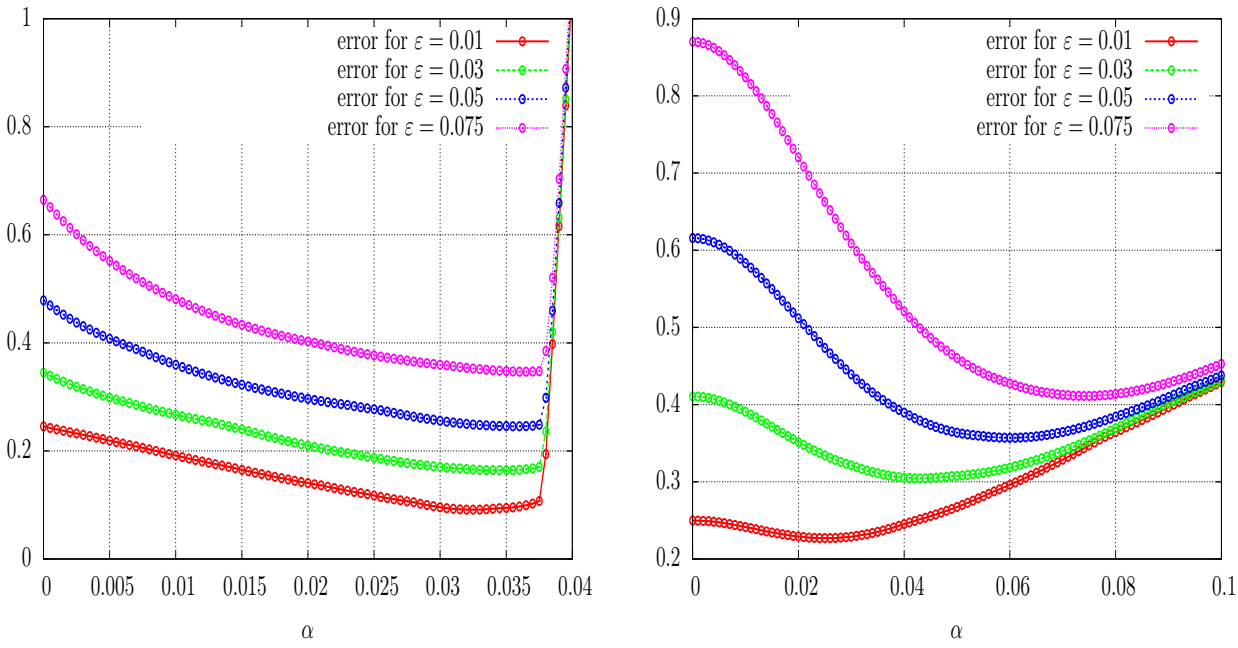

Figure 3.11 – Numerical errors for different values of $\epsilon \neq 0$ with $B = \min(1, \frac{x^2}{10})$, $c = 1$ and $g(x) = x^{1/2}$ in the direct problem. Left : errors by Quasi-reversibility method ($k = 2.34$) . Right : errors by Filtering method.

given individual can give birth to two daughters of inequal sizes. Compared to the work carried out in [158, 67, 97] this last assumption has raised new difficulties, the principal one being that we have no other choice than considering the equation from the "viewpoint" of the daughter cell - what implies to take into account the nonlocal integral term. We established theoretical estimates and built numerical methods to solve it. As shown above by our numerical illustrations however, some issues still remain to be solved, especially the behavior of the algorithm for smaller x and the cancellations of oscillations (also present in [67, 97]).

Chapitre 4

Modèle spécifique de polymérisation avec coalescence pour le Prion

Ce travail est le fruit d'une collaboration avec Pierre Gabriel dans le cadre du projet **PRION** étudié durant le Cemracs'09 sur la modélisation mathématique en médecine. Le but du projet est d'établir un schéma numérique d'ordre élevé et préservant la masse pour des modèles d'agrégation-fragmentation avec coagulation. En s'inspirant des travaux de F. Filbet et P. Laurençot [82], nous écrivons les termes intégraux de coagulation et de fragmentation sous forme conservative ce qui permet d'utiliser un schéma de transport qui préserve la masse. Nous choisissons une discrétisation WENO d'ordre 5 pour ses proriétés à la fois d'ordre èlevé et très peu dissipative puis nous présentons des simulations numériques obtenues à partir de données expérimentales.

Ce travail a fait l'objet d'une publication dans **ESAIM-P**roceedings sous le titre *High-order WENO scheme for polymerization-type equations* [86].

4.1 Introduction

The central mechanism of amyloid diseases is the polymerization of proteins : PrP in Prion diseases, APP in Alzheimer, Htt in Huntington. The abnormal form of these proteins is pathogenic and has the ability to polymerize into fibrils. In order to well understand this process, investigation of the size repartition of polymers is a crucial point. To this end, we discuss in this paper the mathematical modeling of these polymerization processes and we propose numerical methods to investigate the mathematical features of the models.

Mathematical models are already widely used to study the polymerization mechanism of Prion diseases [31, 64, 75, 95, 96, 120, 1, 106, 122, 160], Alzheimer [52, 18, 141] or Huntington [19]. Such models are also used for other biological polymerization processes [11, 21] and even for cell division [17, 62, 156] or in neurosciences [152].

Another field where we find aggregation-fragmentation equations is the physics of aggregates (aerosol and raindrop formation, smoke, sprays...). Among these models (see [115] for a review), one can mention the Smoluchowsky coagulation equation [78, 83, 82, 119, 139] with fragmentation [76, 77, 79, 114, 118, 117] and the Lifshitz-Slyosov system [35, 47, 49, 81, 146, 147, 148, 149]. In [46, 103] a Smoluchowsky coagulation term is added to the Lifshitz-Slyosov equation.

In this paper we are interested in a model including polymerization, coagulation and fragmentation phenomena. We consider a medium where there are monomers (normal proteins for instance) characterized by the concentration $V(t)$ at time t and polymers (aggregates of abnormal proteins) of size x with the concentration $u(t,x)$. The dynamics of the density function $u(t,x)$ is driven by the system

$$\begin{cases} \dfrac{d}{dt}V(t) &= -\displaystyle\int_0^\infty \mathcal{T}\big(V(t),x\big)u(t,x)\,dx, \\ \dfrac{\partial}{\partial t}u(t,x) &= -\dfrac{\partial}{\partial x}\Big(\mathcal{T}\big(V(t),x\big)u(t,x)\Big) + \mathcal{Q}(u)(t,x), \\ u(t,0)=0, \quad u(0,x)=u_0(x)\geq 0 \quad \text{and} \quad V(0)=V_0\geq 0. \end{cases} \tag{4.1}$$

The monomers are attached by polymers of size x with the polymerization rate $k_{\text{on}}(x)$. Depolymerization occurs when monomers detach from polymers with a rate $k_{\text{off}}(x)$. Hence the transport term writes

$$\mathcal{T}(V,x) = Vk_{\text{on}}(x) - k_{\text{off}}(x). \tag{4.2}$$

The two functions k_{on} and k_{off} are piecewise derivable but can be discontinuous. They are positive except that k_{on} can vanish at zero. In this case, or more generally when $\mathcal{T}(V(t),0)\leq 0$, the boundary condition on $u(t,0)$ is not necessary since the characteristic curves outgo from the domain. The choice of the boundary condition $u(t,0)=0$ is justified later.
The coalescence of two polymers and the fragmentation of a polymer into two smaller ones are taken into account by the operator $\mathcal{Q}$. More precisely, denoting by A_x an aggregate of size x we have

$$\begin{aligned} A_x \;+\; A_y \;&\xrightarrow{k_{\text{c}}(x,y)}\; A_{x+y} && \text{coagulation} \\ A_{x+y} \;&\xrightarrow{k_{\text{f}}(x,y)}\; A_x \;+\; A_y && \text{fragmentation.} \end{aligned}$$

Thus the coagulation-fragmentation operator is $\mathcal{Q}=\mathcal{Q}_{\text{c}}-\mathcal{Q}_{\text{f}}$ with

$$\mathcal{Q}_{\text{c}}(u)(x) = \frac{1}{2}\int_0^x k_{\text{c}}(y,x-y)\,u(y)u(x-y)\,dy - u(x)\int_0^\infty k_{\text{c}}(x,y)\,u(y)\,dy, \tag{4.3}$$

$$\mathcal{Q}_{\text{f}}(u)(x) = \frac{1}{2}u(x)\int_0^x k_{\text{f}}(y,x-y)\,dy - \int_0^\infty k_{\text{f}}(x,y)\,u(x+y)\,dy. \tag{4.4}$$

The coalescence of two polymers of size x and y occurs with the symmetric rate $k_{\text{c}}(x,y)=k_{\text{c}}(y,x)$. This rate is a nonnegative function as the fragmentation symmetric rate $k_{\text{f}}(x,y)=k_{\text{f}}(y,x)$ with which a polymer of size $x+y$ produces two fragments of size x and y.

There is a difference between $V(t)$ and $u(t,x=0)$. In biochemical polymerization processes, small polymers are very unstable and thus do not exist. When they appear by detachment from a longer polymer, they are immediately degraded into monomers. Thus, the quantity of small polymers vanishes while the quantity of monomers is very high. To reflect this in the mathematical model, a quantity $V(t)$ of monomers is introduced, which is different from the quantity of small polymers $u(t,x=0)$. The evolution of the first one is given by an ODE while the second one is forced to be equal to zero through the boundary condition $u(t,0)=0$. A consequence of this distinction is that starting from $u_0(x)=0$ and $V_0>0$ there is no evolution : the concentration

of monomers is constant in time, $V(t) = V_0$, and the concentration of polymers remains null, $u(t,x) = 0$. This is a very intuitive and natural behaviour which is important to preserve for biological applications.
In the modeling, the distinction between V and $u(x = 0)$ induces a separation of the polymerization-depolymerization process from the coagulation-fragmentation. Indeed the aggregation of a monomer to a polymer can be seen as a coagulation but the resulting polymer has same size x than the initial one, since a monomer is very small compared to the typical size of a polymer. So a transport term is more accurate to model this phenomenon than an integral term (see [64]).
There is also the fact that when a small polymer is degraded into monomers, it increases the quantity of monomers. In a discrete model, this term appears in the equation on V (see n_0 in [106]). In the continuous model (4.1) this term can be neglected since the quantity of monomers produced by degradation of small polymers is very small compared to the total quantity of monomers.

4.2 Mass Conservation

The mechanism of polymerization is nothing but a rearrangement of the proteins, there is no creation and no disparition. So the total quantity of proteins has to be constant in time and this is the case in model (4.1). We define the total mass of the system as

$$P(t) = V(t) + \int_0^\infty xu(t,x)\,dx, \tag{4.5}$$

since a polymer of size x "contains x monomers". Integrating the equation on $u(t,x)$ multiplied by x and adding the equation on V we obtain

$$\forall t > 0, \qquad \frac{dP}{dt}(t) = 0, \tag{4.6}$$

so the total mass is conserved along time. This is a very important property that we want to keep in the numerical scheme and for this we rewrite equation (4.1) under a conservative form.

4.2.1 Conservative formulation

The classical discretization methods for transport equations are mass preserving. So the idea is to write the coagulation-fragmentation operator $\mathcal{Q}$, which preserves the mass, under a conservative form in order to use a transport scheme. For this we follow the paper [80] where such a transformation is made :

$$\begin{cases} x\mathcal{Q}_{\mathrm{c}}(u)(x) = -\dfrac{\partial \mathcal{C}(u)}{\partial x}(x), \\ x\mathcal{Q}_{\mathrm{f}}(u)(x) = -\dfrac{\partial \mathcal{F}(u)}{\partial x}(x), \end{cases}$$

where the operator $\mathcal{C}(u)$ is given by

$$\mathcal{C}(u)(x) := \int_0^x \int_{x-y}^\infty y k_{\mathrm{c}}(y,z)u(y)u(z)\,dzdy, \tag{4.7}$$

and $\mathcal{F}(u)$ is

$$\mathcal{F}(u)(x) := \int_0^x \int_{x-y}^{\infty} y k_{\mathrm{f}}(y,z) u(y+z)\, dzdy. \tag{4.8}$$

Under this form, the mass conservation is clearer and the use of conservative schemes possible.

A useful consequence of the property (4.6) for the numerical scheme is that the ODE on V can be replaced by a mass conservation equation (see [103])

$$\forall t > 0, \qquad V(t) = V_0 + \int_0^{\infty} x(u_0(x) - u(t,x))\, dx. \tag{4.9}$$

Numerically, this equation is much easier to compute than the ODE to be solved. Moreover (4.9) provides an explicit expression for V as a function of u. So we set

$$\mathcal{G}(u)(x) := \Big(V_0 + \int_0^{\infty} y\big[u_0(y) - u(y)\big] dy\Big) k_{\mathrm{on}}(x) - k_{\mathrm{off}}(x) \tag{4.10}$$

and we obtain a new equation equivalent to (4.1)

$$\begin{cases} x\dfrac{\partial}{\partial t}u(t,x) + \dfrac{\partial\big[\mathcal{G}(u)xu\big]}{\partial x}(t,x) + \dfrac{\partial \mathcal{C}(u)}{\partial x}(t,x) - \dfrac{\partial \mathcal{F}(u)}{\partial x}(t,x) = \mathcal{G}(u)u(t,x), \\ u(t,0) = 0, \qquad u(0,x) = u_0(x). \end{cases} \tag{4.11}$$

In this equation (4.11), we have written the transport term as

$$x\frac{\partial\big[\mathcal{G}(u)u\big]}{\partial x}(t,x) = \frac{\partial\big[\mathcal{G}(u)xu\big]}{\partial x}(t,x) - \mathcal{G}(u)u(t,x). \tag{4.12}$$

This formulation enhances the relation

$$\frac{d}{dt}\int_0^{\infty} xu(t,x)\, dx = \int_0^{\infty} \mathcal{G}(u)u(t,x)\, dx = -\frac{d}{dt}V(t) \tag{4.13}$$

and allows to preserve this property numerically when using conservative transport schemes.

4.2.2 Domain truncation

Numerically, equation (4.11) is solved on a truncated domain $[0,R]$ so the integration bounds have to be changed in order to keep the mass preservation. For the coagulation term, we introduce as in [80]

$$\begin{aligned} \mathcal{C}^R(u)(x) &:= \int_0^x \int_{x-y}^{R-y} y k_{\mathrm{c}}(y,z) u(y)u(z)\, dzdy \\ &= \int_0^x \int_x^R y k_{\mathrm{c}}(y,z-y) u(y)u(z-y)\, dzdy, \end{aligned}$$

and for the fragmentation

$$\begin{aligned} \mathcal{F}^R(u)(x) &:= \int_0^x \int_{x-y}^{R-y} y k_{\mathrm{f}}(y,z) u(y+z)\, dzdy \\ &= \int_0^x \int_x^R y k_{\mathrm{f}}(y,z-y) u(z)\, dzdy. \end{aligned}$$

With this truncation, we have $\mathcal{C}^R(u)(0) = \mathcal{C}^R(u)(R) = \mathcal{F}^R(u)(0) = \mathcal{F}^R(u)(R) = 0$. So the total mass does neither increase nor decrease with respect to time if we consider the coagulation and fragmentation processes. If we look at the effects of this truncation on the original coagulation and fragmentation operators we have

$$Q_{\mathrm{c}}^R(u)(x) := -\frac{1}{x}\partial_x \mathcal{C}^R(u)(x) = \frac{1}{2}\int_0^x k_{\mathrm{c}}(y, x-y)u(u)u(x-y)\,dy - u(x)\int_0^{R-x} k_{\mathrm{c}}(x,y)u(y)\,dy$$

and

$$Q_{\mathrm{f}}^R(u)(x) := -\frac{1}{x}\partial_x \mathcal{F}^R(u)(x) = \frac{1}{2}u(x)\int_0^x k_{\mathrm{f}}(y, x-y)\,dy - \int_x^R k_{\mathrm{f}}(x, y-x)u(y)\,dy.$$

In the coagulation term, the truncation corresponds to the assumption that a polymer of size x cannot coagulate with a polymer of size greater than $R-x$. Concerning the fragmentation term, it is nothing but the assumption that polymers of size greater than R cannot split. Biologically they are the natural assumptions to avoid the loss of mass.

Concerning the transport term, the only way to avoid the loss of mass is to set

$$\mathcal{G}^R(u)(R,t) = 0. \tag{4.14}$$

The meaning we give to this relation in the numerical scheme is exposed in Section 4.3.2. It is useless to do such a truncation for $x = 0$ since $xu(t,x)$ vanishes when $x = 0$.

Finally we obtain a conservative truncated equation for $x \in (0, R)$

$$\begin{cases} x\dfrac{\partial}{\partial t}u_R(t,x) + \dfrac{\partial\left[\mathcal{G}^R(u_R)xu_R\right]}{\partial x}(t,x) + \dfrac{\partial \mathcal{C}^R(u_R)}{\partial x}(t,x) - \dfrac{\partial \mathcal{F}^R(u_R)}{\partial x}(t,x) = \mathcal{G}(u_R)u_R(t,x), \\ u_R(t,0) = 0, \qquad u_R(0,x) = u_0(x). \end{cases} \tag{4.15}$$

When there is no transport term, convergence of the solution of Equation (4.15) to the solution of Equation (4.1) when $R \to \infty$ is proved in [70, 115, 114, 117, 131] under growth conditions on k_{c} and k_{f}.

4.3 A High Order WENO Scheme

In order to obtain a mass preserving scheme, we consider equation (4.11) as a transport equation and for high order accuracy we choose a fifth-order WENO (Weighted Essentially Non Oscillatory) reconstruction for . This high order scheme is comonly used [58, 165] since it is not more complicated to implement than a third order WENO one for instance.

4.3.1 Numerical fluxes

Before using the WENO reconstruction we have to know if the fluxes are positive or negative in order to appropriately upwind the scheme. Concerning the coagulation and the fragmentation terms, we consider a positive upwinding as suggested in [80]. For the transport term $\partial_x\left[\mathcal{G}(u)xu\right]$ we have to make a flux splitting because $\mathcal{G}$ has no sign. A natural splitting here is to put the

terms of $\mathcal{G}$ that are preceded by a plus sign in the positive part and the terms preceded by a minus sign in the negative part, namely $\mathcal{G} = \mathcal{G}_1^+ + \mathcal{G}_1^-$ where

$$\begin{cases} \mathcal{G}_1^+(u)(x) = \Big(V_0 + \int_0^\infty y u_0(y) dy\Big) k_{\text{on}}(x), \\ \mathcal{G}_1^-(u)(x) = -\Big(\int_0^\infty y u(y) dy\Big) k_{\text{on}}(x) - k_{\text{off}}(x). \end{cases} \tag{4.16}$$

An other decomposition is the polymerization-depolymerization one

$$\begin{cases} \mathcal{G}_0^+(u)(x) = \Big(V_0 + \int_0^\infty y\big[u_0(y) - u(y)\big] dy\Big) k_{\text{on}}(x), \\ \mathcal{G}_0^-(u)(x) = -k_{\text{off}}(x). \end{cases} \tag{4.17}$$

The term $\mathcal{G}_0^+$ is necessarily positive because $V_0 + \int_0^\infty y\big[u_0(y) - u(t,y)\big] dy = V(t) \geq 0$. With these two flux splittings, we built others by convex combination. For any $\lambda \in [0,1]$ we set $\mathcal{G}_\lambda = \lambda \mathcal{G}_1 + (1-\lambda)\mathcal{G}_0$ which gives

$$\begin{cases} \mathcal{G}_\lambda^+(u)(x) = \Big(V_0 + \int_0^\infty y\big[u_0(y) - u(y)\big] dy + \lambda \int_0^\infty y u(y) dy\Big) k_{\text{on}}(x), \\ \mathcal{G}_\lambda^-(u)(x) = -\lambda\Big(\int_0^\infty y u(y) dy\Big) k_{\text{on}}(x) - k_{\text{off}}(x). \end{cases} \tag{4.18}$$

We also consider the Lax-Friedrichs scheme which corresponds to

$$\begin{cases} \mathcal{G}_{\text{LF}}^+(u) = \frac{1}{2}\big(\mathcal{G}(u) + m\big), \\ \mathcal{G}_{\text{LF}}^-(u) = \frac{1}{2}\big(\mathcal{G}(u) - m\big), \end{cases} \tag{4.19}$$

with $m = \max_{x \geq 0} |\mathcal{G}(u)|$. This term has to be computed at each time step because $\mathcal{G}(u)$ depends on time.

Finally, the WENO reconstruction is done with

$$\begin{cases} H^+(u) = \mathcal{G}^+(u) x u + \mathcal{C}(u) - F(u), \\ H^-(u) = \mathcal{G}^-(u) x u, \end{cases} \tag{4.20}$$

and the choice among the different flux splittings is discussed in Section 4.4.2.

4.3.2 WENO reconstruction

The point of view adopted here is the finite difference one, as recommanded in [43], because it is better than the finite volume in terms of operation counts. We assume the spatial domain $[0, R]$ is divided into N uniform cells and we denote $x_i = i\Delta x$ for $0 \leq i \leq N$ with $\Delta x = \frac{R}{N}$. We use the WENO formulation of Jiang and Peng [108] which consists in applying WENO to approach the spacial derivative directly on the nodes of the grid. The spatial derivative $\partial_x(H^+(v) + H^-(v))$ is approximated at the point x_i by

$$\frac{1}{\Delta x}\Big[H^+_{i+\frac{1}{2}} + H^-_{i+\frac{1}{2}} - H^+_{i-\frac{1}{2}} - H^-_{i-\frac{1}{2}}\Big]$$

where the fifth order accurate numerical flux $H^+_{i+\frac{1}{2}}$ is given by the WENO reconstruction. For each node x_i we denote by H_i^+ the numerical approximation of $H^+(v(x_i))$. The stencil choice for each flux is specified in Figure 4.1, and $H^\pm_{i\pm\frac{1}{2}}$ are expressed as convex combination of the $H_k^\pm$ of the stencil. Let us detail how we proceed :

- for $H^-_{i-\frac{1}{2}}$ we set $W_1 = H^-_k$, $W_2 = H^-_{k+1}$, $W_3 = H^-_{k+2}$, $W_4 = H^-_{k-1}$, $W_5 = H^-_{k-2}$,
- for $H^-_{i+\frac{1}{2}}$ we set $W_1 = H^-_{k+1}$, $W_2 = H^-_{k+2}$, $W_3 = H^-_{k+3}$, $W_4 = H^-_k$, $W_5 = H^-_{k-1}$,
- for $H^+_{i-\frac{1}{2}}$ we set $W_1 = H^+_{k-3}$, $W_2 = H^+_{k-2}$, $W_3 = H^+_{k-1}$, $W_4 = H^+_k$, $W_5 = H^+_{k+1}$,
- for $H^+_{i+\frac{1}{2}}$ we set $W_1 = H^+_{k-2}$, $W_2 = H^+_{k-1}$, $W_3 = H^+_k$, $W_4 = H^+_{k+1}$, $W_5 = H^+_{k+2}$.

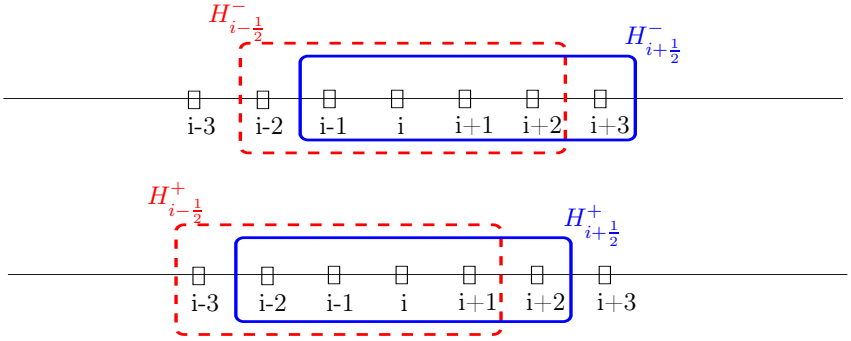

Figure 4.1 – stencil choice

For the regularity coefficients we define for each previous flux

$$\begin{aligned} S_1 &= \frac{13}{12}(W_1 - 2W_2 + W_3)^2 + \frac{1}{4}(W_1 - 4W_2 + 3W_3)^2, \\ S_2 &= \frac{13}{12}(W_2 - 2W_3 + W_4)^2 + \frac{1}{2}(W_2 - W_4)^2, \\ S_3 &= \frac{13}{12}(W_3 - 2W_4 + W_5)^2 + \frac{1}{4}(3W_3 - 4W_4 + W_5)^2. \end{aligned}$$

Then we take the weights

$$w_r = \frac{a_r}{\sum_{j=1}^3 a_j}, \quad \text{with} \quad a_r = \frac{d_r}{(\varepsilon + S_r)^2}, \quad d_1 = \frac{3}{10},\ d_2 = \frac{6}{10},\ d_3 = \frac{1}{10} \qquad r = 1, 2, 3$$

where ε is introduced to prevent the denominator from vanishing. Finally we take the different flux parts given by

$$\begin{cases} H^-_{i\pm\frac{1}{2}} = w_1\left(\frac{W_3}{3} - \frac{7W_2}{6} + \frac{11W_1}{6}\right) + w_2\left(\frac{-W_2}{6} + \frac{5W_1}{6} + \frac{W_4}{3}\right) + w_3\left(\frac{W_1}{3} + \frac{5W_4}{6} - \frac{W_5}{6}\right), \\ H^+_{i\pm\frac{1}{2}} = w_1\left(\frac{W_1}{3} - \frac{7W_2}{6} + \frac{11W_3}{6}\right) + w_2\left(\frac{-W_2}{6} + \frac{5W_3}{6} + \frac{W_4}{3}\right) + w_3\left(\frac{W_3}{3} + \frac{5W_4}{6} - \frac{W_5}{6}\right). \end{cases}$$

Concerning the boundaries $x = 0$ and $x = R$, we compute using the WENO reconstruction with ghost points $x_{-3},\ x_{-2},\ x_{-1}$, and $x_{N+1},\ x_{N+2},\ x_{N+3}$. In the first three points we use that for all time $t \geq 0$,

$$xu(t,x)\big|_{x=0} = \mathcal{C}^R(u)(x = 0, t) = \mathcal{F}^R(u)(x = 0, t) = 0$$

to set $H^\pm_{-3} = H^\pm_{-2} = H^\pm_{-1} = 0$. For the last three ones we use the truncation

$$\mathcal{G}^R(u)(x = R, t) = \mathcal{C}^R(x = R, t) = \mathcal{F}^R(x = R, t) = 0$$

to put $H^\pm_{N+1} = H^\pm_{N+2} = H^\pm_{N+3} = 0$.

4.3.3 Integration method

For the integral terms, we use a fifth order composite rule introduced in [165]. If f_k denotes an approximation of $f(x_k)$, the method can be written as

$$\int_{i\Delta x}^{j\Delta x} f(x)\,dx \simeq \Delta x \sum_{k=i}^{j}{}' f_k$$

where

$$\begin{aligned}\sum_{k=i}^{j}{}' f_k &= \frac{251}{720}f_i + \frac{299}{240}f_{i+1} + \frac{211}{240}f_{i+2} + \frac{739}{720}f_{i+3} \\ &\quad + \frac{739}{720}f_{j-3} + \frac{211}{240}f_{j-2} + \frac{299}{240}f_{j-1} + \frac{251}{720}f_j + \sum_{k=i+4}^{j-4} f_k\end{aligned}$$

if $j - i > 6$. This method is based on polynomial interpolations of the function f.

On the first interval, we integrate without using the boundary value $f_0 = 0$ because the solution can be discontinuous at $x = 0$. So we use the fifth accurate approximation

$$\sum_{k=0}^{1}{}' f_k = \frac{55}{24}f_1 - \frac{59}{24}f_2 + \frac{37}{24}f_3 - \frac{9}{24}f_4.$$

Finally for the intervals at the boundaries we have

$$\sum_{0}^{2}{}' f_k = \frac{8}{3}f_1 - \frac{5}{3}f_2 + \frac{4}{3}f_3 - \frac{1}{3}f_4,$$

$$\sum_{0}^{3}{}' f_k = \frac{21}{8}f_1 - \frac{9}{8}f_2 + \frac{15}{8}f_3 - \frac{3}{8}f_4,$$

$$\sum_{0}^{4}{}' f_k = \frac{21}{8}f_1 - \frac{7}{6}f_2 + \frac{29}{12}f_3 + \frac{1}{6}f_4 - \frac{1}{24}f_5,$$

$$\sum_{0}^{5}{}' f_k = \frac{21}{8}f_1 - \frac{7}{6}f_2 + \frac{19}{8}f_3 + \frac{17}{24}f_4 + \frac{1}{2}f_5 - \frac{1}{24}f_6,$$

$$\sum_{0}^{6}{}' f_k = \frac{21}{8}f_1 - \frac{7}{6}f_2 + \frac{19}{8}f_3 + \frac{2}{3}f_4 + \frac{25}{24}f_5 + \frac{1}{2}f_6 - \frac{1}{24}f_7,$$

$$\sum_{0}^{7}{}' f_k = \frac{21}{8}f_1 - \frac{7}{6}f_2 + \frac{19}{8}f_3 + \frac{2}{3}f_4 + f_5 + \frac{25}{24}f_6 + \frac{1}{2}f_7 - \frac{1}{24}f_8,$$

$$\sum_{N-1}^{N}{}' f_k = \frac{9}{4}f_N + \frac{19}{24}f_{N-1} - \frac{5}{24}f_{N-2} + \frac{1}{24}f_{N-3},$$

$$\sum_{N-2}^{N}{}' f_k = \frac{1}{3}f_N + \frac{4}{3}f_{N-1} + \frac{1}{3}f_{N-2},$$

$$\sum_{N-3}^{N}{}' f_k = \frac{1}{3}f_N + \frac{31}{24}f_{N-1} + \frac{7}{8}f_{N-2} + \frac{13}{24}f_{N-3} - \frac{1}{24}f_{N-4},$$

$$\sum_{N-4}^{N}{}' f_k = \frac{1}{3}f_N + \frac{31}{24}f_{N-1} + \frac{5}{6}f_{N-2} + \frac{13}{12}f_{N-3} + \frac{1}{2}f_{N-4} - \frac{1}{24}f_{N-5},$$

$$\sum_{N-5}^{N}{}' f_k = \frac{1}{3}f_N + \frac{31}{24}f_{N-1} + \frac{5}{6}f_{N-2} + \frac{25}{24}f_{N-3} + \frac{25}{24}f_{N-4} + \frac{1}{2}f_{N-5} - \frac{1}{24}f_{N-6},$$

$$\sum_{N-6}^{N}{}' f_k = \frac{1}{3}f_N + \frac{31}{24}f_{N-1} + \frac{5}{6}f_{N-2} + \frac{25}{24}f_{N-3} + f_{N-4} + \frac{25}{24}f_{N-5} + \frac{1}{2}f_{N-6} - \frac{1}{24}f_{N-7}.$$

We use this quadrature method to discretize the operators $\mathcal{C}^R$ and $\mathcal{F}^R$ with

$$\mathcal{C}_i^R - \mathcal{F}_i^R = (\Delta x)^2 \sum_{j=0}^{i}{}' \sum_{l=i+1}^{N}{}' x_l \big(k^{\mathrm{c}}_{j,l-j} u_j u_{l-j} - k^{\mathrm{f}}_{j,l-j} u_l\big) \tag{4.21}$$

as suggested in [80]. Grouping the two terms in an unique summation is lighter regarding to operation counts.

4.3.4 Time discretization

The time step is denoted by Δt and changes along time because of the CFL stability condition that is time dependent. For the time discretization we choose a third order Runge-Kutta method. To approach the time evolution of an equation $\partial_t u = L(u)$, we compute at time $n\Delta t$

$$u^{(1)} = u^n + \Delta t\, L(u^n) \qquad \text{and} \qquad u^{(2)} = \frac{3}{4}u^n + \frac{1}{4}u^{(1)} + \frac{1}{4}\Delta t\, L(u^{(1)}),$$

where u^n is an approximation of $u(n\Delta t)$. Then the approximation of v at time $(n+1)\Delta t$ is given by

$$u^{n+1} = \frac{1}{3}u^n + \frac{2}{3}u^{(2)} + \frac{2}{3}\Delta t\, L(u^{(2)}).$$

This method is an explicit one, so to ensure the stability we compute the time step Δt at each iteration thanks to the CFL condition

$$\Delta t \leq \min\left\{(G + C + F)^{-1}\right\} \tag{4.22}$$

where

$$G = \frac{1}{\Delta x}\sup_i\left(\mathcal{G}_i^+ - \mathcal{G}_i^-\right), \quad C = \sup_i\left\{\sum_{j=1}^{N}{}' k^{\mathrm{c}}_{i,j} u_j\right\} \quad \text{and} \quad F = \sup_i\left\{\frac{1}{2}\sum_{j=1}^{i-1}{}' k^{\mathrm{f}}_{j,i-j}\right\}.$$

For instance the Lax-Friedrichs decomposition leads to $G_{\mathrm{LF}} = m/\Delta x$.

Since we combine a fifth order WENO reconstruction and a third order time discretization, we predict that our scheme is convergent of third order. To validate it numerically, we compute the solution for different discretization grids with regular parameters and initial data. Comparing

these solutions at time $T = 20$ in the L^∞ space norm (see Table 4.1 for the results), we obtain the numerical order 2.95 which validates the prediction.

Δx	5/40	5/80	5/160
error	81.84	12.44	1.37

Table 4.1 – Error between different discrete solutions and the reference computed with $\Delta x = 5/320$.

4.4 Numerical Simulations

4.4.1 Parameters

Numerical values for the polymerization and fragmentation rates can be found in the biological literature (see [1, 4, 110] for instance). It is of importance to note that the models considered in these papers are discrete ones, so some computations are necessary to deduce adimensional numerical values for the continuous model (4.1). Another point is that the parameters of these models do not depend on the size of polymers, so we can only obtain mean values for the size-dependent parameters.

We choose to use the values of the recent paper [110] to do numerical simulations. The mean length of polymers for the initial distribution is estimated to be 1380. With the continuous model we reduce this value to 0.2 by considering an initial profile equal to a positive constant on $[0, 0.4]$ and null for $x > 0.4$ (see the first plot of Figure 4.5). Thus we define a parameter $\varepsilon = 0.2/1380 \approx 1,4 \times 10^{-4}$ which allows to go from a discrete model to a continuous one (see [64] for more details). The values we find are for instance $2.9 \times 10^{-2} \mu M^{-1} s^{-1}$ for the polymerization rate and $2.1 \times 10^{-9} s^{-1}$ for the fragmentation (where M represents the concentration in *mol* and s the time in *second*). The polymerization rate appears in a derivative term, so the value of the discrete model has to be multiplied by ε to obtain the continuous accurate value $4 \times 10^{-6} \mu M^{-1} s^{-1}$. Conversely, the fragmentation rate which appears in an integral term has to be divided by ε and we find $1.5 \times 10^{-5} s^{-1}$. Concerning the depolymerization and coagulation, they are neglected in the models of [1, 4, 110]. So we consider numerical values that seem to be reasonable compared to the previous ones.

In the present study, the parameters are assumed to be size dependent as suggested in [30, 31] and their choice is now presented and motivated. Concerning the numerical coefficients, they are chosen in order to have mean values of the same order than the values previously obtained from [110].

For the polymerization we assume that small polymers have a different behavior compared to the big ones. We consider a critical size $x_c = 0.5$ such that polymers of size $x < x_c$ convert monomers with the rate

$$k_{\text{on}}^{(1)}(x) = (4x + 0.2) \times 10^{-6} \mu M^{-1} s^{-1},$$

and for $x > x_c$ with a constant rate

$$k_{\text{on}}^{(2)}(x) \equiv 4 \times 10^{-6} \mu M^{-1} s^{-1}.$$

For the fragmentation kernel, we use the classical assumption that the fragmentation probability depends only on the size $x + y$ of the polymer and we set

$$k_{\text{f}}(x, y) = \frac{80(x + y)}{10 + (x + y)} \times 10^{-5} s^{-1}.$$

The depolymerization is assumed to be constant and of the same order as the fragmentation. We discuss the dependence on this parameter by considering different intensities

$$k_{\text{off}}(x) \equiv \eta \times 10^{-6} s^{-1} \qquad \text{with } 2 \leq \eta \leq 8. \tag{4.23}$$

Concerning the coagulation kernel, we do not use a classical one. Even if there is no space in model (4.1), we use a kernel which reflect some space effects. Indeed we consider that small polymers are very mobile and that the big ones, plaques, are very attractant. So the coagulation occurs preferentially between big and small aggregates. The kernel we choose is of the form

$$k_{\text{c}}(x,y) = \frac{4|x-y|^{\frac{3}{2}}}{1+(x+y)} \times 10^{-6} \mu M^{-1} s^{-1}.$$

This kernel satisfies the growth assumption that we can find in [70] to ensure the convergence of the solution when $R \to \infty$ if we consider the only coagulation-fragmentation process.

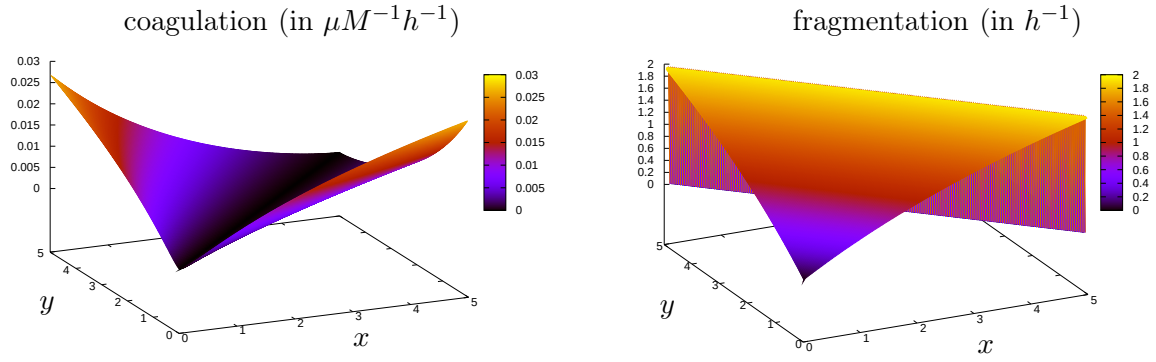

Figure 4.2 – Profiles of the coagulation and fragmentation kernels.

In [110] we also find numerical values for the initial data $V_0 = 98\,\mu M$ and $\displaystyle\int_0^R x u_0(x)\,dx = 0.21 \mu M$. This last value and the fact that the initial distribution of polymers is assumed to be under the form $u_0 = cst \times \mathbb{1}_{[0,0.4]}$ lead to

$$u_0(x) = \begin{cases} 2.6 & \text{if} \quad 0 \leq x \leq 0.4 \\ 0 & \text{if} \quad x > 0.4. \end{cases} \tag{4.24}$$

For the following simulations, the discretization is made on a domain $[0,5]$ with a number of nodes $N = 200$, so the mesh size is $\Delta x = 0.025$.

4.4.2 Choice among the different flux splittings

First we deal with the CFL condition. Thanks to the triangular inequality, we obtain that $G_{\text{LF}} \leq G_0$. Moreover, there is an explicit expression for G_λ

$$G_\lambda^n = \frac{1}{\Delta x} \sup_i \left\{ \left(V_0 + \Delta x \sum_{j=1}^{N}{}' x_j u_j^0 + (2\lambda - 1)\Delta x \sum_{j=1}^{N}{}' x_j u_j^n \right) k_i^{\text{on}} + k_i^{\text{off}} \right\}$$

which shows that G_λ increases with λ. So if $0 \leq \lambda < \Lambda \leq 1$ then at each time step we have $G^n_{\mathrm{LF}} \leq G^n_\lambda \leq G^n_\Lambda$. Notice also that, with the numerical values we have chosen, the quantity of polymers $\Delta x \sum_{j=1}^{N}{}' x_j u^n_j$ increases with n. Indeed we can see in Figure 4.8 that the quantity of monomers $V^n \simeq V(n\Delta t)$ defined by the mass conservation $V^n + \Delta x \sum_{j=1}^{N}{}' x_j u^n_j = V_0 + \Delta x \sum_{j=1}^{N}{}' x_j u^0_j$ decreases. The consequence on the CFL condition is that G^n_λ increases with n if $\lambda > \frac{1}{2}$, decreases if $\lambda < \frac{1}{2}$ and is time independent when $\lambda = \frac{1}{2}$. Thus, regarding to the numerical computation, the fastest scheme is the Lax-Friedrichs one and then the computation time increases significantly with λ.

Let us now turn to the effects of the flux splitting on the size distribution. First we consider a depolymerization corresponding to $\eta = 8$ in (4.23) and investigate the differences between the solutions associated to the decompositions $\mathcal{G}_{\mathrm{LF}}$, $\mathcal{G}_0$ and $\mathcal{G}_1$. We can see in Figure 4.3 that the solutions for $\mathcal{G}_0$ and $\mathcal{G}_1$ are close together for small times and then the behavior of $\mathcal{G}_0$ becomes closer to the Lax-Friedrichs one. The less oscillating scheme for $t = 6h$ is the the Lax-Friedrichs one, but it is also the most oscillating at time $t = 12h$. Finally the solutions associated to the three flux decompositions are quite similar and they all present oscillations at some times, so we do not find with this simulation any reason to discard one of them.

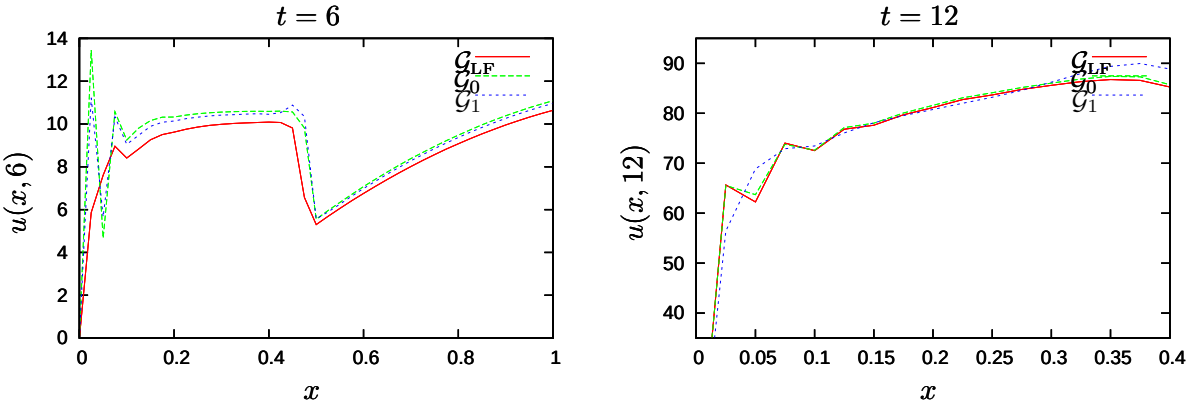

Figure 4.3 – Comparison between the flux splittings $\mathcal{G}_{\mathrm{LF}}$, $\mathcal{G}_0$ and $\mathcal{G}_1$ for $\eta = 8 \times 10^{-6} s^{-1}$.

If we change the depolymerization rate by considering $k_{\mathrm{off}} = 6 \times 10^{-6} s^{-1}$, we remark that the Lax-Friedrichs scheme is unstable (see Figure 4.4) while $\mathcal{G}_0$ is stable. If we continue to decrease η, we find with $k_{\mathrm{off}} = 2 \times 10^{-6} s^{-1}$ that the $\mathcal{G}_0$-scheme becomes unstable while $\mathcal{G}_{0.2}$ is stable. Thus the Lax-Friedrichs scheme and the $\mathcal{G}_\lambda$-schemes with λ small has to be avoided to ensure stability when small depolymerization values are considered.

Knowing that, we compare different stable schemes, namely $\mathcal{G}_\lambda$ with $0.2 \leq \lambda \leq 1$. We can see in Figure 4.5 that for large times ($t = 20h$), the three flux decompositions provide a good behavior where there are strong variations of the solution. These locations are $x = 0$ because of the boundary condition which enforces $u(t, 0)$ to vanish, and $x = 0.5$ because the transport term k_{on} is discontinuous at $x = 0.5$. If we look at smaller times ($t = 6h$ for instance) we can see that the larger λ is, the less oscillating the curves are. But, as we already remarked, the quantity G_λ is higher for λ close to 1 and it increases with time when $\lambda > \frac{1}{2}$. Thus it is penalizing for the computation time to use high values of λ. A good compromise could be to choose $\lambda = \frac{1}{2}$ since $G_{\frac{1}{2}}$ does not depend on time. The other solution is to adapt the λ when we change the parameters.

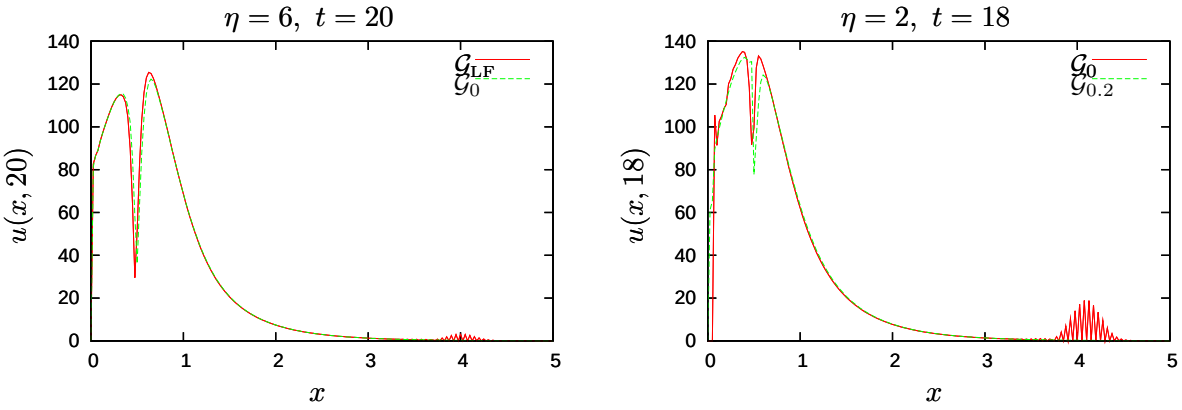

Figure 4.4 – Unstability of some schemes when η decreases. Left : $\mathcal{G}_{\mathrm{LF}}$ becomes unstable for $\eta = 6$. Right : $\mathcal{G}_0$ becomes unstable for $\eta = 2$.

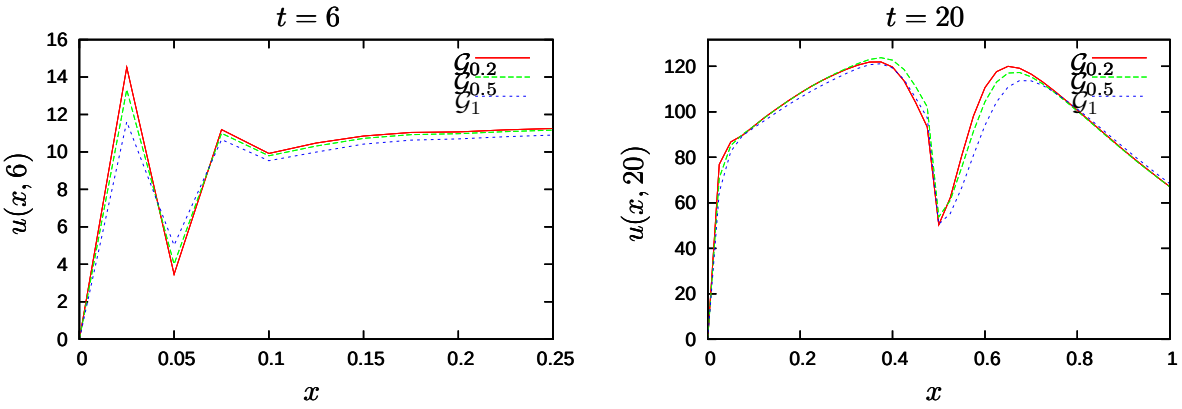

Figure 4.5 – Comparison of the behavior of the solution for different λ with $\eta = 5$.

4.4.3 Interpretation of the numerical results

We have considered that the mean size of the polymers at the initial time $t = 0$ was 1380. This size can be multiplied by 5 along the polymerization process (see Figure 4.6 keeping in mind that the mean size is represented by 0.2 in this continuous model). So if we want to solve the discrete model, we have to consider a system of dimension close to 5000, and the computations are very heavy. If we limit this value to 200 keeping the discrete model, then we lose a lot of precision. It is the same for the continuous model if it is discretized with a first order scheme. That is why we use a high order discretization, and we can see the difference in Figures 4.6 and 4.7 : the high order scheme is able to capture strong variations of amplitude while the first order flattens them. We also remark that the size repartition converges to a bimodal distribution, as observed by [40]. This asymptotic profile is independent of the initial data (see the time $t = 20$ in Figures 4.6 and 4.7) and can be seen as an eigenvector of the operator $\mathcal{Q} - \partial_x \mathcal{T}$ (see [134, 63]).

The evolution of the quantity of monomers $V(t)$ is plotted in Figure 4.8 for different values of the depolymerization rate k_{off}. This quantity decreases since the monomers aggregate to polymers. Thus the mass of polymers increases and the speed of this evolution is similar to those observed by [110]. Concerning the dependence on k_{off}, the difference between the three curves is more significant when the time increases. For small times, when $V(t)$ is close to $V_0 = 98\mu M$,

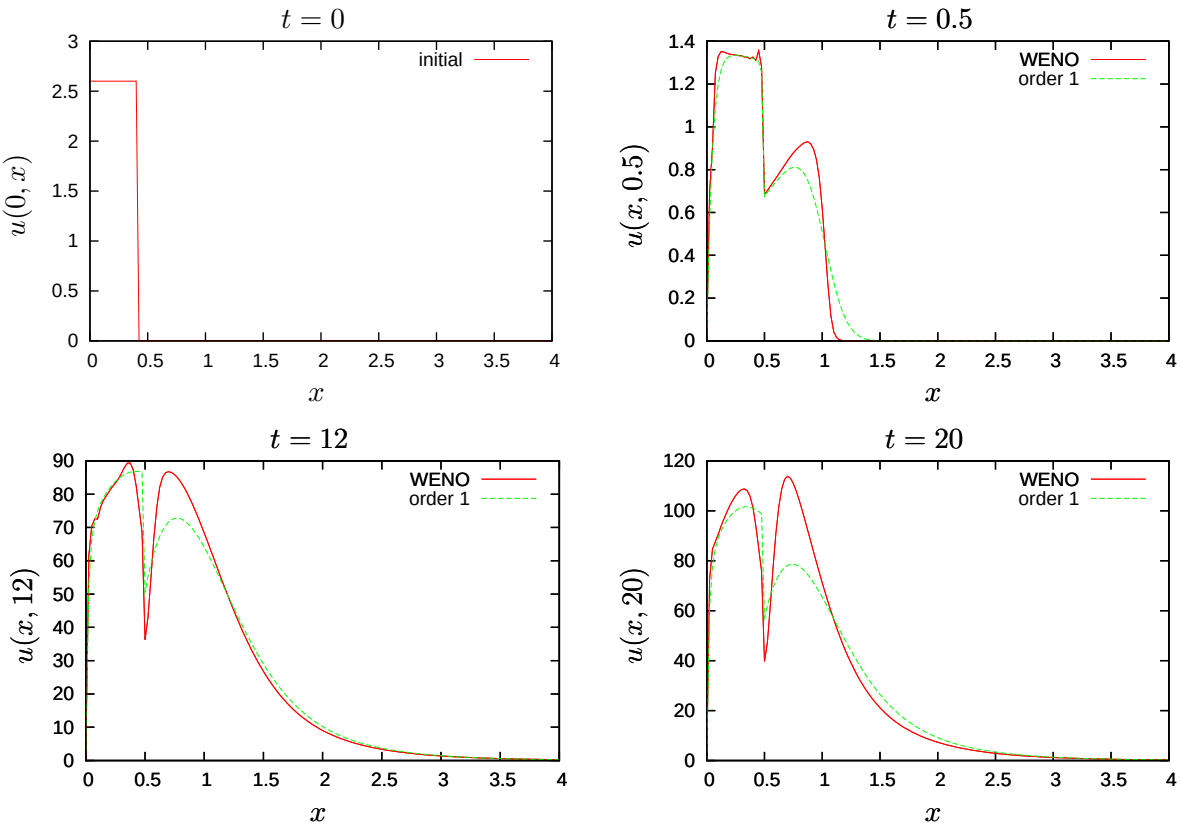

Figure 4.6 – Comparison between the WENO scheme and a first order scheme for the initial size distribution (4.24), with the depolymerization value $k_{\text{off}} = 8 \times 10^{-6} s^{-1}$ and the flux splitting parameter $\lambda = 0.5$

the depolymerization can be neglected since k_{off} is small compared to the product $V(t)k_{\text{on}}(x)$. Conversely, the equilibrium is reached when $\frac{d}{dt}V(t) = 0$, so when $k_{\text{off}} \simeq V k_{\text{on}}$ (see Equation (4.1)). That is why variations of η influence essentially the ratio between the quantity of monomers and the mass of polymers at the equilibrium as we can see in Figure 4.8.

4.5 Conclusion and future work

We have written a high order conservative scheme for a polymerization-type equation. The choice of the flux splitting for the transport term has been discussed but the accurate decomposition remains unclear. It seems that unstabilities can be avoided by adapting the value of λ but the oscillations remain present for any choice of the flux decomposition, even for a regular initial size distribution. A possible explanation for these phenomena can be that the integration method is not "positive" for the intervals at the boundaries. These points remain to be investigated for a better understanding and improvement.

As we have remarked in Section 4.4.3, the size distribution converges toward an equilibrium which corresponds to an eigenvector. The high-order WENO scheme presented in this paper could be used to numerically compute such eigenvectors. Another application of the code is to solve inverse problems (see [67, 158]) in order to determine the size dependence of the different

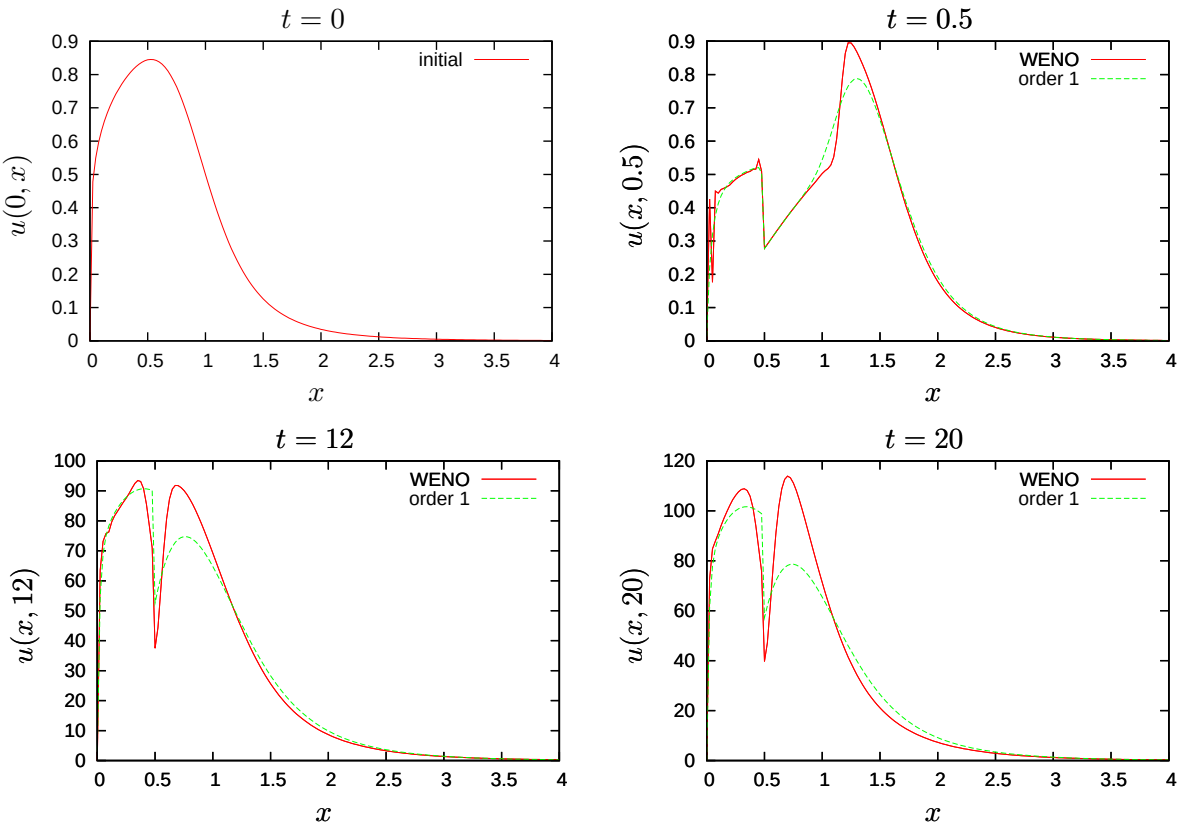

Figure 4.7 – Comparison between the WENO scheme and a first order scheme for a regular initial size distribution, with the depolymerization value $k_{\text{off}} = 8 \times 10^{-6} s^{-1}$ and the flux splitting parameter $\lambda = 0.5$

parameters.

acknowledgement

The authors are thankfull to Vincent Calvez, Marie D Jauffret, Frédéric Lagoutière and Natacha Lenuzza for their help and support during the Cemracs'09 research session.
This work has been done with the financial supports of
- the ANR contract TOPPAZ, allocation grant No. 4243, http ://www-roc.inria.fr/bang/TOPPAZ/
- the CEA-Institute of Emerging Diseases and Innovative Therapies, Route du Panorama, Bat.60, F-92265 Fontenay-aux-Roses.

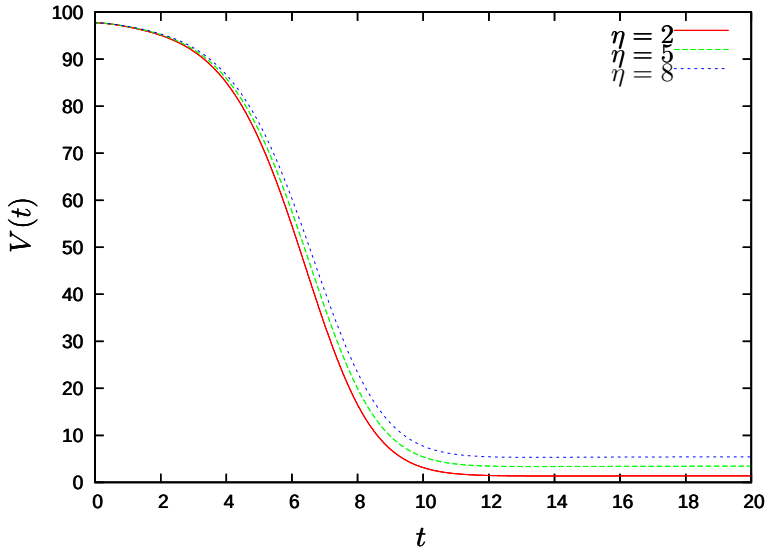

Figure 4.8 – Evolution of the quantity of monomers for different depolymerization rates, with the scheme $\mathcal{G}_{0.2}$.

Chapitre 5

Un modèle d'écoulement particulaires avec coagulation et fragmentation

Ce dernier chapitre du présent mémoire de thèse concerne l'analyse d'un modèle d'interaction fluide-particules avec prise en compte des phénomènes de coagulation et fragmentation entre particules. Cet interaction micro-macroscopique fait interagir des équations de type Euler compressibles pour le fluide et des équations de type Vlasov-Fokker-Planck pour le mouvement microscopique des particules. On s'intéresse à la dérivation d'arguments asymptotiques permettant de comprendre les processus de relaxation du modèle d'interaction. Ainsi en faisant un "rescaling" du modèle on établit une relation de dissipation d'entropie générale liée à l'interaction et aux phénomènes de coagulation-fragmentation. Grâce à cette relation de dissipation d'entropie on a définit deux régimes hydrodynamiques pour l'écoulement suivant un paramètre mesurant le rapport entre le temps de Stockes et le temps d'observation.

Cette étude a été faite en collaboration avec Thierry Goudon et Mamadou Sy.

5.1 Introduction

We are interested in models describing a large set of particles interacting with a fluid. The study of such two–phase flows (where particles represent the disperse phase evolving in a dense fluid) is motivated by applications like dispersion of dusts, smokes or pollutants [85, 54, 170, 173], the modeling of biomedical sprays [14, 140], optimization of combustion processes [73], the formation of powder-snow avalanches [29]... On the mathematical viewpoint the modeling leads to non standard systems of PDEs. The disperse phase is described through a distribution function in phase space, $f(t,x,v,r)$ where $t \geq 0$ stands for the time variable, $x \in \mathbb{R}^3$ the space variable, $v \in \mathbb{R}^3$ the velocity of the particles and $r \geq 0$ is related to their size. The dense phase is described, as usual in fluid mechanics, by macroscopic quantities (say mass density, velocity and temperature) depending only on the time and space variables. Hence the unknowns do not depend on the same set of variables, which makes part of the difficulty for mathematical analysis, together with the fact that we consider systems coupled through highly nonlinear terms. Furthermore, in view of numerical experiments, the kinetic framework leads to high computational cost, both in terms of size and time. This remark motivates to seek reduced models, which are of purely

hydrodynamic type, by means of asymptotic arguments that take advantage of some relaxation processes embodied into the model. Anticipating on the detailed presentation of the model, the evolution of the particle distribution function is driven by the combination of the following phenomena :

- the drag force exerted by the surrounding fluid on the particles,
- the influence of an external potential $x \mapsto \Phi(x)$ (gravity, electrostatic force, centrifugal force...),
- the Brownian motion of the particles,
- coagulation and break-up which modify the size of the particles.

It leads to a Vlasov–Fokker–Planck equation, which furthermore involves a non linear "collision" operator describing the size variations. The fluid quantities obey Euler or Navier-Stokes equations, depending on the physical context. We refer to [176] for introduction to such coupled models in combustion theory ; recent developments can be found in [12, 128]. Investigating existence, uniqueness and regularity issues highly depends on the nature of the coupling and the complexity of the equations used for describing the fluid. We refer for instance to [15] (strong solutions locally in time), [98, 23, 132] (weak solution for viscous flows), [94] (solutions close to equilibrium). Asymptotic analysis is detailed in [89, 88, 133, 36]. Numerical aspects are devised in [6, 37, 154, 153, 125, 90, 93]. Most of these references do not address the question of the influence of the size variations. This is the aim of the present work : we discuss several aspects of the role of a Smoluchowski operator in the stability and dissipation properties of the system, and we study hydrodynamic regimes.

5.2 A fluid-particle model with coagulation and break-up

Here and below, we adopt a discrete modeling of the size variable. Let $i \in \mathbb{N} \setminus \{0\}$. We refer to "a particle of size i" as to be a assembly of i monomers. Therefore, denoting by $a > 0$ the radius of a monomer and ρ_P its mass density

- the volume of a $i-$mer is $\frac{4}{3}\pi a^3 i$,
- the radius is $r_i = a i^{1/3}$,
- the mass is $m_i = \frac{4}{3}\pi a^3 i \rho_P$.

Let $f_i(t,x,v)$ stand for the density of i-mers in phase space : $f_i(t,x,v)\ \mathrm{d}v\ \mathrm{d}x$ represents the number of particles with size i having at time $t \geq 0$ their position and velocity in the infinitesimal domain centered at (x,v) with volume $\mathrm{d}x\ \mathrm{d}v$. Particles are subject to a drag force, which is proportional to the relative velocity with the fluid. The Stokes law defines the proportionality factor as $6\pi\mu a i^{1/3} = 6\pi\mu r_i$, with μ the dynamic viscosity of the fluid. Brownian motion produces velocity fluctuation, described by a diffusion operator with coefficient (Einstein formula)

$$\frac{k\theta 6\pi\mu a i^{1/3}}{(\frac{4}{3}\pi a^3 i\rho_P)^2} = \frac{k\theta}{m_i}\frac{9\mu}{2\rho_P r_i^2},$$

where k is the Boltzmann constant and $\theta > 0$ the temperature of the fluid. Therefore, f_i satisfies the following equation

$$\partial_t f_i + v\cdot\nabla_x f_i - \nabla_x\Phi\cdot\nabla_v f_i = \frac{9\mu}{2\rho_P r_i^2}\nabla_v\cdot\left((v-u)f_i + \frac{k\theta}{m_i}\nabla_v f_i\right) + \frac{1}{\tau_c}Q_i(f). \tag{5.1}$$

In the right hand side the so–called Smoluchowski operator Q describes coagulation and break-up and τ_c is the characteristic time scale of the coagulation and break-up phenomena. The operator

is defined by

$$Q_i(f) = \frac{1}{2}\sum_{j=1}^{i-1} \kappa_{j,i-j} f_j f_{i-j} - \sum_{j=1}^{\infty} \kappa_{i,j} f_i f_j + \sum_{j=i+1}^{\infty} \beta_{j-i,i} f_j - \frac{1}{2}\sum_{j=1}^{i-1} \beta_{j,i-j} f_i$$

according to the formation of $(i+j)-$mers from i-mers and $j-$mers

$$X_i + X_j \to X_{i+j}$$

which occurs with a rate $\kappa_{i,j}$ and the break-up of $i-$mers into smaller pieces with, assuming $j < i$, size j and $i-j$:

$$X_i \to X_{i-j} + X_j.$$

As a specific case, the Becker-Döring operator restricts to the case where, for $i \geq 2$, the coefficients vanish but for $j = 1$: only monomers can be added to or removed from $i-$ mers. Monomers are involved in all reactions so that the collision term Q_1 has a different expression. More precisely, the Becker-Döring [16] cast as follows

$$\begin{aligned} &J_i(f) = k_i f_i f_1 - q_{i+1} f_{i+1}, \\ &Q_i(f) = J_{i-1} - J_i \qquad \text{for } i \geq 2, \\ &Q_1(f) = -2J_1 - \sum_{i=2}^{\infty} J_i \end{aligned}$$

In this expression, k_i is the rate of the coagulation reaction $X_i + X_1 \to X_{i+1}$ and q_{i+1} is the rate of the break-up $X_{i+1} \to X_i + X_1$. For a thorough presentation of the Smoluchowski and Becker-Döring operators, we refer to [45, 151]. The effect of coagulation and break-up is to reduce the total number of particles but to maintain the total mass since

$$\sum_{i=1}^{\infty} Q_i(f) \leq 0, \qquad \sum_{i=1}^{\infty} i Q_i(f) = 0. \tag{5.2}$$

As a consequence of (5.2), we obtain the following local mass conservation law

$$\begin{aligned} \partial_t\Big(\sum_{i=1}^{\infty} i f_i\Big) + v\cdot\nabla_x\Big(\sum_{i=1}^{\infty} i f_i\Big) - \nabla_x\Phi\cdot\nabla_v\Big(\sum_{i=1}^{\infty} i f_i\Big) \\ = \sum_{i=1}^{\infty} \frac{9\mu}{2\rho_P r_i^2}\nabla_v\cdot\Big((v-u) i f_i + \frac{k\theta}{m_i}\nabla_v i f_i\Big). \end{aligned}$$

Note that

$$\tau_i = \frac{m_i}{6\pi\mu r_i} = \frac{2\rho_P r_i^2}{9\mu} = i^{2/3}\ \tau_1$$

has the homogeneity of a time : this is the Stokes setting time, typical of the effect of the drag force on the $i-$particle.

The fluid is described by its density $n(t,x)$ and velocity $u(t,x)$ which obey

$$\begin{aligned} &\partial_t n + \nabla_x\cdot(n\,u) = 0 \\ &\rho_F\partial_t(n\,u) + \rho_F \mathrm{Div}_x(n\,u\otimes u) + \rho_F\alpha n\nabla_x\Phi + \nabla_x p - \mu\Delta_x u = 6\pi\mu\sum_{i=1}^{\infty}\int_{\mathbb{R}^3}(v-u) f_i r_i\,\mathrm{d}v, \end{aligned} \tag{5.3}$$

where ρ_F is a typical mass density for the fluid. The coefficient $\alpha \in \mathbb{R}$ takes into account the fact that external force can act differently on the two phases, both in amplitude and direction. The momentum equation takes into account the drag force exerted on the fluid, at a given position x, by the particles. For the pressure, various options can be considered :

- *incompressible model* in which case p is the Lagrange multiplier associated to the divergence-free constraint $\nabla_x \cdot u = 0$
- *compressible model* which needs an equation of state. We can restrict our discussion to situations where the temperature is assumed to remain constant, at least as seen from the particles. We disregard the energy equation and assume in such a case a simple relation $p = p(n)$, the isothermal case corresponding to $p(n) = n$. More complete models incorporate energy exchanges, as discussed in [22, 90]. We set $p = R\rho\theta$, with R the perfect gas constant, and $E = \frac{u^2}{2} + \frac{R\theta}{\gamma-1}$, the total energy, with $\gamma > 1$ the adiabatic constant. Then, we have

$$\rho_P\big(\partial_t(nE) + \nabla_x \cdot ((nE+p)u) + \alpha n u \cdot \nabla_x \Phi\big) = \sum_{i=1}^{\infty} \int_{\mathbb{R}^3} r_i \frac{v^2}{2} \nabla_v \cdot \big((v-u)f_i + \nabla_v f_i\big)\,\mathrm{d}v \quad (5.4)$$

Note that it can make sense, according to scaling considerations, to neglect the viscous term in (5.3). The following observation is also worthwhile. The right hand side of (5.3) can be recast as

$$\begin{aligned}
&\sum_{i=1}^{\infty} m_i \times \frac{9\mu}{2\rho_P r_i^2} \int_{\mathbb{R}^3} v\nabla_v \cdot \left((v-u)f_i + \frac{k\theta}{m_i}\nabla_v f_i\right)\mathrm{d}v \\
&\qquad = \sum_{i=1}^{\infty} m_i \times \left(\frac{9\mu}{2\rho_P r_i^2} \int_{\mathbb{R}^3} v\nabla_v \cdot \left((v-u)f_i + \frac{k\theta}{m_i}\nabla_v f_i\right)\mathrm{d}v + \int_{\mathbb{R}^3} Q_i(f)\,\mathrm{d}v\right)
\end{aligned}$$

owing to (5.2). A similar remark applies to the energy equation (5.4).

5.3 Dimensionless equations

Following [36], we write the equations in dimensionless form. To this end, we need time and length scales L and T respectively, which defines the velocity unit $U = L/T$. Velocity fluctuations are measured by means of the thermal velocity

$$V_{th} = \sqrt{\frac{k\bar{\theta}}{m_1}}$$

with $m_1 = \frac{4}{3}\pi a^3 \rho_P$, and $\bar{\theta} > 0$ a reference temperature. Denoting $\cdot'$ dimensionless quantities, we set

- $t = Tt'\,;\ x = Lx'\,;\ v = V_{th}v'$
- $n(Tt', Lx') = n'(t', x')\,;\ u(Tt', Lx') = Uu'(t', x')$
- $p(Tt', Lx') = \mathcal{P}p'(t', x')\,;\ f_i'(t', x', v') = \dfrac{4}{3}\pi a^3\ V_{th}^3\ f_i(Tt', Lx', V_{th}v')$,

where $\mathcal{P}$ stands for a suitable pressure unit. If the temperature is not assumed constant, we set similarly $\theta(Tt', Lx') = \bar{\theta}\theta'(t', x')$. For the external potential, we set

$$\Phi(Lx') = \frac{\vartheta_s L}{\tau_1}\Phi'(x')$$

where ϑ_s has the homogeneity of a velocity (for gravity driven flows, it is nothing but the Stokes settling velocity). We arrive at

$$\begin{aligned}\frac{1}{T}\partial_{t'}(f_i') + \frac{V_{th}}{L}v'\cdot\nabla_{x'}(f_i') - \frac{\vartheta_s}{\tau_1 V_{th}}\nabla_{x'}\Phi'\cdot\nabla_{v'}(f_i)\\ = \frac{1}{\tau_i}\nabla_{v'}\cdot\left((v'-\frac{U}{V_th}u')f_i' + \frac{k\theta}{m_i V_{th}^2}\nabla_{v'}f_i'\right) + \frac{1}{\tau_c}Q_i'(f'),\end{aligned}$$

with $Q_i'(f') = Q_i\big(\frac{f}{\frac{4}{3}\pi a^3 V_{th}^3}\big)$. This is coupled to

$$\begin{aligned}&\frac{1}{T}\partial_{t'}n' + \frac{U}{L}\nabla_{x'}\cdot(n'u') = 0,\\ &\frac{U}{T}\partial_{t'}(n'u') + \frac{U^2}{L}\mathrm{Div}_{x'}(n'u'\otimes u') + \alpha\frac{\vartheta_s}{\tau_1}n'\nabla_{x'}\Phi' + \frac{\mathcal{P}}{L\rho_F}\nabla_{x'}p'\\ &\qquad = \frac{\rho_P}{\tau_1\rho_F}\sum_{i=1}^{\infty}\int_{\mathbb{R}^3}(V_{th}v'-Uu')f_i'i^{1/3}\,\mathrm{d}v' + \frac{\mu U}{\rho_F L^2}\Delta_{x'}u'.\end{aligned}$$

(A similar work can be done considering the energy equation if necessary.) The system is governed by the following set of dimensionless parameters

$$\begin{cases}\beta = \dfrac{T}{L}V_{th} = \dfrac{V_{th}}{U}, & \dfrac{1}{\varepsilon} = \dfrac{T}{\tau_1},\\[2ex] \eta = \dfrac{\vartheta_s T}{V_{th}\tau_1}, & \chi = \dfrac{\mathcal{P}T}{\rho_F LU} = \dfrac{\mathcal{P}}{\rho_F U^2},\end{cases}$$

together with the density ratio ρ_P/ρ_F. Finally, we obtain (dropping the fancy symbols)

$$\begin{cases}\partial_t f_i + \beta v\cdot\nabla_x f_i - \eta\nabla_x\Phi\cdot\nabla_v f_i = \dfrac{1}{\varepsilon}\dfrac{1}{i^{2/3}}\nabla_v\cdot\left((v-\dfrac{1}{\beta}u)f_i + \dfrac{\theta}{i}\nabla_v f_i\right) + \dfrac{1}{\tau_c}Q_i(f),\\ \partial_t n + \nabla_x\cdot(n\,u) = 0,\\ \partial_t(n\,u) + \mathrm{Div}_x(n\,u\otimes u) + \alpha\beta\eta\, n\nabla_x\Phi + \chi\nabla_x p = \dfrac{\rho_P}{\varepsilon\rho_F}\displaystyle\sum_{i=1}^{\infty}\int_{\mathbb{R}^3}(\beta v-u)f_i i^{1/3}\,\mathrm{d}v + \mu\Delta_x u.\end{cases}\tag{5.5}$$

Here, μ and τ_c stand for the rescaled and dimensionless version of the fluid viscosity and coagulation relaxation (that are, with the notation in physical units, $\frac{\mu U}{\rho_F L^2}$ and $\frac{T}{\tau_c}$, respectively).

Note that in many applications it is relevant to get rid of the diffusion term in the momentum equation (5.5) because the rescaled viscosity μ is very small, hence dealing with the Euler equations instead of the Navier-Stokes system. In what follows the problem is considered on a domain Ω where

- either $\Omega = \mathbb{R}^3$, in which case the analysis will rely on suitable confining assumption on the potential Φ,
- or Ω is a smooth bounded subset in $\mathbb{R}^3$. In such a case the problem is completed by boundary conditions, for instance specular reflection for the particles and the no-slip condition $u_{|\partial\Omega} = 0$ for the fluid (or $u\cdot\nu = 0$ on $\partial\Omega$, with $\nu(x)$ the unit outward normal at $x\in\partial\Omega$ when working with the Euler equations). More intricate boundary conditions for the particles can be dealt with, see [36].

The initial condition are denoted as follows

$$f_i(t=0,x,v) = f_{\text{init},i}(x,v), \qquad n(t=0,x) = n_{\text{init}}(x), \qquad u(t=0,x) = u_{\text{init}}(x).$$

For further purposes, let us set

$$M_P = \sum_{i=1}^{\infty} \int_\Omega \int_{\mathbb{R}^3} i f_i \,\mathrm{d}v \,\mathrm{d}x, \qquad M_F = \int_\Omega n \,\mathrm{d}x$$

which are thus conserved quantities.

5.4 Equilibria, dissipation and relative entropies

In this section we wish to exhibit some conservation and dissipation properties satisfied by the model. These dissipation properties will induce the existence of equilibrium solutions and their stability, they also provide the basic estimates needed for the analysis of the system.

5.4.1 Detailed balance equilibria ; dissipation properties of the coagulation/break-up operator

First of all, we are interested in sequences $\{\mathscr{M}_1, \mathscr{M}_2, ...\}$ which make the coagulation/break-up operator vanish. The condition $Q_i(\mathscr{M}) = 0$ is equivalent to impose

$$\kappa_{i,j}\mathscr{M}_i\mathscr{M}_j = \beta_{i,j}\mathscr{M}_{i+j} \qquad \text{for any } i,j \geq 1. \tag{5.6}$$

A solution of (5.6), if it exists, is referred to as a "detailed balance equilibrium". Given a detailed balance equilibrium, we set

$$\mathscr{L}(f) = \sum_{i=1}^{\infty} f_i\Big(\ln\Big(\frac{f_i}{\mathscr{M}_i}\Big) - 1\Big). \tag{5.7}$$

When dealing with the free coagulation-break up problem (e. g. without coupling inducing space dependence of the solution) $\mathscr{L}$ plays the role of a Lyapounov functional for the underlying infinite system of ODEs. We refer to [9, 32, 33, 45, 105, 118, 167] for thorough details on the role of the detailed balance assumption and the functional (5.7) in the analysis of coagulation-fragmentation phenomena and of the large time behavior of the solutions.

Using (5.6) with $j = 1$ leads to a recursion formula for defining the equilibria. In turn, detailed balance equilibria can be parametrized by the monomers concentration $\mathscr{M}_1$ as follows :

$$\mathscr{M}_i = \mathscr{Q}_i \ (\mathscr{M}_1)^i,$$

where

$$\mathscr{Q}_1 = 1, \qquad \mathscr{Q}_i = \prod_{j=1}^{i-1} \frac{\kappa_{j,1}}{\beta_{j,1}} \text{ for } i > 1.$$

In the sequel, we assume the existence of detailed balance equilibria. In order to define equilibria with finite mass, it is natural to further request

$$\text{the radius of convergence } Z_\star \text{ of the series } z \mapsto \sum_{i=1}^{\infty} i\mathscr{Q}_i z^i \text{ is } > 0.$$

Note that $Z_\star$ may be finite or not, which strongly influences the large time asymptotics, see [9, 32, 33, 45, 105, 118, 167]. The saturation density is defined by

$$\varrho_\star = \sum_{i=1}^{\infty} i\mathscr{Q}_i Z_\star^i \in (0,\infty].$$

Observe that, given $0 < \rho < \varrho_\star$, there exists a unique detailed balance equilibrium, characterized by $0 < \mathscr{M}_1 < Z_\star$ and the relation

$$\sum_{i=1}^{\infty} i\mathscr{Q}_i \mathscr{M}_1^i = \rho.$$

Finally, the key observation which makes (5.7) a relevant functional for studying the coagulation/break-up dynamics, is simply that

$$\sum_{i=1}^{\infty} Q_i(f) \ln\Big(\frac{f_i}{\mathscr{M}_i}\Big) \le 0,$$

and this entropy dissipation term vanishes iff $f_i = \mathscr{M}_i$.

5.4.2 Detailed balance and stationary solutions

Let us now adapt the discussion to concentrations depending on the phase space variables (x, v). We search for stationary solutions $n_S(x)$, $u_S = 0$, $\tilde{\mathscr{M}}_i(x,v)$ of (5.5) where all terms are turned off. Making the coagulation/break-up term vanish still leads to (5.6), while we have additionally

$$v \cdot \nabla_x \tilde{\mathscr{M}}_i - \nabla_x \Phi \cdot \nabla_v \tilde{\mathscr{M}}_i = 0$$

and

$$\nabla_v \cdot \Big(v\tilde{\mathscr{M}}_i + \frac{\theta}{i}\nabla_v \tilde{\mathscr{M}}_i\Big) = \nabla_v \cdot \Big(\exp(-iv^2/2\theta).\nabla_v\Big(\frac{\tilde{\mathscr{M}}_i}{\exp(-iv^2/2\theta)}\Big)\Big).$$

We thus arrive at

$$\tilde{\mathscr{M}}_i(x,v) = \mathscr{Q}_i \ \big(\tilde{\mathscr{M}}_1(x,v)\big)^i, \qquad \tilde{\mathscr{M}}_1(x,v) = \omega \exp\Big(-\frac{v^2}{2\theta} - \frac{\Phi(x)}{\theta}\Big). \tag{5.8}$$

It can be convenient to rewrite

$$\tilde{\mathscr{M}}_i(x,v) = \mathscr{M}_i \ \exp\Big(-i\frac{v^2}{2\theta} - i\frac{\Phi(x)}{\theta}\Big)$$

where $\mathscr{M}_i = \mathscr{Q}_i \omega^i$ is an equilibrium for the homogeneous equation.

In order to guaranty the finiteness of the mass and energy of the equilibrium, we need to assume the following confinement conditions

(HC0) The potential Φ is bounded from below on Ω : there exists $C \in \mathbb{R}$ such that $\Phi(x) \ge C$ hold for a. e. $x \in \Omega$.

(HC1) $x \mapsto e^{-\Phi(x)} \in L^1(\Omega)$.

(HC2) $x \mapsto \Phi(x)e^{-\Phi(x)} \in L^1(\Omega)$.

The total mass of such an equilibrium is now defined as

$$\sum_{i=1}^{\infty}\int_{\Omega}\int_{\mathbb{R}^3} i\tilde{\mathscr{M}}_i(x,v)\,\mathrm{d}v\,\mathrm{d}x = (2\pi\theta)^{3/2}\ \sum_{i=1}^{\infty}\frac{\mathscr{Q}_i\Gamma_i}{\sqrt{i}}\ \omega^i$$

where we denote from now on

$$\Gamma_i = \int_{\Omega} e^{-i\Phi(x)/\theta}\,\mathrm{d}x.$$

By **(HC0)** and **(HC1)**, the Γ_i's are finite. Therefore, we introduce $\omega_\star > 0$ as to be the radius of convergence of the series $\sum_{i=1}^{\infty}\frac{\mathscr{Q}_i\Gamma_i}{\sqrt{i}}\ z^i$ and we set

$$M_{P\star} = (2\pi\theta)^{3/2}\ \sum_{i=1}^{\infty}\frac{\mathscr{Q}_i\Gamma_i}{\sqrt{i}}\ \omega_\star^i \in (0,\infty].$$

Clearly, for any $0 \le M_P < M_{P\star}$, there exists a unique ω such that the equilibrium parametrized by ω has total mass M_P. Observe that, for a given set of kinetic coefficients, $\omega_\star \neq \rho_\star$ (for instance when the Γ_i's are bounded, we have $\omega_\star \ge \rho_\star$). Similarly, the total energy of an equilibrium is defined as the sum of the kinetic and potential energies, that is

$$\sum_{i=1}^{\infty}\int_{\Omega}\int_{\mathbb{R}^3} i\,\Big(\frac{v^2}{2\theta}+\frac{\Phi(x)}{\theta}\Big)\tilde{\mathscr{M}}_i\,\mathrm{d}v\,\mathrm{d}x = \frac{(2\pi)^{3/2}}{2}\theta^{5/2}\ \sum_{i=1}^{\infty}\frac{\mathscr{Q}_i\tilde{\Gamma}_i}{i^{3/2}}\omega^i$$

with $\tilde{\Gamma}_i = \int_\Omega i\Phi(x)e^{-i\Phi(x)}\,\mathrm{d}x$.

We turn briefly to the stationary solution n_S, recalling the material from [36]. For the sake of concreteness, we detail the computations for a compressible model, assuming that the pressure is define by a simple law $p : n \mapsto p(n)$. The function p is required to satisfy :

(HP1) $p : \mathbb{R}_+ \to \mathbb{R}_+$ is continuous, of class C^2 on $]0,\infty[$, it is increasing and verifies $p(0) = 0$.

(HP2) We set $h(n) := \displaystyle\int_1^n \frac{p'(s)}{s}\,\mathrm{d}s$ (enthalpy function) for $n \in]0,\infty[$. Then, we assume $h \in L^1_{\mathrm{loc}}(]0,\infty[)$.

Owing to **(HP1)**-**(HP2)**, it makes sense to introduce

$$\Pi : n \in [0,\infty[\longmapsto \int_0^n h(s)\,\mathrm{d}s \in \mathbb{R}$$

which can be interpreted as an internal energy. We have $\Pi'(n) = h(n)$ and $n\Pi''(n) = p'(n)$ for any $n \in \mathbb{R}_+$, while $\Pi(0) = \Pi'(1) = 0$. For instance, in the isothermal case, $p(n) = n$ and $\Pi(n) = n\ln(n) - n$, and in the isentropic case $p(n) = n^\gamma$ for some $\gamma > 1$, and $\Pi(n) = \frac{n^\gamma - \gamma n)}{\gamma - 1}$.

At equilibrium, the fluid equation degenerates to

$$\Pi'(n_s(x)) = h(n_S(x)) = Z - \frac{\alpha\beta\eta}{\chi}\Phi(x)$$

where Z is a normalizing constant. Let us introduce the generalized inverse of h

$$\sigma : \mathbb{R} \to [0,\infty], \quad \sigma(s) = \begin{cases} 0 & \text{for} \quad s \le h(0+), \\ h^{-1}(s) & \text{for} \quad h(0+) < s < h(\infty), \\ \infty & \text{for} \quad h(\infty) \le s. \end{cases}$$

and set

$$n_S(x) = \sigma\Big(Z - \frac{\alpha\beta\eta}{\chi}\Phi(x)\Big).$$

The constant Z is defined by the following mass condition

$$M_F = \int_\Omega n_{\text{init}}\,\mathrm{d}x = \int_\Omega n_S\,\mathrm{d}x.$$

Again, the definition makes sense provided some requirements on the potential and the pressure law are fulfilled :

(HC3) $\Phi \in \mathrm{W}^{1,1}(\Omega)$ if Ω is bounded, or $\Phi \in \mathrm{W}^{1,1}_{\text{loc}}(\Omega)$ otherwise.

(HC4) $\alpha\Phi$ is bounded from below on Ω : there exists $C \in \mathbb{R}$ such that $\alpha\Phi(x) \geq C$ a.e. $x \in \Omega$.

(HC5) $\alpha\Phi$ is coercive on Ω : for any $A \in \mathbb{R}$ the set $\{x \in \Omega | \alpha\Phi(x) \leq A\}$ is bounded.

(HC6) Consider the family of functions

$$n_Z(x) = \sigma\left(Z - \frac{\alpha\beta\eta}{\chi}\Phi(x)\right),$$

parametrized by $Z \in \mathbb{R}$. We suppose the existence of some $Z \in \mathbb{R}$ such that $n_Z \in L^1_+(\Omega)$. Hence, we define $\zeta_\star = \sup\{Z \in \mathbb{R} | n_Z \in L^1(\Omega)\}$.

(HC7) For $Z \in (-\infty, \zeta_\star)$, we denote $TM(Z) = \int_\Omega n_Z(x)\,\mathrm{d}x$. Clearly $Z \mapsto TM(Z)$ is strictly increasing. We denote $M_{F\star} = \lim_{Z\to\zeta_\star} TM(Z)$. Hence, for any $\mathcal{M}_F \in (0, M_{F\star})$, there exists a unique normalization constant Z_{M_F} such that the associated equilibrium n_S is well defined and has mass M_{F}.

(HC8) To a non negative integrable function n we associate the quantity, that belongs to $\mathbb{R} \cup \{\infty\}$,

$$E_F(n) = \begin{cases} \displaystyle\int_\Omega \left(\frac{\alpha\beta\eta}{\chi} n\Phi + \Pi^+(n)\right)\mathrm{d}x - \int_\Omega \Pi^-(n)\,\mathrm{d}x & \text{if } \Pi^-(n) \in L^1(\Omega) \\ \infty & \text{otherwise.} \end{cases} . \tag{5.9}$$

The equilibrium n_S is required to have finite free energy. Thus, we further assume : $E_F(n_Z) < \infty$ and $\Pi^-(n_Z) \in L^1(\Omega)$ for any $Z \in (-\infty, \zeta_\star)$.

Remark 1. *In order to clarify this set of assumption, let us discuss relevant examples :*

- *If $h(0^+) > -\infty$ and $h(\infty) = \infty$, which is the case if $p(n) = n^\gamma$, $\gamma > 1$, then hypotheses* **(HC5)**-**(HC7)** *are trivially satisfied with $M_{F\star} = \infty$. Note also that for $p(n) = n^\gamma$, we have*

$$\sigma(s) = \Big(\Big[\frac{\gamma-1}{\gamma}s + 1\Big]^+\Big)^{1/(\gamma-1)}.$$

- *If $h(0^+) = -\infty$ and $h(\infty) = \infty$, which is the case if $p(n) = n$, then $M_{F\star} = \infty$. When $p(n) = n$, hypotheses* **(HC5)**-**(HC7)** *are equivalent to hypotheses* **(HC1)**-**(HC2)** *and $\sigma(s) = e^s$.*
- *When Ω is bounded and Φ is bounded the conditions* **(HC3)**-**(HC7)** *are trivially satisfied.*

The equilibrium n_S can be interpreted has a minimizer of the functional E_F, under the constraint of prescribed mass. In this direction, the following result is proven in [38, Proposition 5, Lemma 6] :

Proposition 5.4.1. *Assuming the conditions* **(HP1)**-**(HP2)** *on the pressure and the conditions* **(HC0)**-**(HC8)** *on the potential, then the functional $E_F(n)$ has a unique minimizer given by*

$$n_S(x) = \sigma\left(Z_{M_F} - \frac{\alpha\beta\eta}{\chi}\Phi(x)\right), \tag{5.10}$$

in the set of non negative integrable functions with total fluid mass M_F. Moreover :

$$E_F(n) - E_F(n_S) \geq \int_\Omega \left[\Pi(n) - \Pi(n_S) - \Pi'(n_S)\,(n - n_S)\right](x)\,\mathrm{d}x \tag{5.11}$$

with equality if and only if

$$\frac{\alpha\beta\eta}{\chi}\Phi(x) + h(n_S(x)) = Z_{M_F}, \quad \textit{for almost all } x \in \Omega.$$

5.4.3 Dissipation and stability properties of the fluid–particles system

We are now in position to derive the crucial dissipation estimate satisfied by the system (5.5). We restrict to the case where (5.5) is closed by the pressure law $p = p(n)$, the temperature $\theta > 0$ in the Fokker–Planck term being fixed ; we assume without loss of generality that the units are such that $\theta = 1$.

Theorem 5.4.2. *We assume that the conditions* **(HP1)**-**(HP2)** *on the pressure and the conditions* **(HC0)**-**(HC8)** *are fulfilled. We suppose that*

$$\frac{\rho_P}{\rho_F} = \frac{1}{\beta^2}, \quad \eta = \beta, \tag{5.12}$$

holds. Let $\mathscr{M}_i$ be a detailed balance equilibrium of the coagulation/break up operator. We define the following free energy functionals, associated respectively to the particles and to the fluid

$$\begin{aligned}
\mathcal{F}_P(f) &= \sum_{i=1}^{\infty}\int_\Omega\int_{\mathbb{R}^3}\left(f_i\Big(\ln\Big(\frac{f_i}{\mathscr{M}_i}\Big) - 1\Big) + i\frac{v^2}{2}f_i + i\Phi\, f_i\right)\mathrm{d}v\,\mathrm{d}x,\\
\mathcal{F}_F(n,u) &= \int_\Omega\left(n\frac{|u|^2}{2} + \chi\Pi(n) + \alpha\beta\eta\, n\Phi\right)\mathrm{d}x.
\end{aligned}$$

Then, the total free energy $\mathcal{F}(f,n,u) = \mathcal{F}_P(f) + \mathcal{F}_F(n,u)$ is dissipated : solutions of (5.5) satisfy

$$\begin{aligned}
&\frac{\mathrm{d}}{\mathrm{d}t}\mathcal{F}(f,n,u) + \mu\int_\Omega |\nabla_x u|^2\,\mathrm{d}x + \frac{1}{\varepsilon}\sum_{i=1}^{\infty}\int_\Omega\int_{\mathbb{R}^3}\left|(v - \frac{1}{\beta}u)\sqrt{i^{1/3}f_i} + \frac{1}{i^{5/6}}\frac{\nabla_v f_i}{\sqrt{f_i}}\right|^2\mathrm{d}v\,\mathrm{d}x\\
&\qquad = \frac{1}{\tau_c}\sum_{i=1}^{\infty}\int_\Omega\int_{\mathbb{R}^3} Q_i(f)\ln\Big(\frac{f_i}{\mathscr{M}_i}\Big)\,\mathrm{d}v\,\mathrm{d}x \leq 0.
\end{aligned} \tag{5.13}$$

Remark that $\mathcal{F}_F$ can be rewritten by means of the functional E_F

$$\mathcal{F}_F(n(t),u(t)) = \int_\Omega n\frac{|u|^2}{2}\,\mathrm{d}x + \chi\left(E_{\mathrm{F}}(n) - E_F(n_S)\right) + \chi E_F(n_S).$$

However, we notice that the right-hand side of (5.11) is positive and equal to zero iff $n = n_S$, so that we can set

$$RE_F((n,u)|(n_S,u_S)) = \int_\Omega n\frac{|u|^2}{2}\,\mathrm{d}x + \chi\left(E_F(n) - E_F(n_S)\right)$$

and consider it as a relative entropy, that is a functional that controls the distance from the pair $(n(t), u(t))$ to the equilibrium solution $(n_S, u_S = 0)$. Similarly, when the total mass M_P is subcritical the free energy $\mathcal{F}_P$ can be interpreted as a relative entropy with respect to the equilibrium having the same mass. In turn, we can establish a non linear stability statement.

Corollary 5.4.3. *We assume that* $0 < M_P \leq M_{P\star}$ *and we denote*

$$\tilde{\mathscr{M}}_i(x,v) = \omega^i \mathscr{Q}_i \exp\Big(- i\frac{v^2}{21} - i\Phi(x)\Big)$$

the equilibrium with total mass M_P*. Therefore, we set*

$$RE_P(f|\tilde{\mathscr{M}}) = \sum_{i=1}^{\infty} \int_\Omega \int_{\mathbb{R}^3} \Big(f_i \ln\Big(\frac{f_i}{\tilde{\mathscr{M}}_i}\Big) - f_i + \tilde{\mathscr{M}}_i\Big)\,\mathrm{d}v\,\mathrm{d}x = \mathcal{F}_P(f) + (2\pi)^{3/2} \sum_{i=1}^{\infty} \frac{\Gamma_i \mathscr{Q}_i}{i^{3/2}} \omega^i.$$

Let n_S *be the equilibrium state defined by* (5.10) *with mass* M_F*. Then, for any* $\delta > 0$*, there exits* $\kappa > 0$ *such that if initially*

$$RE_P(f_{\rm init}|\tilde{\mathscr{M}}) + RE_F((n_{\rm init}, u_{\rm init})|(n_S, 0)) \leq \kappa$$

holds, then, for any $t \geq 0$*, the solution satisfies*

$$\sum_{i=1}^{\infty} \int_\Omega \int_{\mathbb{R}^3} |f_i(t,x,v) - \tilde{\mathscr{M}}_i(x,v)|\,\mathrm{d}v\,\mathrm{d}x \leq \delta, \quad \int_\Omega |n(t,x) - n_S(x)|\,\mathrm{d}x \leq \delta, \quad \int_\Omega n\frac{|u|^2}{2}\,\mathrm{d}x \leq \delta.$$

Corollary 5.4.3 follows exactly as in [36], once the entropy dissipation has been established ; the crucial step is the identification of the relative entropies RE_P and RE_F, which are the appropriate tool to evaluate how far the solution is from the equilibrium. These arguments go back to [27, 61, 162] to which we refer for further details.

Remark 2. *Similar conclusions hold for incompressible models or models including the energy equation. We restrict the discussion to the free space problem, but it applies to problems set on a domain with suitable boundary conditions, say no-slip boundary condition for the velocity u, and specular reflection of the particles. More intricate reflection operator can be considered as well, see [36].*

Remark 3. *The condition* (5.12) *might look a bit arbitrary and artificial; it is adopted for notational convenience only in order not to keep track of complicated coefficients in the energy balance.*

Proof of Theorem 5.4.2. Let us start by computing

$$\begin{aligned}
\frac{\mathrm{d}}{\mathrm{d}t} \sum_{i=1}^{\infty} \int_\Omega \int_{\mathbb{R}^3} \Big(f_i \Big(\ln\Big(\frac{f_i}{\mathscr{M}_i}\Big) - 1\Big) + i\frac{v^2}{2} f_i \Big)\,\mathrm{d}v\,\mathrm{d}x \\
= -\frac{1}{\varepsilon} \sum_{i=1}^{\infty} \int_\Omega \int_{\mathbb{R}^3} \Big((v - \frac{1}{\beta}u) f_i + \frac{1}{i}\nabla_v f_i \Big) \cdot \Big(\frac{1}{i^{2/3}} \frac{\nabla_v f_i}{f_i} + i^{1/3} v \Big)\,\mathrm{d}v\,\mathrm{d}x \\
+ \frac{1}{\tau_c} \int_\Omega \int_{\mathbb{R}^3} \sum_{i=1}^{\infty} \ln\Big(\frac{f_i}{\mathscr{M}_i}\Big) Q(f_i)\,\mathrm{d}v\,\mathrm{d}x - \eta \sum_{i=1}^{\infty} \int_\Omega \int_{\mathbb{R}^3} i\nabla_x \Phi \cdot v f_i\,\mathrm{d}v\,\mathrm{d}x.
\end{aligned}$$

Next the potential energy of the particles satisfies

$$\frac{\mathrm{d}}{\mathrm{d}t}\sum_{i=1}^{\infty}\int_{\Omega}\int_{\mathbb{R}^3} i\Phi f_i\,\mathrm{d}v\,\mathrm{d}x = \beta\sum_{i=1}^{\infty}\int_{\Omega}\int_{\mathbb{R}^3} i\nabla_x\Phi\cdot\, v f_i\,\mathrm{d}v\,\mathrm{d}x.$$

We turn to the kinetic energy of the fluid and we obtain

$$\begin{aligned}\frac{\mathrm{d}}{\mathrm{d}t}\int_{\mathbb{R}^3} n\frac{u^2}{2}\,\mathrm{d}x &= \frac{1}{\varepsilon}\frac{\rho_P}{\rho_F}\sum_{i=1}^{\infty}\int_{\Omega}\int_{\mathbb{R}^3}(\beta v-u)f_i i^{1/3}\cdot u\,\mathrm{d}v\,\mathrm{d}x-\chi\int_{\mathbb{R}^3} u\cdot p'(n)\nabla_x n\,\mathrm{d}x\\ &\quad -\alpha\,\eta\,\beta\int_{\mathbb{R}^3} n\,u\cdot\nabla_x\Phi\,\mathrm{d}x-\mu\int_{\Omega}|\nabla_x u|^2\,\mathrm{d}x.\end{aligned}$$

The evolution of entropy associated to the fluid is driven by

$$\begin{aligned}\frac{\mathrm{d}}{\mathrm{d}t}\int_{\mathbb{R}^3}\chi\Pi(n)\,\mathrm{d}x &= -\chi\int_{\mathbb{R}^3}\nabla_x\cdot(n\,u)\Pi'(n)\,\mathrm{d}x\\ &= \chi\int_{\mathbb{R}^3}\Pi''(n)\nabla_x n\cdot(n\,u)\,\mathrm{d}x=\int_{\Omega}p'(n)\nabla_x n\cdot u\,\mathrm{d}x.\end{aligned}$$

Finally, the potential energy for the fluid satisfies

$$\frac{\mathrm{d}}{\mathrm{d}t}\int_{\mathbb{R}^3} n\Phi\,\mathrm{d}x=\int_{\mathbb{R}^3} n\,u\cdot\nabla_x\Phi\,\mathrm{d}x.$$

We sum all these contributions, using (5.12) and the fact that $\int_{\mathbb{R}^3} u\cdot\nabla_v f_i\,\mathrm{d}v=0$ holds. We obtain

$$\begin{aligned}&\frac{\mathrm{d}}{\mathrm{d}t}\mathcal{F}(f,n,u)+\mu\int_{\Omega}|\nabla_x u|^2\,\mathrm{d}x\\ &\quad=-\frac{1}{\varepsilon}\sum_{i=1}^{\infty}\int_{\Omega}\int_{\mathbb{R}^3}\big(v-\frac{1}{\beta}u\big)^2 f_i i^{1/3}\,\mathrm{d}v\,\mathrm{d}x-\frac{2}{\varepsilon}\sum_{i=1}^{\infty}\int_{\Omega}\int_{\mathbb{R}^3}(v-\frac{1}{\beta}u)\frac{\nabla_v f_i}{i^{2/3}}\,\mathrm{d}v\,\mathrm{d}x\\ &\qquad-\frac{1}{\varepsilon}\sum_{i=1}^{\infty}\int_{\Omega}\int_{\mathbb{R}^3}\frac{1}{i^{5/3}}\frac{|\nabla_v f_i|^2}{f_i}\,\mathrm{d}v\,\mathrm{d}x+\frac{1}{\tau_c}\sum_{i=1}^{\infty}\int_{\Omega}\int_{\mathbb{R}^3}Q(f)\ln\Big(\frac{f_i}{\mathscr{M}_i}\Big)\,\mathrm{d}v\,\mathrm{d}x.\end{aligned}$$

The first three terms in the right hand side can be combined into

$$\sum_{i=1}^{\infty}\int_{\Omega}\int_{\mathbb{R}^3}\Big|(v-u/\beta)\sqrt{i^{1/3}f_i}+\frac{\nabla_v f_i}{\sqrt{i^{5/3}f_i}}\Big|^2\,\mathrm{d}v\,\mathrm{d}x.$$

This observation ends the proof. □

5.5 Hydrodynamic regimes

We are interested in regimes where $0<\varepsilon\ll 1$. As we shall see this regime leads to relaxation effects, which tend to prescribe how the particles concentration depends on the velocity variable v. In turn, we obtain models of purely hydrodynamic nature, where the unknowns depend only

on the time and space variables. Indeed, as ε go to 0, the concentrations f_i tend to make the Fokker–Planck operator vanish. Looking at the dissipation term in (5.13), we guess that

$$f_i(t,x,v) \simeq \frac{\rho_i(t,x)}{(2\pi/i)^{3/2}} \exp\Big(- i\frac{|v-u(t,x)/\beta|^2}{2}\Big) \quad \text{as } \varepsilon \to 0.$$

Then the behavior of the particulate flows can be described through the macroscopic concentration $\rho_i(t,x)$, the velocity $u(t,x)$ and the density $n(t,x)$. Identifying the limit system satisfied by these quantities is the object of the present section. Of course, the asymptotic analysis depends on the prescribed behavior with respect to ε of the other scaling parameters. According to [36], we identify two regimes of interest : the so–called flowing and bubbling regimes.

Before detailing the asymptotic analysis, let us set up a few notation and discuss remarkable estimates, which can be seen as a preliminary step towards a complete justification. We associate to $f_i(t,x,v)$ the following macroscopic quantities

$$\begin{aligned}
\rho_i(t,x) &= \int_{\mathbb{R}^3} f_i(t,x,v)\,\mathrm{d}v,\\
J_i(t,x) &= \beta i \int_{\mathbb{R}^3} v\ f_i(t,x,v)\,\mathrm{d}v,\\
\mathbb{P}_i(t,x) &= i\int_{\mathbb{R}^3} v\otimes v\ f_i(t,x,v)\,\mathrm{d}v.
\end{aligned}$$

Integrating with respect to v the PDE satisfied by f_i we obtain

$$i\partial_t\rho_i + \nabla_x\cdot J_i = \frac{1}{\tau_c}\int_{\mathbb{R}^3} iQ_i(f)\,\mathrm{d}v, \tag{5.14}$$

and

$$\frac{1}{\beta^2}\partial_t J_i + \mathrm{Div}_x\mathbb{P}_i + i\rho_i\nabla_x\Phi = -\frac{1}{\beta^2\varepsilon}\frac{1}{i^{2/3}}(J_i - i\rho_i u) + \frac{1}{\beta\tau_c}\int_{\mathbb{R}^3} ivQ_i(f)\,\mathrm{d}v. \tag{5.15}$$

As a matter of fact, we remark that the system (5.5) conserves the total momentum since we have

$$\partial_t\Big(nu + \frac{1}{\beta^2}\sum_{i=1}^{\infty} J_i\Big) + \mathrm{Div}_x\Big(nu\otimes u + \sum_{i=1}^{\infty}\mathbb{P}_i\Big) + \chi\nabla_x p + \Big(\alpha\beta\eta n + \sum_{i=1}^{\infty} i\rho_i\Big)\nabla_x\Phi = \mu\Delta_x u. \tag{5.16}$$

Let us start by deducing from Theorem 5.4.2 the following a priori estimate.

Proposition 5.5.1. *Assume that* (5.12) *holds and that the conditions* **(HP1)**-**(HP2)** *on the pressure and the conditions* **(HC0)**-**(HC8)** *on the potential are satisfied. Moreover, we assume*

(HC9) $(1+\Phi)\exp(-\frac{1}{2}\Phi(x)) \in \mathrm{L}^1(\Omega)$.

(HP3) *If* $h(0+) = -\infty$ *we assume there exists* $0 < s_1 < 1$ *such that*

$$\sup\left\{\frac{\Pi(n)}{nh(n)}, 0 < n < s_1\right\} < +\infty.$$

We consider an equilibrium $\mathscr{M}_i = \mathscr{Q}_i\omega^i$ *where* $0 < \omega < \omega_\star$ *is such that*

$$\sum_{i=1}^{\infty}\left(\int_\Omega\int_{\mathbb{R}^3}\Big(1 + i\frac{v^2}{2} + i\Phi(x)\Big)e^{-i(v^2/4+\Phi(x)/2)}\,\mathrm{d}v\,\mathrm{d}x\right)\mathscr{M}_i = K < \infty.$$

We suppose that the initial data $(f_{\mathrm{init},i}, n_{\mathrm{init}}, u_{\mathrm{init}})$ *satisfies* $f_{\mathrm{init},i} \geq 0$, $n_{\mathrm{init}} \geq 0$ *and that the quantities*

$$\sum_{i=1}^{\infty} \int_{\Omega}\int_{\mathbb{R}^3} f_{\mathrm{init},i}\Big(1+i+\Big|\ln\Big(\frac{f_{\mathrm{init},i}}{\mathscr{M}_i}\Big)\Big| + i\frac{v^2}{2} + i|\Phi(x)|\Big)\,\mathrm{d}v\,\mathrm{d}x$$

$$\int_{\Omega}\Big(n_{\mathrm{init}} + n_{\mathrm{init}}\frac{|u_{\mathrm{init}}|^2}{2} + |\Pi(n_{\mathrm{init}})| + n_{\mathrm{init}}\beta\eta|\alpha\Phi|\Big)\,\mathrm{d}x$$

are finite and bounded uniformly with respect to all the parameters $\varepsilon, \beta, \eta, \alpha, \rho_P/\rho_F$. *Then, we have :*

(i) The quantity

$$\sum_{i=1}^{\infty} \int_{\Omega}\int_{\mathbb{R}^3} f_i\Big(1+i+\Big|\ln\Big(\frac{f_i}{\mathscr{M}_i}\Big)\Big| + i\frac{v^2}{2} + i|\Phi(x)|\Big)\,\mathrm{d}v\,\mathrm{d}x$$

is bounded uniformly for $t \geq 0$,

(ii) n, $|\Pi(n)|$ *and* $\beta\eta|\alpha\Phi|n$ *are bounded in* $L^\infty(\mathbb{R}^+; L^1(\Omega))$.

(iii) $\sqrt{n}\,u$ *is bounded in* $L^\infty(\mathbb{R}^+; L^2(\Omega))$.

(iv) $\sqrt{\mu}\nabla_x u$ *is bounded in* $L^2(\mathbb{R}^+ \times \Omega)$,

(v) Denoting

$$D_i(t,x,v) = (v - \beta^{-1}u(t,x))\sqrt{i^{1/3}f_i(t,x,v)} + 2\nabla_v\sqrt{i^{-5/3}f_i(t,x,v)},$$

the quantity

$$\sum_{i=1}^{\infty}\int_0^{\infty}\int_{\Omega}\int_{\mathbb{R}^3}\Big|\frac{D_i}{\sqrt{\varepsilon}}\Big|^2\,\mathrm{d}v\,\mathrm{d}x\,\mathrm{d}t$$

is bounded.

In this statement "bounded" means "bounded uniformly with respect to all the parameters $\varepsilon, \beta, \eta, \alpha$, ρ_P/ρ_F*".*

The proof is a consequence of the dissipation estimate in Theorem 5.4.2, combined to the following elementary claim, which allows to control the negative part on $f\ln(f/\mathscr{M})$, see [36, 61]. (We apply this result with $X = \mathbb{N}\times\Omega\times\mathbb{R}^3$, endowed with the measure $\mathscr{M}_i\,\mathrm{d}i\,\mathrm{d}v\,\mathrm{d}x$, where $\mathrm{d}i$ stands for the counting measure on $\mathbb{N}$, $U = \frac{i}{2}(v^2/2 + \Phi(x))$, $\nu = 1/2$ and $g = f_i(t,x,v)/\mathscr{M}_i$.)

Lemma 5.5.2. *Let* X *be a subset of* $\mathbb{R}^D$, *possibly* $\mathbb{R}^D$ *itself. Let* $U : X \to \mathbb{R}^+$ *such that* $(1+U)e^{-\nu U} \in L^1(X)$ *for some* $0 < \nu < 1$. *Let* $g : X \to \mathbb{R}^+$. *Then, we have*

$$0 \leq \int_X g\ln^-(g)\,\mathrm{d}y \leq \nu\int_X Ug\,\mathrm{d}y + \int_X (1+\nu U)e^{-\nu U}\,\mathrm{d}y.$$

With these properties, we already have estimates on the macroscopic quantities, but we can go a step further, identifying leading terms owing to the dissipation term D. To this end, we need an estimate on a higher moment with respect to the size variable, namely, we suppose that

$$\sum_{I=1}^{\infty}\int_{\Omega}\int_{\mathbb{R}^3} i^2\,(1+v^2)\,f_i\,\mathrm{d}v\,\mathrm{d}x \quad \text{is bounded uniformly on } [0,T] \tag{5.17}$$

(uniformly with respect to the scaling parameters) for any $0 < T < \infty$. This condition, the physical interpretation of which is not direct, is however somehow classical when dealing with coagulation-fragmentation problem. It is likely that it can be satisfied under appropriate hypothesis on the initial data and the kinetic coefficients, see [9].

Lemma 5.5.3. *Let the assumptions of Proposition 5.5.1 be fulfilled together with* (5.17)*. Then, we have*

$$J_i = i\rho_i u + \beta\sqrt{\varepsilon}K_i,$$
$$\mathbb{P}_i = \rho_i \mathbb{I} + \beta^{-2} J_i \otimes u + \sqrt{\varepsilon}\mathbb{K}_i$$

where the remainders K and $\mathbb{K}$ are bounded in $L^2(0,T;L^1(\Omega\times\mathbb{N}))$.

Proof. We rewrite

$$J_i = i\rho_i u + \beta i \int_{\mathbb{R}^3} \Big((v-\beta^{-1}u)f_i + \frac{1}{i}\nabla_v f_i\Big)\,\mathrm{d}v = i\rho_i u + \beta\int_{\mathbb{R}^3} D_i\sqrt{i^{5/3}f_i}\,\mathrm{d}v.$$

The last term, that is denoted K_i, can be dominated by using the Cauchy-Schwarz inequality

$$\sum_{i=1}^{\infty}\int_\Omega |K_i|\,\mathrm{d}x \le \beta\sqrt{\varepsilon}\left(\sum_{i=1}^{\infty}\int_\Omega\int_{\mathbb{R}^3}\Big|\frac{D_i}{\sqrt{\varepsilon}}\Big|^2\,\mathrm{d}v\,\mathrm{d}x\right)^{1/2}\left(\sum_{i=1}^{\infty}\int_\Omega\int_{\mathbb{R}^3} i^{5/3}f_i\,\mathrm{d}v\,\mathrm{d}x\right)^{1/2}.$$

We proceed similarly with

$$\mathbb{P}_i = \beta^{-2}J_i\otimes u + \rho_i\mathbb{I} + \int_{\mathbb{R}^3} D_i\otimes v\sqrt{i^{5/3}f_i}\,\mathrm{d}v.$$

□

5.5.1 Flowing regime

For this regime we suppose that both $\rho_P/\rho_F = \beta^{-2}$ and $\eta = \beta$ are fixed, as well as α; we only let ε go to 0. According to the discussion above, we expect that

$$J_i \simeq i\rho_i u, \qquad \mathbb{P}_i \simeq \rho_i\mathbb{I} + \beta^{-2} i\rho_i u\otimes u.$$

Plugging this ansatz into (5.14) and (5.16), we are led to the system

$$\begin{cases} \partial_t\rho_i + \nabla_x\cdot(\rho_i u) = \dfrac{1}{\tau_c}Q_i(\rho), \\ \partial_t n + \nabla_x\cdot(nu) = 0, \\ \partial_t\big((n+\beta^{-2}\nu)u\big) + \mathrm{Div}_x\big((n+\beta^{-2}\nu)u\otimes u + (\chi p+\nu)\mathbb{I}\big) + (\alpha\beta\eta n+\nu)\nabla_x\Phi = \mu\Delta_x u. \end{cases}$$

where we have set

$$\nu = \sum_{i=1}^{\infty} i\rho_i.$$

As a matter of fact, we observe that

$$\partial_t\nu + \nabla_x\cdot(\nu u) = 0.$$

This is a multiphase flow system where particles concentrations are subject to exchanges through coagulation and break-up and advection with the fluid velocity u. The motion of the fluid can be interpreted as a Navier-Stokes (or Euler if $\mu = 0$) system for the composite density $n+\beta^{-2}\nu$ and the velocity u, involving a complex pressure law.

5.5.2 Bubbling regime

For this regime, the scaling assumptions cast as follows

$$\beta = \frac{1}{\sqrt{\varepsilon}} = \eta, \qquad \frac{\rho_P}{\rho_F} = \varepsilon,$$

while we set $\alpha = \mathrm{sgn}(\alpha)\varepsilon$. We guess that, at leading order, the f_i's look like centered Maxwellians

$$f_i(t,x,v) \simeq \frac{\rho_i(t,x)}{(2\pi/i)^{3/2}}\ e^{-iv^2/2}.$$

Accordingly

$$\mathbb{P}_i \simeq i\int_{\mathbb{R}^3} v\otimes v \frac{\rho_i(t,x)}{(2\pi/i)^{3/2}}\ e^{-iv^2/2}\,\mathrm{d}v = \rho_i\mathbb{I}.$$

The relation (5.15) allows to obtain the limiting particles current : letting $\varepsilon = \beta^{-2}$ go to 0 in (5.15) we get

$$J_i \simeq i\rho_i u_i - i^{5/3}\rho_i\nabla_x\Phi - i^{2/3}\nabla_x\rho_i.$$

Coming back to (5.14) and the fluid equations, we arrive at

$$\begin{cases} i\partial_t\rho_i + i\nabla_x\cdot\big(\rho_i(u - i^{2/3}\nabla_x\Phi)\big) = i^{2/3}\Delta_x\rho_i + \dfrac{i}{\tau_c}Q_i(\rho), \\ \partial_t n + \nabla_x\cdot(nu) = 0, \\ \partial_t(nu) + \mathrm{Div}_x(nu\otimes u) + \nabla_x\Big(\chi p + \displaystyle\sum_{i=1}^{\infty}\rho_i\Big) + (\mathrm{sgn}(\alpha)n + \nu)\nabla_x\Phi = \mu\Delta_x u, \end{cases}$$

still with the notation $\nu = \sum_{i=1}^{\infty} i\rho_i$. Now particles concentrations are driven by a convection–diffusion equation, with a size-dependent diffusion coefficient (proportional to the surface of the grain, actually). The particles influence weakly the fluid through the pressure term (which can be incorporated in a common Lagrange multiplier for incompressible flows) and the external force.

Table des figures

Bibliographie

[1] Aguzzi, A., Genoud, N., and Masel, J. Efficient inhibition of prion replication by prp-fc2 suggests that the prion is a prpsc oligomer. *Journal of Molecular Biology 345*, 5 (2005), 1243 –1251.

[2] Aizenmam, M., and Bak, T. A. convergence to equilibrium in a system of reacting polymers. *Comm. Math. Phys. 65* (1979), 203–230.

[3] Aldous, D. J., and Pitman, J. The standard additive coalescent. *Ann. Probab. 26* (1998), 1703–1726.

[4] Ambrosiano, J., Cleland, T., Gray, P., Hlavacek, W., Kim, J. I., Piltch, M., Roberts, R., and Rubenstein, R. Dynamics of the nucleated polymerization model of prion replication. *Biophysical Chemistry 125*, 2-3 (2007), 360 –367.

[5] Amsden, A., Dukowicz, J., O'Rourke, P., and Ramshaw, P. Kiva : a computer program for two- and three- dimensional fluid flows with chemical reactions and fuel sprays. La-10245-ms, hnical Report, Los Alamos National Laboratory, 1985.

[6] Andrews, M. J., and O'Rourke, P. J. The multiphase particle-in-cell (MP-PIC) method for dense particulate flows. *InJ. Multiphase Flow 22* (1996), 379–402.

[7] Arino, O. A survey of structured cell population dynamics. *Acta Biotheor. 43* (1995), 3–25.

[8] Aris, R., Fredrickson, A. G., and Tsuchiya, H. M. Dynamics of microbial cell populations. *Adv. Chem. Eng. 6* (1966), 125–206.

[9] Ball, J. M., Carr, J., and Penrose, O. The Becker–Döring cluster equations : Basic properties and asymptotic behaviour of solutions. *Comm. Math. Phys. 104* (1986), 657–692.

[10] Ball, J. M., Carr, J., and Penrose, O. The becker-döring cluster equations : basic properties and asymptotic behaviour of solutions. *Commun. Math. Phys. 104* (1986), 657–692.

[11] Banasiak, J., and Lamb, W. On a coagulation and fragmentation equation with mass loss. *Proc. Roy. Soc. Edinburgh Sect. A 136*, 6 (2006), 1157–1173.

[12] Baranger, C. *Modélisation, étude mathématique et simulation des collisions dans les fluides complexes.* PhD thesis, ENS Cachan, 2004.

[13] Baranger, C., Boudin, L., Jabin, P.-E., , and Mancini, S. A modeling of biospray for the upper airways. *ESAIM : Proc. 14* (2005), 41–47.

[14] Baranger, C., Boudin, L., Jabin, P.-E., and Mancini, S., Eds. *A modeling of biospray for the upper airways* (2005), vol. 14, ESAIM :Proc.

[15] Baranger, C., and Desvillettes, L. Coupling Euler and Vlasov equations in the context of sprays : local smooth solutions. *Journal of Hyperbolic Differential Equations 3* (2006), 1–26.

[16] Becker, R., and Döring, W. Kinetische behandlung der keimbildung in übersättigten dämpfern. *Ann. Phys. (Leipzig) 24* (1935), 719–752.

[17] Bekkal Brikci, F., Clairambault, J., and Perthame, B. Analysis of a molecular structured population model with possible polynomial growth for the cell division cycle. *Math. Comput. Modelling 47*, 7-8 (2008), 699–713.

[18] Benedek, G. B., Kirschner, D. A., Lomakin, A., and Teplow, D. B. Kinetic theory of fibrillogenesis of amyloid [beta]-protein. *National Academy of Sciences of the United States of America 94*, 15 (1997), 7942–7947.

[19] Bernard, S., Cajavec, B., and Herzel, H. Aggregation in huntington's disease : insights through modelling. *Genome Inform. 16*, 1 (2005), 120–129.

[20] Berthonnaud, P. Limites fluides pour des modèles cinétiques de brouillards de gouttes monodispersés. *C. R. Acad. Sci. 331* (2000), 651–654.

[21] Biben, T., Geminard, J.-C., and Melo, F. Dynamics of bio-polymeric brushes growing from a cellular membrane : Tentative modelling of the actin turnover within an adhesion unit ; the podosome. *J. Biol. Phys. 31* (2005), 87–120.

[22] Boudin, L., Boutin, B., Fornet, B., Goudon, T., Lafitte, P., Lagoutière, F., and Merlet, B., Eds. *Fluid-particles flows : A thin spray model with energy exchanges* (2009), vol. 28, ESAIM : Proc.

[23] Boudin, L., Desvillettes, L., Grandmont, C., and Moussa, A. Global existence of solutions for the coupled Vlasov and Navier-Stokes equations. *Differential and Integral Equations 22* (2009).

[24] Brezis, H. *Analyse Fonctionnelle : Théorie et Applications*. Masson, 1983.

[25] Brown, L. A new examination of classical coarsening theory. *Acta Metall. 37* (1989), 71–77.

[26] Bürger, R., Concha, F., and Wendland, W. Model equations for gravitational sedimentation–consolidation processes. *Z. Angew. Math. Mech. 80*, 2 (2000), 79–92.

[27] Caceres, M. J., Carrillo, J. A., and Dolbeault, J. Nonlinear stability in l^p for a confined system of charged particles. *SIAM J. Math. Anal. 34* (2002), 478–494.

[28] Caflisch, R., and Papanicolaou, G. Dynamic theory of suspensions with brownian effects. *SIAM J. Appl. Math. 43* (1983), 885–906.

[29] Calgaro, C., Creusé, E., and Goudon, T. Simulation of mixture flows : Pollution spreading and avalanches. Tech. rep., INRIA, 2011-12.

[30] Calvez, V., Deslys, J.-P., Doumic, M., Lenuzza, N., Mouthon, F., and Perthame, P. Prion dynamic with size dependency - strain phenomena. *J. of Biol. Dyn. 4*, 1 (2010), 28–42.

[31] Calvez, V., Deslys, J.-P., Laurent, L., Lenuzza, N., Mouthon, F., Oelz, D., and Perthame, B. Size distribution dependence of prion aggregates infectivity. *Math. Biosci. 1* (2009), 88–99.

[32] Carr, J. Asymptotic behaviour of solutions to the coagulation-fragmentation equations. I. The strong fragmentation case. *Proc. Roy. Soc. Edinburgh Sect. A 121* (1992), 231–244.

[33] Carr, J., and da Costa, F. P. Asymptotic behavior of solutions to the coagulation-fragmentation equations. II. Weak fragmentation. *J. Statist. Phys. 77* (1994), 89–123.

[34] Carr, J., and Penrose, O. Asymptotic behavior of solutions to a simplified lifshitz-slyozov equation. *Phys. D. 124* (1998), 166–176.

[35] Carrillo, J. A., and Goudon, T. A numerical study on large-time asymptotics of the lifshitz-slyozov system. *J. Scient. Comp. 18* (2003), 429–473.

[36] Carrillo, J. A., and Goudon, T. Stability and asymptotic analysis of a fluid-particle interaction model. *Comm. PDE 31* (2006), 1349–1379.

[37] Carrillo, J. A., Goudon, T., and Laffite, P. Simulation of fluid and particles flows : Asymptotic preserving schemes for bubbling and flowing regimes. *J. Comput. Phys. 227*, 16 (2008), 7929–7951.

[38] Carrillo, J. A., Jüngel, A., Markowich, P. A., Toscani, G., and Unterreiter, A. Entropy dissipation methods for degenerate parabolic systems and generalized Sobolev inequalities. *Monatshefte für Mathematik 133* (2001), 1–82.

[39] Caswell, H., and Tuljapurkar, S. Structured population models in marine, terrestrial and freshwater ecosystems. *Chapman and Hall, New York, USA* (1997).

[40] Caughey, B., Hayes, S., Hughson, A., Race, R., Raymond, G., Silveira, J., and Sim, V. The most infectious prion protein particles. *Nature 437*, 7056 (09 2005), 257–261.

[41] Châun-Hoàn, L. *Étude de la classe des opérateurs $m-$accrétifs de $L^1(\Omega)$ et accrétifs dans $L^\infty(\Omega)$*. PhD thesis, Université Paris VI, 1977.

[42] Chen, M. K., and Voorhees, P. W. The dynamics of transient ostwald ripening. *Modelling Simul. Mater. Sci. Eng. 1* (1993), 591–612.

[43] Cockburn, B., Shu, C.-W., Johnson, C., and Tadmor, E. *Essentially non-oscillatory and weighted essentially non-oscillatory schemes for hyperbolic conservation laws*, vol. 1697. Springer Berlin / Heidelberg, 1998, pp. 325–432.

[44] Coddington, E. A., and Levinson, N. *Theory of ordinary differential equations*. McGraw-Hill, 1955.

[45] Collet, J.-F. Some modelling issues in the theory of fragmentation-coagulation systems. *Commun. Math. Sci. 2* (2004), 35–54.

[46] Collet, J.-F., and Goudon, T. Lifshitz-slyozov equations : the model with encounters. *Transp. Theory Stat. Phys. 28* (1999), 545–573.

[47] Collet, J.-F., and Goudon, T. On solutions of the lifshitz-slyozov model. *Nonlinearity 13* (2000), 1239–1262.

[48] Collet, J.-F., Goudon, T., Poupaud, F., and Vasseur, A. The becker-döring system and its lifshitz-slyozov limit. *SIAM J. Appl. Math. 62* (2002), 1488–1500.

[49] Collet, J.-F., Goudon, T., and Vasseur, A. Some remarks on large-time asymptotics of the lifshitz-slyozov equations. *J. Stat. Phys. 108* (2002), 341–359.

[50] Collet, J.-F., and Hariz, S. A modified version of the lifschitz-slyozov model. *Applied Math. Lett. 12* (1999), 81–85.

[51] Conlon, J. On a diffusive version of the lifshitz-slyozov-wagner equation. *J. Nonlinear Sc.* (2010), 1432–1467.

[52] Craft, D. L., Selkoe, D. J., and Wein, L. M. A mathematical model of the impact of novel treatments on the a[beta]burden in the alzheimer's brain, csf and plasma. *Bulletin of Mathematical Biology 64*, 5 (2002), 1011–1031.

[53] Dadyburjor, D. B., and Ruckenstein, E. Kinetics of ostwald ripening. *J. Crystal Growth 40* (1977), 279–290.

[54] De Luca, M. *Contribution à la modélisation de la pulvérisation d'un liquide phytosanitaire en vue de réduire les pollutions*. PhD thesis, Univ. Aix–Marseille 2, 2007.

[55] Dellacherie, C., and Meyer, P.-A. *Probabilités et potentiel*. Hermann, 1975, ch. chapitres I à IV.

[56] Després, B., and Lagoutière, F. Contact discontinuity capturing schemes for linear advection and compressible gas dynamics. *J. Scient. Comp. 16* (2001), 479–524.

[57] Devys, A., Goudon, T., and Lafitte, P. A model describing the growth and the size distribution of multiple metastatic tumors. *DCDS-B 12*, 4 (2009), 731–767.

[58] Diekmann, O., Gyllenberg, M., Huang, H., Kirkilionis, M., Metz, J. A. J., and Thieme, H. R. On the formulation and analysis of general deterministic structured population models. *II. Nonlinear theory. J. Math. Biol. 43*, 2 (2001), 157–189.

[59] Diekmann, O., and Metz, J. A. J. *The dynamics of physiologically structured populations*, vol. 68 of *Lecture Notes in Biomathematics*. Springer-Verlag, 1986.

[60] Dolbeault, J., and Rein, G. Time-dependent rescalings and Lyapunov functionals for the Vlasov-Poisson and Euler-Poisson systems, and for related models of kinetic equations, fluid dynamics and quantum physics. *Math. Models Methods Appl. Sci. 11* (2001), 407–432.

[61] Doumic, M. Analysis of a population model structured by the cells molecular content. *Math. Model. Nat. Phenom. 2*, 3 (2007), 121–152.

[62] Doumic, M., and Gabriel, P. Eigenelements of a general aggregation-fragmentation model. *Math. Models Methods Appl. Sci. 20*, 5 (2010), 757–783.

[63] Doumic, M., Goudon, T., and Lepoutre, T. Scaling limit of a discrete prion dynamics model. *Communications in Mathematical Sciences 7*, 4 (2009), 839–865.

[64] Doumic, M., Hoffmann, M., Reynaud-Bouret, P., and Rivoirard, V. Nonparametric estimation of the division rate of a size-structured population.

[65] Doumic, M., Maia, P., and Zubelli, J. On the calibration of a size-structured population model from experimental data. *Acta Biotheoretica 58*, 4 (2010), 405–413.

[66] Doumic, M., Perthame, B., and Zubelli, J. P. Numerical solution of an inverse problem in size-structured population dynamics. *Inverse Problems 25*, 4 (2009), electronic 045008.

[67] Doumic, M., and Tine, L. M. A general inverse problem for aggregation-fragmentation equation. submitted in J.M.B., 2011.

[68] Drake, R. A general mathematical survey of the coagulation equation. in : Topics in current aerosol research (part 2). *International Reviews in Aerosol Physics and Chemistry* (1972), 203–376.

[69] Dubovskii, P. B., and Stewart, I. W. Existence, uniqueness and mass conservation for the coagulation-fragmentation equation. *Math. Methods Appl. Sci. 19* (1996), 571–591.

[70] Edwards, R. *Functional analysis : Theory and Applications*. Dover, 1994.

[71] Einstein, A. On the motion of small particles suspended in liquids at rest required by the molecular-kinetic theory of heat. *Annalen der Physik 17* (1905), 549–560.

[72] Elperin, T., Kleeorin, N., Liberman, M. A., L'vov, V. S., Pomyalov, A., and Rogachevskii, I. Clustering of fuel droplets and quality of spray in Diesel engines.

[73] Engl, H. W., Hanke, M., and Neubauer, A. *Regularization of inverse problems*, vol. 375. Kluwer Academic Publishers Group, Dordrecht, 1996.

[74] Engler, H., Pruss, J., and Webb, G. Analysis of a model for the dynamics of prions ii. *J. of Math. Anal. and App. 324*, 1 (2006), 98–117.

[75] Escobedo, M., Laurençot, P., S., M., and Perthame, P. Gelation and mass conservation in coagulation-fragmentation models. *J. Differential Equations 195*, 1 (2003), 143–174.

[76] Escobedo, M., Mischler, S., and Perthame, B. Gelation in coagulation and fragmentation models. *Comm. Math. Phys. 231*, 1 (2002), 157–188.

[77] Escobedo, M., and S., M. Dust and self-similarity for the smoluchowski coagulation equation. *Ann. Inst. H. Poincaré Anal. Non Linéaire 23*, 3 (2006), 331–362.

[78] Escobedo, M., S., M., and Rodriguez-Ricard, M. On self-similarity and stationary problem for fragmentation and coagulation models. *Ann. Inst. H. Poincaré Anal. Non Linéaire 22*, 1 (2005), 99–125.

[79] Filbet, F. An asymptotically stable scheme for diffusive coagulation-fragmentation models. *Commun. Math. Sci. 6*, 2 (2008), 257–280.

[80] Filbet, F., and Laurençot, P. Numerical approximation of the lifshitz-slyozov-wagner equation. *SIAM J. Numer. Anal. 41* (2003), 563–588.

[81] Filbet, F., and Laurençot, P. Numerical simulation of the smoluchowski coagulation equation. *SIAM J. Sci. Comput. 25* (2004), 2004–2028.

[82] Filbet, F., and Laurençot, P. Mass-conserving solutions and non-conservative approximation to the smoluchowski coagulation equation. *Arch. Math. (Basel) 83*, 6 (2004), 558–567.

[83] Fredrickson, A. G. Population balance equation for cell and microbial cultures. *AIChE Journal 49*, 4 (2003), 1050–1059.

[84] Friedlander, S. K. *Smoke, Dust and Haze : fundamentals of aerosol dynamics.* Topics in chemical engineering. Oxford University Press, 2000.

[85] Gabriel, P., and Tine, L. M., Eds. *High-order WENO scheme for polymerization-type equations* (2010), no. 30, ESAIM Proc.

[86] Gavrilyuck, S., and Teshukhov, V. Kinetic model for the motion of compressible bubbles in a perfect fluid. *Eur. J. Mech. B/Fluids 21* (2002), 469–491.

[87] Goudon, T., Jabin, P., and Vasseur, A. Hydrodynamic limits for the vlasov-navier-stokes equations : Fine particles regime. *Indiana University Math. J. 53* (2004), 1517–1536.

[88] Goudon, T., Jabin, P., and Vasseur, A. Hydrodynamic limits for the vlasov-navier-stokes equations : Light particles regime. *Indiana University Math. J. 53* (2004), 1495–1516.

[89] Goudon, T., Jin, S., and Yan, B. Simulation of fluid–particles flows : Heavy particles, flowing regime and AP–schemes. Tech. rep., INRIA, 2010.

[90] Goudon, T., Lagoutière, F., and Tine, L. M. The lifshitz-slyozov equation with space–diffusion of monomers. 2011.

[91] Goudon, T., Lagoutière, F., and Tine, L. M. Simulations of the lifschitz-slyozov equations : the role of the coagulations terms in the asymptotic behavior. 2011.

[92] Goudon, T., Liu, J.-G., Jin, S., and Yan, B. Asymptotic-preserving schemes for kinetic–fluid modeling of disperse two-phase flows. Tech. rep., INRIA, 2011.

[93] Goudon, T., Moussa, A., He, L., and Zhang, P. The Navier–Stokes–Vlasov–Fokker–Planck system near equilibrium. *SIAM J. Math. Anal. 42* (2010), 2177–2202.

[94] Greer, M. L., Pujo-Menjouet, L., and Webb, G. F. A mathematical analysis of the dynamics of prion proliferation. *J. Theorit. Biol. 242*, 3 (2006), 598–606.

[95] Greer, M. L., van-den Driessche, P., Wang, L., and Webb, G. F. Effects of general incidence and polymer joining on nucleated polymerization in a model of prion proliferation. *SIAM Journal on Applied Mathematics 68*, 1 (2007), 154–170.

[96] Groh, A., Krebs, J., and Wagner, M. Efficient solution of an inverse problem in cell population dynamics. *Inverse Problems 27* (2011).

[97] Hamdache, K. Global existence and large time behaviour of the vlosov-stokes equations. *Japan J. Indust. Appl. 15* (1998), 51–74.

[98] Harten, A. On a class of high resolution total-variation-stable finite difference schemes. *SIAM Jour. of Numer. Anal. 21* (1984), 1–23.

[99] Henson, M. A. Dynamic modeling and control of yeast cell populations in continuous biochemical reactors. *Comput. chem. Eng. 27* (2003), 1185–1199.

[100] Henson, M. A. Dynamic modeling of microbial cell populations. *Curent Opinion in Biotechnology 14* (2003), 460–467.

[101] Herrero, H., Lucquin-Desreux, B., and Perthame, B. On the motion of dispersed balls in a potential flow : a kinetic description of the added mass effect. *SIAM J. Appl. Math. 60* (1999), 61–83.

[102] Herrmann, M., Laurençot, P., and Niethammer, B. Self-similar solutions with fat tails for a coagulation equation with nonlocal drift. *Comptes Rendus Mathematique 347*, 15-16 (2009), 909–914.

[103] Herrmann, M., Niethammer, B., and Velázquez, J. J. L. Self-similar solutions for the LSW model with encounters. *J. Differential Equations 247* (2009), 2282–2309.

[104] Jabin, P.-E., and Niethammer, B. On the rate of convergence to equilibrium in the Becker–Döring equations. *J. Differential Equations 191* (2003), 518–543.

[105] Jansen, V., Masel, J., and Nowak, M. Quantifying the kinetic parameters of prion replication. *Biophysical Chemistry 77*, 2-3 (1999), 139–152.

[106] Jiang, G., and Shu, C. W. Efficient implementation of weighted eno schemes. *J. Comp. Physics 126* (1996), 202–228.

[107] Jiang, J. S., and Peng, D. Weighted eno schemes for hamilton-jacobi equations. *SIAM J. Sci. Comput. 21* (2000), 2126–2143.

[108] Kingman, J. The coalescent. stochastic process. *Stochastic Processes and Applications* (1982), 235–248.

[109] Knowles, T. P. J., Waudby, C. A., Devlin, G. L., Cohen, S. I. A., Aguzzi, A., Vendruscolo, M., Terentjev, E. M., Welland, M. E., and Dobson, C. M. An analytical solution to the kinetics of breakable filament assembly. *Science 326*, 5959 (2009), 1533–1537.

[110] Laurençot, P. The lifshitz-slyozov equation with encounters. *Math. Models Methods Appl. Sci. 11* (2001), 731–748.

[111] Laurençot, P. Weak solutions to the lifshitz-slyozov-wagner equation. *Indiana Univ. Math. J. 50* (2001), 1319–1346.

[112] Laurençot, P. The lifshitz-slyozov-wagner equation with conserved total volume. *SIAM J. Math. Anal. 34* (2003), 257–272.

[113] Laurençot, P., and Mischler, S. From the discrete to the continuous coagulation-fragmentation equations. P. R. S. Edinburgh, Ed., vol. 132 of *Sect. A*, pp. 1219–1248.

[114] Laurençot, P., and Mischler, S. On coalecence equations and related models. *Model. Simul. Sci. Eng. Technol.* (2004), 321–356.

[115] Laurençot, P., and Perthame, B. Exponential decay for the growth-fragmentation/cell-division equation. *Comm. Sci. 7*, 2 (2009), 503–510.

[116] Laurençot, P., and Mischler, S. The continuous coagulation-fragmentation equations with diffusion. *Archive for Rational Mechanics and Analysis 162* (2002), 45–49.

[117] Laurençot, P., and Mischler, S. Convergence to equilibrium for the continuous coagulation-fragmentation equation. *Bull. Sci. Math. 127*, 3 (2003), 179–190.

[118] Laurençot, P., and Mischler, S. Liapunov functionals for smoluchowski's coagulation equation and convergence to self-similarity. *Monatsh. Math. 146*, 2 (2005), 127–142.

[119] Laurençot, P., and Walker, C. Well-posedness for a model of prion proliferation dynamics. *J. Evol. Equ. 7*, 2 (2007), 241–264.

[120] Le Roux, A.-Y. A numerical conception of entropy for quasi-linear equations. *Math. of Comp. 31* (1977), 848–872.

[121] Lenuzza, N. *Modélisation de la réplication des Prions : implication de la dépendance en taille des agrégats de PrP et de l'hétérogénéité des populations cellulaires.* PhD thesis, CEA, Paris, 2009.

[122] Lifschitz, I. M., and Pitaevski, L. *Cinétique Physique, Cours de Physique Théorique*, vol. 10. Mir, 1990.

[123] Lifshitz, E. M., and Slyozov, V. V. The kinetics of precipitation from supersaturated solid solutions. *J. Phys. Chem. Solids 19* (1961), 35–50.

[124] Liu, H., Wang, Z., and Fox, R. A level set approach for dilute non-collisional fluid-particle flows. *J. Comput. Phys. 230* (2011), 920–936.

[125] Lushnikov, A. Some new aspect of coagulation theory. *Izv. Akad. Nauk SSSR, Ser. Fiz. At-mosfer. I Okeana. 14* (1978), 738–743.

[126] Marcus, A. Stochastic coalescence. *Technometrics 10* (1968), 133–143.

[127] Mathiaud, J. *Etude de systèmes de type gaz-particules.* PhD thesis, ENS Cachan, 2006.

[128] McKendrick, A. Applications of mathematics to medical problems. *Proc. Edingburgh Math. Soc. 44* (1926), 98–130.

[129] Meerson, B., and Sasorov, P. Domain stability, competition, growth, and selection in globally constrained bistable systems. *Phys. Rev. E. 53* (1996), 3491–3494.

[130] Meister, E., and Stewart, I. W. A global existence theorem for the general coagulation-fragmentation equation with unbounded kernels. *Math. Methods Appl. Sci. 11* (1989), 627–648.

[131] Mellet, A., and Vasseur, A. Global weak solutions for a Vlasov-Fokker-Planck/Navier-Stokes system of equations. *Math. Mod. Meth. Appl. Sci. 17* (2007), 1039–1063.

[132] Mellet, A., and Vasseur, A. Asymptotic analysis for a Vlasov–Fokker–Planck/compressible Navier–Stokes system of equations. *Comm. Math. Phys. 281* (2008), 573–596.

[133] Michel, P. Existence of a solution to the cell division eigenproblem. *Model. Math. Meth. Appl. Sci. 16*, suppl. issue 1 (2006), 1125–1153.

[134] Michel, P., Mischler, S., and Perthame, B. General entropy equations for structured population models and scattering. *C. R. Acad. Sc. Paris, Sér. I 338* (2004), 697–702.

[135] Michel, P., Mischler, S., and Perthame, B. General entropy equations for structured population models and scattering. *C. R. Math. Acad. Sci. Paris 338*, 9 (2005), 697–702.

[136] Michel, P., Mischler, S., and Perthame, B. General relative entropy inequality : an illustration on growth models. *J. Math. Pures et Appl. 84*, 9 (2005), 1235–1260.

[137] Mischler, S., Perthame, B., and Ryzhik, L. Stability in a nonlinear population maturation model. *Math. Models Meth. Appl. Sci. 12* (2002), 1751–1772.

[138] Mischler, S., and Rodriguez-Ricard, M. Existence globale pour l'équation de smoluchowski continue non homogène et comportement asymptotique des solutions. *C. R. Math. Acad. Sci. Paris 336*, 5 (2003), 407–412.

[139] Moussa, A. *Etude mathématique et numérique du transport d'aérosols dans le poumon humain*. PhD thesis, ENS Cachan, 2009.

[140] Murphy, R. M., and Pallitto, M. M. A mathematical model of the kinetics of [beta]-amyloid fibril growth from the denatured state. *Biophysical Journal 81*, 3 (2001), 1805–1822.

[141] Niethammer, B. A scaling limit of the becker-döring equations in the regime of small excess density. *J. Nonlinear Sci. 14*, 5 (2004), 453–468.

[142] Niethammer, B., and Otto, F. Ostwald ripening : the screening length revisited. *Calc. Var. Partial Differential Equations 13* (2001), 33–68.

[143] Niethammer, B., and Pego, R. Non-self-similar behavior in the lsw theory of ostwald ripening. *J. Stat. Phys. 95* (1999), 867–902.

[144] Niethammer, B., and Pego, R. On the initial-value problem in the lifshitz-slyozov-wagner theory of ostwald ripening. *SIAM J. Math. Anal. 31* (2000), 467–485.

[145] Niethammer, B., and Pego, R. The lsw model for domain coarsening : Asymptotic behavior for conserved total mass. *J. Stat. Phys. 104* (2001), 1113–1144.

[146] Niethammer, B., and Pego, R. L. Well-posedness for measure transport in a family of nonlocal domain coarsening models. *Indiana Univ. Math. J. 54*, 2 (2005), 499–530.

[147] Niethammer, B., and Velazquez, J. J. L. Global well-posedness for an inhomogeneous lsw model in unbounded domains. *Math. Ann. 328* (2004), 481–501.

[148] Niethammer, B., and Velázquez, J. J. L. On the convergence to the smooth self-similar solution in the lsw model. *Indiana Univ. Math. J. 55* (2006), 761–794.

[149] Niethammer, B., and Velázquez, J. J. L. On screening induced fluctuations in ostwald ripening. *J. Stat. Phys. 130* (2008), 415–453.

[150] Norris, J. R. Smoluchowski's coagulation equation : uniqueness, non-uniqueness and hydrodynamic limit for the stochastic coalescent. *Ann. Appl. Probab. 9* (1999), 78–109.

[151] Pakdaman, K., Perthame, B., and Salort, D. Dynamics of a structured neuron population. *Nonlinearity 23* (2010), 55–75.

[152] Patankar, N. A., and Joseph, D. D. Lagrangian numerical simulation of particulate flows. *Int. J. Multiphase Flow 27* (2001), 1685–1706.

[153] Patankar, N. A., and Joseph, D. D. Modeling and numerical simulation of particulate flows by the Eulerian–Lagrangian approach. *Int. J. Multiphase Flow 27* (2001), 1659–1684.

[154] Penrose, O. The becker-döring equations at large times and their connection with the lsw theory of coarsening. *J. Stat. Phys. 89*, 1-2 (1997), 305–320.

[155] Perthame, B. *Transport equations in biology.* Frontiers in mathematics. Birkhäuser, 2007.

[156] Perthame, B., and Ryzhik, L. Exponential decay for the fragmentation or cell-division equation. *Journal of Differential Equations 210*, Issue 1 (2005), 155–177.

[157] Perthame, B., and Zubelli, J. P. On the inverse problem for a size structured population model. *Inverse Problem 23* (2007), 1037–1052.

[158] Phillips, T. Trouble with lifshitz, slyozov and wagner, science news, nasa science.

[159] Pruss, J., Pujo-Menjouet, L., Webb, G., and Zacher, R. Analysis of a model for the dynamics of prion. *Dis. Cont. Dyn. Sys. Ser. B 6*, 1 (2006), 225–235.

[160] Ramkrishna, D. Population balances : Theory and applications to particulate processes in engineering. *Academic Press, New York* (2000).

[161] Rein, G. Non-linear stability of gaseous stars. *Arch. Rat. Mech. Anal. 168* (2003), 115–130.

[162] Sagalovich, V. V., and Slyozov, V. V. Diffusive decomposition of solid solutions. *Sov. Phys. Usp. 30* (1987), 23–44.

[163] Shen, J., Shu, C. W., and Zhang, M. A high order weno scheme for a hierarchical size-structured population model. *J. Sci. Comput. 33*, 3 (2007), 279–291.

[164] Simon, J. Compact sets in $l^p(0,t;b)$. *Ann. Mat, Pura ed Appl. CXLVI* (1987), 65–96.

[165] Slemrod, M. Trend to equilibrium in the Becker–Döring cluster equation. *Nonlinearity 2* (1989), 429–443.

[166] Smoluchowski, M. Drei vorträge über diffusion, brownsche molekularbewegung und koagulation von kolloidteilchen. *Physik. Zeitschr 17* (1916), 557–599.

[167] Smoluchowski, M. Versuch einer mathematichen theorie der koagulationskinetic kolloider lösungen. *Zeitschrift f. physik. Chemie 92* (1917), 129–168.

[168] Sportisse, B. *Modélisation et simulation de la pollution atmosphérique.* Habilitation à diriger les recherches, sciences de l'univers, Université Pierre et Marie Curie, 2007.

[169] Trèves, F. *Topological vector spaces, distributions and kernels.* Dover, 2006.

[170] Vinkovic, I. *Dispersion et mélange turbulents de particules solides et de gouttelettes par une simulation de grande échelle et une modélisation stochastique lagrangienne. Application à la pollution de l'atmosphère.* PhD thesis, Ecole Centrale de Lyon, 2005.

[171] Vinkovic, I. *Dispersion et mélange turbulents de particules solides et de gouttelettes par une simulation des grandes échelles et une modélisation stochastique lagrangienne. Application à la pollution de l'atmosphère.* PhD thesis, Ecole Centrale de Lyon, 2005.

[172] VonFoerster, H. *Some remarks on changing populations*, f. stohlman, ed. ed. 1959.

[173] Williams, F. Spray combustion and atomization. *Phys. Fluid 1* (1958), 541–555.

[174] Williams, F. *Combustion Theory.* Benjamin Cummings Publishing, 1985.